TOWARDS MICRORNA-BASED THERAPEUTICS

FOR CARDIOVASCULAR DISEASES

PhD Dissertation

by Zhiyong Lei

Promoter: Prof. dr. P.A.F.M. Doevendans

Co-promoters: Dr. J.P.G. Sluijter
                                              Dr. H. el Azzouzi

Beoordelingscommissie :

        Prof.dr. J.P.W.M. Bakkers

        Prof.dr. M.C. Verhaar

        Prof.dr. R. Goldschmeding

        Prof.dr. R.M. Schiffelers

        Prof.dr. J. van der Velden

Contact Information

Zhiyong Lei
Department of Experimental Cardiology
University Medical Center Utrecht
Internal mail G02.523
PO Box 85500
3508 GA Utrecht
Email: zlei@umcutrecht.nl

Table of Contents

Chapter 1   introduction

Targeted Delivery Of miRNA Therapeutics for cardiovascular diseases: Opportunities and Challenges

Zhiyong Lei[2,#], Rick F J Kwekkeboom[1,#], Pieter A. Doevendans[2,3], René J P Musters[1, *], Joost P G Sluijter[2, 3, *]

1. Department of Physiology, VU University Medical Center, Van der Boechorststraat 7, 1081 BT, Amsterdam, the Netherlands

2. Department of cardiology, Division of heart and lungs, Experimental Cardiology laboratory, University Medical Center Utrecht, P.O. Box 85500, 3508 GA, Utrecht, the Netherlands

3. ICIN, Netherlands Heart Institute, Catharijnesingel 52, 3511 GC Utrecht, the Netherlands
# These authors contributed equally to this paper

* Correspondence to J.Sluijter@umcutrecht.nl

In 2012, 17.5 million people died because of various cardiovascular diseases worldwide, which may increase to an estimated 23.6 million by 2030. In America, around 0.8 million people died of CVDs in 2011 which counts for 31.3% of total deaths[1]. In Europe, about 4 million people died from CVD in 2011[2], which makes cardiovascular diseases one of the leading causes of morbidity and mortality worldwide. The major risk factors currently associated with cardiovascular diseases such as high blood pressure, high blood cholesterol, tobacco smoking, unhealthy diet, physical inactivity, diabetes, and advanced aging will continuously increase these numbers, especially in developing countries, which will led to a steep increase in mortality rates by cardiovascular diseases[1]. This worldwide growing burden of cardiovascular diseases prompt to continuously search for new therapeutic possibilities which definitively demand a better understanding of the molecular mechanism underlying cardiovascular diseases.

microRNA basics

A novel molecular level of gene control was identified a decade ago called microRNAs(miRNAs). miRNAs are small regulatory non-coding RNA molecules, 19-22 nucleotides (nt) in length, which bind to the 3'-UTR region of the mRNAs and regulate mRNA expression via degradation or inhibition of their translation [3, 4]. miRNAs are transcribed in the nucleus by RNA Polymerase II, like mRNAs, and subsequently processed into a pre-miRNA by a combination of proteins including nuclear located endonuclease Pasha and Drosha[5]. After being transported out of the nucleus into the cytosol by ATP-consuming exportin-5 [6, 7], pre-miRNAs are further processed into mature miRNAs by RNA endonuclease Dicer [8, 9].This step is followed by the binding of the RNA induced silencing complex (RISC)[10], after which miRNAs are ready to fulfill their inhibitory roles.

The complexity of the action of miRNAs

miRNA-mRNA interactions

The action of miRNAs-targets interaction are surprisingly diverse. Although miRNAs are previously believed to regulate their targets solely by binding to the 3'-UTR region of the targeted mRNAs and thereby causing their degradation or inhibition of translation [11-13], recent observations suggest that they may bind to other region of targeted mRNAs as well, including mRNA coding regions, 5'-UTR, intron and even non-coding RNA targets [14-16]. While most of miRNAs bind to their target via a so called "seed sequence", thereby requiring 6-8 nt complementary to the targets in its 5' ends , some other miRNAs may bind to their target sequences complementary to a more centered region that is 10-12 nt in length [14]. Even within the seed region, mismatches are well tolerant [14-16]. These

---

[1] World Health Organization, 2015

characteristics for target binding makes it possible for one miRNA to have potentially many different targets [14-16], even having predictions over 200 different candidates, and thereby makes mechanistic understanding of their down-stream effects difficult. Although most of the miRNAs fulfill their function in the cytoplasm where mRNAs are transcribed, some miRNAs could be transport back to the nucleus after maturation in the cytosol, indicated that miRNAs may play a cis-acting regulatory role in the nucleus or may have RNA targets localized in the nucleus [17-19].

miRNA-targets interaction depends on the abundance of the miRNA itself and their targets, the complementarity to each other, and the accessibility to the targeted site for the miRNAs [13, 20-23]. Thus, factors that interfere with these can influence the interaction between miRNAs and their targets as well. For example, miRNAs sharing same targets can influence each other indirectly via competing endogeneous RNA species ceRNA including long non-coding RNAs, pseudogenes and circular RNAs or natural microRNA sponges [24]. When miRNA A expression goes up, the abundance of its targets (ceRNA, sponges) goes down. As a result, more free microRNA B is available for targeting other targets, a phenomena called endogenous competing. As many RNA binding proteins also bind to 3'-UTR regions of the mRNA, miRNA-target interaction can be affected by the binding of these RNA binding proteins. Whether it is competing or facilitating depends on the properties of the RNA binding protein. For examples, Dnd1 and huR can competitively replace microRNA silencing complexes [25, 26]. Some RNA binding can also regulate the microRNA-targets interactions by changing the secondary structure of the mRNA thereby affecting the accessibility of the targets. For instance, in quiescent cells both miR-221 and miR-222 and their targets p21 accumulate in the cell. Once stimulated with growth factors, Pum-1 is upregulated, phosphorylated and binds the 3'-UTR of p21 which induces structural changes of p21 mRNA. As a result, miR-221 and miR-222 gain access to the p21 3'-UTR, suppress p21, and eventually allow cells to undergo cell cycling [27].

Prediction based MicroRNA targets identification

To facilitate microRNA studies, many algorithms were developed based on the property of the microRNA-target interaction, the energy of their interaction, and/or conservation of the targets site between difference species, sometimes, experimental evidence is also taken into account [13, 28, 29].

Experimental validation of microRNA targets

Algorithm-predicted microRNA targets need to be validated experimentally [13]. One of most commonly used approach is a luciferase assay, in which the 3'-UTR region of a putative target is cloned between the stop codon and the polyA signal of the luciferase gene. After co-transfection of microRNA and scramble-control mimics and this reporter constructs, luciferase activity was measured and normalized by β-gal activity which do not carry this 3'-UTR sequence. To rule out the possibility of suppression of luciferase activity is not due to indirect effects, site specific mutagenesis within the

seed region of target sites can be introduced. A lot of microRNA targets were subsequently validated, however, this assay assumes that the structure of 3'-UTR will be the same as the endogenous structure and concentration of microRNA mimics used is physiological relevant. In fact, neither of these assumption is necessarily correct.

Other commonly used techniques for target validation at RNA and protein level are qPCR and Western Blotting. microRNAs inhibit its targets either via causing degradation of the targeted mRNA or inhibition of its translation. These techniques are very important and useful in microRNA target identification. However, besides some intrinsic problems with these method as discussed above, they are also time-consuming and usually it is not feasible to get a full picture of the microRNA and its targets.

Micro-arrays were the first approaches used to identify microRNA targets more generally. By transfecting human cells with miR-124, a brain enriched microRNA, or miR-1, a muscle specific microRNA, they identified over 100 genes shifted towards a brain and muscle phenotype, respectively[30]. Although promising, one of the potential drawbacks of this approach is its difficulty to distinguish if the change in transcription is direct or indirect related to the microRNA. This problem is partially solved by combining micro-array profiling with target prediction algorithms[31]. However, due to the fact that micro-array technology is a hybridization-based technology, it is almost impossible to use it for quantitative analysis. Another attempt to identify microRNA targets on a large scale, is RNA immunoprecipation. By pulling down RNA-induced silencing complex(RISC) after miR-210 overexpression, 31 predicted targets are identified[32]. Using AIN/GW182 protein immunoprecipitation approaches, Zhang. et al. systematic identified 1589 microRNA targets at different stages of *C. elegans* development[33]. Nonne et al. tried to improve this approach by introducing tandem affinity purification technology, in which mRNA/microRNA complexes are sequentially purified first via Ago moiety and then via biotin labeled microRNA mimic (TAP-tar)[34]. However, compared with the small microRNA, the influence of biotin modification on the miRNA-targets interaction is not neglectable. In order to identify microRNA targets in a cardiovascular context, we decided to modify these strategies and apply it in a "simple cell" system which is lacking most of the microRNAs due to loss of the microRNA biogenesis gene Dgcr8 (see chapter 3). In this system, we can introduce one microRNA of interested into a simple cell lacking most of the microRNAs and then pull-down the RISC complexes, containing the microRNA introduced and its targets.

MiRNAs in cardiovascular diseases

In the last decade, miRNAs have been investigated extensively. In mammalians, they are involved in many biological processes, if not all, including embryonic stem cell (ESC) pluripotency[35], cellular proliferation [36-42], driving and directing differentiation [43, 44], regulating apoptosis [45, 46], and aging [47-49]. The overall importance of miRNAs in the cardiovascular system was established by knocking out key miRNA processing components. For example, cardiac-specific knockout of Dicer leads to dilated cardiomyopathy, heart failure, and eventually lethality in mice [50]. These Dicer knock-out mice have deregulated cardiac contractile proteins and profound sarcomere disarray [50]. Similar to Dicer knock-out mice, postnatal inactivation of Pasha in the heart, leads to left ventricular malfunction, dilated cardiomyopathy, and lethality in adult mice [51]. The importance of miRNAs is not limited to cardiomyocytes, since specific knockout of Dicer or Pasha in smooth muscle cells (SMC) leads to reduced proliferation and impaired contractility [52, 53], and in endothelial cells (ECs) to impaired postnatal angiogenesis [54]. Furthermore, specific miRNAs were found to have pivotal roles in cardiovascular diseases as was explored extensively in different animal models as shown in Fig. 1. For example, Van Rooij *et al.* showed that inhibition of dysregulated miRNA-208 in pressure overloaded hearts preserved cardiac function and reduced mortality [55, 56]. In addition, when the heart is under stress, cardiomyocytes produce more "waste-products" which needs to be removed via autophagy [57]. Ucar A. et al showed that misregulated miR-132/212 in the pressure overloaded heart suppressed cardiomyocyte autophagy, which turned out to be detrimental to cardiac function. Pharmaceutical inhibition of miR-132/212 rescued autophagic responses and preserved cardiac function [58]. In another study, systemic inhibition of mir-92a enhanced vessel growth and functional recovery of damaged tissue in a mouse hind limb ischemia model and myocardial infarction [59]. Similar results were reported in a large animal study in which inhibition of mir-92a reduced infarct size and resulted in improved ejection fraction [60]. Due to limited space, we refer to table 1 and recent reviews for the role of several individual miRNAs [61-65].

The potential of miRNA therapeutics for cardiovascular diseases

miRNA gain-of-function

An advantage of miRNAs as potential therapeutic targets is their synergistic effects. miRNAs bind to their targets in a partial complementary manner and increasing evidence suggests that a single miRNA can target several genes within a similar signaling pathway [66, 67]. The effect of a miRNA on an individual mRNA target sometimes is low, but due to the simultaneous regulation of multiple targets within a pathway, the combined effect is more pronounced [67]. For example, miR-29 regulates the level of fibrosis through direct targeting of different collagens, fibrillins and elastins, which are all components of the extracellular matrix and collectively determine tissue stiffness, whereas each component individually is only partly inhibited [68]**.** Therefore, one advantage of using miRNA

mimics is the inhibitory effect they have on a selected pathway, by blocking several targets and leading to pronounced effects, both *in vitro* and *in vivo*.

Another advantage of using miRNA as a therapeutic target is their gain-of-function is easy to achieve by using miRNA mimics or viral approaches. Depending on the vendor, the synthesized structure of miRNA mimics varies, but they all have similar structures. The structure either resembles endogenous present pre-miRNAs with a stem-loop or consists of a double stranded RNA to help the mimic get incorporated into RISC complexes. Many of miRNA mimics were shown to be functional *in vitro* by numerous labs, including our own [37, 69-72]. miRNAs are relatively stable in the cell when compared to other RNA species with a half-life ranging from 28 hours to 5 days, which is about 10 times longer than mRNA molecules [73]. The long half-life of miRNAs indicates that potentially miRNA mimics may have long-lasting effects. As we discussed above, Eva van Rooij et al. was among the first that tried to overexpress miR-29 mimics by systematic injection of cholesterol-tagged microRNA mimics at a dose of 80mg/kg body weight and showed modest down-regulation of the miR-29 targeted genes, but accompanied by less fibrotic remodeling [68]. Only few *in vivo* applications of miR mimics can be found in literature, however, viral approaches, especially adeno-associated viruses (AAV) mediated miRNA gain of function, are more widely used [74, 75]. Due to its low immunogenicity, the transgene can remain active for months [74]. Eulalio, A. et al used AAV9, a cardiac tropism of AAV serotypes, to overexpress miR-590-3p and miR-199a-3p and induced a marked cardiac regeneration after myocardial infarction [74]. The long-lasting high level transgene expression make AAV virus an ideal tool for research, with potential future clinical applications.

miRNA inhibition

miRNAs can be inhibited by synthetic miRNA inhibitors *in vitro* as well as *in vivo [76]*. The synthesis of miRNA inhibitors is even easier compared to miRNA mimics as they are single stranded. Anti-miRs, widely used for *in vitro* studies, are chemically engineered single-stranded oligonucleotides completely complementary to the 20nt long targeted miRNAs. To facilitate entry into the cell, anti-miRs can be modified with cholesterol into a so called antagomiR [77]. Upon systemic intravenous injection, this cholesterol-tagged antagomiR could efficiently and specifically silence endogenous miRNAs throughout the body, except for the brain [77].

miRNA inhibitors do not require incorporation into the RISC complex to become functional but bind to endogenously present miRNAs and block their activities. This makes it possible to modify their structure and thereby improve resistance to nucleases and specificity by increasing their affinity to targeted miRNA. Several miRNA inhibitors were designed with different modifications on the 2' position of the sugar molecule [77, 78]. Among these,2'-O-Me, 2'-O-methoxyethyl (2'-MOE) and 2'-fluoro modification are the most commonly used [79-81]. Another type of modification, named locked nucleic acid (LNA) and using an O, 4'-C methylene bridge to lock the furanose ring in the sugar-

phosphate backbone, displayed enhanced affinity to their targeted miRNA [82-87]. In fact, LNA-miRNA binding affinity is so high that tiny LNA molecules, complementary to only the 7nt long seed sequence of a family of miRNAs, can effectively block the whole miRNA family [88]. The effect of a single injection can last several months and this long-lasting inhibition of endogenous miRNA targets probably originates from anti-miRs having a different structure than natural RNA species so that endogenous RNases cannot recognize them anymore.

The challenges of miRNA therapeutics for cardiovascular diseases

miRNA gain-of-function

The capacity to induce a long-lasting high level of transgene expression in combination with low production cost, makes the AAV an ideal tool for miRNA gain-of-function research [74, 75]. However, the safety of AAV in clinical applications is still under debate, and using viruses for gene therapy still carries a negative connotation from failures in the past. It has been reported that neutralization antibodies against AAV virus can be detected in healthy populations [89] and transgene products itself can induce cell-mediated and humoral responses [90]. Besides, a definitive cardiac specific serotype is not yet fully developed. For example, AAV9 is considered to be a cardiac tropism serotype [91-95], however, AAV9 transgenes are also expressed in other tissues such as liver, brain [90, 96, 97]. AAV-viruses are promising and further developments might very well make them an successful clinical tool, however, the negative public opinion regarding virus-based transgene delivery methods will most likely frustrate developments.

Even though miRNA mimics are powerful and widely used for *in vitro* studies, *in vivo* delivery of miRNA mimics is challenging. Synthetic miRNA mimics, as siRNAs, have a very short half-life in the blood [98]. As we mentioned previously, miRNA mimics have to be double stranded or need a stem-looped precursor structure so that they can be processed correctly and functionally incorporated into the RISC complex. This makes it difficult to modify their structure to improve their stability, like miRNA inhibitors, while maintaining their biological function. Interestingly, endogenously expressed miRNAs are stable in serum for 4-6 years when stored at -20°C, while other RNA species had been degraded [99].These 'circulating' miRNAs may form complexes with miRNA effector protein Ago2 [98] , high density lipoprotein HDL [100], or can be incorporated into microvesicles such as exosomes, microvesicular bodies, and apoptotic bodies, thereby protected from RNase degradation [98, 101]. Based on these observations, it might be possible to improve the stability of miRNA mimics in circulation by forming complexes with protective proteins, polymers, or loaded into vesicles before injecting them into the body.

miRNA inhibition

Different from miRNA mimics, miRNA inhibitors are already chemically modified RNA molecules, which may be recognized by our body as foreign materials and thereby induce inflammation as is observed for siRNAs[102]. It is well documented that foreign single or double stranded synthetic siRNAs can induce innate immune response through activation of Toll-like receptor (TLR) receptors [102, 103]. For instance, bacterial DNA or even mitochondrial DNA fragments can induce inflammation through TLR9 signaling upon myocardial infarction [104].

Although very useful, the high stability of miRNA therapeutics(antagomiRs, LNA) is a double-edged sword. As we mentioned previously, the effect of antagomiRs is very long-lasting compared to conventional pharmaceuticals. With a single injection of antagomiR at a dose of 80mg/kg, inhibition of endogenous miRNAs can still be observed over a month [58, 75], probably due to lack of nuclease that can recognize them in mammalian cells. This long-lasting systemic effects of antagomiR or LNA will increase the chance of potential side effects in healthy parts or other organs of the body.

General challenges for miRNA mimics and inhibitors

Besides these specific challenges for miRNA mimics or inhibitors, there are some common challenges for both of them. miRNA mimics and inhibitors are negatively charged. It is therefore difficult for them to leave the blood stream and enter the cell. Various delivery vehicles have been used to help them enter the cell such as liposomes and polymers, which significantly enhance cellular uptake and which will be discussed later in detail. However, 90% of the mimics are still trapped into endolysosomal vesicles and cannot escape into the cytosol of the cell [105]. Thus, agents which can disrupt the endolysosomal compartments and help them escape from endolysosome degradation or new delivery techniques are needed for further developments.

Lack of effective organ specific (e.g. cardiac-specific delivery methods) is another problem for both miRNA mimics and inhibitors. *In vivo* administration of miRNA mimics and inhibitors mainly rely on systemic injection, with related issues such as high costs, potential side effect and low efficacy. It costs up to 250 euro per mouse with a dose of 80mg/kg via systemic injection using antagomir[106]. Given the body weight of a human, it will cost more than half a million euro for a single treatment for humans. Even though lower dose (<10mg/Kg) repetitive injections [72] or using low dose LNAs [88] have been shown to be effective and cheaper, it will still cost around 100,000 euro for using them in human trials. The cost may be reduced in the future with the development of synthesis technology and more potent miRNA inhibitors. Another problem with systemic delivery of miRNA therapeutics is the potential side effects. First, one miRNA can have multiple targets, thus one miRNA may have different functions in different organs or cell types. For example, miR-214 has been shown to play an inhibitory role in angiogenesis [79, 107],however, this miRNA is also essential in regulating calcium homeostasis in cardiomyocytes [108]. Therefore, systemic inhibition of miR-214 may improve neovascularization in the heart, but it may also cause problems in myocardial calcium handling.

In summary, successful implementation of miRNA therapeutics relies on the strategies to improve the stability in the circulation, to reach high efficient and tissue/cell-specific delivery, to have effective cellular uptake and eventually to escape from endolysosomal compartments.

Overcoming challenges: lessons learned from siRNA delivery

Several of the previously mentioned challenges for using miRNA as therapeutic modalities, both mimics and inhibitors, also apply when using siRNA as a therapeutic molecule. siRNAs are double-stranded RNA-molecules, 21-23 nucleotides in length, that can be synthetically produced. After cytosolic delivery they are incorporated into the RISC complex like miRNAs. siRNAs have a completely complementary sequence to its target mRNA and binding of the siRNA-RISC complex to their targets results in mRNA degradation [109]. Like miRNA mimics, siRNAs have similar problems, like being susceptible for degradation in the blood, not leaving the blood vessels readily, and not readily being taken up by cells. To overcome these challenges several siRNA delivery vehicles, like liposomal delivery vehicles, polymeric delivery vehicles and ultrasound microbubbles, have been studied. In order to overcome these challenges for miRNA-based treatment, we can learn important lessons from these siRNA delivery vehicles. An overview of these commonly used delivery vehicles is provided in Table 2.

Liposomal delivery vehicles

Liposomes are the most-studied and oldest delivery vehicle for siRNA, as was recently reviewed by Buyens et al. [110]. In circulation, it has been extensively shown that liposomes protect the siRNA from RNase degradation and remain stable in blood [110, 111]. Additionally, Elbashir et al. showed that cationic liposomes could induce cellular uptake of siRNA in cell culture through endocytosis, overcoming the challenge of low uptake of naked siRNAs by cells [112]. Subsequently, cationic liposomes have been used to successfully treat liver metastasis in mice by increasing apoptosis via targeting the bcl-2 oncogene in cancer cells [113]. Specific delivery of siRNA for CD31 to endothelial cells, inhibited angiogenesis and decreased tumor growth [114], thereby demonstrating that liposomes not only facilitate cellular uptake, but also help in the exit of siRNAs from blood vessels into the tissue and become biologically active *in vivo* at several doses of 1-4 mg/kg body weight. However, after intravenous (*i.v.*) injection, siRNA loaded liposomes tend to end up in the liver, kidney, lung, tumors, spleen and bone [111, 115, 116],but not in the heart. Hereby liposomes can solve major challenges for miRNA, antimiR and siRNA delivery, including stability, cellular uptake and targeting of blood vessels or specific organs, but still there is a need to increase delivery to the myocardium for cardiac applications in order to improve therapeutic effectsand avoid off-target side-effects.

Polymeric delivery vehicles

Another strategy to overcome the challenges is the use of polymers, which have been used with mixed successes [109, 117, 118]. There are many polymers that have been used to improve siRNA delivery, and most commonly used are polyethylenimine (PEI), chitosan, poly(lactic-*co*-glycolic acid) (PLGA), poly-l-lysine (PLL) and dendrimers. These polymers mostly rely on their cationic charge to bind siRNA and subsequently protect the siRNA from degradation in the blood. Additionally, a cationic charge also induces endocytosis, thereby increasing cellular uptake of the delivery vehicle. PEI was found to protect siRNA from RNase degradation in circulation and after i.v. injection, siRNA ended up in tumors, liver, spleen, lung, kidney and to a low extent to the heart of mice [119].Upon i.v. treatment with a specific PEI-siRNA complex against vascular endothelial growth factor receptor-2, this decreased tumor growth [119].Similarly, chitosan was found to protect siRNA from degradation for at least 7 h, whereas naked siRNAs are degraded within minutes upon systemic injection[120]. In addition, after i.v.injection of siRNA carrying chitosan in mice, the siRNA could be found in the brain, liver, lungs, kidney, spleen, to a very low degree in the heart and abundantly in tumors[121]. These delivered siRNAs for POSTN, FAK or PLXDC1 were subsequently capable of reducing tumor size in mice [121].

Another polymer, PLGA, has been studied as siRNA delivery vehicle because it is FDA-approved and provides a slow release of siRNA due to hydrolysis of PLGA [122], thereby making therapeutic effects last longer. However, PLGA is not cationic and is not readily taken up by cells which makes loading PLGA with siRNA more difficult and additional functionalities to improve cellular uptake have to be added [123]. If these additional functionalities are used, the resulting composite polymer is capable of protecting siRNA from degradation, enabling exit of siRNA out of the blood stream into tissue and subsequently inhibiting tumor growth [123]. Cardiac accumulation of these particles, however, was not reported and besides providing protection from degradation, the challenges for siRNA delivery where not necessarily overcome by the characteristics of PLGA, but rather by adding other polymers or moieties.

PLL has been shown to deliver siRNA for luciferase into cells, knocking down protein expression up to 80% *in vitro* [124]. However, when trying to translate the use of PLL to *in vivo* models, several issues were encountered like blood instability [125] and severe toxicity [124]. Additionally, PLL-siRNA delivery vehicles mainly accumulate in the liver, spleen and tumors [126].

Dendrimers are branching polymers and chemically challenging to produce [127]. For siRNA and oligonucleotide delivery, polypropylenimine (PPI) or Poly(amido amine) (PAMAM) have received most interest because of their cationic nature [127]. Dendrimers have proven to be able to cross cell membranes and deliver siRNA intracellularly [128]. However, low dendrimer-siRNA stability in the blood has been reported [129]. After i.v. injection, dendrimers are capable of transferring siRNA out of the blood stream after which they accumulate in the liver, kidney and spleen [128] or in tumors after

the addition of tumor targeting functionalities like a synthetic analog of luteinizing hormone-releasing hormone [128], but no studies have reported specific uptake and use for the heart.

Several challenges have been conquered by using polymers to deliver siRNA *in vivo*. This resulted in successful therapeutic effects in laboratory animals at several doses of siRNA, ranging from 1-3 mg/kg body weight, whereas antagomiRs are administered at 20-80 mg/kg body weight. By using polymers like chitosan, PEI and PLGA it is possible to provide protection against degradation in the blood, transfer the siRNA out of the blood stream and into cells to facilitate mRNA degradation. An overview of the characteristics of discussed polymers is given in Table 2. However, these siRNA-polymers mostly end up in the liver, spleen, kidneys and tumors, and not in other organs like the heart, introducing the additional challenge of specifically targeting these delivery vehicles to the myocardium.

Cardiovascular application of liposomal and polymeric delivery devices

As previously mentioned, liposomal and polymeric delivery vehicles for siRNA naturally accumulate in tumors, liver or spleen, and not in the vasculature and heart. Due to this biodistribution, targeting the cardiovascular system with synthetic delivery vehicles is quite difficult. On top of that, the heart muscle is a difficult organ to transfect, and it is even believed that direct injection of naked nucleotides results in higher cardiac uptake then nucleotides combined with a delivery vehicle [130]. It has been hypothesized that the cationic nature of delivery vehicles caused them to get attached to the densely packed anionic extracellular matrix of the heart [131]. Even so, several approaches have been used to target the cardiovascular system using siRNA delivery vehicles.

To circumvent issues with biodistribution, delivery vehicles can be directly injected into the myocardium [131-133] (Figure 2: delivery route 1). Kim et al. used a PEI-based delivery vehicle to deliver siRNA against Src homology domain 2 (SH2)-containing tyrosine phosphatase-1 (SHP-1) to the myocardium of rats in an ischemia-reperfusion model, resulting in a successful knockdown of SHP-1, and thereby reducing apoptotic cell death and subsequently leading to a 50% reduction in infarction size [131]. Alternatively, Somasuntharam et al. used pH-sensitive nanoparticles for intramyocardial siRNA delivery in a mouse model with a permanent ligation in the left anterior descending coronary. As a result of Nox2 knock-down, fractional shortening of the heart improved to non-infarcted myocardial levels [133]. Additionally, direct injection of liposomes carrying miR-590 and miR-199 in heart of neonatal rats successfully increased cardiomyocyte proliferation within 3 days [74].

Even though biodistribution of cationic liposomes after i.v. injection does not favor the heart, the i.v. approach to achieve cardiac effects has been reported (Figure 2: delivery route 2). For instance, Santel et al. successfully knocked down CD31 mRNA levels by 40% in the heart after i.v. injection of liposomes loaded with siRNA in mice [134], CD31 is an endothelial cell specific marker and was used

in this study to prove endothelial targeting of the delivery vehicle. Betigeri et al. furthermore used i.v. injection of liposomes, loaded with siRNA against c-Jun N-terminal kinase-1 (JNK1), to decrease apoptosis in the heart of mice during hypoxia, knocking down JNK1 by 80% and significantly reducing apoptosis [135]. Both studies mention, however, that uptake of liposomes in organs other than the heart is much higher [134, 135].

Another approach to affect the cardiovascular system is by indirect targeting via organs which are easier to transfect, like the liver [136, 137] or spleen [138, 139], which naturally show high accumulation of delivery vehicles (Figure 2: delivery routes 3 and 4). In the liver, both PEI-based delivery vehicles and liposomes were successfully used to knockdown ApoB, resulting in a reduction in serum cholesterol levels and thereby preventing atherosclerosis [136, 137]. In another approach siRNA against C-C chemokine receptor type 2 (CCR2) was intravenously injected after complexion with cationic liposomes. These liposomes accumulated in the spleen and transfected monocytes, macrophages and neutrophils, leading to less responsiveness of these cells to macrophage chemo-attractant protein 1 (MCP-1), a chemo-attractant which is released from the infarcted heart. As a result, monocyte numbers were reduced by 70% in infarcted hearts which led to a 34% reduction in infarct size (Figure 2: delivery route 5) [139]. In a follow up study, the same group found that the reduction in infarct size also leads to increased left ventricular ejection fraction [138]. This approach was also used to decrease the number of macrophages and monocytes in atherosclerotic plaques, leading to a 82% reduction of macrophages/monocytes in the plaque [139].

The main issue in treating the heart with siRNA remains the low accumulation of delivery vehicles and siRNA. While liposomal-siRNA formulations have entered the clinical arena for treatment of cancer [140] and the liver [141], the heart still lags behind, creating a need for improved cardiac homing of siRNA delivery vehicles. Interestingly, promising alternative methods are being developed to treat myocardial infarction or atherosclerosis by targeting organs like the liver or spleen with subsequent effects on the heart, although these are still in an early preclinical phase and mostly rely on a reduction in total cholesterol levels or modulating the immune responses.

Microbubbles

Microbubbles (MB) are micrometer-diameter gas-filled spheres with a flexible shell which can be modified in order to bind nucleic acids like DNA or siRNA [142-144]. The characteristic that makes MB really interesting as a drug delivery vehicle, is their ultrasound (US) responsiveness. Having a core of gas, MB react to US pressure waves. During the peak positive pressure phase the gas-filled MB will be compressed and during the peak negative phase the MB will expand, causing the MB to oscillate on the US wave. Increasing the peak-to-peak pressure of the US-wave to a certain point causes the MB to collapse, thereby releasing its therapeutic payload and permeabilizing cells [145, 146] and blood vessels [147]. This results in an increased local delivery and uptake of therapeutic

payload if US is applied locally [148]. The MB has been used for the local delivery of liposomes, nanoparticles, plasmid DNA (pDNA) and also siRNA [149].

MB have been found to protect siRNA from RNase degradation in circulation and for transferring themout of the blood vessel into cells in tumor tissue, subsequently slowing down tumor growth [142]. Similarly, Un et al. used MB to deliver siRNA against ICAM-1 to the liver and successfully delivered siRNA in endothelial cells, Kupffer cells and hepatocytes, thereby providing protection against ischemia-reperfusion damage in the liver [150]. MB are therefore capable of protecting siRNA, enable siRNA to exit the blood stream, and induce the entry of siRNA into cells.

Furthermore, the capability to use a physical force to induce local delivery makes the MB suitable to target tissues in which delivery vehicles do not naturally accumulate, and MB+US was thereby used to deliver siRNA or oligonucleotides to the heart [151, 152]. In 2005, Tsunoda et al. successfully delivered siRNA against GFP in GFP transgenic mice. They found that delivery was confined to the endothelial cells in the heart [151] and was not observed in cardiomyocytes, in contrast to delivery of pDNA, which did enter cardiomyocytes as well as endothelial cells after MB+US treatment [151]. Alter et al., showed that also single stranded oligonucleotides could be delivered locally to the heart, inducing the transcription of dystrophin in cardiomyocytes [152]. Both studies showed successful delivery of small oligoncleotides to compartments of the heart while retaining biological activity without off-target effects in other organs. Where Tsunoda et al. only found tissue penetration to endothelial cells by using double stranded siRNA, Alter et al. observed tissue penetration reaching the cardiomyocytes by using single stranded oligonucleotides, an interesting difference between these RNA analogues.

MB+US induced local delivery techniques look promising for local miRNA delivery in cardiovascular approaches. Small RNA molecules are only delivered to organs where US is applied andtherefore also the heart can be reached, in contrast to the other discussed synthetic delivery vehicles. Penetration of siRNA into tissue, however, only extends to endothelial cells. For miRNA mimics, similar results can be expected as these molecules are double stranded as well. For antimiR molecules, being single-stranded, affecting both endothelial cells and cardiomyocytes seems feasible. Although promising, MB+US induced delivery of siRNA is still rather complex and many factors are known to influence the success of local delivery, including MB type [152], US intensity [153], US frequency [154], US pulsing [149], and MB dose [152]. Furthermore, cavitating MB can cause stress to blood vessels and cells [143]. However, when all these factors are well adjusted, MB+US induced delivery of miRNA mimics is a very promising technique for treatment in cardiovascular disease, including the myocardium.

Improving cardiac delivery

Strategies to improve homing of delivery vehicles to the heart include the use of antibodies, endothelial cell or cardiac targeting peptides (CTPs), or pH sensitive targeting moieties. These cardiac targeting agents take advantage of distinct properties of cardiac tissue, such as cardiac specific cell surface markers which can be recognized by antibodies or targeting peptides. Ko et al. modified liposomes with a cell-penetrating peptide TATp for increased cellular uptake and an anti-myosin antibody for cardiac targeting. This approach resulted in increased accumulation of DNA-liposome complexes in the ischemic myocardium [155]. Another well studied targeting peptide is RGD that specifically binds to integrin αvβ3 and αvβ5, which is enriched on the endothelial cells surface. This RGD peptide has been used for targeted delivery of siRNA to endothelial cells in combination with delivery vehicles such as chitosan nanoparticles [121], PEI [156] and liposomes [157]. Using another approach, Sosunov, E. A. et al reported that a low pH sensitive insertion peptide accumulates only in the ischemic myocardium but not the healthy regions, as the pH in the ischemic myocardium is lower [158]. These strategies improve cardiac homing but have not been used in combination with siRNA or miRNA therapeutics yet. It will be interesting to see how these promising targeting strategies, by themselves or as a combination, improve cardiac homing of delivery vehicles for siRNA and miRNA therapeutics.

Improving endosomal release and cytosolic delivery of miRNA therapeutics

Cellular entry of siRNA or miRNA therapeutics using delivery vehicles is usually endocytosis mediated, thus resulting in endolysosomal localization. The last challenge for small RNA therapeutic delivery after its entry into cells is their release from its carriers and escape from the endolysosomal compartment. To this end, fusogenic peptides have been used to facilitate endo-lysosomal escape and improve cytosolic delivery of therapeutic molecules after internalization of drug delivery vehicles [159]. Hatakeyama et al. showed that introduction of pH-responsive fusogenic GALA peptide into a drug delivery vehicle improved gene silencing due to more efficient endosomal escape [160, 161]. By combining fusogenic peptides and cell penetrating peptides, even more efficient knockdown has been achieved [162, 163]. Many protein/peptides like GALA have been identified and can enhance endosomal release, which can be considered for incorporation in the miRNA therapeutics delivery complex [164].

Future perspectives

miRNAs have been shown to play important roles in many different aspects of cardiovascular diseases. Some properties that make the miRNA an excellent therapeutic target are the ability to influence whole cellular processes instead of a single gene, the easy manipulation of miRNA acitivity

in vivo using miRNA inhibitors, the high intracellular stability of miRNA therapeutics, and their involvement in regenerative processes in cardiovascular disease. Actually, the first successful phase 2 clinical trial with antimiR-122 [165], a hepatitis C targeting antimiR, has been carried out and will definitely encourage the introduction of more miRNA therapeutics towards clinical practice, also for the cardiovascular field.

However, the intrinsic nature of miRNAs targeting multiple target mRNAs can achieve synergistic effects but may also cause un-expected off-target side effects since no organ or tissue selectivity is achieved, especially the heart is difficult to reach. Moreover, *in vivo* delivery of miRNA mimicking molecules to enhance miRNA function is limited and mainly achieved by viral overexpression. There is therefore a persistent need for methods to increase miRNA therapeutic delivery, prevent off-target uptake and increase tissue-specific uptake.

Recent developments in drug delivery vehicles for siRNA have resulted in successful protection of siRNA in the blood, successful exit from the circulation, and intracellular delivery of siRNA and important lessons can be learned from these siRNA delivery methods. Three important challenges have been conquered using liposomal and polymeric delivery vehicles. However, the big issue remains that these delivery vehicles end up in tumors, spleen, liver and lungs, not readily in the heart. For cardiac application, one would need high systemic doses of siRNA to reach therapeutic levels in the myocardium, resulting in large off-target effects and low therapeutic benefit. Strategies to circumvent this problem include local injection or indirectly treating the heart by targeting other organs with known effects on the heart. However, local injections are invasive and targeting the immune system is not cardiac specific and can result in major side-effects. An alternative approach is the use of MB and US, which are known to have low off-target effects. However, cardiac delivery of siRNA by MB has not been studied extensively and data so far points towards the direction of low tissue penetration of siRNA. For cardiac application of siRNA (or miRNA) therapy, cardiac targeting remains an issue. However, several strategies to improve cardiac uptake and targeting of delivery vehicles are being developed and encouraging results are being obtained with antibodies, cardiac targeting peptides, and pH sensitive targeting peptides (for an overview see Figure 3). These results, however, still need to be translated to delivery vehicles for miRNA therapeutics. A growing body of knowledge is available but needs to be combined with experimental and translational efforts to open-up successful delivery for miRNAs, at this point the most potent therapeutic small RNA available.

Scope of this thesis

The aim of this thesis was to identify novel miRNA targets that are involved in cardiovascular diseases and explore the feasibility of using specific miRNA therapeutics for interventions. To search for novel miRNA targets, we have applied state of art technology to identify dynamic regulated microRNAs in cardiovascular disease models (Chapter 4). To understand the biological role of these microRNAs, we used various techniques including a multicolor microRNA *in situ* hybridization technique (Chapter 2), a microRNA-free Simple cell system for targets identification and individual microRNA functional studies (Chapter 3), and use of transgenic knockout mice models to study the mechanistic role of microRNAs (Chapter 4, 5, 6 and 7). Our studies show that one microRNA can play different roles under different tissue or cellular context, for instance, increased miR-132/212 level is needed to promote arteriogenesis during ischemia (Chapter 4) while sustained upregulated miR-132/212 levels in the stressed heart could also impair cardiac contractility (Chapter 6). These observations suggest that targeted tissue or organ-specific delivery might be essential for microRNA based interventions. Moreover, this may explain why miR-132/212 knockout mice show no advantage long-term functional benefits over their wild-type litter mates after myocardial infarction (Chapter 7). To further explore the possibility of targeted delivery, we designed and tested new delivery systems, including ultrasound-exposed microbubbles and nanopolymers for targeted delivery of microRNA therapeutics in the cardiovascular system (Chapter 8 and 9).

References

1. Go, A.S., et al., Heart disease and stroke statistics--2014 update: a report from the American Heart Association. Circulation, 2014. **129**(3): p. e28.
2. Nichols, M., et al., Cardiovascular disease in Europe 2014: epidemiological update. European heart journal, 2014: p. ehu299.
3. Guo, H., et al., Mammalian microRNAs predominantly act to decrease target mRNA levels. Nature, 2010. **466**(7308): p. 835-40.
4. Baek, D., et al., The impact of microRNAs on protein output. Nature, 2008. **455**(7209): p. 64-71.
5. Tomari, Y. and P.D. Zamore, MicroRNA biogenesis: drosha can't cut it without a partner. Curr Biol, 2005. **15**(2): p. R61-4.
6. Yi, R., et al., Exportin-5 mediates the nuclear export of pre-microRNAs and short hairpin RNAs. Genes Dev, 2003. **17**(24): p. 3011-6.
7. Bohnsack, M.T., K. Czaplinski, and D. Gorlich, Exportin 5 is a RanGTP-dependent dsRNA-binding protein that mediates nuclear export of pre-miRNAs. RNA, 2004. **10**(2): p. 185-91.
8. Jiang, F., et al., Dicer-1 and R3D1-L catalyze microRNA maturation in Drosophila. Genes Dev, 2005. **19**(14): p. 1674-9.
9. Chendrimada, T.P., et al., TRBP recruits the Dicer complex to Ago2 for microRNA processing and gene silencing. Nature, 2005. **436**(7051): p. 740-4.
10. Forstemann, K., et al., Drosophila microRNAs are sorted into functionally distinct argonaute complexes after production by dicer-1. Cell, 2007. **130**(2): p. 287-97.
11. Zheng, W., et al., Identification of microRNA target genes in vivo. Mol Biotechnol, 2011. **47**(3): p. 200-4.
12. Chi, S.W., G.J. Hannon, and R.B. Darnell, An alternative mode of microRNA target recognition. Nat Struct Mol Biol, 2012. **19**(3): p. 321-7.
13. Ritchie, W., J.E. Rasko, and S. Flamant, MicroRNA target prediction and validation. Adv Exp Med Biol, 2013. **774**: p. 39-53.
14. Helwak, A., et al., Mapping the human miRNA interactome by CLASH reveals frequent noncanonical binding. Cell, 2013. **153**(3): p. 654-65.
15. Chi, S.W., et al., Argonaute HITS-CLIP decodes microRNA-mRNA interaction maps. Nature, 2009. **460**(7254): p. 479-86.
16. Haecker, I., et al., Ago HITS-CLIP expands understanding of Kaposi's sarcoma-associated herpesvirus miRNA function in primary effusion lymphomas. PLoS Pathog, 2012. **8**(8): p. e1002884.
17. Hwang, H.W., E.A. Wentzel, and J.T. Mendell, A hexanucleotide element directs microRNA nuclear import. Science, 2007. **315**(5808): p. 97-100.
18. Jeffries, C.D., H.M. Fried, and D.O. Perkins, Nuclear and cytoplasmic localization of neural stem cell microRNAs. RNA, 2011. **17**(4): p. 675-86.
19. Liang, H., et al., Nuclear microRNAs and their unconventional role in regulating non-coding RNAs. Protein Cell, 2013. **4**(5): p. 325-30.
20. Heikham, R. and R. Shankar, Flanking region sequence information to refine microRNA target predictions. J Biosci, 2010. **35**(1): p. 105-18.
21. Liu, H., et al., Improving performance of mammalian microRNA target prediction. BMC Bioinformatics, 2010. **11**: p. 476.
22. Marin, R.M. and J. Vanicek, Efficient use of accessibility in microRNA target prediction. Nucleic Acids Res, 2011. **39**(1): p. 19-29.
23. Witkos, T.M., E. Koscianska, and W.J. Krzyzosiak, Practical Aspects of microRNA Target Prediction. Curr Mol Med, 2011. **11**(2): p. 93-109.
24. Tay, Y., J. Rinn, and P.P. Pandolfi, The multilayered complexity of ceRNA crosstalk and competition. Nature, 2014. **505**(7483): p. 344-352.
25. Kedde, M., et al., RNA-binding protein Dnd1 inhibits microRNA access to target mRNA. Cell, 2007. **131**(7): p. 1273-86.

26. Epis, M.R., et al., The RNA-binding protein HuR opposes the repression of ERBB-2 gene expression by microRNA miR-331-3p in prostate cancer cells. J Biol Chem, 2011. **286**(48): p. 41442-54.

27. Kedde, M., et al., A Pumilio-induced RNA structure switch in p27-3' UTR controls miR-221 and miR-222 accessibility. Nat Cell Biol, 2010. **12**(10): p. 1014-20.

28. Ritchie, W. and J.E. Rasko, Integrated miRNA expression analysis and target prediction. Methods Mol Biol, 2012. **822**: p. 289-93.

29. Lewis, B.P., C.B. Burge, and D.P. Bartel, Conserved seed pairing, often flanked by adenosines, indicates that thousands of human genes are microRNA targets. Cell, 2005. **120**(1): p. 15-20.

30. Lim, L.P., et al., Microarray analysis shows that some microRNAs downregulate large numbers of target mRNAs. Nature, 2005. **433**(7027): p. 769-73.

31. Wang, X. and X. Wang, Systematic identification of microRNA functions by combining target prediction and expression profiling. Nucleic Acids Res, 2006. **34**(5): p. 1646-52.

32. Fasanaro, P., et al., An integrated approach for experimental target identification of hypoxia-induced miR-210. J Biol Chem, 2009. **284**(50): p. 35134-43.

33. Zhang, L., et al., Systematic analysis of dynamic miRNA-target interactions during C. elegans development. Development, 2009. **136**(18): p. 3043-55.

34. Nonne, N., et al., Tandem affinity purification of miRNA target mRNAs (TAP-Tar). Nucleic Acids Res, 2010. **38**(4): p. e20.

35. Heinrich, E.M. and S. Dimmeler, MicroRNAs and stem cells: control of pluripotency, reprogramming, and lineage commitment. Circ Res, 2012. **110**(7): p. 1014-22.

36. Jin, C., et al., MicroRNA-21 mediates the rapamycin-induced suppression of endothelial proliferation and migration. FEBS Lett, 2013. **587**(4): p. 378-85.

37. Sluijter, J.P., et al., MicroRNA-1 and -499 regulate differentiation and proliferation in human-derived cardiomyocyte progenitor cells. Arterioscler Thromb Vasc Biol, 2010. **30**(4): p. 859-68.

38. Wu, W.H., et al., MicroRNA-130a mediates proliferation of vascular smooth muscle cells in hypertension. Am J Hypertens, 2011. **24**(10): p. 1087-93.

39. Chen, J.F., et al., The role of microRNA-1 and microRNA-133 in skeletal muscle proliferation and differentiation. Nat Genet, 2006. **38**(2): p. 228-33.

40. Choe, N., et al., The microRNA miR-132 targets Lrrfip1 to block vascular smooth muscle cell proliferation and neointimal hyperplasia. Atherosclerosis, 2013. **229**(2): p. 348-55.

41. Chen, J., et al., mir-17-92 cluster is required for and sufficient to induce cardiomyocyte proliferation in postnatal and adult hearts. Circ Res, 2013. **112**(12): p. 1557-66.

42. Porrello, E.R., et al., Regulation of neonatal and adult mammalian heart regeneration by the miR-15 family. Proc Natl Acad Sci U S A, 2013. **110**(1): p. 187-92.

43. Marson, A., et al., Connecting microRNA genes to the core transcriptional regulatory circuitry of embryonic stem cells. Cell, 2008. **134**(3): p. 521-33.

44. Ohtani, K. and S. Dimmeler, Control of cardiovascular differentiation by microRNAs. Basic Res Cardiol, 2011. **106**(1): p. 5-11.

45. Subramanian, S. and C.J. Steer, MicroRNAs as gatekeepers of apoptosis. J Cell Physiol, 2010. **223**(2): p. 289-98.

46. Li, P., MicroRNAs in cardiac apoptosis. J Cardiovasc Transl Res, 2010. **3**(3): p. 219-24.

47. Smith-Vikos, T. and F.J. Slack, MicroRNAs and their roles in aging. J Cell Sci, 2012. **125**(Pt 1): p. 7-17.

48. Jansen, F., et al., Role, Function and Therapeutic Potential of MicroRNAs in Vascular Aging. Curr Vasc Pharmacol, 2013.

49. Boon, R.A., et al., MicroRNA-34a regulates cardiac ageing and function. Nature, 2013. **495**(7439): p. 107-10.

50. Chen, J.F., et al., Targeted deletion of Dicer in the heart leads to dilated cardiomyopathy and heart failure. Proc Natl Acad Sci U S A, 2008. **105**(6): p. 2111-6.

51. Rao, P.K., et al., Loss of cardiac microRNA-mediated regulation leads to dilated cardiomyopathy and heart failure. Circ Res, 2009. **105**(6): p. 585-94.

52. Albinsson, S., et al., MicroRNAs are necessary for vascular smooth muscle growth, differentiation, and function. Arterioscler Thromb Vasc Biol, 2010. **30**(6): p. 1118-26.
53. Chen, Z., et al., DiGeorge syndrome critical region 8 (DGCR8) protein-mediated microRNA biogenesis is essential for vascular smooth muscle cell development in mice. J Biol Chem, 2012. **287**(23): p. 19018-28.
54. Suarez, Y., et al., Dicer-dependent endothelial microRNAs are necessary for postnatal angiogenesis. Proc Natl Acad Sci U S A, 2008. **105**(37): p. 14082-7.
55. Callis, T.E., et al., MicroRNA-208a is a regulator of cardiac hypertrophy and conduction in mice. J Clin Invest, 2009. **119**(9): p. 2772-86.
56. Montgomery, R.L., et al., Therapeutic inhibition of miR-208a improves cardiac function and survival during heart failure. Circulation, 2011. **124**(14): p. 1537-47.
57. Gatica, D., et al., Molecular mechanisms of autophagy in the cardiovascular system. Circulation research, 2015. **116**(3): p. 456-467.
58. Ucar, A., et al., The miRNA-212/132 family regulates both cardiac hypertrophy and cardiomyocyte autophagy. Nat Commun, 2012. **3**: p. 1078.
59. Bonauer, A., et al., MicroRNA-92a controls angiogenesis and functional recovery of ischemic tissues in mice. Science, 2009. **324**(5935): p. 1710-3.
60. Hinkel, R., et al., Inhibition of MicroRNA-92a Protects Against Ischemia-Reperfusion Injury in a Large Animal Model. Circulation, 2013.
61. Small, E.M., R.J. Frost, and E.N. Olson, MicroRNAs add a new dimension to cardiovascular disease. Circulation, 2010. **121**(8): p. 1022-32.
62. van Rooij, E. and E.N. Olson, MicroRNA therapeutics for cardiovascular disease: opportunities and obstacles. Nat Rev Drug Discov, 2012. **11**(11): p. 860-72.
63. Ono, K., Y. Kuwabara, and J. Han, MicroRNAs and cardiovascular diseases. FEBS J, 2011. **278**(10): p. 1619-33.
64. Lorenzen, J.M., S. Batkai, and T. Thum, Regulation of cardiac and renal ischemia-reperfusion injury by microRNAs. Free Radic Biol Med, 2013.
65. Sluijter, J.P., MicroRNAs in Cardiovascular Regenerative Medicine: Directing Tissue Repair and Cellular Differentiation. ISRN Vascular Medicine, 2013. **2013**.
66. Backes, C., et al., A dictionary on microRNAs and their putative target pathways. Nucleic Acids Res, 2010. **38**(13): p. 4476-86.
67. Cloonan, N., et al., MicroRNAs and their isomiRs function cooperatively to target common biological pathways. Genome Biol, 2011. **12**(12): p. R126.
68. van Rooij, E., et al., Dysregulation of microRNAs after myocardial infarction reveals a role of miR-29 in cardiac fibrosis. Proc Natl Acad Sci U S A, 2008. **105**(35): p. 13027-32.
69. Xiao, J., et al., MicroRNA-204 is required for differentiation of human-derived cardiomyocyte progenitor cells. J Mol Cell Cardiol, 2012. **53**(6): p. 751-9.
70. van Mil, A., et al., microRNA-1 enhances the angiogenic differentiation of human cardiomyocyte progenitor cells. J Mol Med (Berl), 2013. **91**(8): p. 1001-12.
71. Liu, J., et al., MicroRNA-155 prevents necrotic cell death in human cardiomyocyte progenitor cells via targeting RIP1. J Cell Mol Med, 2011. **15**(7): p. 1474-82.
72. Grundmann, S., et al., MicroRNA-100 regulates neovascularization by suppression of mammalian target of rapamycin in endothelial and vascular smooth muscle cells. Circulation, 2011. **123**(9): p. 999-1009.
73. Gantier, M.P., et al., Analysis of microRNA turnover in mammalian cells following Dicer1 ablation. Nucleic Acids Res, 2011. **39**(13): p. 5692-703.
74. Eulalio, A., et al., Functional screening identifies miRNAs inducing cardiac regeneration. Nature, 2012. **492**(7429): p. 376-81.
75. Dirkx, E., et al., Nfat and miR-25 cooperate to reactivate the transcription factor Hand2 in heart failure. Nat Cell Biol, 2013. **15**(11): p. 1282-93.
76. van Mil, A., P.A. Doevendans, and J.P. Sluijter, The potential of modulating small RNA activity in vivo. Mini Rev Med Chem, 2009. **9**(2): p. 235-48.
77. Krutzfeldt, J., et al., Silencing of microRNAs in vivo with 'antagomirs'. Nature, 2005. **438**(7068): p. 685-9.

78.   Krutzfeldt, J., et al., Specificity, duplex degradation and subcellular localization of antagomirs. Nucleic Acids Res, 2007. **35**(9): p. 2885-92.

79.   van Mil, A., et al., MicroRNA-214 inhibits angiogenesis by targeting Quaking and reducing angiogenic growth factor release. Cardiovasc Res, 2012. **93**(4): p. 655-65.

80.   Meister, G., et al., Sequence-specific inhibition of microRNA- and siRNA-induced RNA silencing. RNA, 2004. **10**(3): p. 544-50.

81.   Hutvagner, G., et al., Sequence-specific inhibition of small RNA function. PLoS Biol, 2004. **2**(4): p. E98.

82.   Fabani, M.M. and M.J. Gait, miR-122 targeting with LNA/2'-O-methyl oligonucleotide mixmers, peptide nucleic acids (PNA), and PNA-peptide conjugates. RNA, 2008. **14**(2): p. 336-46.

83.   Elmen, J., et al., LNA-mediated microRNA silencing in non-human primates. Nature, 2008. **452**(7189): p. 896-9.

84.   Varallyay, E., J. Burgyan, and Z. Havelda, Detection of microRNAs by Northern blot analyses using LNA probes. Methods, 2007. **43**(2): p. 140-5.

85.   Orom, U.A., S. Kauppinen, and A.H. Lund, LNA-modified oligonucleotides mediate specific inhibition of microRNA function. Gene, 2006. **372**: p. 137-41.

86.   Naguibneva, I., et al., An LNA-based loss-of-function assay for micro-RNAs. Biomed Pharmacother, 2006. **60**(9): p. 633-8.

87.   Kloosterman, W.P., et al., In situ detection of miRNAs in animal embryos using LNA-modified oligonucleotide probes. Nat Methods, 2006. **3**(1): p. 27-9.

88.   Hullinger, T.G., et al., Inhibition of miR-15 protects against cardiac ischemic injury. Circ Res, 2012. **110**(1): p. 71-81.

89.   Boutin, S., et al., Prevalence of serum IgG and neutralizing factors against adeno-associated virus (AAV) types 1, 2, 5, 6, 8, and 9 in the healthy population: implications for gene therapy using AAV vectors. Hum Gene Ther, 2010. **21**(6): p. 704-12.

90.   Ciesielska, A., et al., Cerebral infusion of AAV9 vector-encoding non-self proteins can elicit cell-mediated immune responses. Mol Ther, 2013. **21**(1): p. 158-66.

91.   Ying, Y., et al., Heart-targeted adeno-associated viral vectors selected by in vivo biopanning of a random viral display peptide library. Gene Ther, 2010. **17**(8): p. 980-90.

92.   Sands, M.S., AAV-mediated liver-directed gene therapy. Methods Mol Biol, 2011. **807**: p. 141-57.

93.   Pleger, S.T., et al., Cardiac AAV9-S100A1 gene therapy rescues post-ischemic heart failure in a preclinical large animal model. Sci Transl Med, 2011. **3**(92): p. 92ra64.

94.   Katwal, A.B., et al., Adeno-associated virus serotype 9 efficiently targets ischemic skeletal muscle following systemic delivery. Gene Ther, 2013. **20**(9): p. 930-8.

95.   Bish, L.T., et al., Adeno-associated virus (AAV) serotype 9 provides global cardiac gene transfer superior to AAV1, AAV6, AAV7, and AAV8 in the mouse and rat. Hum Gene Ther, 2008. **19**(12): p. 1359-68.

96.   Geisler, A., et al., microRNA122-regulated transgene expression increases specificity of cardiac gene transfer upon intravenous delivery of AAV9 vectors. Gene Ther, 2011. **18**(2): p. 199-209.

97.   Foust, K.D., et al., Intravascular AAV9 preferentially targets neonatal neurons and adult astrocytes. Nat Biotechnol, 2009. **27**(1): p. 59-65.

98.   Arroyo, J.D., et al., Argonaute2 complexes carry a population of circulating microRNAs independent of vesicles in human plasma. Proc Natl Acad Sci U S A, 2011. **108**(12): p. 5003-8.

99.   Jung, M., et al., Robust microRNA stability in degraded RNA preparations from human tissue and cell samples. Clin Chem, 2010. **56**(6): p. 998-1006.

100.   Vickers, K.C., et al., MicroRNAs are transported in plasma and delivered to recipient cells by high-density lipoproteins. Nat Cell Biol, 2011. **13**(4): p. 423-33.

101.   Valadi, H., et al., Exosome-mediated transfer of mRNAs and microRNAs is a novel mechanism of genetic exchange between cells. Nat Cell Biol, 2007. **9**(6): p. 654-9.

102.   Judge, A.D., et al., Sequence-dependent stimulation of the mammalian innate immune response by synthetic siRNA. Nature biotechnology, 2005. **23**(4): p. 457-462.

103.   Sioud, M., Induction of inflammatory cytokines and interferon responses by double-stranded and single-stranded siRNAs is sequence-dependent and requires endosomal localization. Journal of molecular biology, 2005. **348**(5): p. 1079-1090.

104.   Arslan, F., D.P. de Kleijn, and G. Pasterkamp, Innate immune signaling in cardiac ischemia. Nat Rev Cardiol, 2011. **8**(5): p. 292-300.

105.   Thomson, D.W., et al., On measuring miRNAs after transient transfection of mimics or antisense inhibitors. PLoS One, 2013. **8**(1): p. e55214.

106.   Thum, T., et al., MicroRNA-21 contributes to myocardial disease by stimulating MAP kinase signalling in fibroblasts. Nature, 2008. **456**(7224): p. 980-4.

107.   Chan, L.S., et al., Role of microRNA-214 in ginsenoside-Rg1-induced angiogenesis. Eur J Pharm Sci, 2009. **38**(4): p. 370-7.

108.   Aurora, A.B., et al., MicroRNA-214 protects the mouse heart from ischemic injury by controlling Ca(2)(+) overload and cell death. J Clin Invest, 2012. **122**(4): p. 1222-32.

109.   Whitehead, K.A., R. Langer, and D.G. Anderson, Knocking down barriers: advances in siRNA delivery. Nat Rev Drug Discov, 2009. **8**(2): p. 129-38.

110.   Buyens, K., et al., Liposome based systems for systemic siRNA delivery: stability in blood sets the requirements for optimal carrier design. J Control Release, 2012. **158**(3): p. 362-70.

111.   Jiang, N., et al., A novel in vivo siRNA delivery system specifically targeting liver cells for protection of ConA-induced fulminant hepatitis. PLoS One, 2012. **7**(9): p. e44138.

112.   Elbashir, S.M., et al., Duplexes of 21-nucleotide RNAs mediate RNA interference in cultured mammalian cells. Nature, 2001. **411**(6836): p. 494-8.

113.   Yano, J., et al., Antitumor activity of small interfering RNA/cationic liposome complex in mouse models of cancer. Clin Cancer Res, 2004. **10**(22): p. 7721-6.

114.   Santel, A., et al., RNA interference in the mouse vascular endothelium by systemic administration of siRNA-lipoplexes for cancer therapy. Gene Ther, 2006. **13**(18): p. 1360-70.

115.   Zhang, G., et al., A delivery system targeting bone formation surfaces to facilitate RNAi-based anabolic therapy. Nat Med, 2012. **18**(2): p. 307-14.

116.   Lin, S.Y., et al., Sterically polymer-based liposomal complexes with dual-shell structure for enhancing the siRNA delivery. Biomacromolecules, 2012. **13**(3): p. 664-75.

117.   Li, R.C., et al., In vivo suppression of microRNA-24 prevents the transition toward decompensated hypertrophy in aortic-constricted mice. Circ Res, 2013. **112**(4): p. 601-5.

118.   Singha, K., R. Namgung, and W.J. Kim, Polymers in small-interfering RNA delivery. Nucleic Acid Ther, 2011. **21**(3): p. 133-47.

119.   Schiffelers, R.M., et al., Cancer siRNA therapy by tumor selective delivery with ligand-targeted sterically stabilized nanoparticle. Nucleic Acids Res, 2004. **32**(19): p. e149.

120.   Katas, H. and H.O. Alpar, Development and characterisation of chitosan nanoparticles for siRNA delivery. J Control Release, 2006. **115**(2): p. 216-25.

121.   Han, H.D., et al., Targeted gene silencing using RGD-labeled chitosan nanoparticles. Clin Cancer Res, 2010. **16**(15): p. 3910-22.

122.   Alshamsan, A., et al., STAT3 silencing in dendritic cells by siRNA polyplexes encapsulated in PLGA nanoparticles for the modulation of anticancer immune response. Mol Pharm, 2010. **7**(5): p. 1643-54.

123.   Zhou, J., et al., Octa-functional PLGA nanoparticles for targeted and efficient siRNA delivery to tumors. Biomaterials, 2012. **33**(2): p. 583-91.

124.   Meyer, M., et al., Synthesis and biological evaluation of a bioresponsive and endosomolytic siRNA-polymer conjugate. Mol Pharm, 2009. **6**(3): p. 752-62.

125.   Buyens, K., et al., Monitoring the disassembly of siRNA polyplexes in serum is crucial for predicting their biological efficacy. J Control Release, 2010. **141**(1): p. 38-41.

126.   Kano, A., et al., Grafting of poly(ethylene glycol) to poly-lysine augments its lifetime in blood circulation and accumulation in tumors without loss of the ability to associate with siRNA. J Control Release, 2011. **149**(1): p. 2-7.

127.   Wang, Y. and S.M. Grayson, Approaches for the preparation of non-linear amphiphilic polymers and their applications to drug delivery. Adv Drug Deliv Rev, 2012. **64**(9): p. 852-65.

128.   Taratula, O., et al., Surface-engineered targeted PPI dendrimer for efficient intracellular and intratumoral siRNA delivery. J Control Release, 2009. **140**(3): p. 284-93.

129. Merkel, O.M., et al., Molecular modeling and in vivo imaging can identify successful flexible triazine dendrimer-based siRNA delivery systems. J Control Release, 2011. **153**(1): p. 23-33.
130. Wolff, J.A. and V. Budker, The mechanism of naked DNA uptake and expression. Adv Genet, 2005. **54**: p. 3-20.
131. Kim, D., et al., Anti-apoptotic cardioprotective effects of SHP-1 gene silencing against ischemia-reperfusion injury: use of deoxycholic acid-modified low molecular weight polyethyleneimine as a cardiac siRNA-carrier. J Control Release, 2013. **168**(2): p. 125-34.
132. Saliba, Y., et al., A new method of ultrasonic nonviral gene delivery to the adult myocardium. J Mol Cell Cardiol, 2012. **53**(6): p. 801-8.
133. Somasuntharam, I., et al., Delivery of Nox2-NADPH oxidase siRNA with polyketal nanoparticles for improving cardiac function following myocardial infarction. Biomaterials, 2013. **34**(31): p. 7790-8.
134. Santel, A., et al., A novel siRNA-lipoplex technology for RNA interference in the mouse vascular endothelium. Gene Ther, 2006. **13**(16): p. 1222-34.
135. Betigeri, S., et al., Non-viral systemic delivery of siRNA or antisense oligonucleotides targeted to Jun N-terminal kinase 1 prevents cellular hypoxic damage. Drug Deliv Transl Res, 2011. **1**(1): p. 13-24.
136. Kang, J.H., et al., Efficient reduction of serum cholesterol by combining a liver-targeted gene delivery system with chemically modified apolipoprotein B siRNA. J Control Release, 2012. **163**(2): p. 119-24.
137. Tadin-Strapps, M., et al., siRNA-induced liver ApoB knockdown lowers serum LDL-cholesterol in a mouse model with human-like serum lipids. J Lipid Res, 2011. **52**(6): p. 1084-97.
138. Majmudar, M.D., et al., Monocyte-directed RNAi targeting CCR2 improves infarct healing in atherosclerosis-prone mice. Circulation, 2013. **127**(20): p. 2038-46.
139. Leuschner, F., et al., Therapeutic siRNA silencing in inflammatory monocytes in mice. Nat Biotechnol, 2011. **29**(11): p. 1005-10.
140. Strumberg, D., et al., Phase I clinical development of Atu027, a siRNA formulation targeting PKN3 in patients with advanced solid tumors. Int J Clin Pharmacol Ther, 2012. **50**(1): p. 76-8.
141. Coelho, T., et al., Safety and efficacy of RNAi therapy for transthyretin amyloidosis. N Engl J Med, 2013. **369**(9): p. 819-29.
142. Carson, A.R., et al., Ultrasound-targeted microbubble destruction to deliver siRNA cancer therapy. Cancer Res, 2012. **72**(23): p. 6191-9.
143. Christiansen, J.P., et al., Targeted tissue transfection with ultrasound destruction of plasmid-bearing cationic microbubbles. Ultrasound Med Biol, 2003. **29**(12): p. 1759-67.
144. Hernot, S. and A.L. Klibanov, Microbubbles in ultrasound-triggered drug and gene delivery. Adv Drug Deliv Rev, 2008. **60**(10): p. 1153-66.
145. Tlaxca, J.L., et al., Analysis of in vitro transfection by sonoporation using cationic and neutral microbubbles. Ultrasound Med Biol, 2010. **36**(11): p. 1907-18.
146. Meijering, B.D., et al., Ultrasound and microbubble-targeted delivery of macromolecules is regulated by induction of endocytosis and pore formation. Circ Res, 2009. **104**(5): p. 679-87.
147. Choi, J.J., et al., Noninvasive and localized blood-brain barrier disruption using focused ultrasound can be achieved at short pulse lengths and low pulse repetition frequencies. J Cereb Blood Flow Metab, 2011. **31**(2): p. 725-37.
148. Chappell, J.C., et al., Targeted delivery of nanoparticles bearing fibroblast growth factor-2 by ultrasonic microbubble destruction for therapeutic arteriogenesis. Small, 2008. **4**(10): p. 1769-77.
149. Kinoshita, M. and K. Hynynen, A novel method for the intracellular delivery of siRNA using microbubble-enhanced focused ultrasound. Biochem Biophys Res Commun, 2005. **335**(2): p. 393-9.
150. Un, K., et al., Efficient suppression of murine intracellular adhesion molecule-1 using ultrasound-responsive and mannose-modified lipoplexes inhibits acute hepatic inflammation. Hepatology, 2012. **56**(1): p. 259-69.
151. Tsunoda, S., et al., Sonoporation using microbubble BR14 promotes pDNA/siRNA transduction to murine heart. Biochem Biophys Res Commun, 2005. **336**(1): p. 118-27.

152.   Alter, J., et al., Microbubble stability is a major determinant of the efficiency of ultrasound and microbubble mediated in vivo gene transfer. Ultrasound Med Biol, 2009. **35**(6): p. 976-84.

153.   Saito, M., et al., Sonoporation mediated transduction of pDNA/siRNA into joint synovium in vivo. J Orthop Res, 2007. **25**(10): p. 1308-16.

154.   Haag, P., et al., Microbubble-enhanced ultrasound to deliver an antisense oligodeoxynucleotide targeting the human androgen receptor into prostate tumours. J Steroid Biochem Mol Biol, 2006. **102**(1-5): p. 103-13.

155.   Ko, Y.T., et al., Gene delivery into ischemic myocardium by double-targeted lipoplexes with anti-myosin antibody and TAT peptide. Gene Ther, 2009. **16**(1): p. 52-9.

156.   Kim, J., S.W. Kim, and W.J. Kim, PEI-g-PEG-RGD/small interference RNA polyplex-mediated silencing of vascular endothelial growth factor receptor and its potential as an anti-angiogenic tumor therapeutic strategy. Oligonucleotides, 2011. **21**(2): p. 101-7.

157.   Holig, P., et al., Novel RGD lipopeptides for the targeting of liposomes to integrin-expressing endothelial and melanoma cells. Protein Eng Des Sel, 2004. **17**(5): p. 433-41.

158.   Sosunov, E.A., et al., pH (low) insertion peptide (pHLIP) targets ischemic myocardium. Proc Natl Acad Sci U S A, 2013. **110**(1): p. 82-6.

159.   Bongartz, J.P., et al., Improved biological activity of antisense oligonucleotides conjugated to a fusogenic peptide. Nucleic Acids Res, 1994. **22**(22): p. 4681-8.

160.   Hatakeyama, H., et al., A pH-sensitive fusogenic peptide facilitates endosomal escape and greatly enhances the gene silencing of siRNA-containing nanoparticles in vitro and in vivo. J Control Release, 2009. **139**(2): p. 127-32.

161.   Sakurai, Y., et al., Endosomal escape and the knockdown efficiency of liposomal-siRNA by the fusogenic peptide shGALA. Biomaterials, 2011. **32**(24): p. 5733-42.

162.   Ye, S.F., et al., Synergistic effects of cell-penetrating peptide Tat and fusogenic peptide HA2-enhanced cellular internalization and gene transduction of organosilica nanoparticles. Nanomedicine, 2012. **8**(6): p. 833-41.

163.   Choi, S.W., et al., Multifunctional siRNA delivery system: polyelectrolyte complex micelles of six-arm PEG conjugate of siRNA and cell penetrating peptide with crosslinked fusogenic peptide. Biotechnol Prog, 2010. **26**(1): p. 57-63.

164.   Varkouhi, A.K., et al., Endosomal escape pathways for delivery of biologicals. J Control Release, 2011. **151**(3): p. 220-8.

165.   Janssen, H.L., et al., Treatment of HCV infection by targeting microRNA. N Engl J Med, 2013. **368**(18): p. 1685-94.

166.   Kuhnert, F., et al., Attribution of vascular phenotypes of the murine Egfl7 locus to the microRNA miR-126. Development, 2008. **135**(24): p. 3989-93.

167.   Yin, K.J., et al., Vascular endothelial cell-specific microRNA-15a inhibits angiogenesis in hindlimb ischemia. J Biol Chem, 2012. **287**(32): p. 27055-64.

168.   Spinetti, G., et al., MicroRNA-15a and microRNA-16 impair human circulating proangiogenic cell functions and are increased in the proangiogenic cells and serum of patients with critical limb ischemia. Circ Res, 2013. **112**(2): p. 335-46.

169.   Zhou, Q., et al., Regulation of angiogenesis and choroidal neovascularization by members of microRNA-23~27~24 clusters. Proc Natl Acad Sci U S A, 2011. **108**(20): p. 8287-92.

170.   Fiedler, J., et al., MicroRNA-24 regulates vascularity after myocardial infarction. Circulation, 2011. **124**(6): p. 720-30.

171.   Meloni, M., et al., Local Inhibition of MicroRNA-24 Improves Reparative Angiogenesis and Left Ventricle Remodeling and Function in Mice With Myocardial Infarction. Mol Ther, 2013. **21**(7): p. 1390-402.

172.   van Rooij, E., et al., Control of stress-dependent cardiac growth and gene expression by a microRNA. Science, 2007. **316**(5824): p. 575-9.

173.   Huang, Z.P., et al., MicroRNA-22 regulates cardiac hypertrophy and remodeling in response to stress. Circ Res, 2013. **112**(9): p. 1234-43.

174.   da Costa Martins, P.A., et al., MicroRNA-199b targets the nuclear kinase Dyrk1a in an auto-amplification loop promoting calcineurin/NFAT signalling. Nat Cell Biol, 2010. **12**(12): p. 1220-7.

175. Ganesan, J., et al., MiR-378 controls cardiac hypertrophy by combined repression of mitogen-activated protein kinase pathway factors. Circulation, 2013. **127**(21): p. 2097-106.
176. Care, A., et al., MicroRNA-133 controls cardiac hypertrophy. Nat Med, 2007. **13**(5): p. 613-8.
177. Pan, Z., et al., MicroRNA-101 inhibited postinfarct cardiac fibrosis and improved left ventricular compliance via the FBJ osteosarcoma oncogene/transforming growth factor-beta1 pathway. Circulation, 2012. **126**(7): p. 840-50.
178. Duisters, R.F., et al., miR-133 and miR-30 regulate connective tissue growth factor: implications for a role of microRNAs in myocardial matrix remodeling. Circ Res, 2009. **104**(2): p. 170-8, 6p following 178.
179. Ali, R., et al., miR-1 mediated suppression of Sorcin regulates myocardial contractility through modulation of Ca2+ signaling. J Mol Cell Cardiol, 2012. **52**(5): p. 1027-37.
180. Lu, Y., et al., MicroRNA-328 contributes to adverse electrical remodeling in atrial fibrillation. Circulation, 2010. **122**(23): p. 2378-87.
181. Grueter, C.E., et al., A cardiac microRNA governs systemic energy homeostasis by regulation of MED13. Cell, 2012. **149**(3): p. 671-83.
182. Noh, S.M., et al., Pegylated poly-l-arginine derivatives of chitosan for effective delivery of siRNA. J Control Release, 2010. **145**(2): p. 159-64.
183. Ghosn, B., et al., Efficient gene silencing in lungs and liver using imidazole-modified chitosan as a nanocarrier for small interfering RNA. Oligonucleotides, 2010. **20**(3): p. 163-72.
184. Thibault, M., et al., Excess polycation mediates efficient chitosan-based gene transfer by promoting lysosomal release of the polyplexes. Biomaterials, 2011. **32**(20): p. 4639-46.
185. Holzerny, P., et al., Biophysical properties of chitosan/siRNA polyplexes: profiling the polymer/siRNA interactions and bioactivity. J Control Release, 2012. **157**(2): p. 297-304.
186. Yuan, X., et al., The development and mechanism studies of cationic chitosan-modified biodegradable PLGA nanoparticles for efficient siRNA drug delivery. Pharm Res, 2010. **27**(7): p. 1285-95.
187. Kolhar, P., N. Doshi, and S. Mitragotri, Polymer nanoneedle-mediated intracellular drug delivery. Small, 2011. **7**(14): p. 2094-100.
188. Shen, M., et al., An MRI-visible non-viral vector for targeted Bcl-2 siRNA delivery to neuroblastoma. Int J Nanomedicine, 2012. **7**: p. 3319-32.
189. Zheng, M., et al., Enhancing in vivo circulation and siRNA delivery with biodegradable polyethylenimine-graft-polycaprolactone-block-poly(ethylene glycol) copolymers. Biomaterials, 2012. **33**(27): p. 6551-8.
190. Gao, S., et al., The effect of chemical modification and nanoparticle formulation on stability and biodistribution of siRNA in mice. Mol Ther, 2009. **17**(7): p. 1225-33.
191. Lee, D., et al., Bioreducible crosslinked polyelectrolyte complexes for MMP-2 siRNA delivery into human vascular smooth muscle cells. Pharm Res, 2012. **29**(8): p. 2213-24.
192. Liu, P., et al., A mPEG-PLGA-b-PLL copolymer carrier for adriamycin and siRNA delivery. Biomaterials, 2012. **33**(17): p. 4403-12.
193. Qi, R., et al., Biodegradable copolymers with identical cationic segments and their performance in siRNA delivery. J Control Release, 2012. **159**(2): p. 251-60.
194. Sato, A., et al., Polymer brush-stabilized polyplex for a siRNA carrier with long circulatory half-life. J Control Release, 2007. **122**(3): p. 209-16.
195. Kang, H., et al., Tat-conjugated PAMAM dendrimers as delivery agents for antisense and siRNA oligonucleotides. Pharm Res, 2005. **22**(12): p. 2099-106.
196. Arima, H., et al., Folate-PEG-appended dendrimer conjugate with alpha-cyclodextrin as a novel cancer cell-selective siRNA delivery carrier. Mol Pharm, 2012. **9**(9): p. 2591-604.

Table 1. miRNA interventions in cardiovascular diseases

	miRNA	Disease model	Interventionand effect	Targetedgenes or pathway
Proliferation cardiac regeneration	15	IR	KO; Systematic LNA	Arl2 and Bcl2[42, 88]
	~17-92	MI	cKO	PTEN[41]
	590/199a	MI	Lipid transfection reagent; AAV9	Homer1, Hopxand Clic5[74]
angiogenesis	92a	HI and MI	SystematicantagomiR	ITGA5[59]
	214	In vivo Matrilgel plug	Systematic antagomiR	QKI[79]; eNOS[107]
	126	HI	antagomiR	Spred1[166]
	15a	HI	Genetic knockout Lentivirus	VEGF and FGF2[167]
	15a/16-1	HI	antagomiR	VEGF and AKT-3[168]
	23/24/27	laser-induced choroidal neovascularization mouse model	LNA	Sproty2, Sema6A[169]
	100	HI	Systematic antagomiR	mTOR[72]
	24	MI	Adenovirus mediated decoys	GATA2, PAK4 [170] ;eNOS[171]
cardiomyocytes hypertrophy	208a	TAB	KO, transgenic	Thrap1[172]; myostatin[55]
	22	isoproterenol infusion and calcineurin transgene	KO	Sirt1 and Hdac4[173];
	199b	n.a.	Transgenicmice and antagomiR	Dyrk1a[174]
	378	TAC	adenovirus	MAPK pathway[175]
	133	n. a.	Systematic antagomiR	Rhoa[176], Cdc42 and NELFA/Whsc2[176]
	24	TAC	antagomiR	junctophilin-2[117]
	132/212	TAC	KO, Systematic antagomiR	Foxo3[58]
cardiac fibrotic remodeling	21	TAC	antagomiR	Spry1[106]
	29	MI	Systematic antagomiR	Col1A1, Col1A2, Col3A1, FBN1 and ELN1[68]
	101a/b	MI[177]	andenovirus	FBJ; c-fos[177]
	133a	TAC	transgenic	CTGF[178]
contractility, conduction and arrhythmias	1	n.a.	antagomiR	Sorcin[179]
	328	n.a.	adenovirus	CACNA1C and CACNB1[180]

|	25	TAC	antagomiR	Hand2[75]
Cardiac metabolic regulation	208a	High fat diet	KO	MED13[181]

HI: hindlimb ischemia; MI: myocardial infarction; IR: myocardial infarction and reperfusion; TAB: trans aorta binding; TAC: trans-aorta constriction; KO: knockout; LNA: locked nucleic acid

Table 2: Commonly used polymeric delivery devices for siRNA delivery

Polymer:	Size	Charge	Intracellular delivery	RNAseprotection	Biodistribution	*In vivo*success
Chitosan	100 – 400 nm[182, 183]	Cationic	+[184]	++[185]	Liver, brain, tumor, spleen.[121]	ApoB knockdown in liver[183] / tumor size reduction[121]
PLGA	100 – 1000 nm[186]	Anionic	-[187]	+/- [186]	Tumors[123]	Reduction of tumor size in mice[123]
PEI	50 – 500 nm[119, 188, 189]	Cationic	++[189, 190]	+/-[189, 191]	Liver, spleen, lung.[119, 189]	Reduction of tumor size and survival in mice[119]
PLL	25 – 300 nm[192, 193]	Cationic	+/-[125]	-[125, 194]	Tumor, liver, spleen.[126, 192]	Tumor-homing of siRNA-PLL particles[126]
Dendrimers	40 – 300 nm[129]	Cationic	+/-[195]	-[129, 195]	Liver, kidney, spleen, tumor.[128, 129]	Tumor-homing of siRNA [128, 196]

Polymer: polymer type, Size: measured radius of delivery vehicles, Charge: surface charge of delivery vehicles, Intracellular delivery: capability of delivery vehicles to deliver siRNAintracellularly (++=very capable, +=capable, +/-=slightly capable, -=low capability, --=very low capability), Blood stability: capability of deliver y vehicle to protect and stabilize siRNA in the presence of blood (++=very capable, +=capable, +/-=slightly capable, -=low capability, --=very low capability), Biodistribution: reported tissues/organs where the delivery vehicles can be found after *in vivo* application, *In vivo* success: examples of successful applications of delivery vehicles.

**Figure 1: miRNAs involved in cardiovascular diseases**
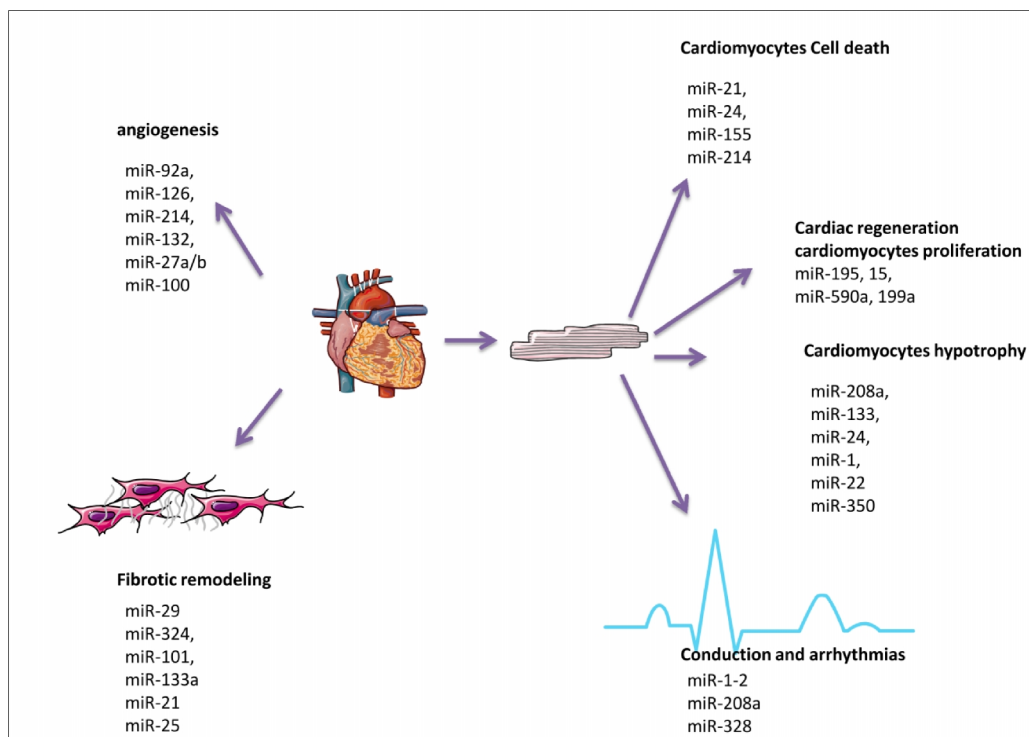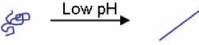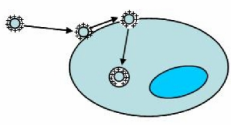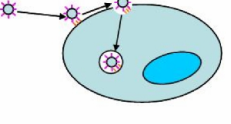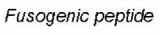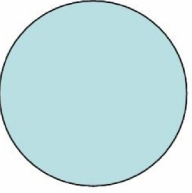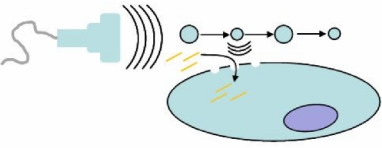
miRNAs are reported to be involved in many different types of cardiovascular diseases and in different cell types such as in angiogenesis for endothelial cells, in cardiac fibrotic remodeling for myofibroblasts, and in proliferation, cell death, conduction and arrhythmias for cardiomyocytes.

Figure 2: Targeting the heart with siRNA delivery vehicles.
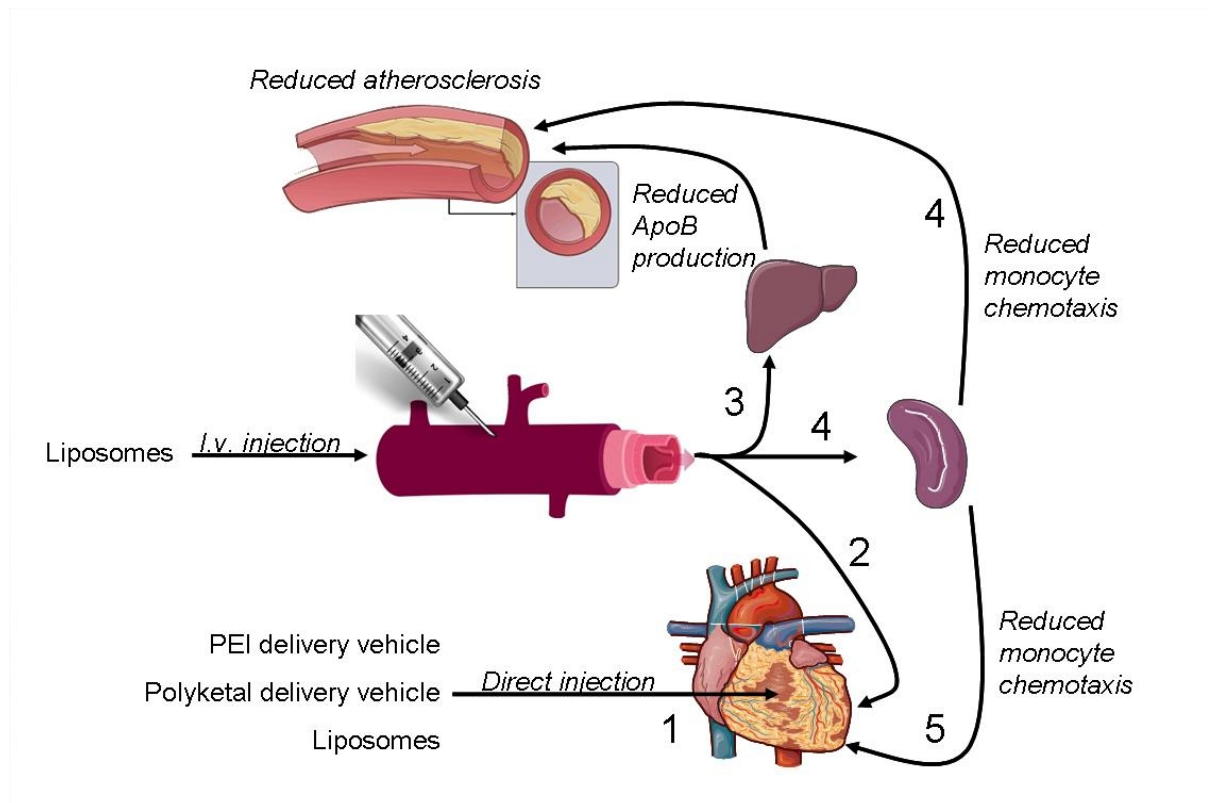
Cardiac application of siRNA delivery vehicles can occur via different application routes. Delivery strategies either rely on (1) intramyocardial injection of siRNA-carrying delivery vehicles, or intravenous injection routes (2, 3, 4). After intravenous injection, delivery vehicles can directly enter the heart (2) or enter off-target organs like the liver (3) or the spleen (4). Subsequently, secondary effects of those organs can have therapeutic effects on atherosclerosis by reducing ApoB levels (3) or by reducing monocyte chemotaxis (4). Reduced chemotaxis of monocytes from the spleen can also reduce infarct size after myocardial infarction (5).

Figure 3: Delivery vehicles for siRNA, targeting options and improving cytosolic delivery.

Delivery vehicles that can be used for siRNA delivery are represented in the left column, the size of the circles represents the size of the delivery vehicle. In the middle column, tissue targeting options which can be combined with delivery vehicles from the left column are depicted. Additionally, the right column gives an overview for options to increase cellular entry and endosomal escape.

Chapter 2

MMISH: Multicolor MicroRNA *In Situ* Hybridization for

Paraffin Embedded Samples

Zhiyong Lei[1], Alain van Mil[1], Junjie Xiao[2], Corina H.G. Metz[1], Esther C.M. van Eeuwijk[1], Pieter A. Doevendans[1,3] and Joost. P.G. Sluijter[1,3*]

1. Department of Cardiology, Division Heart and Lungs, University Medical Center Utrecht, Utrecht, the Netherlands

2. Regeneration and Ageing Lab, School of Life Science, Shanghai University, Shanghai, China
3. ICIN, Netherlands Heart Institute, Moreelsepark 1, 3511 EP, Utrecht, the Netherlands

Abstract

Through advances in miRNA discovery methods and ways to modulate miRNA activity, the impact of microRNA (miRNA) function in physiological and pathological processes is found to be ever-increasing. It has become more and more evident that miRNA actions are often tissue or cell-type specific. To understand and assess the roles of miRNAs, visualization of the expression patterns of specific miRNAs is needed at the cellular level in a wide variety of different tissue types. Although miRNA *in situ* hybridization techniques have been greatly improved in recent years, they remain difficult to routinely perform due to the complexity of the procedure. In addition, as it is crucial to define which tissues or cells are expressing a particular miRNA in order to elucidate the biological function of the miRNA, incorporation of additional staining for different cellular markers is necessary. Here, we describe a robust and flexible <u>m</u>ulticolor <u>mi</u>RNA <u>in situ</u> <u>h</u>ybridization (MMISH) technique for paraffin embedded sections. We show that the miRNA *in situ* protocol is sensitive and highly specific and can successfully be combined with both immunohistochemical and immunofluorescent staining.

Introduction

microRNAs (miRNAs) are short non-coding RNAs, which have been shown to play important roles in many different biological processes, pathological development and disease progression [1]. To explore the potential differential expression of one or many specific miRNAs in a physiological or pathological context, several techniques, such as Northern blot, qPCR, microarray, and next generation deep sequencing technologies can be used [2]. However, these techniques will provide the levels using a mixed sample of different cell types. In addition, not only expression levels, but also their locations, the cell type identification within the tissue are important [3]. A miRNA can only fulfill its function when its expression is temporal-spatial correlated with its targeted mRNAs. Thus a robust technique to define the expression patterns of specific miRNAs at the cellular level is crucial to elucidate their functions [4-9].

One way to visualize miRNAs at the cellular level is by performing miRNA *in situ* hybridization [10, 11]. The concept is straightforward and in general similar to the traditional *in situ* hybridizations for long coding mRNAs: a pre-labeled nucleic acid sequence, called probe, complementary to the selected miRNA is used to visualize the localization of the specific miRNA. Based on these well-established mRNA *in situ* procedures, several protocols have been developed to detect miRNA expression, which have advanced our understanding of how and where miRNAs are located [12-18].

MiRNA *in situ* techniques have been greatly improved and made less complicated, but even so, they are still laborious and difficult to perform routinely. Several modifications have been implemented to improve the sensitivity of the technique: 1) the use of Locked Nucleic Acid (LNA) based probes has significantly improved the hybridization signal and reduced the background [13]; 2) by using double-labeled probes, increased signal-to-noise ratios have been achieved; 3) by the introduction of an extra 1-Ethyl-3-[3-dimethylaminopropyl]carbodiimide hydrochloride (EDC)-based fixation step, free miRNAs were prevented from escaping into hybridization buffers [18]. However, one major drawback of EDC fixation is that it destroys the epitope of cell surface markers, which makes it difficult to perform subsequent immunohistochemical staining [18]. Still, to date only highly abundant miRNAs

have been localized and defined by *in situ* hybridization [12-18], suggesting still low sensitivity of this technique and the need for further optimization. Moreover, most of the available protocols require cryopreserved tissue samples [12, 13], while most clinical grade patient samples are paraffin embedded to better preserve morphology.

Here, we provide a non-toxic urea-based miRNA *in situ* hybridization protocol for paraffin embedded samples in combination with different visualization methods. By using our protocol, a multicolor image can be created by combining high sensitive *in situ* hybridization with immunofluorescent stainings, thereby allowing to visualize the expression of miRNAs at the cellular and even subcellular level.

Materials and Methods:

<u>REAGENTS</u>

Tissue-Tek® Tissue-Clear® Xylene Substitute (Cat. 1426, SAKURA), proteinase K (Cat. 03115828001, Roche); PBS 1x (Cat. 10010023, Life Technologies); Tris (Cat. T1503); glycine (Cat. G8898, Sigma); Paraformaldehyde (PFA) (Cat. P-6148, Sigma), Diethylpyrocarbonate (DEPC) (Fluka, 32490); Triethanolamine (Fluka, 90279); HCl (Riedel, 30721); Acetic anhydride (Sigma, A6404); 50x Denhardt's (Cat. 750018, Life technologies); Yeast tRNA (Cat. 10109495001, Roche) Anti-digoxigenin antibody (Roche, 1093274); Levamisole (Cat. X3021, DAKO); NBT/BCIP (Cat. K0598, DAKO); chromogen (Cat. K0640, DAKO); Fast Red Substrate (Dako, K0699); CHAPS (Sigma, C5070-5G); Tween (Cat. 93773, Fluka); NaCl (sigma); MgCl2 (Cat. 2320946, sigma); 20 X SSC (Cat. 15557-044, Life technologies); fluoromount-G (Cat.0100-1, SourthernBiotech); 1-Ethyl-3-[3-dimethylaminopropyl]carbodiimide hydrochloride (EDC) (Cat. 77149, Thermo Fisher); Heparin (Cat. H4784, Sigma)

Used antibodies: Anti-Digoxigenin-AP, Fab fragments antibody (Cat. 11093274910 Roche); anti-CD31 (Cat. 550274, BD Pharmingen); anti-cardiac Troponin I(Cat. ab47003, Abcam); anti-Vimentin (Cat. ab45939, Abcam); anti-Actinin (sarcomeric) (Cat. A7811, Sigma); Hoechst (Cat. H1399, Life technologies); Lectin BS-1 (Cat. L2895, Sigma).

5'- and 3'- double DIG-labeled miRCURY LNA™ Detection probes: miR-132 (Cat. 38031-15, Exiqon), miR-222 (Cat. 38499-15, Exiqon), miR-155 (Cat. 88083-15, Exiqon), miR-25 (Cat. 18122-15, Exiqon), miR-159a (Cat. 99003-15, Exiqon), and U6 (Cat. 99002-15, Exiqon).

<u>EQUIPMENT</u>

Coverslips (Menzel-Gläser, 24 x 60 mm)

Antigen retriever 2100 (Aptum Biologics Ltd)

Microscope (Olympus, BX53)

<u>REAGENT SETUP</u>

1. DEPC-treated PBS (1 liters): Add 1 ml of DEPC to 1 liters of PBS and mix vigorously. Keep at 37ºC overnight, then autoclave.

2. DEPC-treated water (1 liter): Add 1 ml of DEPC to 1 liter of milliQ water, keep at 37ºC overnight, then autoclave.

3. Proteinase K digestion buffer: 5 mM Tris, 1 mM EDTA, 1 mM NaCl, pH 7.4

4. EDC fixation buffer: 0.13 M 1-methylimidazole in 0.3 M NaCl, pH 8.0.

5. Acetylation buffer: Add 6.67 ml triethanolamine, 875 μl HCL (37%), 1.25 ml acetic anhydride in 493 ml H_2O.

6. Pre-hybridization blocking buffer: Urea (2 M), 2.5x SSC, 1x Denhardt's, 200 μg/ml yeast tRNA, 0.1% CHAPS, 0.1% Tween, 50 ug/ml heparin.

7. *In situ* hybridization buffer: Urea (2 M), 2.5x SSC, 1x Denhardt's, 200 μg/ml yeast tRNA, 0.1% CHAPS, 0.1% Tween, 50 ug/ml heparin.

8. Blocking buffer: 0.5% BSA, 10% normal goat serum in TBST (0.1% tween 20).

9. Antigen retrieving buffer: 10 mM Tris Base, 1 mM EDTA Solution, 0.05% Tween 20, pH 9.0.

10. Primary and secondary antibody incubation buffer: 0.5% BSA, 10% normal goat serum in TBST (0.1% tween 20).

11. Washing solution I: 0.1 M Tris, pH 7.5, 0.15 M NaCl, 0.1% Tween 20.

12. Washing solution II: 0.1 M Tris, pH 9.0, 0.15 M NaCl.

A step by step guide:

Slide preparation

1. Fix adult tissue in freshly prepared 4%PFA at 4ºC overnight under rotation. The fixation time for embryonic tissue can be reduced to 1 hour.

2. Cut paraffin embedded samples at 10 μm, dry the section for 1 hour at a 56 ºC plate.

3. Start the deparaffinization with fresh tissue clear for 2x 10 min.

4. Rehydrate sections subsequently with 99% ethanol, 95% ethanol, 70% ethanol, 50% ethanol, and PBS. 5 min for each step.

Proteinase K treatment

5. Optional: Delimit the sections with a DAKO Pen.

6. Transfer the slides in their holder into pre-warmed Proteinase K solution (5 mg/ml, 37°C) for 7 min.

7. Wash slides with 0.2% glycine in PBS for 2x 10 min to remove Proteinase K.

EDC fixation

8. Wash slides in EDC fixation buffer for 2x 10 min to remove residual phosphate groups from PBS.

9. Cover section with 200 ul 0.16 M EDC solution in EDC fixation buffer for 1 hour at room temperature.

10. Wash slides for 10 min to remove residual EDC with 0.2% glycine in PBS.

Acetylation

11. Transfer to acetylation solution for 30 min at room temperature.

12. Wash slides in washing solution I for 10 min.

Hybridization

13. Apply 200 μl pre-hybridization buffer on each slide at room temperature for 1 hour.

14. Recover probe in appropriate amount of hybridization buffer. The final concentration is probe specific, depending on the abundance of the miRNA of interest and the affinity of the probe to the target. For U6 5 nM is sufficient, miRNA probes were used at 10 nM. We recommend to first test a range of 1 to 40 nM.

15. Replace the pre-hybridization buffer with 100 ul hybridization solution, including the probe and cover the section with a 60 mm x 24 mm coverslip to avoid evaporation.

16. Place slides on a 65ºC hot plate to denature the probe and miRNA targets.

17. Incubate slides overnight at 30ºC below their Tm, as provided by the supplier. For example, Tm (miR-132) is 86ºC, Tm (miR-155) is 76ºC, Tm (miR-222) is 88ºC, Tm (miR-159) is 87ºC. Therefore, the sections for miR-132 are incubated at 56ºC, miR-155 at 46ºC, miR-222 at 58ºC and miR-159a at 57 ºC.

18. Soak slides in pre-warmed 5x SSC and carefully remove coverslips at their hybridization temperature.

19. Wash slides 2 times in 5x SSC, 10 min each at their hybridization temperature.

20. Wash slides for 4 times in 0.2x SSC, 10 min each at their hybridization temperature.

21. Wash slides in wash buffer I for 10 min at room temperature.

Staining

22. Block sections by applying 0.5% BSA and 10% normal goat serum in TBST for 1 hour.

23. Remove the blocking solution and apply 100 ul anti-DIG-alkaline phosphatase antibody in 5% BSA (1:1500) for 1 hour at room temperature.

24. Wash slides for 2 times in washing solution I, 5 min each.

Visualization

25. Wash slides for 10 min in washing solution II. Mix 3 ml BCIP/NBT solution with 3 drops levamisole solution, apply 200 μl to each slide and incubate at room temperature.

26. Regularly check the staining under the microscope. The incubation time needed for each probe will differ, depending on the expression level of each miRNA/ probe sensitivity. For high abundant targets, such as U6, a strong nuclear staining is visible within 15 min, but for low abundant miRNAs the incubation time can be extended to several hours. However, incubation time longer than 6 hours usually hardly improves the signal further.

Immunofluorescent staining

27. Wash slides in TBS for 5 min and place the slides in an antigen retrieval chamber, filled with appropriate antigen retrieval buffer, place the chamber holder in antigen retriever 2100, turn on the antigen retriever. It takes about 2 hours for the antigen retriever to complete the procedure and cool down.

28. Take out the slides and wash them in TBS for 10 min.

29. Optional: delimit the sections again with a DAKO pen.

30. Block with 0.5% BSA and 10% normal goat serum in TBST for 1 hour at room temperature.

31. Dilute antibodies in blocking solution, apply 100 ul to the slides and incubate overnight at 4ºC .

32. Wash slides 3 times in washing buffer I, 10 min each, with gentle agitation.

33. Dilute appropriate fluorescent-labeled secondary antibodies and apply to the sections for 1 hour at room temperature.

34. Wash slides 3 times in washing buffer, 10 min each, with gentle agitation.

35. Dilute Hoechst (1 mg/ml) in PBS and apply to the slides for 10 min at room temperature.

36. Wash slides 2 times in washing buffer I, 5 min each.

37. Apply 100 ul fluoromount-G solution and seal slides with 24 mm x 60 mm coverslips.

38. Dry the slides in the dark. When dry, they are ready for microscopy.

Results and discussion

To show the specificity and feasibility of our *in situ* protocol, we first performed miR-132 *in situ* hybridization on paraffin embedded mouse brain [11, 19-21]. As expected, miR-132 is expressed in the cytoplasm of neural cells, compared to the exclusive nuclear location of U6 (Figure 2). miR-159a, a plant specific miRNA, which is not present in mammalian cells , is used here as a negative control. In addition, we performed *in situ* hybridization for U6, miR-132 and miR-159a on paraffin embedded mouse embryo (E14.5) sections. As expected, U6 showed a strong nuclear staining throughout the embryo; miR-132 showed high expression in the brain, but is visible in other tissues as well (Figure 3) [19-27].

Subsequently, we showed that our *in situ* protocol can be combined with additional colorimetric stainings. Immediately after the miRNA *in situ* section, antigen retrieval was performed with "antigen retriever" as described previously [28]. The high temperature stops alkaline phosphatase activity of the miRNA probes and helps the cellular surface epitope to recover. After *in situ* hybridization for U6, miR-132, miR-222 and miR-155 in cardiac tissue, we identified the cellular types by immunofluorescent staining for CD31 (Endolthelium), Lectin BS-1 (Endothelium), cardiac Troponin I (Cardiomyoyctes) and Vimentin (Fibroblasts), respectively. As shown in Figure 4, the *in situ* hybridization miRNA signal is shown in purple/blue, whereas the cell types by antibody staining were visualized via chromogen in red. We show that miR-132 in expressed predominantly in cardiomyocytes, miR-222 is present in the nuclei of the smooth muscle cells, while miR-155 is lowly expressed in cardiomycoytes. Depending on the combination, signals are sometimes difficult to

distinguish from one another. We therefore set up a protocol where we can combine the colorimetric *in situ* hybridization with immunofluorescent stainings for cell-specific markers.

As described above, we first performed *in situ* hybridization for U6, miR-132 and miR-155 on various paraffin embedded mouse tissues, including heart and spleen, and subsequently stained these sections to visualize endothelial cells (Lectin BS-1) and myofibroblasts (Vimentin). The signals from the different channels were digitally merged into a 4-channel fluorescent image by using ImageJ. U6 is exclusively localized in the nuclei, miR-132 is expressed in the cardiomyocytes and large vessels (Vimentin positive), and miR-155 is highly expressed in B cells in the spleen which are small, lectinBS-1 and Vimentin negative cells, in some small cells in the infarcted area and is also detectable in cardiomyocytes after myocardial infarction.

As in other *in situ* hybridization protocols, there are many crucial steps and some steps must be optimized case by case. The time needed for PFA fixation before embedding can be different depending on the type of tissue and the size of the tissue. Fixation duration will also influence the time needed for proteinase K treatment and antigen retrieval later on . Therefore, the concentration and time of proteinase K treatment should be optimized. In practice, after proteinase K treatment, a quick Hoechst staining is very helpful as, in general, a bright nuclear signal with a clear nuclear edge suggests proteinase K treatment is optimal. Additionally, the hybridization temperature should be determined experimentally. The annealing temperature provided by the supplier is determined in silico and can be significantly different in reality. At last, the time for development of the *in situ* signal differs between different miRNAs and tissues, as it is directly related to the abundance of the targets.

Notes:
We used urea in our buffers which has previously been used successfully in RNA gel electrophoresis to prevent RNA from forming secondary structures [29], and recently, also for antigen retrieval [30]. Thus, urea may play a dual role by keeping the miRNA molecules and probes linear, thereby enhancing the target-probe affinity by preventing intermolecular interaction within miRNAs or individual probes, and by reversing the EDC fixation induced epitope loss by denaturing the antigens.

A great advantage of our protocol is *in situ* hybridization can be combined with immunofluorescent stainings. In the final steps of the *in situ*, NBT/BCIP is converted into a dark blue stable crystal by alkaline phosphatase. This signal is so stable that it is still present after autoclave treatment. This makes it possible to follow-up with standard immunofluorescent stainings, and allows different antigen retrieval procedures. Our protocol is not limited to paraffin embedded samples only and will also work for cryopreserved samples. In our experience, cryosections usually show stronger signals than paraffin-embedded tissues. However, a well-performed cryopreservation procedure is critical to prevent RNA degradation and cryo-damaging of the tissue during freezing.

Limitations

We found that nuclear Hoechst signals can be affected when NBT/BCIP was used for detection of U6 in the *in situ* hybridization due to steric hindrance of abundant overlaying signals. Moreover, this technique is semi-quantitative: one can compare the expression of a specific miRNA between different conditions, but direct comparison of two different miRNAs is limited unless the labeling property of different probes have been proven to be the same.

Application and advantages over other methods: Our protocol uses urea in the hybridization buffer, as compared to toxic deionized formamide, and it can be easily combined with different immune-labeling procedures, which allows one to analyze the expression and precise (sub)cellular location of the miRNA of interest.

Ethical Standards

The use of mice tissue was granted by the Animal Ethical Experimental committee of Utrecht University and was performed under the Guide for the Care and Use of Laboratory Animals.
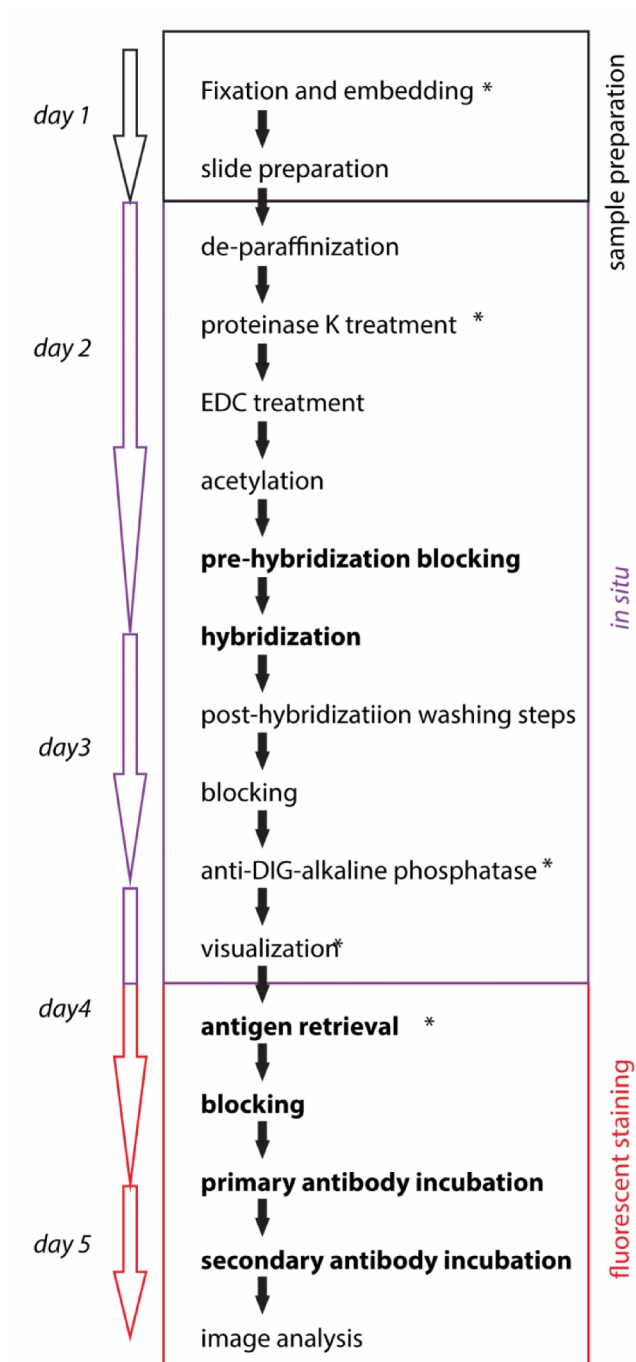
Figure 1.The workflow of MMISH which covers most of the critical points presented in this paper, including the time needed for each steps and sections. Steps marked with a * require optimization. Steps with bold characterization contain differences from other reported methods.
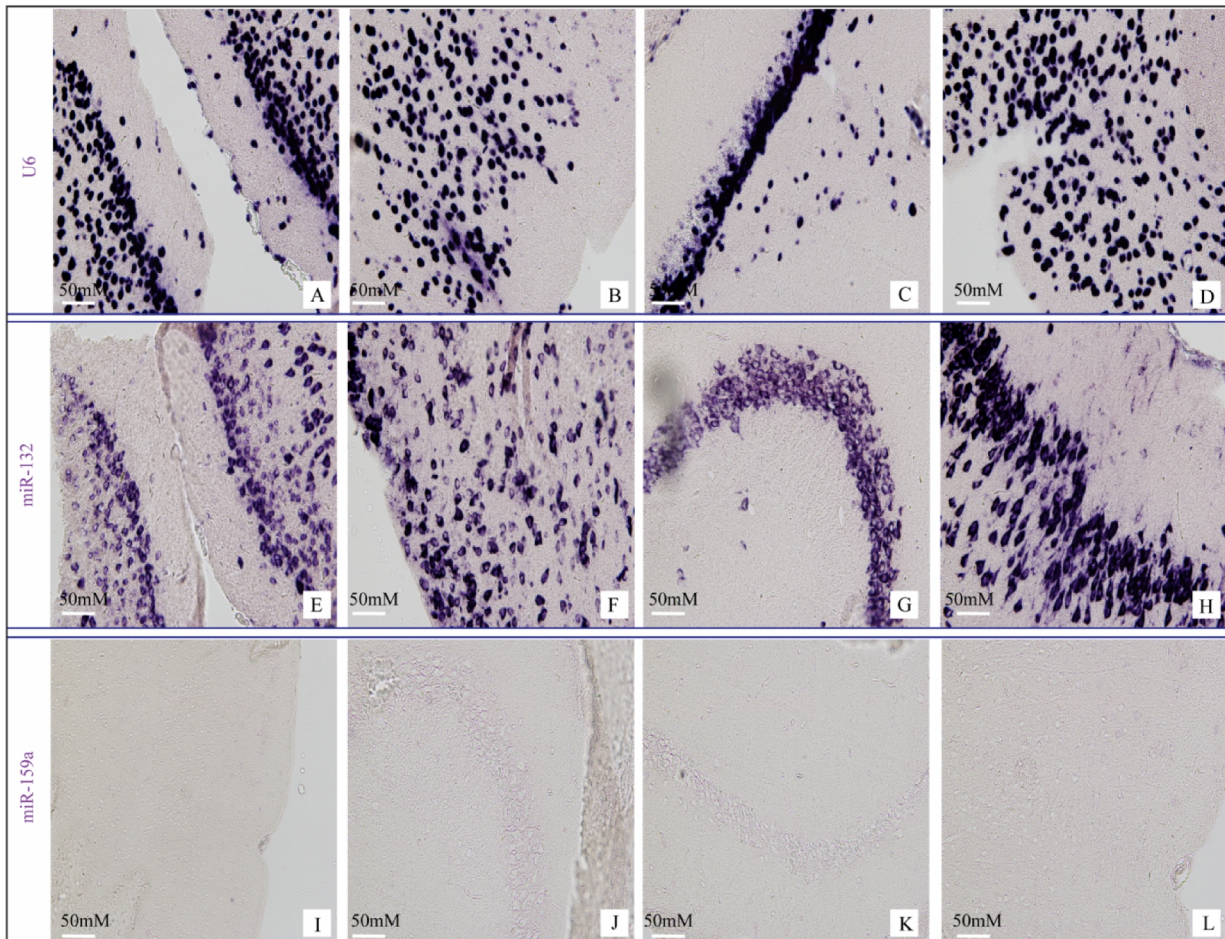
Figure 2. Representative images of miRNA *in situ* hybridization for U6 (A, B, C and D), miR-132 (E, F, G and H) and miR-159a (I, J K and L) in paraffin embedded mouse brain. U6 is used as a positive control and plant specific miR-159a serves as a negative control.
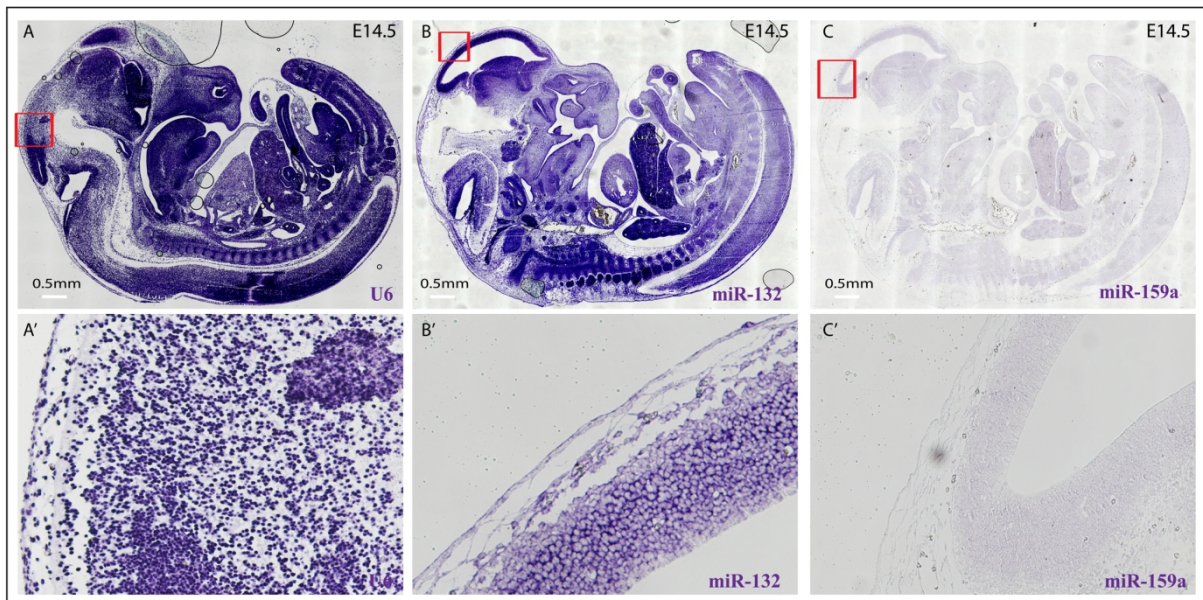
Figure 3. Representative images of miRNA *in situ* hybridization for U6 (A), miR-132 (B) and miR-159a (C) in paraffin embedded mouse embryo at E14.5. U6 is used as a positive control and plant specific miR-159a serves as a negative control. Figure A', B' and C' show high magnifications of the red box indicated areas in A, B and C.

Figure 4. Representative images of miRNA *in situ* hybridization for U6 (A), miR-132 (B), miR-222 (C) and miR-155(D) in paraffin embedded mouse heart in combination with immunohistochemical stainings. A: endothelial cells (CD31), B: endothelial cells (lectin BS-1), C: cardiomyocytes (Troponin I) and D: (myo)fibroblasts (Vimentin). (miRNAs in purple/blue, cell-specific markers in red)
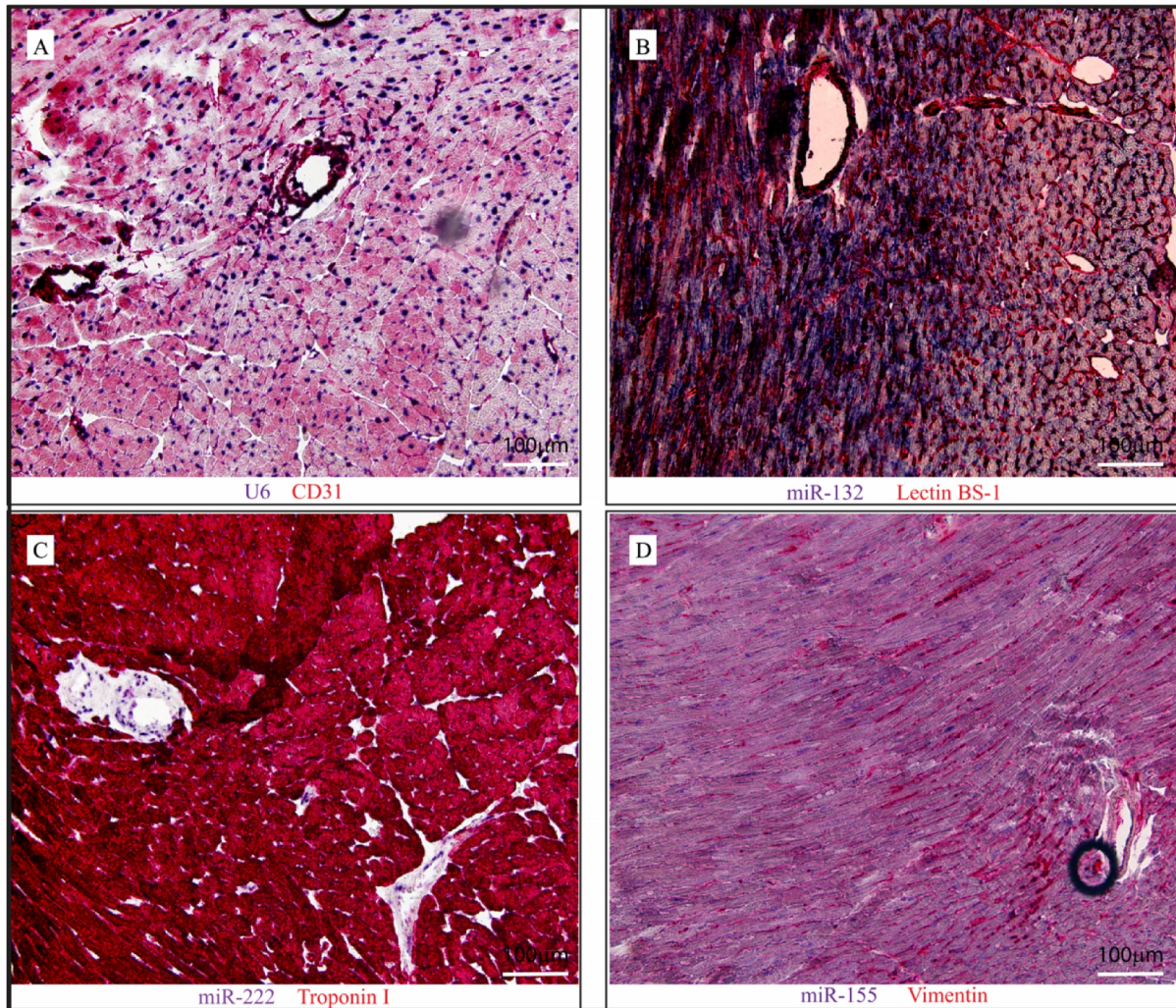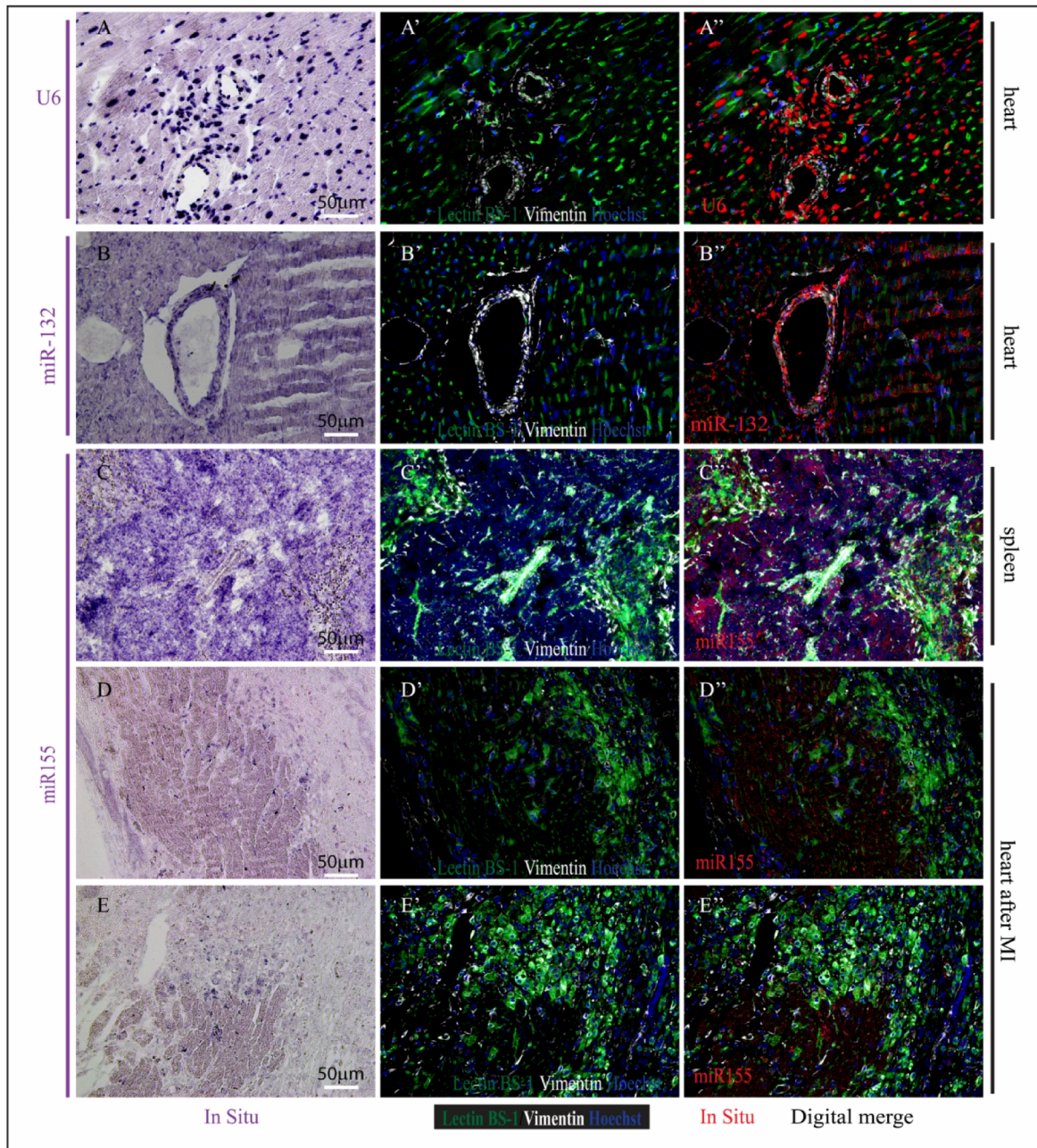
Figure 5. Representative images of miRNA *in situ* hybridization for U6 (A), miR-132 (B) and miR-155 (C, D and E) in paraffin embedded healthy mouse heart (A, B), spleen (C) or myocardial infarcted heart (D, E) in combination with immunofluorescent stainings. Nuclei are stained with Hoechst, endothelial cells with Lectin BS-1 in green, and (myo)fibroblasts in white. Digital merged images from *in situ* and immunofluorescent signals are shown on the right with nuclei in blue; endothelial cells in green; (myo)fibroblasts in white, and the *in situ* signal digitally converted into red.

Reference

1. Kwekkeboom, R.F., et al., Targeted delivery of miRNA therapeutics for cardiovascular diseases: opportunities and challenges. Clin Sci (Lond), 2014. **127**(6): p. 351-65.
2. van Rooij, E., The art of microRNA research. Circ Res, 2011. **108**(2): p. 219-34.
3. Park, C.Y., et al., A resource for the conditional ablation of microRNAs in the mouse. Cell Rep, 2012. **1**(4): p. 385-91.
4. Wahlquist, C., et al., Inhibition of miR-25 improves cardiac contractility in the failing heart. Nature, 2014. **508**(7497): p. 531-5.
5. Liu, X., et al., A necessary role of miR-221 and miR-222 in vascular smooth muscle cell proliferation and neointimal hyperplasia. Circ Res, 2009. **104**(4): p. 476-87.
6. Heymans, S., et al., Macrophage microRNA-155 promotes cardiac hypertrophy and failure. Circulation, 2013. **128**(13): p. 1420-32.
7. Schneider, M., et al., Cell-specific detection of microRNA expression during cardiomyogenesis by combined in situ hybridization and immunohistochemistry. J Mol Histol, 2011. **42**(4): p. 289-99.
8. Nazari-Jahantigh, M., et al., MicroRNA-155 promotes atherosclerosis by repressing Bcl6 in macrophages. J Clin Invest, 2012. **122**(11): p. 4190-202.
9. Kuwabara, Y., et al., Increased microRNA-1 and microRNA-133a levels in serum of patients with cardiovascular disease indicate myocardial damage. Circ Cardiovasc Genet, 2011. **4**(4): p. 446-54.
10. Deo, M., et al., Detection of mammalian microRNA expression by in situ hybridization with RNA oligonucleotides. Dev Dyn, 2006. **235**(9): p. 2538-48.
11. Thompson, R.C., M. Deo, and D.L. Turner, Analysis of microRNA expression by in situ hybridization with RNA oligonucleotide probes. Methods, 2007. **43**(2): p. 153-61.
12. Silahtaroglu, A.N., et al., Detection of microRNAs in frozen tissue sections by fluorescence in situ hybridization using locked nucleic acid probes and tyramide signal amplification. Nat Protoc, 2007. **2**(10): p. 2520-8.
13. Obernosterer, G., J. Martinez, and M. Alenius, Locked nucleic acid-based in situ detection of microRNAs in mouse tissue sections. Nat Protoc, 2007. **2**(6): p. 1508-14.
14. Turnock-Jones, J.J. and J.P. Le Quesne, MicroRNA in situ hybridization in tissue microarrays. Methods Mol Biol, 2014. **1211**: p. 85-93.
15. Shi, Z., J.J. Johnson, and M.S. Stack, Detecting microRNA in human cancer tissues with fluorescence in situ hybridization. Methods Mol Biol, 2013. **1039**: p. 19-27.
16. Sempere, L.F. and M. Korc, A method for conducting highly sensitive microRNA in situ hybridization and immunohistochemical analysis in pancreatic cancer. Methods Mol Biol, 2013. **980**: p. 43-59.
17. Nielsen, B.S. and K. Holmstrom, Combined microRNA in situ hybridization and immunohistochemical detection of protein markers. Methods Mol Biol, 2013. **986**: p. 353-65.
18. Renwick, N., et al., Multicolor microRNA FISH effectively differentiates tumor types. J Clin Invest, 2013. **123**(6): p. 2694-702.
19. Magill, S.T., et al., microRNA-132 regulates dendritic growth and arborization of newborn neurons in the adult hippocampus. Proc Natl Acad Sci U S A, 2010. **107**(47): p. 20382-7.
20. Miller, B.H., et al., MicroRNA-132 dysregulation in schizophrenia has implications for both neurodevelopment and adult brain function. Proc Natl Acad Sci U S A, 2012. **109**(8): p. 3125-30.
21. Scott, H.L., et al., MicroRNA-132 regulates recognition memory and synaptic plasticity in the perirhinal cortex. Eur J Neurosci, 2012. **36**(7): p. 2941-8.
22. Shaked, I., et al., MicroRNA-132 potentiates cholinergic anti-inflammatory signaling by targeting acetylcholinesterase. Immunity, 2009. **31**(6): p. 965-73.
23. Anand, S., et al., MicroRNA-132-mediated loss of p120RasGAP activates the endothelium to facilitate pathological angiogenesis. Nat Med, 2010. **16**(8): p. 909-14.
24. Eskildsen, T.V., et al., Angiotensin II Regulates microRNA-132/-212 in Hypertensive Rats and Humans. Int J Mol Sci, 2013. **14**(6): p. 11190-207.

25.   Shaltiel, G., et al., Hippocampal microRNA-132 mediates stress-inducible cognitive deficits through its acetylcholinesterase target. Brain Struct Funct, 2013. **218**(1): p. 59-72.

26.   Eskildsen, T.V., et al., The microRNA-132/212 family fine-tunes multiple targets in Angiotensin II signalling in cardiac fibroblasts. J Renin Angiotensin Aldosterone Syst, 2014.

27.   Huang, Y., et al., MicroRNA-132 silencing decreases the spontaneous recurrent seizures. Int J Clin Exp Med, 2014. **7**(7): p. 1639-49.

28.   Xu, X., et al., β cells can be generated from endogenous progenitors in injured adult mouse pancreas. Cell, 2008. **132**(2): p. 197-207.

29.   Priyakumar, U.D., et al., Urea destabilizes RNA by forming stacking interactions and multiple hydrogen bonds with nucleic acid bases. Journal of the American Chemical Society, 2009. **131**(49): p. 17759-17761.

30.   Inoue, D. and J. Wittbrodt, One for all—a highly efficient and versatile method for fluorescent immunostaining in fish embryos. PLoS One, 2011. **6**(5): p. e19713.

Chapter 3

Dgcr8 is indispensable for cardiac lineage specification in embryonic stem cells

Zhiyong Lei[1], Alain van Mil[1], Annebel M. van de Vrugt[1], Pieter A. Doevendans[1,2] and Joost. P.G. Sluijter[1,2*]

1. Department of Cardiology, Division Heart and Lungs, University Medical Center Utrecht, Utrecht, the Netherlands
2. ICIN, Netherlands Heart Institute, Moreelsepark 1, 3511 EP, Utrecht, the Netherlands

Abstract

Objective: microRNAs have been shown to play important roles in cellular behavior and lineage specification including cardiogenic differentiation. However, full understanding of their roles in cardiomyocyte differentiation have been impeded due to lack of proper cellular model. Here, we used an embryonic stem cell (ESC) that is lacking the important microprocessor Dgcr8 (or Pasha), which allows the introduction of individual miRNAs to study their role in cardiac differentiation and for more precise target selection.

Methods: Dgcr8 KO ESC were cultured in LIF-supplemented ESC medium with mouse embryonic fibroblast feeders and cardiac differentiation was induced using an embryonic body-based differentiation protocol. Differentiation was monitored by measuring mRNA and protein levels of cardiogenic markers and heterochromatin changes using immunofluorescent staining and semi-quantitative PCR.

Results and conclusion: We showed that Dgcr8 KO ESCs indeed are lacking a large population of small RNAs, including but not limited to mature microRNAs. The KO cells had a lower proliferation rate and were unable to differentiate into the cardiac lineage. To our surprise, in addition to a defect in microRNA processing, Dgcr8 KO embryonic stem cells are unable to form proper heterochromatin and to inactivate genotoxic centromeric repetitive elements. Our results argue that, in addition to controlling microRNA processing, Dgcr8 may serve a previously unrecognized role in heterochromatin silencing.

Introduction

microRNAs (miRNAs) have been shown to play important roles in cardiac differentiation [1-6], pathological development and progression of cardiac diseases [7-12]. Full understanding of their role in these conditions requires identification of their precise target genes and studying their function in the relevant cell types. Several different cell types, such as HEK293 or COS7, or organs like the mouse heart have been used for identification and validation of different miRNA targets [13, 14]. A major hurdle for target identification is that the cells used are either not relevant for the studied process, thereby not having the correct target mRNAs present, or the redundancy caused by other miRNAs that may compete with the miRNA of interest and thereby interfere with the effect of overexpression or inhibition of the miRNA of interest [15, 16]. Therefore, an ideal cell model to study the effects of a single miRNA including its targets in a cardiac context, would be a cardiomyocyte without any mature miRNAs present, a very "Simple Cell" as it were.

Most of the currently known miRNAs go through canonical miRNA processing. They are transcribed as normal mRNAs by RNA Polymerase II and subsequently processed into mature miRNAs by microprocessor complexes including Dgcr8 and Drosha [17]. After being exported into the cytosol[18, 19], precursor miRNAs are further processed into mature miRNAs by Dicer [20, 21]. Therefore, cells lacking Dgcr8 or Dicer are not able to produce canonical mature miRNAs. Dicer has been shown to have miRNA independent roles and commercial miRNA mimics are provided as precursor or precursor like structures, which require processing by Dicer to become functional. Thus, knocking out Dgcr8 in embryonic stem cells (ESC) has become the first choice to create a versatile miRNA-free cell model. In this cell model, the miRNA population will be eliminated, however, the activity for precursor processing will be kept intact and the cells may hold their potential to differentiate into any cell type of interest, e.g. cardiomyocytes. Although inactivation of Dgcr8 was used to explore the role of the total miRNA population in a particular cell type or tissue in vivo [22-25], the consequence of the loss of Dgcr8 on cardiac lineage specification of ESCs, and whether or not we can create the "simple cardiomyocyte" from Dgcr8 KO ESCs, is unknown.

Methods and Materials:

Embryonic stem cell (ESC) culture and embryonic bodies (EB) preparation and differentiation

Wild-type ESCs V6.5 and Dgcr8 knockout (KO) ESCs (Novus Biologicals, NBA1-19349) were cultured on a MEF feeding layer in ESC medium, containing DMEM (Gibco, cat. no. 41965), 15% FBS (Gibco, cat. no. 16141-079), 1x penicillin/streptomycin (Sigma, cat. no. P4458), 1x MEM-nonessential amino acids (PAA, cat. no. M11-003), 1x Leukemia Inhibitory Factor, and 0.0007% β-mercaptoethanol. Cells were detached using Accutase (Chemicon Millipore, SF006) and before differentiation, preplated for 0.5-2 h in non-coated plates. The supernatant including ESCs was collected, and EBs were formed in low attachment plates (6 well) with 2 million cells per well in differentiation medium, containing IMDM (Gibco, cat. no. 21980), Ham's F12 nutrient mixture with GlutaMAX-I (Gibco, cat. no. 31765), 2% Horse serum (Gibco, 16050-122), 1x MEM-nonessential amino acids (BioWhittaker, BE13-114E), 1x Insulin transferrin-selenium (Gibco, 41400-045), 1x penicillin/streptomycin (Sigma, cat. no. P4458), and 25 µg/mL ascorbic acid (Sigma, A-4034). The cells were incubated at 37 ºC while shaking (circa 50 rotations/min) for 2 days to induce EB formation.

Proliferation rate assay

To determine the degree of proliferation, cells were trypsinized into single cells and 10,000 cells were seeded in a 24-well plate, pre-coated with MEFs. Cells were trypsinized into single cells at 48 and 72 hours after seeding and counted with a Bio-Rad TC-10 automatic cell counter.

RNA isolation, small RNA profiling and semi-quantitative PCR analysis

Total DNA-free RNA was isolated with Tripure Isolation Reagent following manufactory's instructions (Roche Applied Science) and analyzed by using the Agilent Small RNA Kit (Agilent Technologies, cat. no. 5067-1548) according to the manufacturer's guidelines. Results were obtained using the Agilent Bioanalyzer 2100 and data was analyzed with 2100 Expert Software.

Total RNA was treated with RNase-free DNase I (Qiagen), checked to be DNA free, and cDNA was made using the iScript™ cDNA Synthesis Kit (Bio-Rad). Quantitative real-time polymerase chain reaction (qRT-PCR) was performed with iQ SYBR Green Supermix (Bio-Rad) and specific primers with the following sequences: *Gapdh* forward 5'-GGCATGGACTGTGGTCATGA-3' and reverse 5'-TTCACCACCATGGAGAAGGC-3'; *Hprt* forward 5' TCAGTCAACGGGGGACATAAA-3' and reverse 5'- GGGGCTGTACTGCTTAACCAG -3'; *Oct4* forward 5'- AGAGGATCACCTTGGGGTACA-3' and reverse 5'- CGAAGCGACAGATGGTGGTC -3'; *Sox2* forward 5'- GCGGAGTGGAAACTTTTGTCC-3' and reverse 5'- CGGGAAGCGTGTACTTATCCTT -3'; *Nanog* forward 5'- TCTTCCTGGTCCCCACAGTTT-3' and reverse 5'- GCAAGAATAGTTCTCGGGATGAA -3'; *Hnf4α* forward 5'- GTGGCGAGTCCTTATGACACG-3' and reverse 5'- GCTGTTGGATGAATTGAGGTTGG -3'; *TnT* forward 5'- CAGAGGAGGCCAACGTAGAAG-3' and reverse 5'- CTCCATCGGGGATCTTGGGT -3'; *α-MHC* forward 5'-ATCCTGTCCAACAAGAAGCC-3' and reverse 5'-ACCTCTCCCTGAGAGACGAA-3'; *β-actin* forward 5'-CTCTTTTCCAGCCTTCCTTC-3' and reverse 5'-TCTCCTTCTGCATCCTGTC-3'; *Pasha* exon 3 forward 5'-CACGGCTAAAGCAATCGTTCAA-3' and reverse 5'-GCTCTGTAGGTGGACGGCCAC-3'; LINE-1 forward 5'- GAACAGACGAGGACACTGAAAA-3' and reverse 5'- CTGGCTTCTCATTCGCATTCT-3'; IAP forward 5'-AGCAAGAAAAGAAGCCCGTGA-3' and reverse 5'- ATGCCAGAACATGTGTCAAGTG-3'; *Major* forward 5'- GACGACTTGAAAAATGACGAAATC-3' and reverse 5'-CATATTCCAGGTCCTTCAGTGTGC-3'; *Minor* forward 5'- CATGGAAAATGATAAAAACC-3' and reverse 5'- CATCTAATATGTTCTACAGTGTGG-3'. For minor and major satellite RNA RT-PCR, PCR products were separated using agarose gels (2%) and images were taken using UV exposure and detection with the ChemiDoc XRS System (Bio-Rad).

Western blotting

Total protein was isolated with protein lysis buffer (Roche Applied Science). Protein amounts were determined using the Pierce BCA Protein Assay (Thermo Scientific). Equal amounts of protein were loaded, separated, and transferred to a PVDF membrane using the Novex® NuPAGE® SDS-PAGE Gel System and the iBlot® Transfer System (Invitrogen). PVDF membranes were blocked in 5% non-

fat dry milk in 0.1% TBST with 2% normal goat serum or 5% non-fat dry milk in 0,1% PBST with 2% normal goat serum. Blocked membranes were incubated with primary antibodies against Pasha (Dgcr8; 1:1000, Proteintech, cat. no. 10996-1-AP) or β-actin (1:5000, Sigma, cat. no. A5441), and subsequently probed with horseradish peroxidase-conjugated goat-anti-rabbit (1:2000, Dako, P0448) or goat-anti-mouse (1:1000, Dako, P0447). The signal was visualized with Chemiluminescent Peroxidase Substrate (Sigma) and detected with the ChemiDoc XRS System (Bio-Rad). Image Lab software was used for analysis.

Fluorescent immunohistochemistry

EBs were fixed with 4% PFA in PBS, incubated in 30% sucrose PBS, and preserved in Tissue-Tek® O.C.T.^{TM} (Sakura). Cryosections were stained for α-actinin (1:800, Sigma, cat. no. A7811), and Troponin I (1:100, Abcam, cat. no. ab47003). The secondary antibodies used were Alexa Fluor-488 goat-anti-mouse (1:400, Invitrogen, A11001) and Alexa Fluor-555 goat-anti-rabbit (1:400, Invitrogen, A21458). Nuclei were counterstained with 1 μg/mL Hoechst 33342 (Invitrogen) and sections were mounted in Fluoromount-G (SouthernBiotech). Images were captured using confocal laser scanning microscopy (Carl Zeiss LSM 700) and associated software.

Statistical analysis

Data are presented as mean ± SEM. Student's t-tests were performed for comparison between WT and KO and differences were considered statistically significant when p values were < 0.05, as indicated by an asterisk (*).

Results

Characterization of mouse Dgcr8 KO ESCs

To confirm the absence of Dgcr8 in KO ESCs, we designed primers which amplify the 3' part of intron 2 and the 5' part of intron 4 and performed a PCR with WT and KO genomic DNA. As expected, PCR products from KO are smaller (100 bp) compared with WT products (248 bp) (Figure 1B). Additionally, we performed Western blotting with an anti-Dgcr8 antibody with protein lysate of WT and KO ESC. We indeed confirmed the absence of the predicted 86 kD-signal in the KO samples (Figure 1C). The loss of Dgcr8 in the KO ESC was further confirmed by immunofluorescent staining, as is illustrated by the absence of nuclear Dgcr8 in KO ESC cells (Figure 1D).

Dgcr8 KO ESCs were viable and displayed typical mouse ESC morphology when cultured on a mouse embryonic fibroblast feeder layer. Interestingly, KO ESC colonies were smaller as compared with WT colonies (Figure 1E). And we also noticed Dgcr8 KO ESCs proliferate much slower than WT cells (Figure 1F).

Dgcr8 was first identified as a Drosha interacting protein by Drosha immunoprecipitation, and therefore its function was mainly associated with miRNA biogenesis. To evaluate the consequence of Dgcr8 loss on the cellular RNA profile, we isolated total RNA from WT and KO ESCs and compare the small RNA profiles (1-150 bp) using a Bioanalyzer small RNA chip. We observed that Dgcr8 KO cells are not only lacking miRNAs, as indicated by the miRNA spike in control (20 bp), but also a large population of small RNA species ranging from 4-40 bp (Figure 1G and H).

Dgcr8 KO EBs do not differentiate into the cardiac lineage

To assess the effect of the Dgcr8 KO on the cardiogenic differentiation of ESCs, we induced cardiac differentiation using a well-established EB-based differentiation protocol [26]. We observed that Dgcr8 KO ESCs can form EBs, but their size is smaller and their shape is more irregular compared to WT ESC derived EBs (Figure 2A). Upon induction of differentiation, WT ESCs undergo typical

morphological and phenotypical changes, such as forming of cyst-like structures and spontaneous contraction (Figure 2B) . In contrast, KO EBs did not show cyst-like structures and did not contract (Figure 2A+B) .

To further characterize the cardiogenic differentiation of EBs, we performed qRT-PCR for pluripotency (Oct4), early mesoderm (Brachyury T), and cardiogenic lineage markers (αMHC and TnT). Consistent with our previous observations, we found that the expression of Oct4 decreased upon differentiation, associated with an increased level of Brachyury T in WT cells. Prolonging the differentiation reduced the expression of Brachyury T and increased the levels of cardiac markers αMHC and Troponin in WT EBs on day 10. These results indicate loss of pluripotency and induced mesoderm and subsequent cardiac differentiation in the WT EBs. In the Dgcr8 KO cells, however, the expression of pluripotency markers Oct4, Sox2, and Nanog did not change, only very low levels of Brachyury T could be detected, and the expression of αMHC and Troponin was absent, even 10 days after differentiation (Figure 2C). We further confirmed these findings by immunofluorescent staining of EBs for the cardiac markers α-Actinin and Troponin. Indeed, we could detect α-Actinin and Troponin positive regions in the WT EBs after 10 days of differentiation, which were not observed in the KO EBs (Figure 2D).

Dgcr8-KO ESCs are deficient in heterochromatin silencing and centromeric repeat sequence RNA inactivation

Although miRNA processing was the first role ascribed to Dicer, defects in the formation of heterochromatin have been linked to failure of differentiation and induction of apoptosis in Dicer KO ESCs [27, 28]. Centromeric heterochromatin regions contain a lot of transposable elements, which have to be silenced by the formation of heterochromatin rich regions. RNAi mediated heterochromatin assembly has been reported to play a critical role in ESC differentiation, genome stability and protection from viral invasion [29]. Recently, a Dgcr8 RNA immune-precipitation study has greatly expanded its target spectrum and has shown its physical interaction with several other non-coding RNAs (ncRNA), including retro-transposable elements as well as Major Satellite and Minor Satellite

centromeric repeat RNA species [30], thereby regulating retro-transposon activities [31]. Dgcr8 null ESCs are not able to produce a large population of endo-siRNA, or shRNA [32], essential components of siRNA induced chromatin silencing complexes. Therefore, we investigated if there were any differences in heterochromatin formation between WT and Dgcr8 KO ESCs. Using a H3K9ME3 antibody, a well established heterochromatin marker [27, 33], we performed immunofluorescent staining on WT and Dgcr8 KO ESCs before and after differentiation. Although we found no differences before differentiation (Figure 3A), upon differentiation we did observe a clear condensation pattern only in WT cells (Figure 3B). A clear example of heterochromatin condensation is seen in differentiated fibroblast (Figure 3C). This pattern is not seen in the KO ESCs, suggesting there is a defect in the formation of heterochromatin regions in KO ESCs.

To further confirm this finding, we selected four centromeric repeat sequences: minor and major satellite repeats, and LINE-1, all identified as Dgcr8-interacting RNAs [30], and IAP, and performed a semi-quantitative PCR using WT and KO ESC RNA samples. As predicted, we found that the expression of LINE-1, and minor and major satellite transcripts is more abundant in the KO ESCs compared to WT ESC, before and after differentiation (Figure 4 A and B). The expression of these three RNA transcripts is less pronounced upon differentiation in the WT ESCs (Figure 4 B and Supplement figure E), which correlates with the widespread heterochromatin formation as shown by the H3K9ME3 staining (Figure 3 A and B). The higher expression of these three transcripts in the KO ESCs indicates a defect in heterochromatin silencing (Figure 4B and Supplement figure E). Interestingly, another retro-transposon-like element, IAP, did not show any difference (Supplement figure F).

Discussion

In this study, we aimed to characterize and generate a miRNA-free cell that potentially can be used for miRNA functional analysis in cardiomyocytes. Our results show that Dgcr8 KO ESCs proliferate slower and are lacking a large population of small RNA species ranging from 4-40 bp, including mature miRNAs (~20 bp). However, Dgcr8 KO ESCs are unable to undergo cardiogenic differentiation. Furthermore, we observed that centromeric regions of KO ESCs have a higher transcriptional activity upon induction of differentiation as compared to WT controls. Therefore, Dgcr8 KO ESCs are unable to fully inactivate their heterochromatin regions like WT ESCs, which is likely leading to the defect in cardiac differentiation.

Consistent with a previous study, we found that Dgcr8 KO ESCs exhibit slower proliferation rates. It has been shown that the miR-290 family is involved in the regulation of ESC proliferation [34] and overexpression of this family could partially rescue the proliferation defect of Dgcr8 KO ESCs [34]. Additionally, we observed a defect in cardiomyogenic differentiation in the Dgcr8 KO ESCs, as shown by the lack of spontaneous contraction and absence of myogenic differentiation markers which agree with previous observation that Dgcr8 KO ESC is not capable to form teratoma [34]. Dicer is also involved in miRNA processing, which is downstream of Dgcr8. Similar to Dgcr8 KO ESCs, Dicer KO ESCs display a similar phenotype [27], but show a more pronounced defect in heterochromatin silencing even before differentiation [27].

How and if microprocessors like Dgcr8 or Dicer control ESC differentiation through miRNA processing is not known. Although a lack of miRNA processing seems the most obvious explanation for the defect in differentiation, more and more studies point to a miRNA biogenesis-independent role of the microprocessor. In fission yeast, which does not have miRNAs, RNAi-mediated heterochromatin silencing has been shown to play important roles in protection of virus invasion and genome integrity. There, RNA transcripts from centromeric chromatin regions are used as a template by the RNA dependent RNA Polymerase (RdRP) to generate dsRNAs which are subsequently processed into short dsRNAs. The short dsRNAs serve as a guide for the RNA-induced Silencing

Complex (RISC) containing Ago-complexes for both Post-Transcriptional Gene Silencing (PTGS) and Chromatin Dependent Gene Silencing (CDGS) [29]. In mammals, small RNAs, that play an important role in silencing genotoxic transposable genetic regions[35, 36], have also been identified, both in ESCs and germ cells [32]. In germ cells, for example, a class of small RNAs called Piwi-associated RNAs (piRNAs), which are longer than miRNAs (26-31 nt), have been shown to play an important role in silencing genotoxic transposable genetic regions [35, 36]. These small RNAs have also been found in ESCs, however, the function of these small RNAs in ESCs is unclear. Before differentiation, centromeric chromatin regions are slightly more open in the Dgcr8 KO cells as shown by Minor and Major satellite RNA semi-quantitative RT-PCR. Upon differentiation, centromeric chromatin regions are inactivated in WT but not in the Dgcr8 KO cells. The functional importance of major satellite RNA transcripts is in line with a recent study, in which manipulation of major satellite RNA completely blocked embryonic differentiation at 2-cell stages [37]. Our results suggest that Dgcr8 might carry a previously unrecognized small RNA related function which is independent of miRNA biogenesis, as was also reported for Dicer [27]. Future studies are needed to fully understand its function during this process and to identify its substrates and working partners [32].

How the defective heterochromatin silencing in Dgcr8 KO ESCs prevents their differentiation into the cardiac lineage is not clear. However, recent studies about LINE1 may shed some lights on this question. LINE1, one of redundant retro-transposon derived RNA species, which are distributed in the heterochromatin regions across the genome, is inactivated upon differentiation. In oocytes, the level of the LINE1 is used to determine which cell will go into apoptosis, a well conserved phenomena called fetal oocyte attrition (FOA) [38]. Oocytes with low LINE1 activity are selected and the ones with high LINE1 levels are eliminated [38]. Interestingly, Dgcr8 KO ESCs show accumulation of LINE-1 and a defect in inactivation of LINE-1 upon cardiac differentiation. It is conceivable that a failure in inactivation of heterochromatin regions in differentiated cells will result in an accumulation of these long transposable transcripts, which thereby trigger an interferon-response via Toll-Like Receptors 8/9 [32]. Interestingly, ESCs and germ cells are still innocent in their TLR-induced interferon response, but once they are differentiated, the cells are no longer tolerant to long dsRNA

stimulation. If the cells fail to inactivate these heterochromatin regions, this control mechanism clears these cells to prevent malignant growths (Figure 5).

Dgcr8 null ESCs have a lower proliferation rate and an absence of cardiomyogenic differentiation. Although a defect in miRNA processing might be a direct mechanism, our results suggest that Dgcr8 is also involved in heterochromatin silencing, thereby adding another dimension to gene regulation at the epigenetic level. Furthermore, this dual role of Dgcr8 suggests that previous reported defects in Dgcr8 conditional KO mice could, in addition to a loss of small RNA biogenesis, may also be related to heterochromatin maintenance
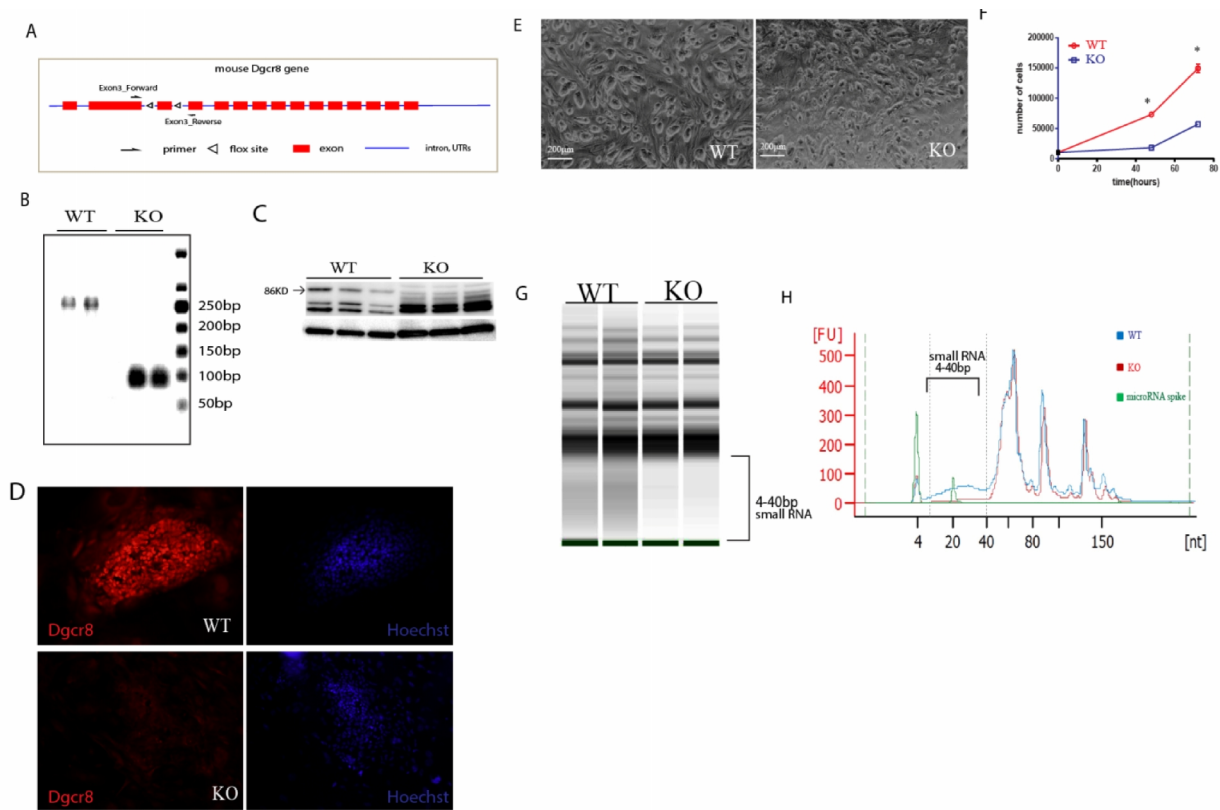
Figure 1. Characterization of Dgcr8 KO mouse embryonic stem cell. A. Illustration of the mouse Dgcr8 gene, including the locations of 2 flox sites that were used for gene targeting and the design of genotyping primers, as used in figure 1C. B. Validation of the loss of Dgcr8 protein in the Dgcr8 KO-ESCs by Western blotting. C. Genotyping of WT and KO ESCs with primers franking exon2 and exon4. WT display a band at 248 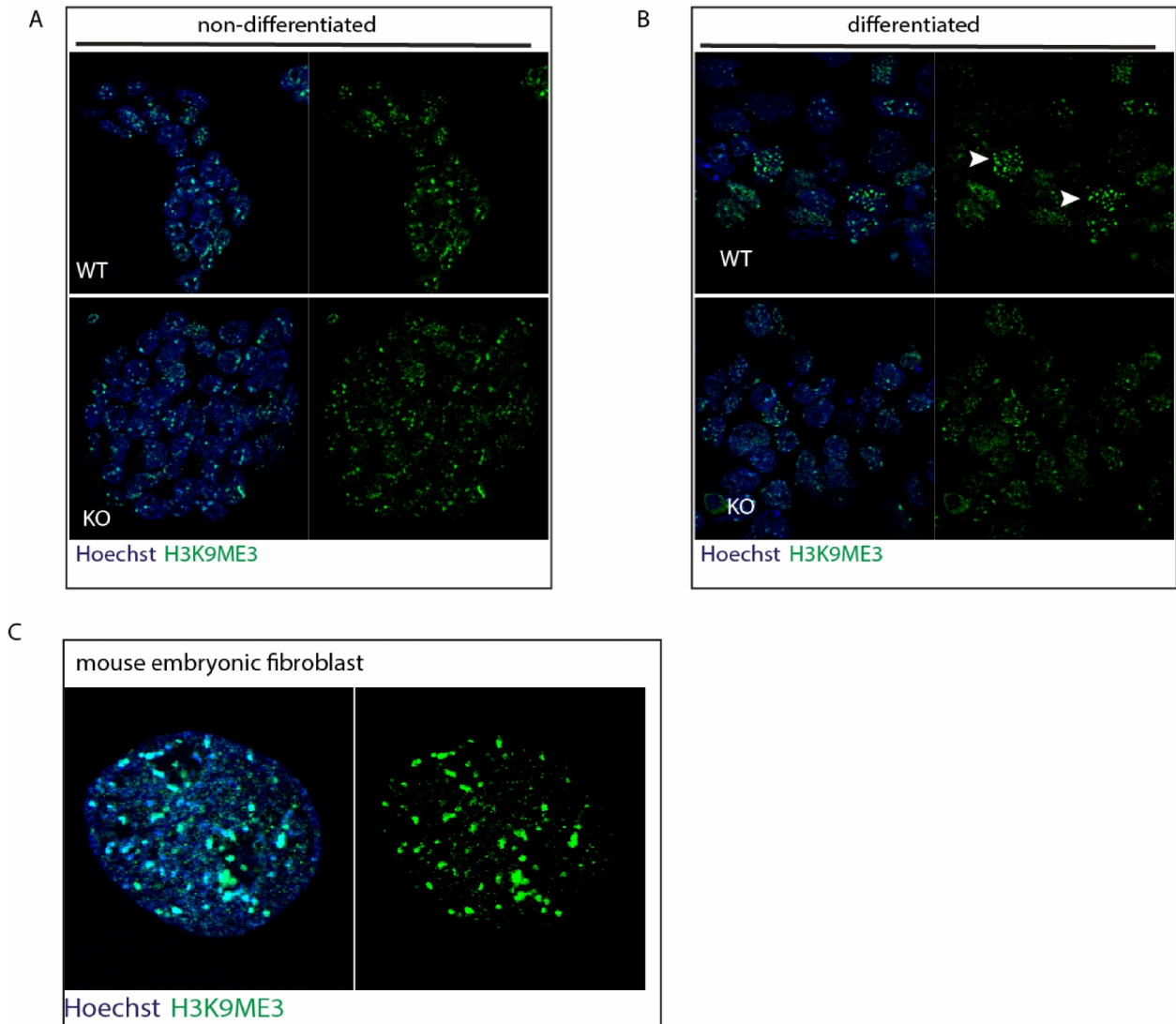bp and KO at 100bp. D. Immunofluorescent staining of Dgcr8 on WT and KO ESC colonies. Note the nuclear staining of dgcr8 in the WT colony. E. Representative images of WT and Dgcr8 KO ESCs in culture. F. Comparison of WT and Dgcr8 KO ESC proliferation rate in culture. G. Representative images of total RNA profiles from WT and Dgcr8 KO ESCs using bioanalyzer 2100. Note the absence of small RNA species in Dgcr8 KO ESCs, ranging from 4-40 nt long. F. Histogram of the profiles of the total RNA from WT and Dgcr8 KO ESCs using bioanalyzer 2100. Note the absent of small RNA species in Dgcr8 KO ESCs ranging from 4-40 nt long.
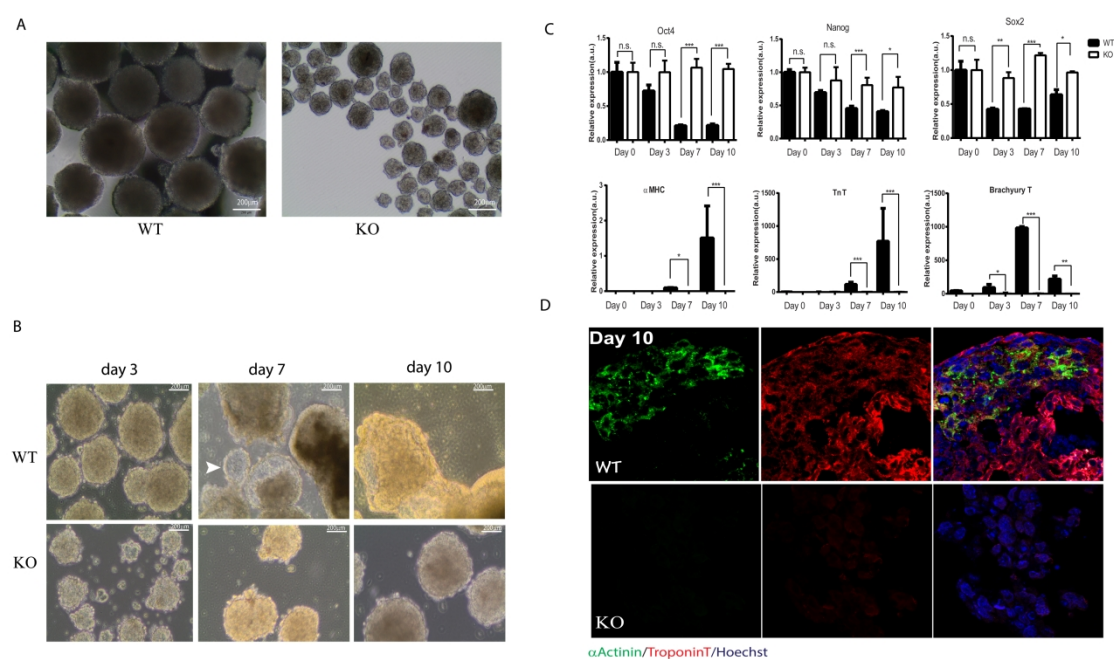
Figure 2. Dgcr8 KO ESCs are defect in cardiogenic differentiation. A. Morphology of WT and Dgcr8 KO EBs, note the irregular shape/size of Dgcr8 KO EBs. B. Morphology of WT and Dgcr8 KO EBs 3, 7 and 10 days after initiation of differentiation. Note Dgcr8 KO EBs are smaller, and lack of cyst-like structures which are present in WT EBs after 7 and 10 days differentiation. C. qPCR analysis of Oct4, a stem cell pluripotency marker, and differentiation marker Brachyury T, Troponin T (TnT) and αMHC. D. Immunofluorescent staining for cardiac marker α-Actinin and Troponin T in WT and KO cells after 10 days of differentiation.

Figure 3. Dgcr8 KO ESC are deficient in heterochromatin silencing during differentiation. A. H3K9ME3 immunofluorescent staining on non-differentiated WT and KO ESC. B. H3K9ME3 immunofluorescent staining on 7 days differentiated WT and KO ESCs. Note the H3K9ME3 condense staining in the different WT cells, as indicated with white arrows which is absent in the Dgcr8 KO ESCs. C. H3K9ME3 immunofluorescent staining on mouse embryonic fibroblast served as a positive control.
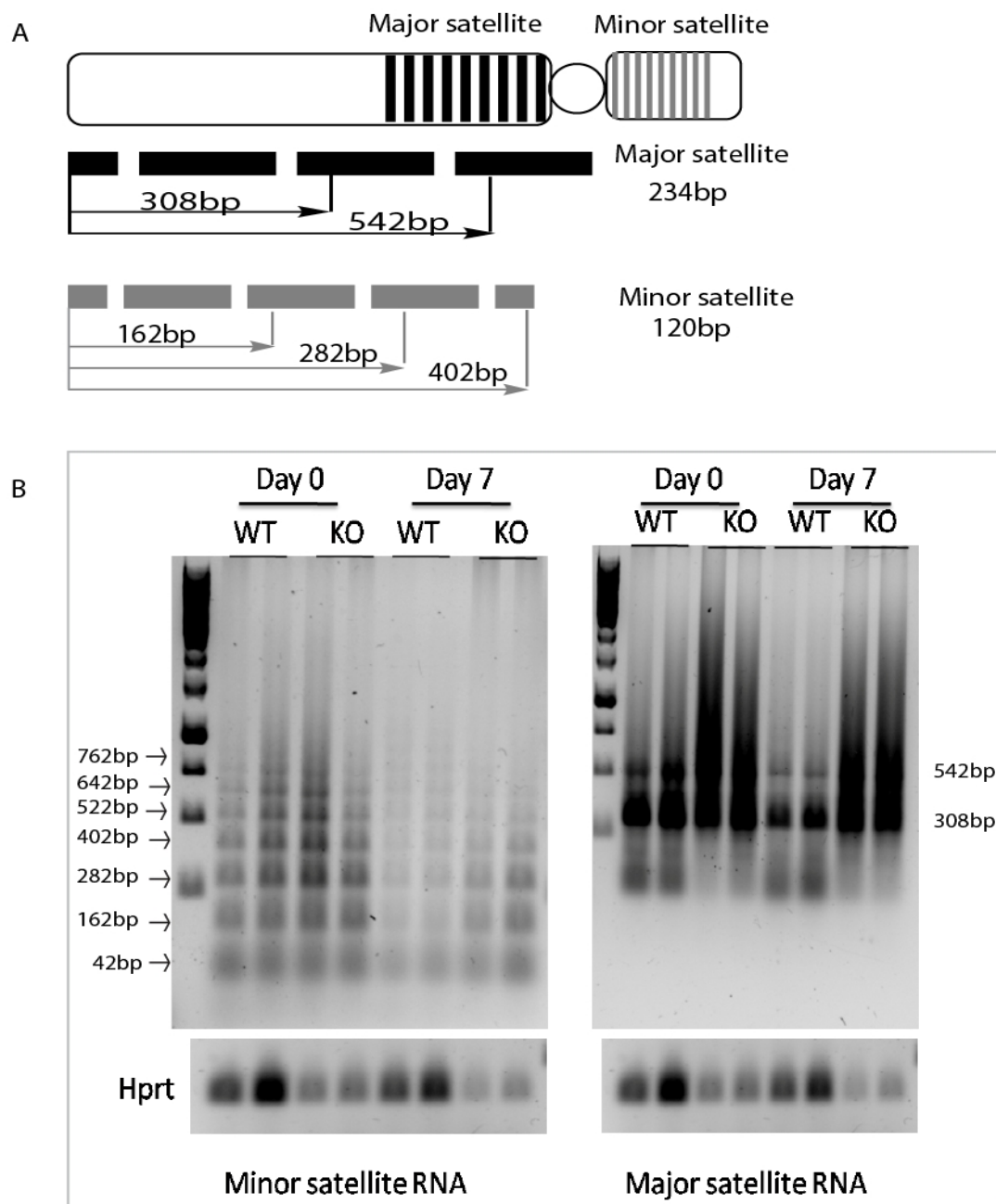
Figure 4. Semi-quantitative RT-PCR analysis from centromeric minor satellite RNA and major satellite RNA species. A. Illustration of the Major and Minor satellite repeat, including the different lengths of the fragment of PCR amplicons. B. RT-PCR products using Minor and Major satellite transcription specific primers to detect Minor and Major satellite RNA transcripts. PCR products are separated on DNA agarose gels with Hprt as input control.
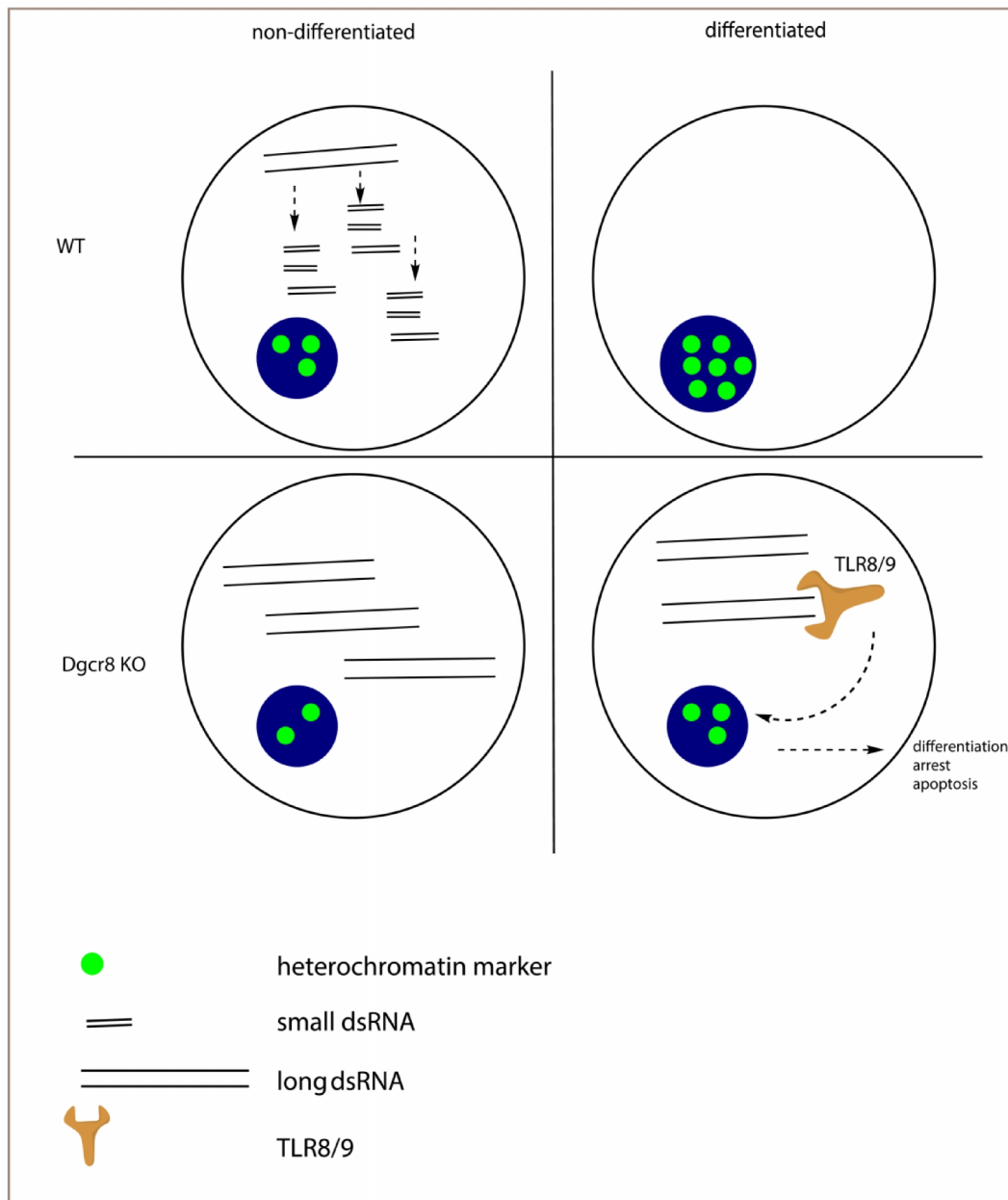
Figure 5. A working model for Dgcr8 in ESC heterochromatin silencing. Before differentiation, both WT and KO ESCs can maintain proper genome structure with moderate heterochromatin. However, KO ESCs are lacking a large population of small RNAs. Upon differentiation, in WT ESCs the endo-siRNA is blocked while KO cells are defective in this heterochromatin inactivation, which results in accumulation of long dsRNA. Long dsRNAs activate the interferon response via TLR8/9, leading to an arrest in differentiation and apoptosis.

Reference

1.   Sluijter, J.P., et al., MicroRNA-1 and -499 regulate differentiation and proliferation in human-derived cardiomyocyte progenitor cells. Arterioscler Thromb Vasc Biol, 2010. **30**(4): p. 859-68.

2.   van Mil, A., et al., MicroRNA-1 enhances the angiogenic differentiation of human cardiomyocyte progenitor cells. J Mol Med (Berl), 2013. **91**(8): p. 1001-12.

3.   Cai, B., et al., microRNA-124 regulates cardiomyocyte differentiation of bone marrow-derived mesenchymal stem cells via targeting STAT3 signaling. Stem Cells. **30**(8): p. 1746-55.

4.   Glass, C. and D.K. Singla, MicroRNA-1 transfected embryonic stem cells enhance cardiac myocyte differentiation and inhibit apoptosis by modulating the PTEN/Akt pathway in the infarcted heart. Am J Physiol Heart Circ Physiol. **301**(5): p. H2038-49.

5.   Chen, J.F., et al., The role of microRNA-1 and microRNA-133 in skeletal muscle proliferation and differentiation. Nat Genet, 2006. **38**(2): p. 228-33.

6.   Takaya, T., et al., MicroRNA-1 and MicroRNA-133 in spontaneous myocardial differentiation of mouse embryonic stem cells. Circ J, 2009. **73**(8): p. 1492-7.

7.   Callis, T.E., et al., MicroRNA-208a is a regulator of cardiac hypertrophy and conduction in mice. The Journal of clinical investigation, 2009. **119**(9): p. 2772-86.

8.   Care, A., et al., MicroRNA-133 controls cardiac hypertrophy. Nature medicine, 2007. **13**(5): p. 613-8.

9.   Fiedler, J., et al., MicroRNA-24 regulates vascularity after myocardial infarction. Circulation. **124**(6): p. 720-30.

10.   Gurha, P., et al., Targeted deletion of microRNA-22 promotes stress-induced cardiac dilation and contractile dysfunction. Circulation. **125**(22): p. 2751-61.

11.   Ganesan, J., et al., MiR-378 controls cardiac hypertrophy by combined repression of mitogen-activated protein kinase pathway factors. Circulation, 2013. **127**(21): p. 2097-106.

12.   van Rooij, E., et al., A signature pattern of stress-responsive microRNAs that can evoke cardiac hypertrophy and heart failure. Proceedings of the National Academy of Sciences of the United States of America, 2006. **103**(48): p. 18255-60.

13.   Matkovich, S.J., et al., RISC RNA sequencing for context-specific identification of in vivo microRNA targets. Circ Res, 2011. **108**(1): p. 18-26.

14.   Karginov, F.V., et al., A biochemical approach to identifying microRNA targets. Proc Natl Acad Sci U S A, 2007. **104**(49): p. 19291-6.

15.   Cesana, M., et al., A long noncoding RNA controls muscle differentiation by functioning as a competing endogenous RNA. Cell, 2011. **147**(2): p. 358-69.

16.   Tay, Y., J. Rinn, and P.P. Pandolfi, The multilayered complexity of ceRNA crosstalk and competition. Nature, 2014. **505**(7483): p. 344-52.

17.   Tomari, Y. and P.D. Zamore, MicroRNA biogenesis: drosha can't cut it without a partner. Curr Biol, 2005. **15**(2): p. R61-4.

18.   Yi, R., et al., Exportin-5 mediates the nuclear export of pre-microRNAs and short hairpin RNAs. Genes Dev, 2003. **17**(24): p. 3011-6.

19.   Bohnsack, M.T., K. Czaplinski, and D. Gorlich, Exportin 5 is a RanGTP-dependent dsRNA-binding protein that mediates nuclear export of pre-miRNAs. RNA, 2004. **10**(2): p. 185-91.

20.   Jiang, F., et al., Dicer-1 and R3D1-L catalyze microRNA maturation in Drosophila. Genes Dev, 2005. **19**(14): p. 1674-9.

21.   Chendrimada, T.P., et al., TRBP recruits the Dicer complex to Ago2 for microRNA processing and gene silencing. Nature, 2005. **436**(7051): p. 740-4.

22.   Chen, Z., et al., DiGeorge syndrome critical region 8 (DGCR8) protein-mediated microRNA biogenesis is essential for vascular smooth muscle cell development in mice. J Biol Chem, 2012. **287**(23): p. 19018-28.

23.   Wang, Y., et al., DGCR8 is essential for microRNA biogenesis and silencing of embryonic stem cell self-renewal. Nat Genet, 2007. **39**(3): p. 380-5.

24. Yi, R., et al., DGCR8-dependent microRNA biogenesis is essential for skin development. Proc Natl Acad Sci U S A, 2009. **106**(2): p. 498-502.

25. Rao, P.K., et al., Loss of cardiac microRNA-mediated regulation leads to dilated cardiomyopathy and heart failure. Circ Res, 2009. **105**(6): p. 585-94.

26. Buikema, J.W., et al., Wnt/beta-catenin signaling directs the regional expansion of first and second heart field-derived ventricular cardiomyocytes. Development, 2013. **140**(20): p. 4165-76.

27. Kanellopoulou, C., et al., Dicer-deficient mouse embryonic stem cells are defective in differentiation and centromeric silencing. Genes Dev, 2005. **19**(4): p. 489-501.

28. Murchison, E.P., et al., Characterization of Dicer-deficient murine embryonic stem cells. Proc Natl Acad Sci U S A, 2005. **102**(34): p. 12135-40.

29. Buhler, M. and D. Moazed, Transcription and RNAi in heterochromatic gene silencing. Nat Struct Mol Biol, 2007. **14**(11): p. 1041-8.

30. Macias, S., et al., DGCR8 HITS-CLIP reveals novel functions for the Microprocessor. Nat Struct Mol Biol, 2012. **19**(8): p. 760-6.

31. Heras, S.R., et al., The Microprocessor controls the activity of mammalian retrotransposons. Nat Struct Mol Biol, 2013. **20**(10): p. 1173-81.

32. Babiarz, J.E., et al., Mouse ES cells express endogenous shRNAs, siRNAs, and other Microprocessor-independent, Dicer-dependent small RNAs. Genes Dev, 2008. **22**(20): p. 2773-85.

33. Fodor, B.D., et al., Jmjd2b antagonizes H3K9 trimethylation at pericentric heterochromatin in mammalian cells. Genes Dev, 2006. **20**(12): p. 1557-62.

34. Wang, Y., et al., Embryonic stem cell-specific microRNAs regulate the G1-S transition and promote rapid proliferation. Nat Genet, 2008. **40**(12): p. 1478-83.

35. Riedmann, L.T. and R. Schwentner, miRNA, siRNA, piRNA and argonautes: news in small matters. RNA Biol, 2010. **7**(2): p. 133-9.

36. Chuma, S. and T. Nakano, piRNA and spermatogenesis in mice. Philos Trans R Soc Lond B Biol Sci, 2013. **368**(1609): p. 20110338.

37. Casanova, M., et al., Heterochromatin reorganization during early mouse development requires a single-stranded noncoding transcript. Cell Rep, 2013. **4**(6): p. 1156-67.

38. Malki, S., et al., A role for retrotransposon LINE-1 in fetal oocyte attrition in mice. Dev Cell, 2014. **29**(5): p. 521-33.

39. Andersen, C.L., J.L. Jensen, and T.F. Orntoft, Normalization of real-time quantitative reverse transcription-PCR data: a model-based variance estimation approach to identify genes suited for normalization, applied to bladder and colon cancer data sets. Cancer Res, 2004. **64**(15): p. 5245-50.

A

B

Gene name	Stability value	Standard error
Hprt	0.082	0.030
βActin	0.097	0.031
Gapdh	0.037	0.048

C

D

Hnf4α

E

F
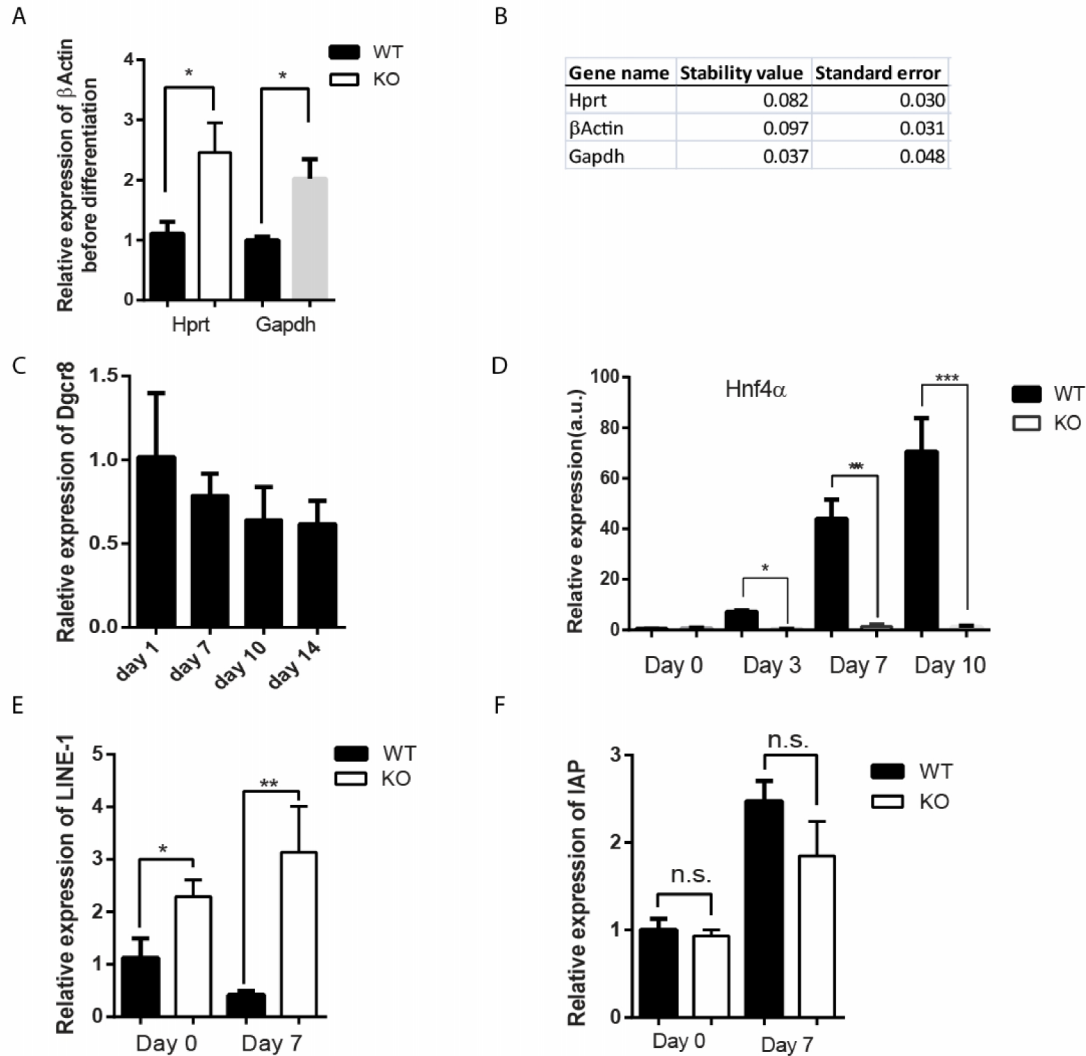
Supplement figures A. The expression of β-Actin in WT and KO ESC normalized by Hprt and Gapdh. B. The stability of Hprt, β-Actin and Gapdh as a housekeeping during WT and KO ESC differentiation as analyzed using Normfinder [39]. C. The expression Dgcr8 during differentiation in WT ESC. D. The expression of Hnf4a during differentiation in WT and KO ESC. E. The expression of LINE-1 before and after differentiation. F. The expression of IAP before and after differentiation.

Chapter 4

MicroRNA-132/212 family enhances arteriogenesis after hindlimb ischemia through modulation of the Ras-MAPK pathway

Zhiyong Lei[1], Alain van Mil[1], Maarten M. Brandt[3], Sebastian Grundmann[5], Imo Hoefer[1], Michiel Smits[1], Hamid el Azzouzi[1], Taru Fukao[2], Caroline Cheng[3, 4], Pieter A. Doevendans[1,6] and Joost. P.G. Sluijter[1,6*]

1. Department of Cardiology, Division Heart and Lungs, University Medical Center Utrecht, Utrecht, the Netherlands
2. Max Planck Institute of Immunobiology and Epigenetics, Freiburg, Germany
3. Experimental Cardiology, Erasmus Medical Center, the Netherlands
4. Nephrology &Hypertension, University Medical Center Utrecht, the Netherlands
5. Department of Cardiology and Angiology I, University Heart Center Freiburg - Bad Krozingen, Freiburg, Germany
6. ICIN, Netherlands Heart Institute, Catharijnesingel 52, 3511 GC Utrecht, the Netherlands

Abstract

Background: Arteriogenesis is a complicated process induced by increased local shear-and radial wall-stress, leading to an increase in arterial diameter. This process is enhanced by growth factors secreted by both inflammatory and endothelial cells in response to physical stress. Although therapeutic promotion of arteriogenesis is of great interest for ischemic diseases, little is known about the modulation of the signaling cascades via microRNAs.

Methods and Results: We observed that miR-132/212 expression was significantly upregulated after occlusion of the femoral artery. miR-132/212 knockout(KO) mice display a slower perfusion recovery after hind-limb ischemia compared to wild type (WT) mice. Immunohistochemical analysis demonstrates a clear trend towards smaller collateral arteries in KO mice. Although Ex vivo aortic ring assays score similar number of branches in miR-132/212 knockout mice compared to WT, it can be stimulated with exogenous miR-132, a dominant member of the miR-132/212 family. Moreover, in in vitro pericyte-endothelial co-culture cell assays, overexpression of miR-132 and mir-212 in endothelial cells results in enhanced vascularization, as shown by an increase in tubular structures and junctions. Our results suggested that miR-132/212 may exert their effects by enhancing the Ras-MAPK signaling pathway through direct inhibition of Rasa1, and Spred1.

Conclusions: the miR-132/212 cluster promotes arteriogenesis by modulating Ras-MAPK signaling via direct targeting of its inhibitors Rasa1 and Spred1.

Keywords:

miR-132/212, arteriogenesis, Ras-MAPK, hindlimb ischemia

Introduction

Under physiological circumstances, normal adult blood vessels stay quiescent by using various inhibitors to counteract pro-angiogenic signal fluctuation [1]. Dysregulation of this balance may cause diseases such as capillary and arterio-venous malformations [2]. However, under ischemic conditions, the compensatory growth of blood vessels is an appreciated response, which can be achieved in two ways: by branching from existing vessels (called angiogenesis), or by enlargement of pre-existing collaterals (termed arteriogenesis) [3]. The increase in diameter via arteriogenesis weights much more than the number of newly formed capillaries via angiogenesis and has therefore the potential to become a future therapeutic approach [4]in chronic and acute ischemic diseases. Many attempts have been made to modulate the pro- and anti-arteriogenic balance [5-7]. However, effective therapeutic approaches to promote arteriogenesis are still lacking.

Initial studies have shown an important role for microRNAs (miRNAs) in neovascularization [8-14], but a clear understanding of all players involved is still lacking. It has previously been shown that miR-132 is upregulated in endothelial cells by various pro-angiogenic stimuli such as hypoxia[15], VEGF [10, 15], and angiotensin II [16].Overexpression of miR-132 in HUVECs promoted proliferation and migration *in vitro,* and transplanting these cells promoted vascularization *in vivo* [17]. In cancer, miR-132 promoted angiogenesis by suppressing one of the GTPase-activating proteins, called RASA1 [10]. Very Low Density Lipoprotein Receptor (*Vldlr*) knockout mice, displayed an aberrant neovascularization in the retina, associated with increased expression of miR-132. Moreover, inhibition of miR-132 in the retina could reduce aberrant neovascularization[18] or corneal neovascularization [19]. Although, the role of this microRNA family was explored for angiogenesis, its influence on hind-limb ischemia induced arteriogenesis has not been explored. In this study, we combine *in vitro* assays and *in vivo* animal models to explore the role of miR-132/212 in vascular growth during arteriogenesis and to unravel the underlying mechanism.

Materials and Methods

Generation and genotyping of miR-132/212 KO mice

The generation of miR-132/212 KO mice has been described as previously [20]. For genotyping, DNA samples were obtained by ear clipping and used in a GC-Rich PCR kit (Roche, cat. 12140306001) with the MiR-132/212 primers as shown in the supplementary table 1. PCR product were revealed on a 1% agarose gel: WT genotype shows a predicted band at 1076 bp and the KO genotype at 392 bp.

Hind-limb ischemia

This study was approved by the Animal Ethical Experimentation Committee(Utrecht University) and was carried out in accordance with the Guide for the care and use of Laboratory Animals. Hind-limb ischemia was applied on 10-12 week old mice (10 WT (C57B6) and 13 miR-132/212 KO) as described previously[21]. In brief, mice were anesthetized with fentanyl (0.05mg/kg), midazolam(5mg/kg) and medetomidine (0.5mg/kg) by intraperitoneal injection and surgical procedures were performed under sterile conditions. A vertical longitudinal incision was made in the right hind-limb and the femoral artery was dissected. To achieve slower recovery, ligation was performed using an electricoagulator at the most proximal position and thereby separating them into two parts. After closure, mice received atipamezole (2.5mg/kg) and flumazenil (0.5mg/kg) to recover. Temgesic (0.1mg/kg) was given every 8 hours after surgery for 6 times. Measurement of blood flow was performed by scanning both rear paws with an LDI analyzer (Moor Infrared Laser Doppler Imager Instrument, Wilmington, Delaware), before and after the surgical procedure (days 0, 4, 7, and 14). During the procedure, the animal was kept under 2% isoflurane anesthesia and its body temperature was strictly maintained between 36.5°C- 37.5°C. The images obtained were quantitatively converted into histograms with Moor LDI processing software as described before [22]. Data were reported as the ratio of blood flow in the right over left (R/L) hindlimb.

MicroRNA in situ hybridization

The procedure for microRNA *in situ* hybridization has been described previously with slight modification [23]. Cryosections were fixed by 4% paraformaldehyde for 10 min, acetylated for 10 min

followed with 10 min proteinase K treatment (10 μg/ml). Hybridization was performed following manufacturer's suggestions with DIG labeled miRCURY LNA miRNA detection probes (Exiqon) for miR-132 (38031-15), negative control miR-159 (99003-15) and positive control U6 (99002-15). Sections were subsequently blocked for 1h before overnight incubation with anti-DIG alkaline phosphatase antibody (1:1,500, Roche). To block endogenous alkaline phosphatase activity, sections were incubated with levamisole solution (DAKO), followed by Liquid Permanent Red (DAKO) incubation for visualization. Blood vessels were stained with lectin BS-1 (1:100, Sigma). Nuclei were stained with Hoechst 33342 (Life Technologies). Images were taken by Zeiss LSM710 and analyzed using Zen2012 (Zeiss).

RNA isolation and RT-PCR

DNA-free RNA was extracted with Tripure (Roche applied science). To perform qPCR for gene expression RNA is transcribed to cDNA using the iScript cDNA Synthesis Kit (Bio-Rad) according to manufacturer's instructions, and quantitative real-time polymerase chain reaction was performed on a MyIQ single-color qRT-PCR system (Bio-Rad) as described previously [24].All the primers used for qPCR analysis are listed in the supplementary table 1.Mature miR-132 and miR-212 expression levels were measurement by TaqMan® MicroRNA Assay following manufactory's instruction, using U6 as control.

Immunofluorescent staining

The following primary antibodies were used: Rasa1 (clone B4F8, ab2922, Abcam 1:100), Spred1 (Millipore, ABS186, 1:500), Spry1 (Cell signaling, 13013, 1:500), αSMA-FITC (Sigma, F3777, 1:400), followed by secondary antibodies goat anti-mouse and goat anti-rabbit Alexa 555 (Life technologies, 1:500) for detection. In brief, tissues were imbedded in Tissue-Tek® O.C.T™ (SAKURA) and sectioned to 7 μm thick slices. For the Spred1 and spry1 staining, sections were fixed with cold methanol and subsequently blocked with 10% normal goat serum plus 2% BSA in TBST, containing 0.1% tween 20. Then sections were incubated with primary antibodies diluted in 0.5% BSA in TBST overnight at 4°C. Before incubation with a secondary antibody, slides were washed three

times for 10 min each. For RASA1, sections were first cleared with 1% tween for 30 min, then blocked with affini-pure Fab fragment goat anti-mouse IgG (Jackson immunoresearch laboratory, 115-007-003, 100 µg/ml) with 10% normal goat serum. Anti-RASA1 antibody was diluted in 0.5% BSA in TBST, applied on the sections overnight at 4˚C, followed by biotin-sp-conjugated affini-pure Fab fragment goat anti-mouse IgG(H+L) (Jackson immunoresearch laboratory, 115-067-003, 1:500) and streptavidin-conjugated Alexa 555. Images were taken by Zeiss LSM700 and analyzed using ZEN 2012 software (Zeiss)

Western blotting

The following primary antibodies were used for western blotting: Rasa1 (clone B4F8, ab2922, Abcam 1:200), Spred1 (Millipore, ABS186, 1:1000), Spry1 (Cell signaling #13013, 1:1000), β-actin (Sigma, 1:15000), p44/42 MAPK(ERK1/2) (Cell Signaling #9102, 1:1000), phosopho-p44/42 MAPK(ERK1/2) (Cell Signaling#9101, 1:1000). Adductor muscles were lysed with EDTA-free lysis buffer (Roche Applied Science, Cat.04719964001) with 1x protease/phosphatase inhibitor cocktail (Cell Signaling, #5872). Protein concentrations were measured with BCA protein assay kit (Thermo Scientific, 23227), separated with NuPAGE bis-tris Precast gels (Life Technologies), and transferred to PVDF membrane with an iblot western blotting system (Life Technologies), according the manufacturer's instructions. Membranes were first blocked with 5% blotting grade blocker (Bio-Rad #170-6404) with exception of the detection of phosoph-ERK1/2 in which 5% BSA was used. After washing, HRP-conjugated secondary antibody was used for ECL detection (Sigma).

Aortic Ring Assay

Aortas from both WT and miR-132/212 KO mice were surgically isolated, cleaned, dissected into 0.5 mm segments and embedded into fibrin as described before [25]. For rescue, aortic ring segments were transfected overnight either with 50 nmol/L microRNA mimics as indicated by siPORT NeoFX prior to embedding. 25 ng/ml recombinant mouse vascular endothelial cell growth factor (VEGF164) (R&D, 493-MV-005) was added and replaced on day 4. Pictures were taken on day 7 and the number of branches were counted under an inverted microscope.

Cell culture and transfection

Human umbilical venous endothelial cells (HUVECs)(Lonza) were cultured in EGM2 according to manufacturer's instructions, and all experiments were performed before passage 7. HUVECS were transfected with either 20 nmol/L Spred1 (s46287), Spry1 (s20026), Rasa1 (120290), Silencer select negative control#1 (4390843), or with mirVana miRNA mimic negative control (4464085), hsa-miR-132-3p mimics (MC10166), hsa-miR-212-3p mimics (MC10340), mirVana miRNA inhibitor negative control1 (4464077), hsa-miR-132-3p inhibitor (AM10166), hsa-miR-212-3p inhibitor (AM10340), using Lipofectamine 2000 (all from Life technologies).

3'-untranslated region (3'-UTR) reporter generation and luciferase assay

A 1 kb fragment, which flanks conserved miR-132-binding sequences of the *spred1* 3'-untranslated region (UTR), and the full-length *Spry1* 3-'UTR were cloned into the pMIR-REPORT Luciferase vector (Ambion), as described previously [23]. Mutations in the seed-region were generated by Q5 Site-Directed Mutagenesis kit (New England Biolabs). All the primers used for cloning and mutagenesis are listed in the supplementary table 1. To determine suppression efficiency of miR-132 and 212 on these targets, HEK293 cells were co-transfected with 200 ng of pMIR-REPORT- 3'-UTR Luciferase vectors, or one of the mutated vectors, and a pMIR-REPORTβ-gal control plasmid to normalize for transfection efficiency. In addition, 25 nmol/L miR mimic controls, miR-132 mimics, or miR-212 mimics were introduced by using Lipofectamine 2000 (Life Technologies). Luciferase and β-

galactosidase activity was assessed after 48h with the Luciferase Assay System and β-galactosidase Enzyme Assay System (both from Promega), respectively, as previously described [24].

In vitro angiogenesis assay

Human Umbilical Vein Endothelial Cells (HUVECs; Lonza) and Human Brain Vascular Pericytes (HBVPs; Sciencell #1200) were cultured on gelatin-coated plates in EGM2 medium (EBM2 medium supplemented with EGM2 bullet kit and 2% FCS; Lonza) and DMEM (10% FCS; Lonza), respectively, in 5% CO_2 at 37˚C. Lentiviral transfected HUVECs expressing green fluorescent protein (GFP) and pericytes were used at passage 6-8. miR-132 and miR-212 were inhibited or enhanced in HUVECs only, either by using anti-miR-132 and anti-miR-212, or by supplementing miR-132 mimics and miR-212 mimics, respectively. Control cells were transfected with non-targeting miR and anti-miR controls. In order to monitor the effects of miR-132 and miR-212 in angiogenesis, transfected HUVEC-GFP and PKH26 stained pericytes were suspended in a 2.5 mg/ml collagen type I (BD Biosciences) as described by Stratmani[26]. Co-cultures were imaged after 96h incubation in 5% CO_2 at 37 ˚C by fluorescence microscopy, thereby acquiring 4 planes of images, followed by 3D-analysis using a commercial analysis system (Angiosys, Buckingham, UK).

Phospho-ERK1/2 Bio-PlexPro^{TM} assay

In brief, 48 hours after transfection of indicated siRNAs or microRNA mimics, EGM2 was removed and replaced with EBM2 for 3 hours to starve the HUVECs. Subsequently, 25 ng/ml recombinant human VEGF165 (R&D, 293-E-010) was added and cells were harvested at indicated time points and lysed with EDTA-free lysis buffer (Roche Applied Science, Cat. 04719964001) with 1x protease/phosphatase inhibitor cocktail (Cell Signaling, #5872). Protein concentrations were measured with the BCA protein assay kit (Thermo Scientific, 23227) and diluted into 200 µg/ml. Phospho-ERK1/2 Bio-PlexPro^{TM} assay was performed according to the manufacture's instruction. Of each sample, 100 µl was incubated with capture antibodies (Bio-Rad, 171-v50006M, 171-v60003M), and after washing, streptavidin-PE was applied for visualization. Samples were processed with the Bio-plex 200 (Bio-Rad) and data was analyzed with Bio-Plex Data Pro software (Bio-Rad) and Graphpad Prism 6.0.

Data was analyzed using Graphpad Prism 6 and comparisons were performed with t-test or paired t-test between two groups, and ANOVA for multiple comparisons. Data are presented as mean ± SEM. P-values are indicated as follows: *$p<0.05$; **$p<0.01$;***$p<0.001$, $p<0.05$ is considered as significant.

Results

MiRNA-132 and miR-212 is upregulated upon hind-limb ischemia

To understand the function of miR-132 and miR-212 in arteriogenesis, we performed hind-limb ischemia on wild-type (WT) mice and checked the expression of these two microRNAs in the thigh muscle at different time points after hind-limb ischemia. By quantitative reverse-transcriptase polymerase chain reaction (qRT-PCR), we found that miR-132 and miR-212 levels were significantly increased on day 4 and day 7 (Figure1A and B) after hindlimb ischemia in the adductor muscle.

The miR-132/212 locus is positioned in the first intron of the human 1700016p03 gene, whose function remains to be investigated. miR-132 and 212 are transcribed as a single transcript and further processed into two mature microRNAs, which are highly conserved among different species (Supplementary Figure 1A). Although these two miRNAs share the same seed sequences and hereby belong to the same miRNA family, the level of mature miR-132 expression is significantly higher than that of miR-212 in the thigh muscle, indicating that miR-132 might be more active in the arteriogenic response, as previously reported for miR-212 being a more dominant miRNA in angiogenesis.(Figure 1A).

To further understand its function, we analyzed which cell types express miR-132 in hind-limb tissue by *in situ* hybridization. As expected, we found that miR-132 is expressed in endothelial cells (lectin BS-1 positive cells) of blood vessels and in cells surrounding the endothelial cell layer in WT mice only (Fig S1B).

MicroRNA-132/212 is involved in arteriogenesis after hindlimb ischemia

The increased expression upon hindlimb ischemia and the vascular localization of miR-132 suggests that miR-132 may play a role in vascular growth, for example, in arteriogenesis. To test this, we compared the arteriogenic response between WT and KO mice. Blood flow perfusion ratio in the miR-132/212 knockout mice was significantly lower compared to their WT litters at day 7 and 14 as measured by laser Doppler (Figure 2A and 2B), indicating a slower perfusion restoration. The total number of alpha-smooth muscle actin (αSMA) positive vessels in the adductor muscle was similar between WT and KO mice (Figure 2C), but there is a clear trend towards smaller collateral arteries in KO mice, as determined by the cross-sectional diameter of αSMA-positive arteries (Figure2D + E).

miR-132/212 promotes endothelial cells neovascularization responses *in vitro*

To further investigate the effect of microRNA-132/212 on vascular growth, we modulated miR-132/212 activity with overexpression or inhibition approaches in different *in vitro* neovascularization assays.

Firstly, we performed WT and miR-132/212 KO mice-derived aortic ring assay [25]. In the growth factor rich environment, we observed a slight decrease in the number of branches in aortic rings from KO mice compared to WT control. Interestingly, transfection of miR-132 mimics rescued, and even significantly enhanced activation via increasing vascular branching. Although similar effect were observed with miR-212, the effects were less pronounced as compared with miR-132.(FigureS1C and D).

Secondly, we performed a HUVEC and pericyte co-culture assay, thereby better mimicking the *in vivo* situation by taking the interplay between endothelial cells and pericytes into account [26]. As shown in Figure 3A, supplementing miR-132 and miR-212 mimics to HUVECs enhanced the total number of junctions, tubules, and tubule length compared to that of miR controls. Conversely, inhibiting miR-132 and miR-212 using anti-miRs resulted in some decline in the total number of junctions, tubules, and tubule length (Figure 3B).

***Spred-1, Spry1* and *Rasa1* are direct targets of the microRNA-132/212 family**

Based on Ago-Hits-clip [27], PAR-CLIP [28] and CLASH studies [29] and our results above, we

decided to focus on targets related to growth factor signaling. In combination with bioinformatics

target site prediction algorithms (Targetscan), we selected *Rasa1*, *Spred1* and *Spry1* which have a high

prediction context score and are conserved among species, as shown in Figure 4A and 4D. Since

Rasa1 was already a confirmed miR-132 target [10], we only cloned the 3'-UTR of *Spred1* and *Spry1*

into a luciferase reporter vector and analyzed whether miR-132 and miR-212 could suppress luciferase

activity in HEK293 cells. We found that both miR-132 and miR-212 can significantly suppress the

Spred1-3'UTR and *Spry1*-3'UTR luciferase activity at 25nm/L, compared with scramble control

miRNAs (Figure 4B and E). Additionally, we performed a dose-response assay with *Spred1*-3'UTR,

Spry1-3'UTR and 3'-UTRs with three mutated nucleotides in indicated binding regions (Figure 4A and

D). Inhibitory effects were dose-dependent and mutations within the seed region significantly affected

the suppressing effects on luciferase activity, even completely abolishing the suppressive effect at a

concentration of 1nm/L (Figure 4C and F).

We next investigated the direct regulation of these targets in HUVEC cells. Following overexpression

of miR-132 and miR-212 in HUVECs in the co-culture assays, we detected reduced levels of Spred1,

Spry1 and Rasa1 protein; while inhibition of the miR-132 and miR-212 led to elevated Spred1, Spry1

and Rasa1 expression. This indicates that these genes are also regulated by miR-132/212 in HUVECs

(Figure 4G and H).

miR-132/212 modulates growth factor-activated Ras-MAPK signaling in HUVECs

Spred1, Spry1 and Rasa1 are known inhibitors of Ras-MAPK signaling and their inhibition can

prolong Ras-MAPK signaling upon growth factor stimulation [30-33]. We therefore tested whether

miR-132/212 could prolong Ras-MAPK signaling by inhibiting *Spred1, Spry1* and *Rasa1* in HUVECs.

Compared with siRNA controls and miR controls, overexpression of miR-132 and miR-212 or

knockdown of *Spred1*, *Spry1*and *Rasa1*, indeed prolonged ERK1/2 phosphorylation (Figure 5A-D).

By using a non-linear one-phase exponential decay model and interpolation of the time of

phosphorylated ERK1/2$T_{1/2}$ to reach 50%, we observed that $T_{1/2}$ was prolonged both by overexpression of miR-132/212 and by knockdown of its targets (Figure 5E).

Spred1, Spry1 and *Rasa1* knockdown promotes endothelial cells neovascularization responses *in vitro*

We have shown that overexpression of miR-132 or miR-212 promotes endothelial cells neovascularization. As microRNA functions by inhibiting its targets, we reason that knockdown of *Spred1, Spry1* and *Rasa1* should have similar effect as overexpression of miR132 and miR-212. As expected, subsequent knockdown of *Spred1, Spry1*, *Rasa1* and a combination of these three via siRNA knockdown in HUVECs (Figure 6C) showed similar neovascularization responses as overexpression of miR-132 or miR-212, total number of junctions, tubules, and tubule length were increased compared to control conditions (Figure 6A-B).

miR-132/212 family modulates Ras-MAPK signaling by targeting *Spred1, Spry1* and *Rasa1in vivo*

We reasoned that if *Spred1, Spry1* and *Rasa1* are *in vivo* targets of miR-132 or 212, they should be expressed in the arteries of the thigh muscle. By immunofluorescent staining, we observed that *Spred1, Spry1* and *Rasa1* could all be detected in the vascular wall (Supplemental Figure 2). By comparing the expression of *Spred1, Spry1* and *Rasa1* in the adductor muscle from WT and KO after femoral artery ligation using Western blot, we observed that Spred1 and Rasa1 are significantly more present in the KO mice (Figure 7A and B). Surprisingly we found that there is no difference in the Spry1 protein between WT and KO mice (Figure 7A and B). Next we asked if higher level of Spred1 and Rasa1 expression could have an effect on the Ras-MAPK pathway. By Western blotting we detected lower phosphorylated ERK1/2 in the area of blood vessel growth in knockout mice14 days after hindlimb ischemia (Figure 7C-D).

Discussion

Here, we show that upregulation of miR-132 and miR-212 upon hindlimb ischemia is involved in the arteriogenic response: microRNA-132/212 KO animals display delayed perfusion restoration upon femoral artery occlusion. Furthermore, we demonstrate that this effect is attributable to miR-132/212 modulation of the Ras-MAPK signaling pathway through direct targeting of *Spred1 and Rasa1*. To the best of our knowledge, this is the first study showing a single microRNA family, and probably mediated via the more abundantly expressed miR-132, that can facilitate the arteriogenic responses by suppressing multiple targets within the Ras-MAPK pathway.

The Ras-MAPK pathway is very important in neovascularization during development and after ischemic challenges. In the developing retina, for example, this physiological pathway only becomes apparent in active sprouting endothelial cells[18]. Reduced ERK1/2 activation leads to reduced lumen formation, whereas excessive activation of ERK1/2 results in larger arteries [34, 35]. Upon ischemic challenge, e.g. in hindlimb ischemia models, shear stress-stimulated endothelial cells induce Monocyte Chemotactic Protein 1(*MCP-1)* expression, which in turn attracts neutrophil granulocytes and macrophages [36]. These circulating inflammatory cells start producing growth factors which eventually activate Ras-MAPK signaling pathway in the smooth muscle cells and endothelial cells further and promote their proliferation and extracellular matrix remodeling. Recently, attempts have been made to interfere in arteriogenesis through manipulation of Ras-MAPK signaling genetically and chemically, for example by suppression of Sproutys to promote blood flow recovery in the hindlimb ischemia model [7]. Since therapeutic activation of Ras-MAPK signaling is still challenging, inhibition of their endogenous inhibitors using microRNA therapeutics holds a great promise as an alternative strategy.

We confirmed that *Rasa1* is a direct target of miR-132 and miR-212, and further expanded their target spectrum thereby including *Spred1* and *Spry1*. Using 3'-UTR reporters of *Spred1* and *Spry1*, we demonstrated a direct binding of miR-132 and 212, which was abolished by disrupting the

83

corresponding binding sites. Knockdown of these three targets mimicked overexpression of miR-132 or miR-212 in the *in vitro* neovascularization assay and on the modulation of phosphorylated ERK1/2. Our data shows that Rasa1 is the most potent regulator among the three targets in promoting neovascularization and prolonging pERK1/2 activation in HUVECs, probably as being the most upstream signaling molecule as compared to Spry1 and Spred1. Another possibility is genetic redundancy, in which the loss of *Spred1* or *Spry1* can be compromised partially by other family members; Spry1 has at least four homologues [37] and Spred1 has at least two homologues in mice [38]. Our *in vitro* observations were confirmed *in vivo* where levels of Rasa1 and Spred1 were significantly higher in the adductor muscle in the miR-132/212 KO mice upon hind-limb ischemia. Although Spred1 and Rasa1 protein levels were higher in miR-132/212 KO mice, Spry1 expression levels were similar between WT and KO mice. Accordingly, we demonstrated lower levels of phosphorylated ERK1/2 as a downstream effect of lower active Ras-MAPK signaling.

The biological function of miR-132 and miR-212 may be different, although they share the same seed sequence. It has been shown that microRNA targets determination is beyond the seed sequence [39]. Consistent with this notion, we observe different effects in various assays. Since both miR-132 and miR-212 are removed in the knockout mice, it is impossible to determine which one should be responsible for the impaired arteriogenesis response. Given the fact that the expression of the mature miR-132 is 40 fold higher than miR-212 (Fig S1A), we tend to believe that miR-132 plays a major role in the arteriogenic response after hindlimb ischemia. However, it is still possible that a specific cell population, highly expressing miR-212 but not miR-132, is more important for the vascular growth after hindlimb ischemia . In line with this hypothesis, a recent study showed that miR-212 is stronger in the regulation of vasodilatation than miR-132 [40].To exclusively clarify the different roles and locations of these two microRNAs, improved microRNA in situ techniques with higher sensitivity are needed that can detect low abundant expressed microRNA in combination with mice with individual microRNA knockouts. Our results demonstrate a new role for miR-132 and miR-212 in the facilitation of the arteriogenic responses after hind-limb induced by targeting and enhancing Ras-MAPK signaling. This extends the role for miR-132 beyond the ischemic challenges and

promoting angiogenesis. It would be interesting to test if we can enhance arteriogenesis by specifically deliver these two microRNAs in the ischemia vasculature or in combination with other Ras-MAPK activators such as growth factors to further boost their pro-arteriogenic capacity. However, local delivery strategies should still be further improved [41].
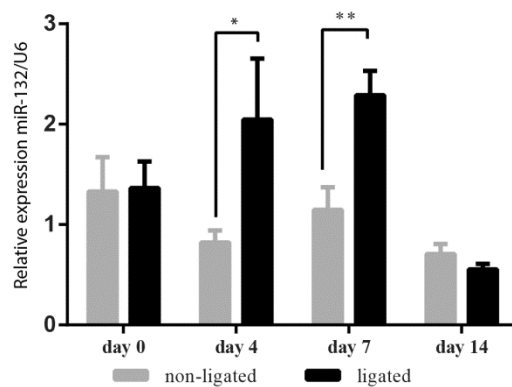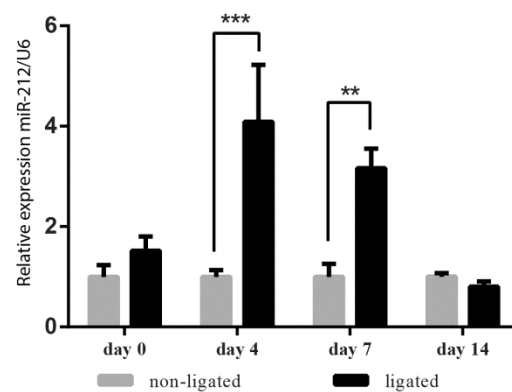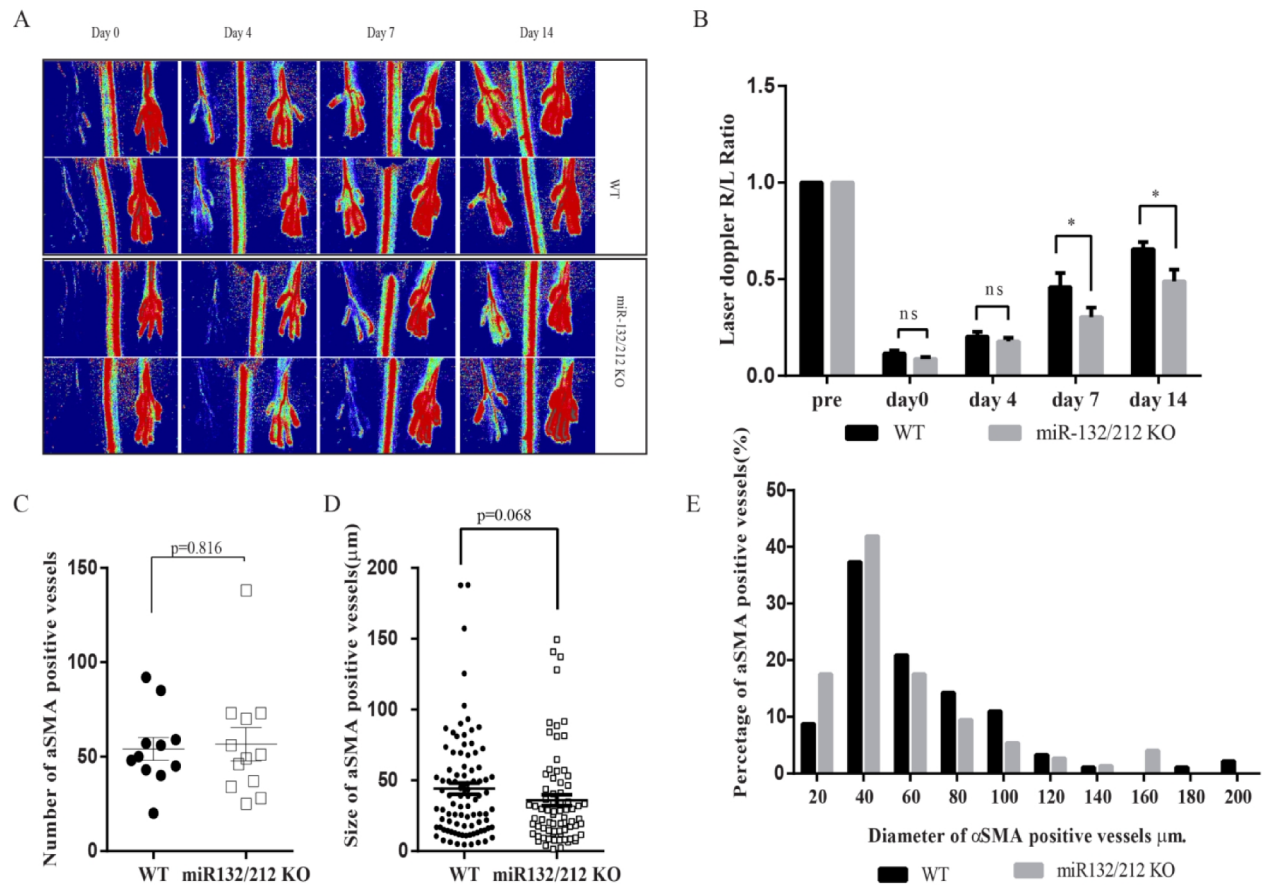

Figure 1. miR-132/212 expression after hind-limb ischemia. A. miR-132 expression as measured by qPCR assays. B. miR-212 expression as measured by qPCR assays (B).

Figure 2. miR-132/212 knockout mice show slower blood flow recovery rate after hindlimb ischemia. A. Laser Doppler images of WT and miR-132/212 KO at0, 4, 7 and 14 days after ligation of femoral artery. Low or no perfusion is displayed as dark blue, whereas the highest degree of perfusion is displayed as red. B. Quantification of laser Doppler image (Ratio R/L) as shown in A.. C. Quantification of number of αSMA positive vessels as determined by αSMA staining on adductor muscle on day 14. D. Quantification of the diameter of αSMA positive vessels as determined by αSMA staining on adductor muscle on day 14. E. Quantitative analysis the percentage of arteries in different size range. Note the higher percentage in the small vessels(ϕ400 a.u.) but lower in the larger vessel in the miR-132/212 KO mice..
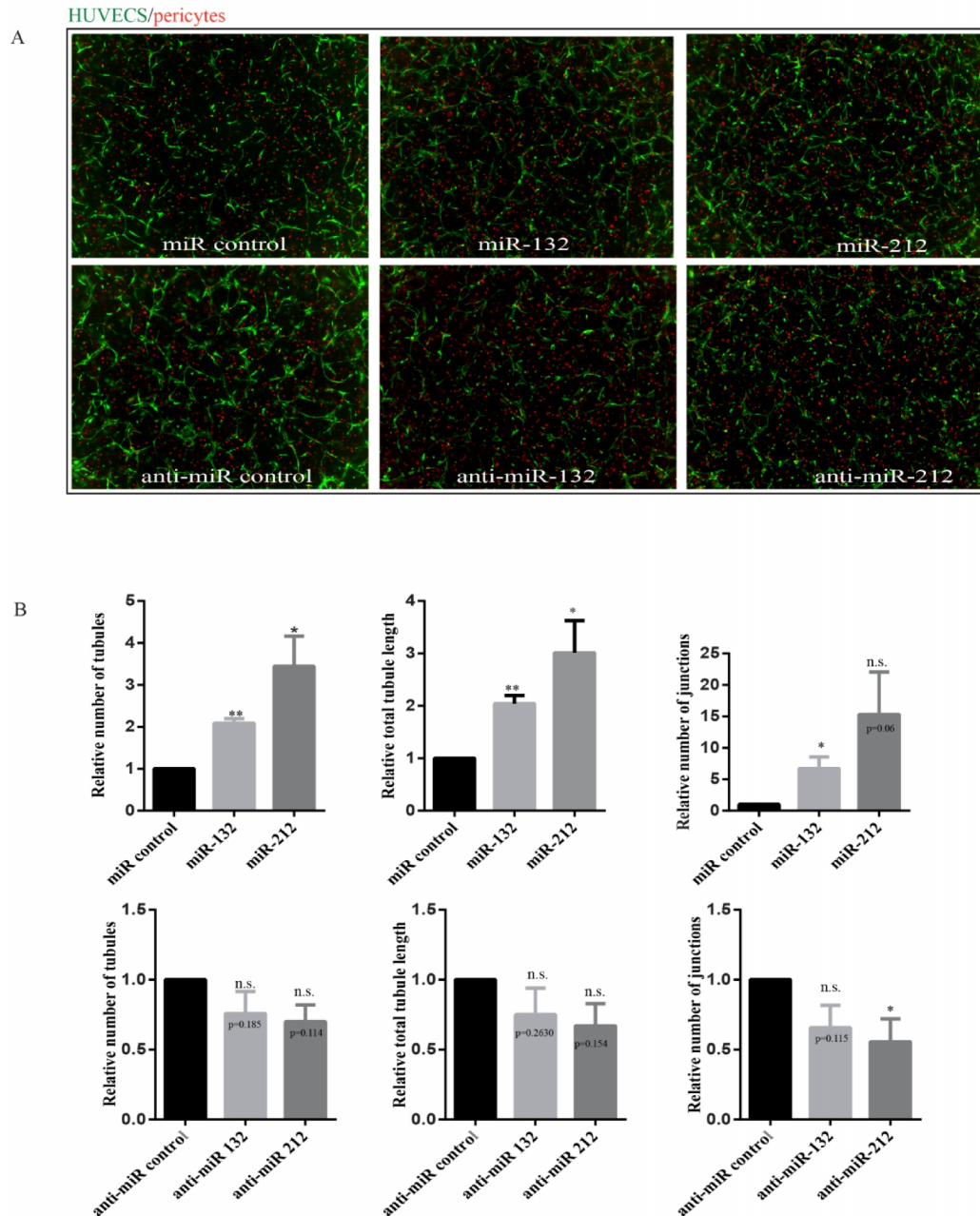
Figure 3:Effect of miR132 and miR212 in HUVECs angiogenesis in co-culture with pericytes. A. Representative image from HUVECs and pericytes co-culture assay with miR-132 and 212 transfection. HUVECs labeled in green with GFP, pericytes in labeled with PKH26 in red. B. Quantification of the HUVECs and pericytes co-culture assay with anti-miR-132 and 212 transfection.
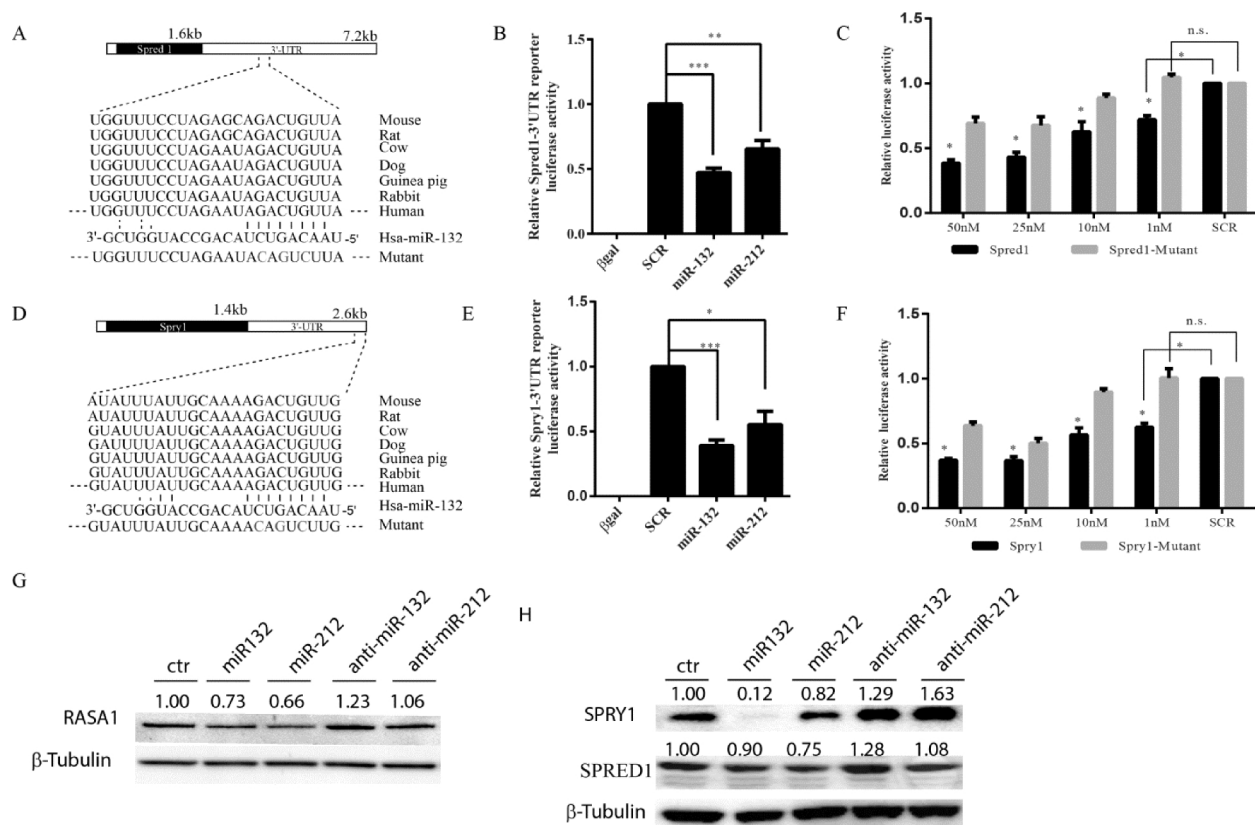
Figure 4:Identification of*Spred1* **and** *Spry1* **as direct miR-132/212 targets by luciferase assay and in cultured HUVECs.** A. the position of predicted miR-132 and miR212 targets of Spred1 by Targetscan and mutant form of 3'UTR as indicated in red. B. Luciferase assay of *Spred1*-3'UTR reporter in response to transfection with indicated scramble or microRNA mimics at final concentration of 25nM. C. Luciferase activity of wildtype and mutant *Spred1*-3'UTR in response to different dose of miR-132. D. The position of predicted miR-132 and miR212 targets of Spred1 by Targetscan and mutant form of 3'UTR as indicated in red. E. Luciferase assay of Spred1-3'UTR reporter in response to transfection with indicated scramble or microRNA mimics at final concentration of 25nM. F. Luciferase activity of wildtype and mutant Spred1-3'UTR in response to different final concentration of miR-132 mimics transfection. G.RASA1 expression after miR-132 , miR212 overexpression and inhibition in HUVECs. The number above indicate the relative expression compared with sham normalized by β-Tubulin expression. H.SPRED1 and SPRY1 expressions after miR-132 , miR212 overexpression and inhibition in HUVECs. The number above indicate the relative expression compared with sham normalized by β-Tubulin expression.
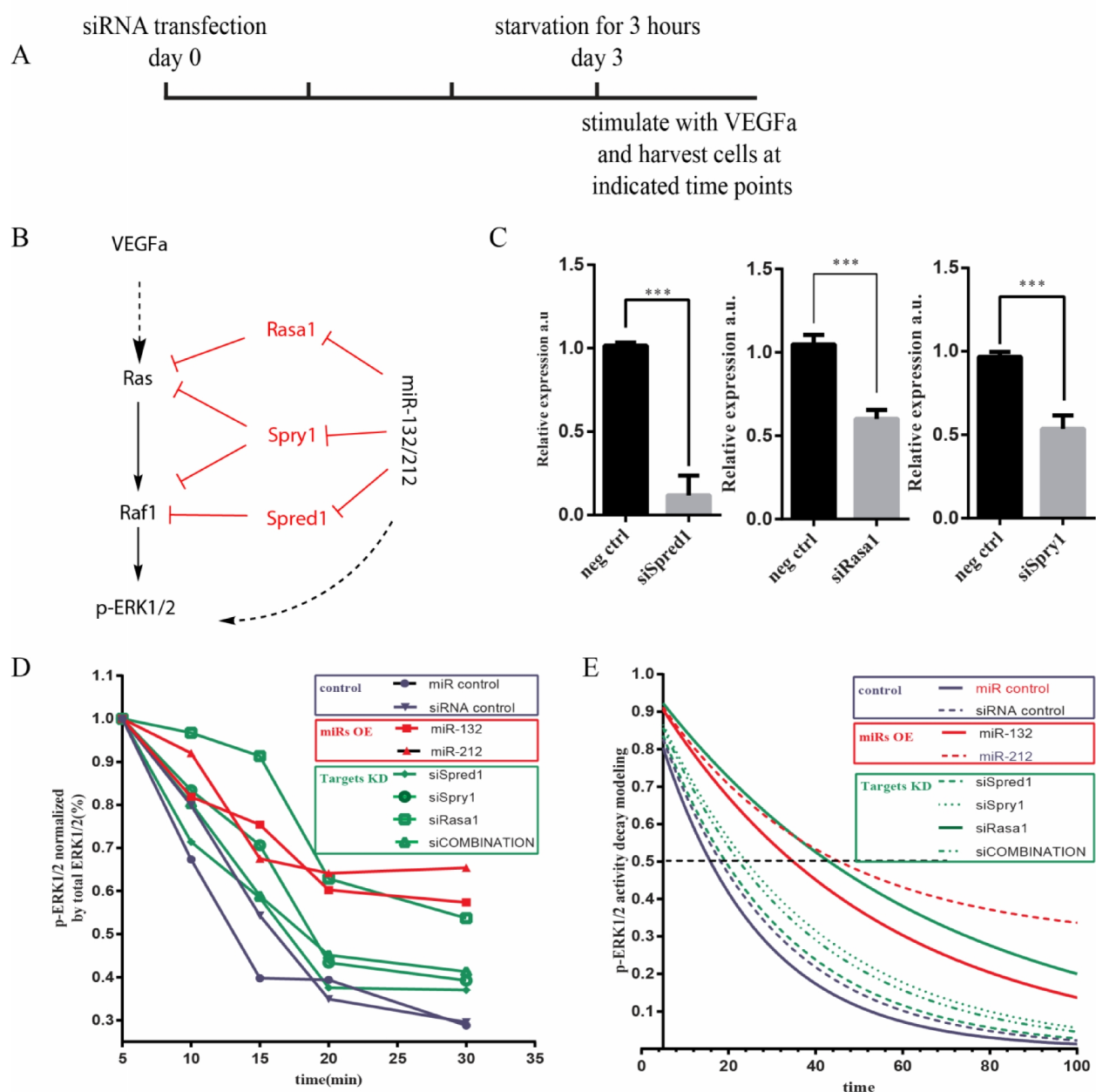
Figure 5: miR-132/212 modulate Ras-MAPK signaling by suppressing Rasa1, Spred1 and Spry1 in HUVECs. A. Experimental setting for quantitative measure of active ERK1/2 using Bio-plex phosopho-ERK1/2 assay. B. A working model for miR-132/212 in modulation of Ras-MAPK pathway. C. Quantification of Spred1, Spry1 or Rasa1 expression level after siRNA transfection against Spred1, Spry1 or Rasa1 in HUVECs . D. Quantification of phosophorylated ERK1/2 level by Bio-plex pro phosopho-ERK1/2 set. Note the sustain ERK1/2 phosphorylation is prolonged after miR-132, 212 transfection or siRNA against Spred1, Spry1, Rasa1 or combinations of the three. E. Modeling the decay of phosophorylated ERK1/2 level from D.
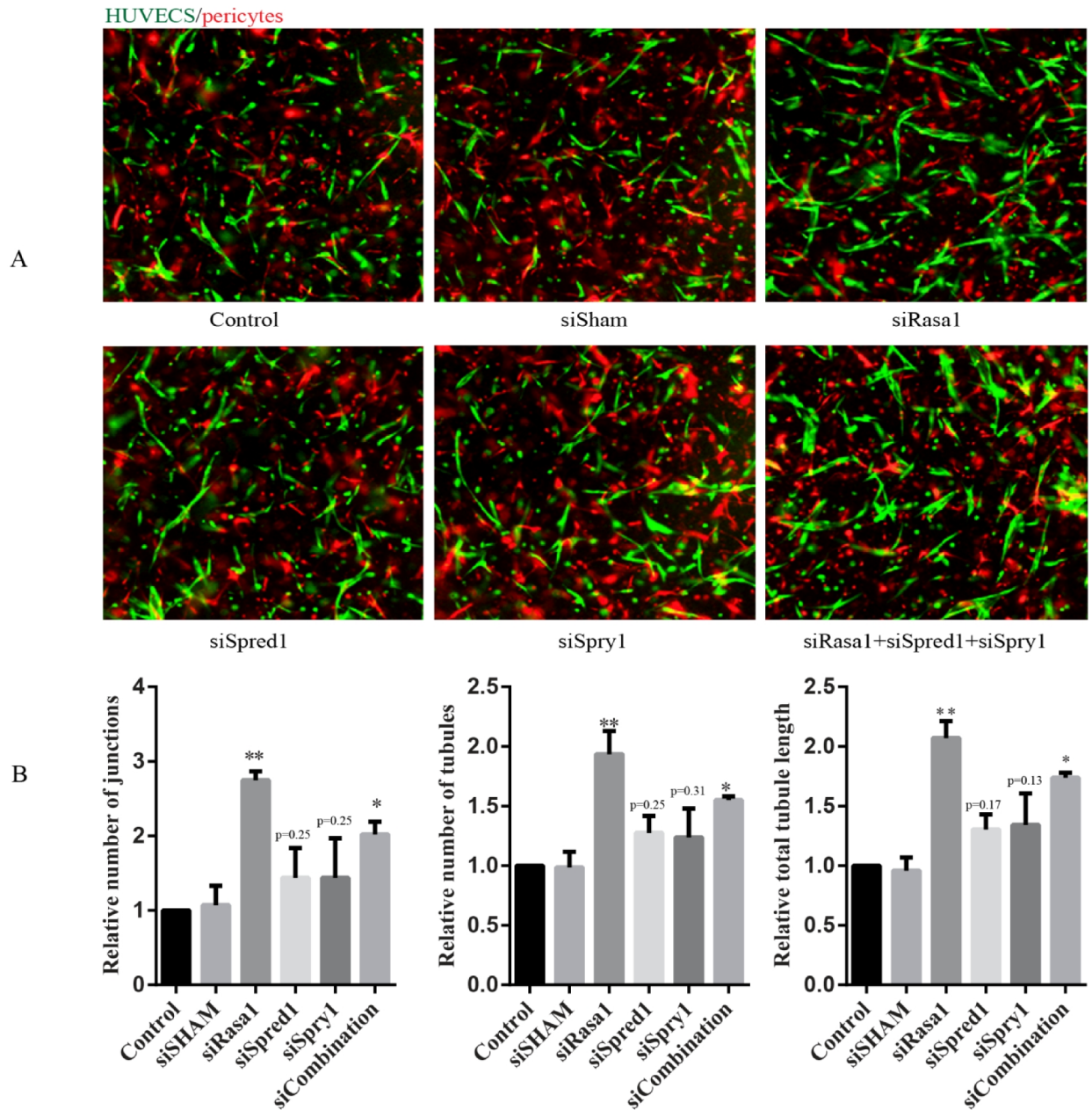
Figure 6. Knockdown targets of miR132 and miR212 Rasa1, Spred1 and Spry1 mimics effect of miR-132 and miR-212 in HUVECs pericytes neovascularization assay. A. Representative image from HUVECs and pericytes coculture assay after transfection with siRNAs against Spred1, Spry1, Rasa1 and combination of these three siRNA. B.Quantification of the number of tubules, junctions and total tubule length in the HUVECs and pericytes coculture assay after transfection with siRNAs against Spred1, Spry1 and Rasa1.

A

B

C

D
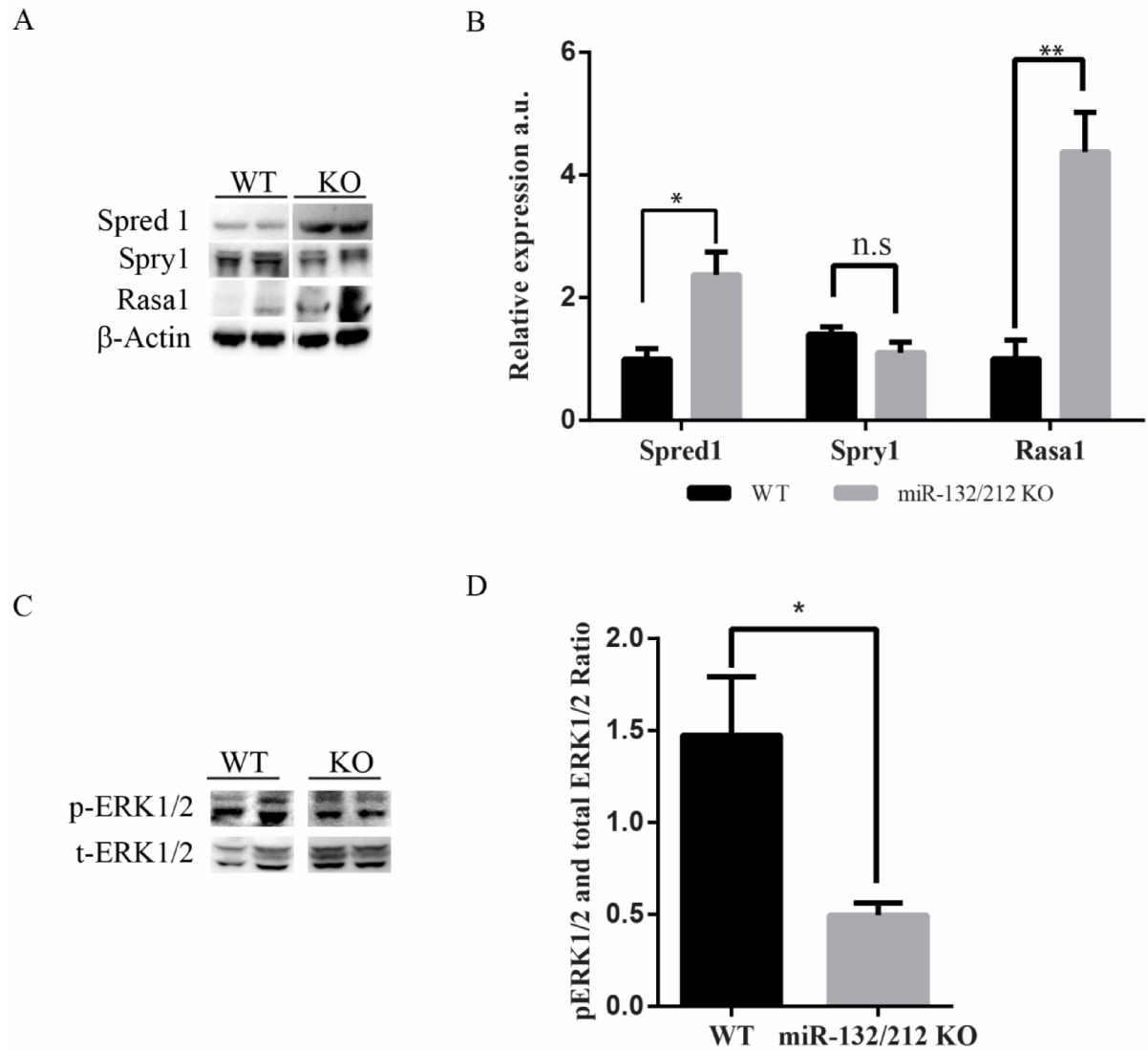
Figure 7. Expression of miR-132/212 targets and phosophorylated ERK1/2 in ischemia limb. A. Spred1, Rasa1 and Spry1 expression as determined by Western Blot, normalized by β-Actin. B. Quantification Spred1, Rasa1 and Spry1 expression as determined by Western Blot. C. Phosophorylated ERK1/2 expression in the thigh WT and KO mice on 14 days after hindlimb ischemia as determined by Western Blot on day 14. D. Quantification of phosophorylated ERK1/2 expression in the thigh WT and KO mice on 14 days after hindlimb ischemia as determined by Western Blot, normalized by β-Actin

References

1. Carmeliet, P. and R.K. Jain, Molecular mechanisms and clinical applications of angiogenesis. Nature, 2011. **473**(7347): p. 298-307.
2. Revencu, N., et al., RASA1 mutations and associated phenotypes in 68 families with capillary malformation-arteriovenous malformation. Hum Mutat, 2013. **34**(12): p. 1632-41.
3. Heil, M., et al., Arteriogenesis versus angiogenesis: similarities and differences. J Cell Mol Med, 2006. **10**(1): p. 45-55.
4. Troidl, K. and W. Schaper, Arteriogenesis versus angiogenesis in peripheral artery disease. Diabetes Metab Res Rev, 2012. **28 Suppl 1**: p. 27-9.
5. Shimpo, M., et al., AAV-mediated VEGF gene transfer into skeletal muscle stimulates angiogenesis and improves blood flow in a rat hindlimb ischemia model. Cardiovasc Res, 2002. **53**(4): p. 993-1001.
6. Jacobi, J., et al., Adenoviral gene transfer with soluble vascular endothelial growth factor receptors impairs angiogenesis and perfusion in a murine model of hindlimb ischemia. Circulation, 2004. **110**(16): p. 2424-9.
7. Taniguchi, K., et al., Suppression of Sproutys has a therapeutic effect for a mouse model of ischemia by enhancing angiogenesis. PLoS One, 2009. **4**(5): p. e5467.
8. van Mil, A., et al., MicroRNA-1 enhances the angiogenic differentiation of human cardiomyocyte progenitor cells. J Mol Med (Berl), 2013. **91**(8): p. 1001-12.
9. Zhou, Q., et al., Regulation of angiogenesis and choroidal neovascularization by members of microRNA-23~27~24 clusters. Proc Natl Acad Sci U S A, 2011. **108**(20): p. 8287-92.
10. Anand, S., et al., MicroRNA-132-mediated loss of p120RasGAP activates the endothelium to facilitate pathological angiogenesis. Nat Med, 2010. **16**(8): p. 909-14.
11. Fish, J.E., et al., miR-126 regulates angiogenic signaling and vascular integrity. Dev Cell, 2008. **15**(2): p. 272-84.
12. Fiedler, J., et al., MicroRNA-24 regulates vascularity after myocardial infarction. Circulation, 2011. **124**(6): p. 720-30.
13. Bonauer, A., et al., MicroRNA-92a controls angiogenesis and functional recovery of ischemic tissues in mice. Science, 2009. **324**(5935): p. 1710-3.
14. Kuehbacher, A., et al., Role of Dicer and Drosha for endothelial microRNA expression and angiogenesis. Circ Res, 2007. **101**(1): p. 59-68.
15. Katare, R., et al., Transplantation of human pericyte progenitor cells improves the repair of infarcted heart through activation of an angiogenic program involving micro-RNA-132. Circ Res, 2011. **109**(8): p. 894-906.
16. Jin, W., et al., Small RNA sequencing reveals microRNAs that modulate angiotensin II effects in vascular smooth muscle cells. J Biol Chem, 2012. **287**(19): p. 15672-83.
17. Devalliere, J., et al., Sustained delivery of proangiogenic microRNA-132 by nanoparticle transfection improves endothelial cell transplantation. FASEB J, 2014. **28**(2): p. 908-22.
18. Westenskow, P.D., et al., Ras pathway inhibition prevents neovascularization by repressing endothelial cell sprouting. J Clin Invest, 2013. **123**(11): p. 4900-8.
19. Mulik, S., et al., Role of miR-132 in angiogenesis after ocular infection with herpes simplex virus. Am J Pathol, 2012. **181**(2): p. 525-34.
20. Kayo, H., et al., miR-212 and miR-132 are dispensable for mouse mammary gland development. Nat Genet, 2014. **46**(8): p. 802-4.
21. Grundmann, S., et al., MicroRNA-100 regulates neovascularization by suppression of mammalian target of rapamycin in endothelial and vascular smooth muscle cells. Circulation, 2011. **123**(9): p. 999-1009.
22. van den Borne, P., et al., Absence of chemokine (C-x-C motif) ligand 10 diminishes perfusion recovery after local arterial occlusion in mice. Arterioscler Thromb Vasc Biol, 2014. **34**(3): p. 594-602.
23. Sluijter, J.P., et al., MicroRNA-1 and -499 regulate differentiation and proliferation in human-derived cardiomyocyte progenitor cells. Arterioscler Thromb Vasc Biol, 2010. **30**(4): p. 859-68.

24. van Mil, A., et al., MicroRNA-214 inhibits angiogenesis by targeting Quaking and reducing angiogenic growth factor release. Cardiovasc Res, 2012. **93**(4): p. 655-65.

25. Baker, M., et al., Use of the mouse aortic ring assay to study angiogenesis. Nat Protoc, 2012. **7**(1): p. 89-104.

26. Stratman, A.N., et al., Pericyte recruitment during vasculogenic tube assembly stimulates endothelial basement membrane matrix formation. Blood, 2009. **114**(24): p. 5091-101.

27. Chi, S.W., et al., Argonaute HITS-CLIP decodes microRNA-mRNA interaction maps. Nature, 2009. **460**(7254): p. 479-86.

28. Hafner, M., et al., Genome-wide identification of miRNA targets by PAR-CLIP. Methods, 2012. **58**(2): p. 94-105.

29. Helwak, A. and D. Tollervey, Mapping the miRNA interactome by cross-linking ligation and sequencing of hybrids (CLASH). Nat Protoc, 2014. **9**(3): p. 711-28.

30. Pamonsinlapatham, P., et al., p120-Ras GTPase activating protein (RasGAP): a multi-interacting protein in downstream signaling. Biochimie, 2009. **91**(3): p. 320-8.

31. Casci, T., J. Vinos, and M. Freeman, Sprouty, an intracellular inhibitor of Ras signaling. Cell, 1999. **96**(5): p. 655-65.

32. Hanafusa, H., et al., Sprouty1 and Sprouty2 provide a control mechanism for the Ras/MAPK signalling pathway. Nat Cell Biol, 2002. **4**(11): p. 850-8.

33. Wakioka, T., et al., Spred is a Sprouty-related suppressor of Ras signalling. Nature, 2001. **412**(6847): p. 647-51.

34. Lanahan, A., et al., The neuropilin 1 cytoplasmic domain is required for VEGF-A-dependent arteriogenesis. Dev Cell, 2013. **25**(2): p. 156-68.

35. Deng, Y., et al., Endothelial RAF1/ERK activation regulates arterial morphogenesis. Blood, 2013. **121**(19): p. 3988-96, S1-9.

36. Schaper, W., Collateral circulation: past and present. Basic Res Cardiol, 2009. **104**(1): p. 5-21.

37. Mason, J.M., et al., Sprouty proteins: multifaceted negative-feedback regulators of receptor tyrosine kinase signaling. Trends Cell Biol, 2006. **16**(1): p. 45-54.

38. Bundschu, K., U. Walter, and K. Schuh, Getting a first clue about SPRED functions. Bioessays, 2007. **29**(9): p. 897-907.

39. Grimson, A., et al., MicroRNA targeting specificity in mammals: determinants beyond seed pairing. Mol Cell, 2007. **27**(1): p. 91-105.

40. Kumarswamy, R., et al., Vascular importance of the miR-212/132 cluster. European Heart Journal, 2014. **35**(45): p. 3224-3231.

41. Kwekkeboom, R.F., et al., Targeted delivery of miRNA therapeutics for cardiovascular diseases: opportunities and challenges. Clin Sci (Lond), 2014. **127**(6): p. 351-65.

A. Relative expression in skeletal muscle normalized by U6

B. Lectin BS-1/miR-132/Hoechst

C.

D.
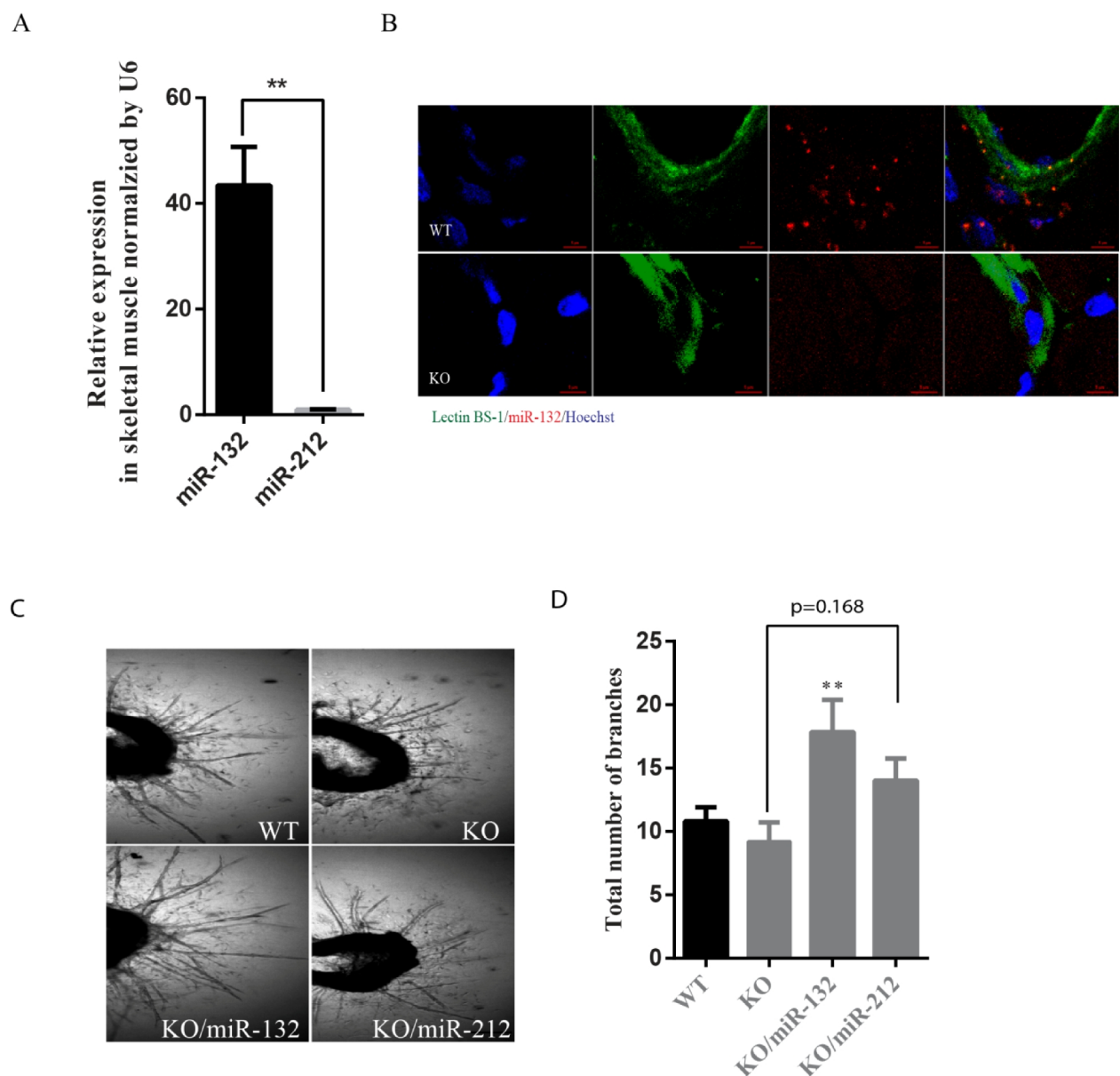
Supplementary Figure 1. The expression of the miR-132/212 and their roles in Ex vivo neovascularization assay. A. qPCR analysis the expression of miR-132 and 212 in thigh muscle. B. miR-132 expression in the endothelial cells in the thigh muscle blood vessel as detected by miR-132 in situ, miR-132 in red, endothelial cells in green, nuclei in blue, bar=5μm. C. Representative pictures from aorta ring assays. bar=200μM. D. Quantification of aorta ring branching from WT, KO, and KO transfected with miR-132 and 212 precursors.
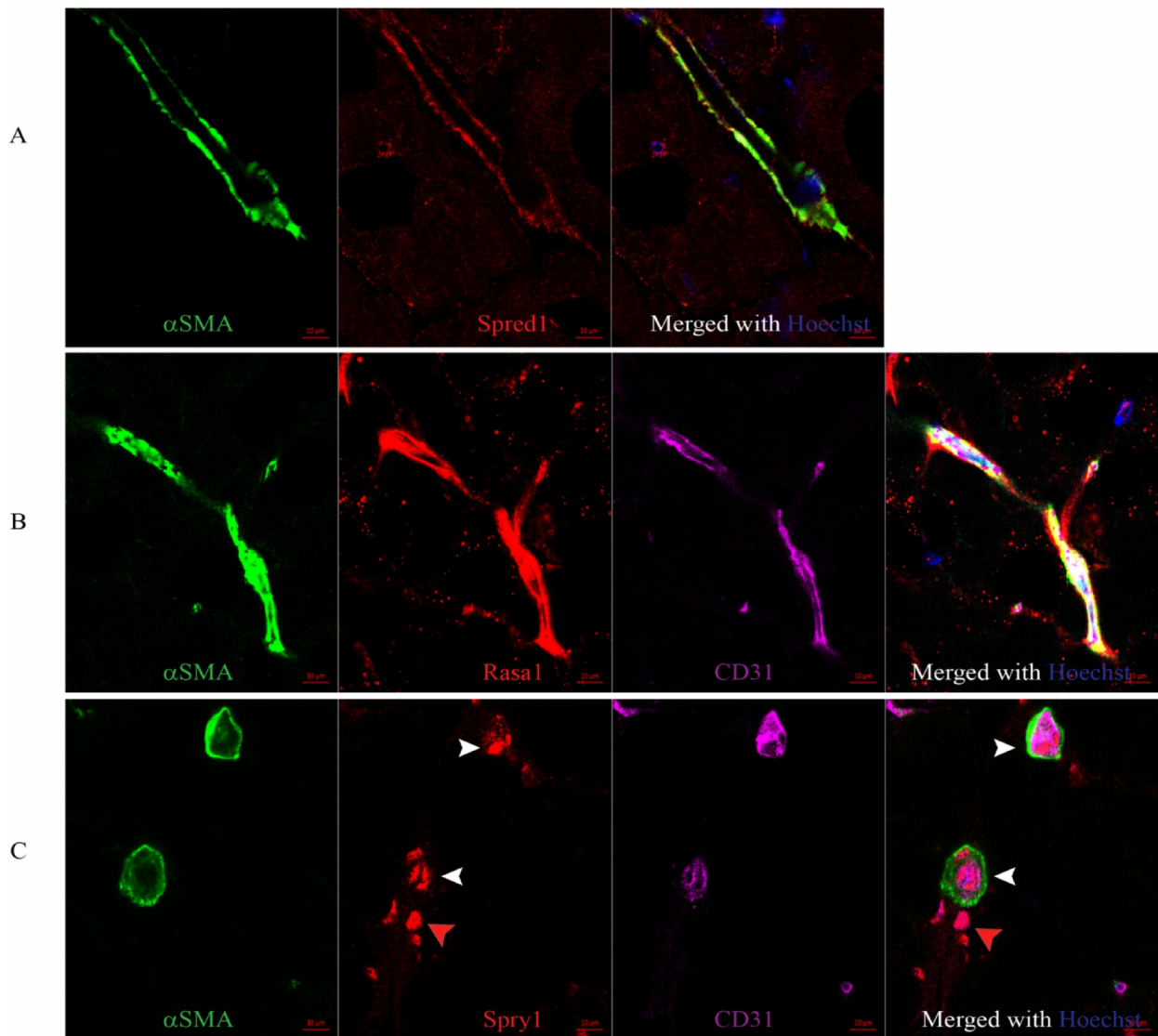
Supplementary Figure 2.The expression of miR-132/212 targets Spred1, Spry1 and Rasa1 in wildtype thigh blood vessels characterized by immunofluorescent staining. Note the overlapping expression of Spred1 (in A), Rasa1(in B) with αSMA. Spry1 are expressed in the interior layer CD31 positive cells layers in the vessel as shown in C with white arrow and also expressed in the cells which are either CD31 or αSMA positive as indicated by red arrow. Spred1, Rasa1 and Spry1 in red, αSMA in green, CD31 in purple, nuclear was stained with DAPI in blue. Bar=10mm

Supplementary Table 1. Primers and oligos nucleotides used in this study.

Primer name	Sequence(5'-3')	Application
Mir132-KO-GT-P1	ATCCTTTCAAGAAAGTGGGGAGA	genotyping
Mir132-KO-GT-P2	TCTGAGGAGGATGTTCAGACAC	genotyping
hSpred-utr_SDM1_F	TCCTAGAATAcagtcTTAACTTTCAAAATTTTTATTGGTG	mutagenesis
hSpred-utr_SDM1_R	AACCAAGTTTAGCTGAAAAC	mutagenesis
hSpry1utr_SDM1_F	TATTGCAAAAcagtcTTGAAATGTACTCATGTTTG	mutagenesis
hSpry1utr_SDM1_R	AATACCATAAAATAATAGAGATTCG	mutagenesis
hSpred1-3UTR_F1	ATCGGCTAGCAAGAAGAGGGTATTTCTA	cloning
hSpred1-3UTR_R1	ATCGAAGCTTATACACATGTTTAAGAAT	cloning
hSpry1-3'UTR_F1	ATCGGCTAGCGGAGGTGGGTTGTACCTC	cloning
hSpry1-3'UTR_R1	ATCGAAGCTTGACAGTTTCATTAATTAA	cloning
hSpry1_F1	GCAGTGGCAGTTCGTTAGTTG	qPCR
hSpry1_R1	CAGTAGGCTGAATCTCTCTCTCA	qPCR
hSpred1_F1	AAGGATGCCCCGAATCAAAAA	qPCR
hSpred1_R1	GGCTTG[ii]GCTTTGCATGTAGAC	qPCR
hRASA1_F1	GGGAGCTGGACTGACAGG	qPCR
hRASA1_R1	AGAGTCTCAGCAAGCAACGA	qPCR
mACTB_F1	GGCTGTATTCCCCTCCATCG	qPCR
mACTB_R1	CCAGTTGGTAACAATGCCATGT	qPCR
Gapdh_F2	GGCATGGACTGTGGTCATGA	qPCR
Gapdh_R2	TTCACCACCATGGAGAAGGC	qPCR
mSpry1_F1	ATGGATTCCCCAAGTCAGCAT	qPCR
mSpry1_R1	CCTGTCATAGTCTAACCTCTGCC	qPCR
mSpred1_F1	GAGATGACTCAAGTGGTGGATG	qPCR
mSpred1_R1	TCTGAAAGGTAAGGCCAAACTTC	qPCR
mRasa1_F1	GTGGTGTACAGCAGCACGTA	qPCR
mRasa1_R1	ATTACCACGGTGGGCATACT	qPCR

Chapter 5

Inhibition of miRNA-132/212 Suppresses VHL-Regulated Pathophysiological Angiogenesis

Zhiyong Lei[1#], Timothy D. Klasson[2#], Maarten M. Brandt[3], Glenn van de Hoek[4], Ive Logister[2],

Caroline Cheng[2, 3], Pieter A. Doevendans[1,5], Joost. P.G. Sluijter[1, 5*] and Rachel H. Giles[2*]

1. Department of Cardiology, Division Heart and Lungs, University Medical Center Utrecht, Utrecht, the Netherlands

2. Department of Nephrology & Hypertension, Division Internal Medicine, University Medical Center Utrecht, Heidelberglaan 100, 3584CX Utrecht, the Netherlands

3. Experimental Cardiology, Erasmus Medical Center, the Netherlands

4. Department of Medical Genetics, University Medical Center Utrecht, Heidelberglaan 100, 3584CX Utrecht, the Netherlands
5. ICIN, Netherlands Heart Institute, Catharijnesingel 52, 3511 GC Utrecht, the Netherlands
   # These authors contributed equally to this paper

Abstract:

Objective:

Clear cell renal cell carcinoma (ccRCC) is the most common form of sporadic and inherited kidney cancer, and is highly associated with biallelic mutations in the *von Hippel-Lindau* (*VHL*) tumor suppressor gene and an activated PI3k-AKT pathway. Although upregulation of the miR-132/212 and disturbed VHL signaling have both been linked with pathogenic angiogenesis, no evidence of a possible connection between the two has yet been made.

Approach and Results:

We show that miRNA132/212 levels are increased after loss of functional pVHL, the protein product of the *VHL* gene, *in vivo* and *in vitro*. We also show that PTEN levels are down regulated in models lacking endogenous *VHL* or after *VHL* knockdown in wild-type cells, at least partially due to the action of miRNA132/212. Furthermore, we show that blocking miRNA132/212 with anti-miRs can significantly alleviate the excessive vascular branching phenotype characteristic of *vhl*$^{-/-}$ mutant *zebrafish*. Moreover, using human umbilical vascular endothelial cells (HUVECs) and an endothelial cell/pericyte coculture system, we observed that *VHL* knockdown promotes endothelial cells' neovascularization capacity *in vitro*, an effect which can be inhibited by anti-miR-132/212 treatment.

Conclusions:

Taken together, our results demonstrate an important role for miRNA132/212 in angiogenesis induced by loss of VHL and suggest an interesting opportunity for pharmaceutical intervention using an inhibitor of miR-132/212 to inhibit tumor growth for ccRCC patients.

Keywords: VHL loss of function, microRNA-132/212, pathological angiogenesis, ccRCC

Introduction:

Clear cell renal cell carcinoma (ccRCC), the most common form of sporadic and inherited kidney cancer, is highly associated with mutations in the von Hippel-Lindau (*VHL*) gene. [1, 2] The protein product of the *VHL* gene (pVHL) is an E3 ubiquitin ligase involved in the degradation of hypoxia-inducible transcription factor subunits (HIFα). Under normal oxygen conditions, hydroxylated HIFα can be recognized by an ubiquitin ligase complex containing pVHL and rapidly degraded. Upon hypoxia or loss of functional pVHL, HIFα-subunits can no longer be hydroxylated and begin to accumulate. Stabilized HIFα activates the expression of a large suite of downstream target genes (including *EPO, VEGF*), the actions of which are vital to promote angiogenesis. However, many of the changes initiated by the stabilization of HIFα, such as increased angiogenesis, an upregulation of anti-apoptotic signaling and a shift to anaerobic glycolosis, can contribute to tumor growth and survival. People born with a mutation in one *VHL* allele will acquire somatic mutations in the second allele, resulting in consequent angiogenic symptoms and a variety of tumors, including ccRCC [3]. Another hallmark of ccRCC is activated PI3k/AKT pathway signaling, higher levels of which is significantly correlated with a worse survival rate[2], although the mechanism by which this occurs is still not fully understood.

MicroRNAs (miRNAs) are small non-coding RNAs that post-transcriptionally regulate the expression of groups of target genes by inhibition of the translation of their targeting messenger RNAs (mRNAs) or marking these mRNAs for degradation. miRNAs are key regulators in many physiological and pathological processes [4], including the dynamic regulation of ccRCC during tumor progression[2]. By promoting the expression of vascular endothelial growth factor (*VEGF*), VHL/HIF signaling increases cAMP response element binding protein (CREB) levels, a transcription factor which upregulates the expression of pro-angiogenic miR-132/212 [5]. This implies that pVHL loss-of-function would stimulate miR-132/212 expression and thereby contribute to excessive angiogenesis. In this study, using a combination of cellular models, patient ccRCC material with biallelic loss of *VHL* and a previously described *vhl*$^{-/-}$ mutant *zebrafish* model, we show that miR-132/212 is upregulated after *VHL* knockdown or mutation and that this upregulation is at least partially responsible for

increased angiogenesis, possibly by targeting phosphatase and tensin homolog (*PTEN)*. A scarcity of functional pVHL induces excessive vascular outgrowth which can be inhibited by pharmaceutical inhibition of miR-132/212, thereby providing an exciting potential therapy target for reducing the growth and burden of tumors associated with *VHL* mutations.

Materials and methods:

Materials and Methods are available in the online-only data supplement.

Results:

We first examined the expression of miR-132 in relation to VHL loss-of-function and (pseudo)-hypoxia signaling. We found that cells grown in hypoxic conditions display significantly elevated levels of miR-132 expression (Figure 1.A). We observe similar effects in HUVECs transfected with siRNA targeting *VHL* mRNA relative to those treated with non-targeting siRNA (Figure 1.B). To confirm the effect *in vivo,* we used a previously established *zebrafish* model of *VHL* deficiency [6-8]. MiR-132/212 is well conserved in most species, including *zebrafish* (Supplementary Figure 1.A). Like our cell models, *vhl*^{-/-} *zebrafish* also show an increased level of expression of miR-132 (Figure 1.C). In isogenic cell lines taken from human ccRCC *VHL*^{-/-} tumors, the expression of miR-132 is reduced upon *VHL* reconstitution with ectopic *VHL* (Figure 1.D). Lastly, we examined miR-132 expression in histology slides taken from ccRCC tumors using microRNA *in situ* hybridization. In agreement with our previous qPCR results, we observed widespread overexpression of miR-132 in tumor material from ccRCC samples with biallelic *VHL* mutations proven by sequencing (Figure 1.E). These results demonstrate that miR-132/212 are increased in response to the (pseudo-)hypoxia induced by the lack of functional pVHL which eventually leads to overexpression of miR-132/212.

To assess the functional consequences of miR-132/212 expression in a *VHL*-null environment, we used an *in vitro* co-culture assay designed to gauge angiogenesis. In agreement with the important role of VHL in HIFα degradation, knockdown of VHL in HUVEC/pericyte coculture shows significantly more vascular junctions, tubule number, and total tubular length as compared to siSham control treatment (Figure 2.A-C). To evaluate whether the pro-angiogenic effects of *VHL* silencing are

mediated by a downstream increase in miR-132/212, GFP-labelled HUVECs were treated with anti-miRs against miR-132/212 in combination with siRNA targeting *VHL*. Inhibiting the action of miR-132/212 reduced the excessive angiogenesis response induced by the silencing of *VHL* significantly (Figure 2.D), suggesting that VHL-regulated angiogenesis is at least partially mediated by the upregulation of miR-132/212.

vhl^{-/-} *zebrafish* embryos display a phenotype of post-vascularization branching/sprouting around the intersomitic vessels. Counting these sprouts is a quantitative measure of angiogenesis in *zebrafish* [7]. *vhl*^{-/-} *zebrafish* were injected at a one-cell stage with anti-miRs directed against miR-132 or miR-212 and four days later tails of the living fish were imaged with a confocal microscope (Figure 3.A). The cloaca of the *zebrafish* is placed in the center of the image and the branches sprouting from the inter-somitic vessels were counted for the four vessels anterior and the four vessels posterior to the cloaca (Figure 3.B). Anti-miR injections against miR-132/212 significantly reduced the extent of inter-somitic vessel sprouting in *vhl*^{-/-} fish (Figure 3.C-D). In addition, injecting wild-type *zebrafish* with miRNA132/212 mimics partially recapitulated the *vhl* mutant vessel sprouting phenotype (supplemental figure B, C).

Therefore, in light of the fact that miR-132/212 expression is linked to vessel sprouting in *vhl*^{-/-} *zebrafish*, which phenocopies *zebrafish* with loss of both *ptena* and *ptenb* [9], we proceeded to look at the expression of PTEN in our VHL-null models. PTEN, a phosphatidylinositol-3,4,5-trisphosphate 3-phosphatase, antagonizes the activity of phosphatidylinositol-4,5-bisphosphate 3-kinase (PI3K), suppressing cellular proliferation, cell survival and angiogenesis by inactivating the PI3K-driven AKT signaling pathway [10]. *PTEN* has been predicted to be a potential target of miR-132/212 in humans by targetscan (Figure 4.A) and the rat homologue of *PTEN* has been shown to be targeted by miRNA-132/212 in rat vascular smooth muscle cells [11]. Moreover, downregulation of PTEN has been significantly correlated with lower survival rate in ccRCC patients [2]. We reasoned that upregulated miR-132/212 upon mutation or silencing of *VHL* could result in the subsequent reduction of PTEN. We therefore first looked at the regulation of PTEN in *vhl*^{-/-} *zebrafish* and in HUVECs after

knockdown of *VHL*. *Zebrafish*, as opposed to mammals, have two copies of the *pten* gene: *ptena* and *ptenb*. *ptenb* is a predicted target of miRNA132/212 in targetscan, but not *ptena* (Figure 4.B). Accordingly, we found significantly reduced *ptenb* expression in *vhl*^{-/-} *zebrafish* with no significant changes observed in *ptena* (Figure 4.C). In HUVECs, overexpression of miR-132 or miR-212 combined with *VHL* knockdown caused a reduction in PTEN mRNA (Figure 4.D) and protein levels (Figure 4.E-F) showing that PTEN is indeed targeted by miR-132/212 in our *in vitro* as well as *in vivo* models.

Discussion:

In this study we used patient material, human cells and *zebrafish* to examine the role of the miRNA132/212 family in the pathophysiology of neovascularization caused by the loss of functional pVHL. We observed that miR-132/212 is upregulated in response to *VHL* mutation both in *zebrafish* model systems and in human patient ccRCC tumor material carrying biallelic inactivating *VHL* mutations. We demonstrated that the excessive angiogenesis attributable to *VHL* mutation is strongly affected by miRNA132/212. Indeed, targeting these miRNAs with anti-miRs can significantly reduce angiogenesis in both *in vitro* and *in vivo* models of *VHL* deficiency. We identified the tumor suppressor PTEN as one of the targets affected by miRNA132/212 in *VHL*-null models. Taken together, our results implicate miRNA132/212 as an important intermediate in pathological angiogenesis after loss of functional pVHL or tissue hypoxia. In addition, the effects of miRNA132/212 on *PTEN* suggest a possible role for these miRNAs in tumorigenesis.

The miRNA132/212 family is clustered in the genome and is highly conserved in vertebrates. MiR-132/212 are initially expressed as one primary miRNA and then processed into two mature miRNA with the same target-defining "seed" sequence [12]. This miRNA family plays a number of roles in the promotion of angiogenesis. Mice without functional miR-132/212 show impaired arteriogenesis response after hindlimb ischemia [13]. The pro-angiogenic potential of miR-132 has been used to increase angiogenesis in endothelial cell grafts and after ischemic injury [14]. MiR-132/212 frequently act as a promoter of cell proliferation and increases in their expression levels have also been suggested

as contributors to tumorigenesis in addition to their angiogenic role. MiR-132 has previously been shown to induce pathological neovascularization in the endothelium by targeting p120 Ras GTPase activating protein [5]. In addition, anti-miR-132 has also been shown to reduce tumor burden in a mouse xenograft model of human breast carcinoma [5].

This study supports the previously reported role of miRNA132/212 in pathophysiological angiogenesis and expands upon its role in the context of VHL-regulated hypoxia signaling. When VHL is mutated or downregulated, miRNA132/212 and PI3K are consequently upregulated. MiRNA-132/212 targeting of *PTEN* mRNA ensures that PI3K has a chance to activate AKT (Figure 5). Uncontrolled proliferation and angiogenesis are hallmarks of cancer and many tumors contain mutations leading to hyper-activation of the RAS or AKT signaling networks which act to promote these processes [15-17]. Differential expression of miRNA has been previously reported in tumors including ccRCC [18] and is widely believed to be an important player in tumorigenesis [19-21]. MiR132/212 is therefore an interesting potential target for the treatment of cancer.

In human patients, ccRCC is almost always associated with *VHL* mutations. However, von Hippel-Lindau patients born with a single germline mutation in *VHL* initially develop non-cancerous cysts in the kidney and do not develop ccRCC until around 35 years of age on average[22]. In addition, mouse models with *Vhl* mutations do not develop renal tumors [23]. In contrast, *zebrafish vhl* mutants develop dysplastic lesions within 6 days post fertilization (dpf). Therefore it is believed that *VHL* mutations in mammals create a pre-cancerous cystic phenotype but an additional mutation to another ancillary oncogene is required before tumor formation [24]. Although the recently developed *Vhl* mutant mouse with heterozygous mutations in BRCA1 associated protein 1 (*Bap1*) is perhaps the most physiologically relevant mouse model of human ccRCC [25], *Pten* $^{-/-}$ *Vhl* $^{-/-}$ double mutant mice develop benign squamous metaplasia and cystadenoma [24] and display kidney cysts that are very similar to those taken from the kidneys of human VHL patients, implying that activation of the AKT signaling pathway is important in the development of pre-cancerous cysts. Indeed, cysts taken from VHL patients display hyper-activation of PI3K signaling [24]. MiRNA-132/212 mediated reduction of PTEN, which is an important suppressor of the PI3K/AKT pathway, may at least partially explain this

expression pattern. In addition, biallelic *PTEN* mutations are rare in ccRCC [26, 27] but loss of a single *PTEN* allele through mutation is not uncommon [28]. MiRNA-132/212 expression may be the reason that this is sufficient to cause hyper-activation of AKT signaling despite the presence of a functional PTEN allele. Hyper-activation of AKT signaling and loss of *PTEN* are common in many other tumor types because tumor growth requires angiogenesis. Thus, miRNA-132/212 expression may fulfill an important role in the development of ccRCC tumors.

One of the hallmarks of ccRCC is resistance to cytotoxic treatment. Anti-apoptotic signaling is upregulated after HIFα hyper-stabilization in ccRCC tumors. Many experimental treatments focus on inhibiting the action of downstream anti-apoptosis proteins such as mammalian target of rapamycin (mTOR), an important pro-survival protein induced by activated AKT signaling [29]. Our results and the results of other studies suggest that miR-132/212 may act as a promoter of tumorigenesis by targeting inhibitors of proliferation, survival and angiogenesis presenting an interesting opportunity for pharmaceutical intervention. Treatments which inhibit the action of miR-132/212 might therefore be a useful method to inhibit tumor growth by targeting angiogenesis and increase the sensitization of tumors to apoptotic signaling, increasing the effectiveness of cytotoxic therapies for ccRCC.
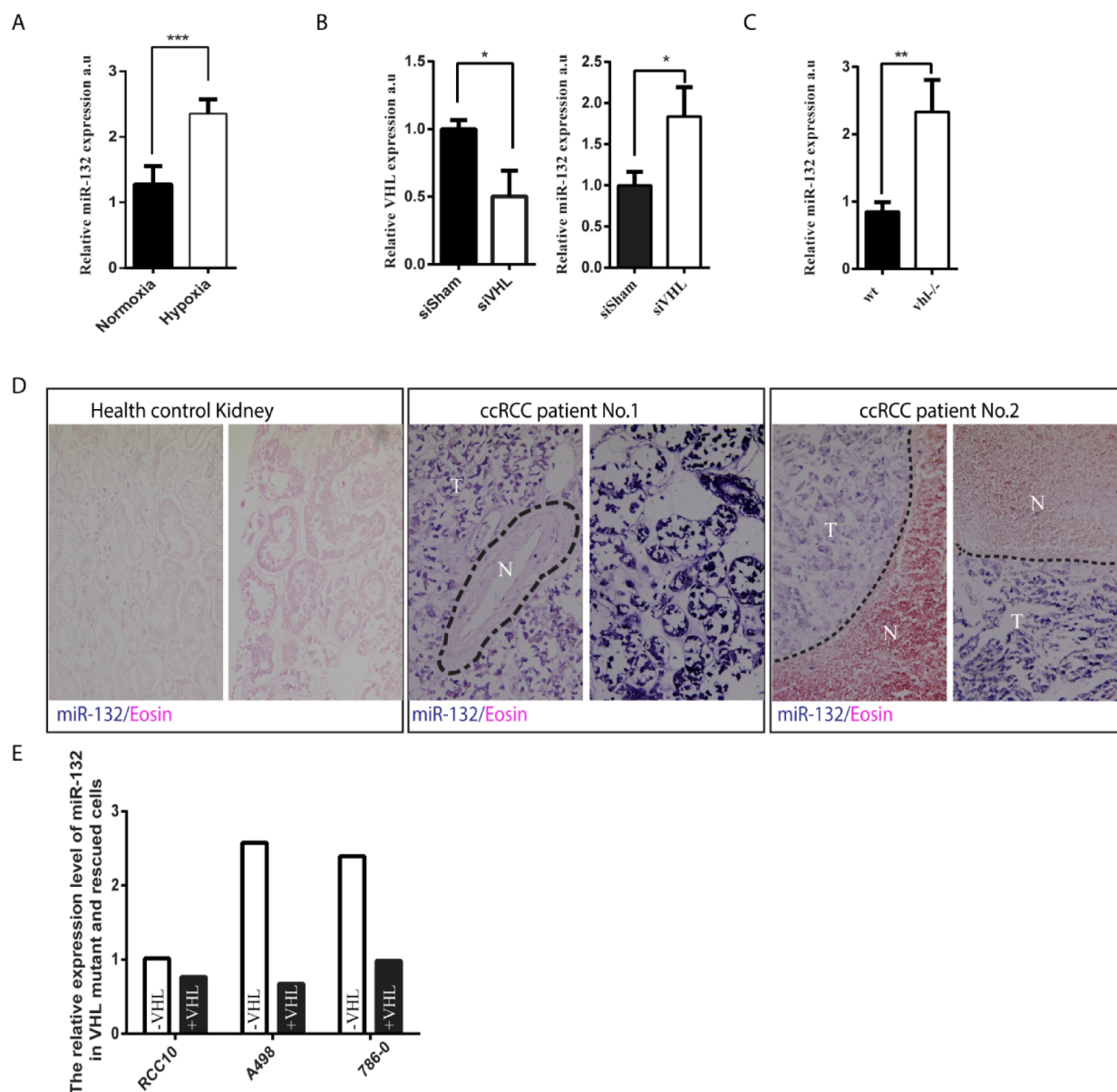
Figure 1. Characterization of miR-132 expression under hypoxic and pseudo-hypoxic conditions.
A. The expression of miR-132 in HUVECs cells under normoxia and hypoxia as compared by qPCR.
B. The expression of miR-132 in siSham and siVHL transfected HUVECs as compared by qPCR. C.
The expression of miR-132 in WT and *vhl*^{-/-} *zebrafish*. D. The expression of miR-132 in healthy kidney tissue and ccRCC from two patients with known bilateral VHL mutations in their tumor as shown by miR-132 in situ hybridization. MiR-132 in situ signal is shown in purple blue. Light eosin counterstaining appears in pink. Dashed line in Patient 2 indicates normal parenchyma (N) vs ccRCC tumor (T) material. E. The expression of miR-132 in established VHL^{-/-} lines RCC10, A498 and 786-0 ectopic VHL expression.
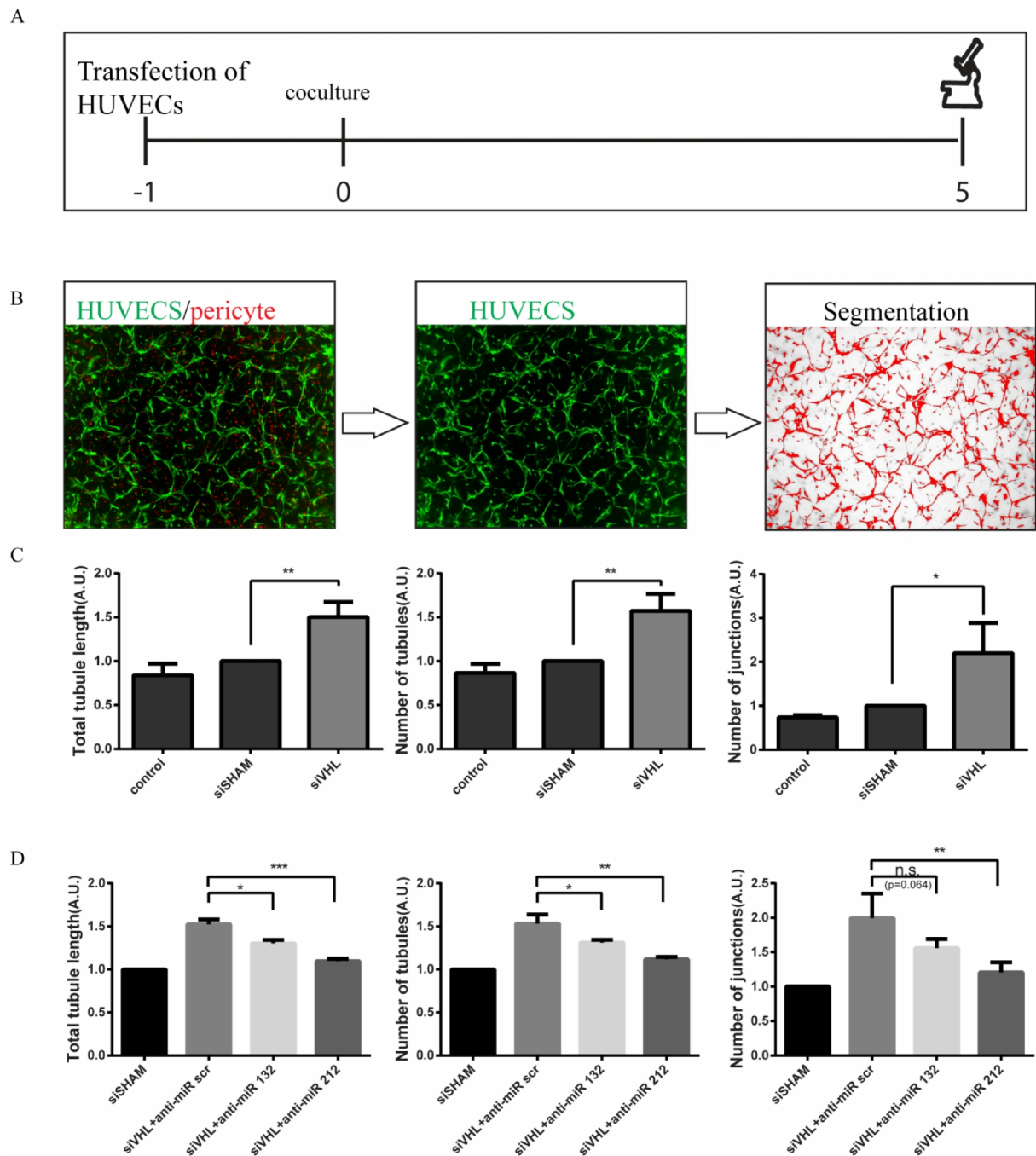
Figure 2. Reduced levels of VHL enhance endothelial cell neovascularization capacity and can be inhibited by blocking miR-132 or miR-212. A. The schematic outline of the coculture experiment with HUVECs and pericytes. B. Schematic cartoon shows the analysis process of tubular structures in the endothelial cells and pericytes coculture assay. C. VHL siRNA knockdown in HUVECs enhances endothelial cell neovascularization capacity. D. Blocking miR-132 or -212 inhibits VHL-induced neovascularization enhancement.
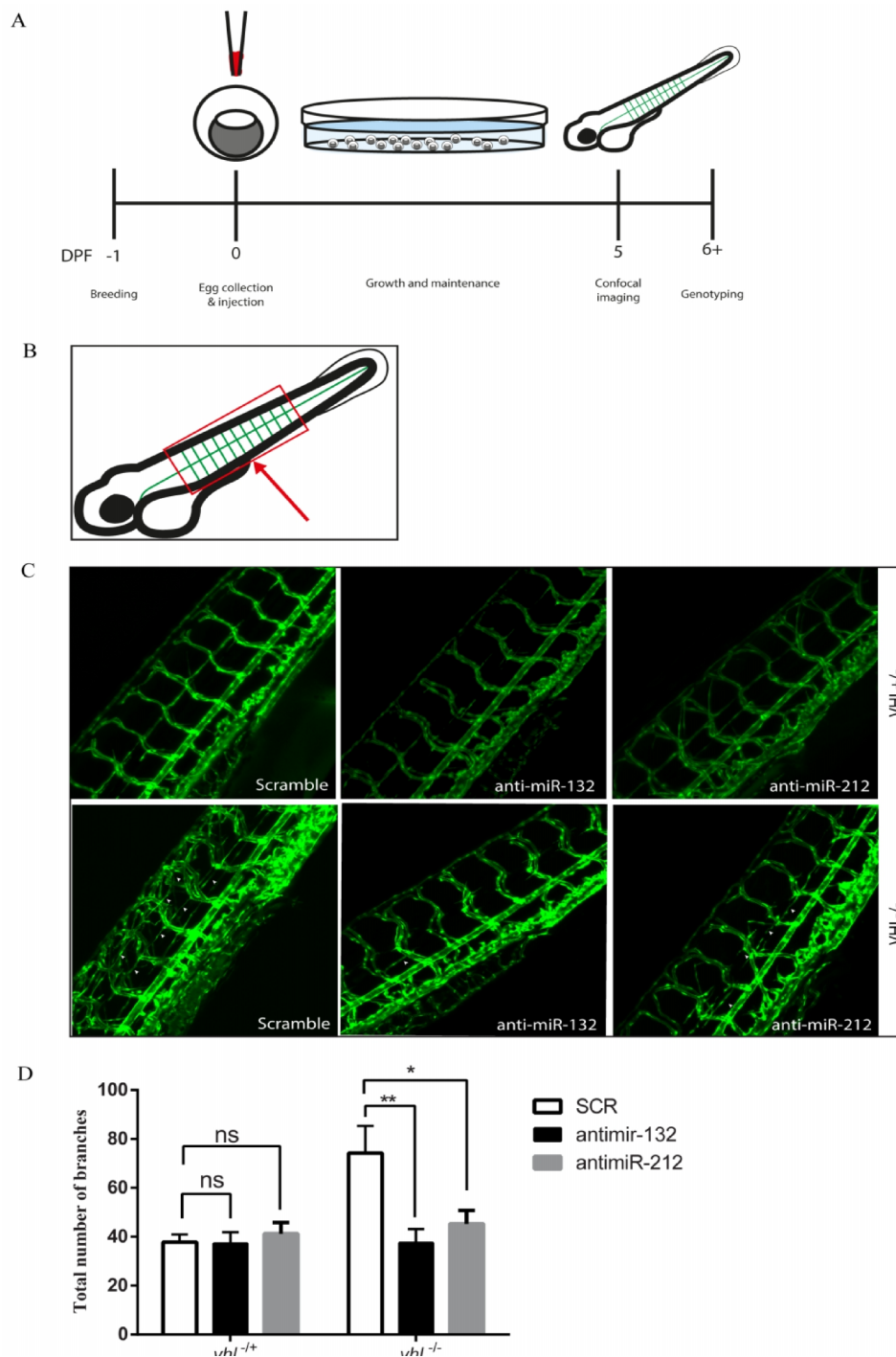
Figure 3. Inhibition of miR-132/212 normalized vasculature outgrowth in *vhl$^{-/-}$* zebrafish. A. The diagram of microinjection of microRNA mimics and antimiRs in *zebrafish* embryos. B. The diagram of intersomitic vasculature of the fish embryo on 5pdf. C. Representative images of tail vascular structures in *vhl$^{+/-}$* and *vhl$^{-/-}$ zebrafish* after injected with scrambled or miR-132, miR-212 inhibitors. D. Quantification of vascular branching after injected with scrambled, miR-132, or miR-212 inhibitors.
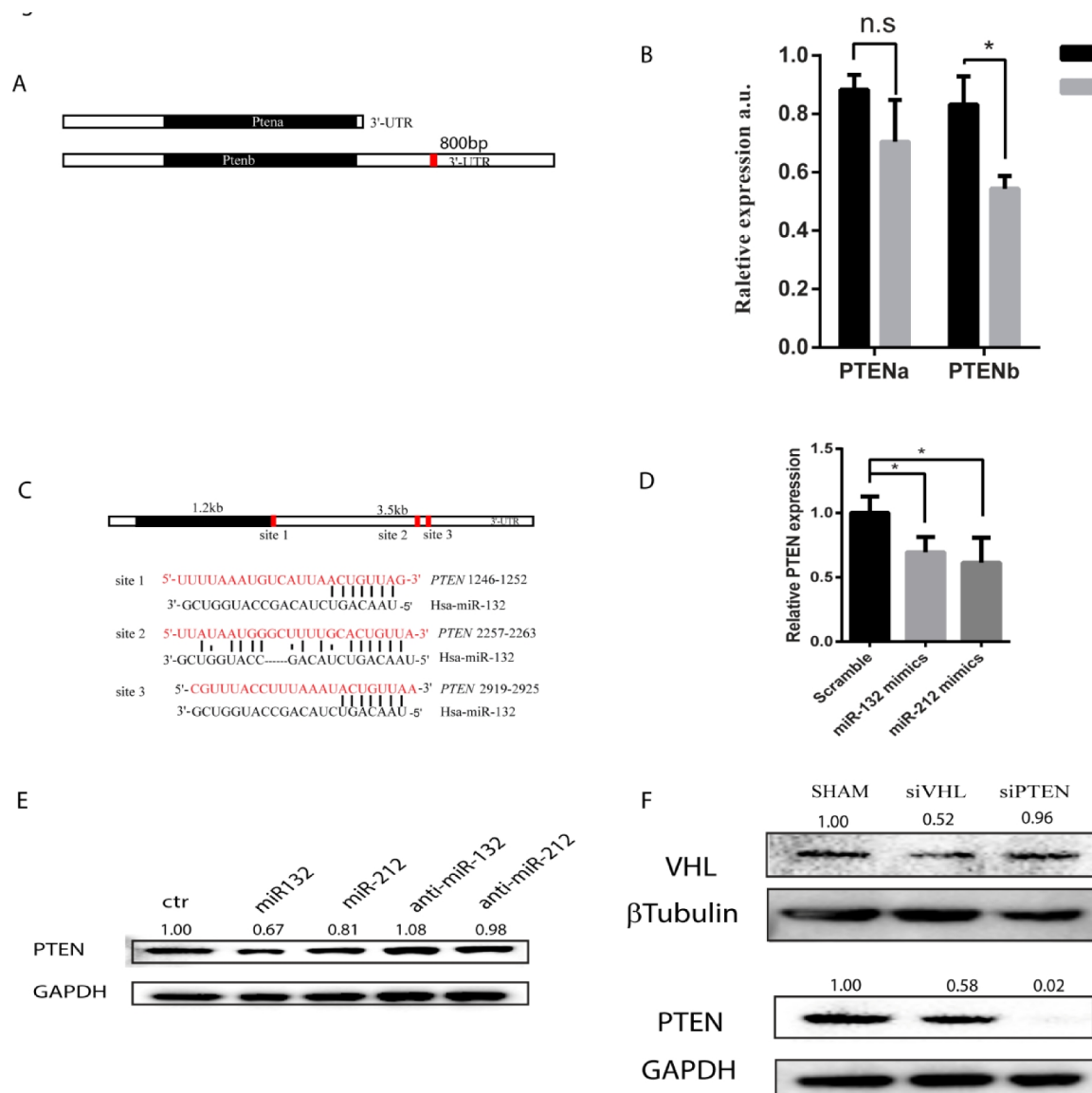
Figure 4. PTEN is a potential target of miR-132/212. A. The position of predicted miR-132 targets on *zebrafish* orthologues ptena and ptenb by Targetscan. Note only ptenb has predicted miR-132 targeting site on the 3'-UTR (red). B. The expression levels of ptena and ptenb in WT and vhl-/- *zebrafish* by qPCR. C. Three predicted miR-132 target sites of PTEN predicted by Targetscan in human. D. PTEN mRNA expression after miR-132, miR-212 overexpression. E. PTEN protein levels after miR-132, miR-212 overexpression and inhibition in HUVECs. The numbers above indicate the relative expression compared with sham normalized by GAPDH. F. The expression of PTEN after VHL or PTEN knockdown by Western Blot.
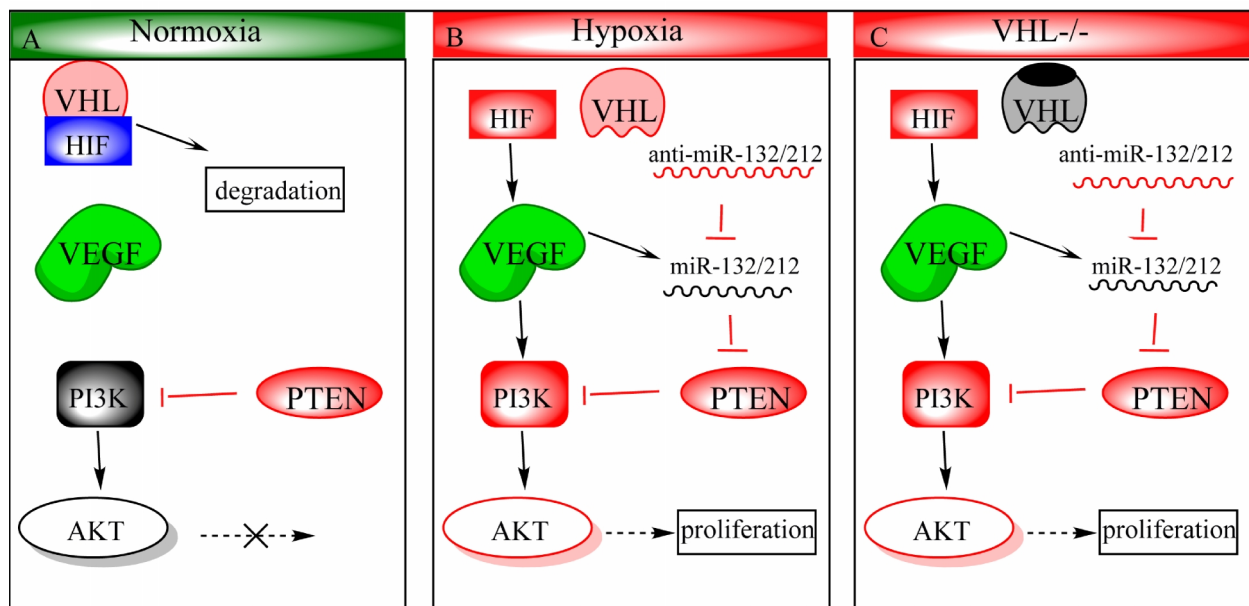
Figure 5. Proposed mechanism of miR-132/212 in modulation of VHL/PI3K/AKT pathways. A. During normoxia, HIFα is ubiquitinated by the VHL-ubiquinition complex, targeting it for degradation. PTEN antagonizes PI3k to prevent AKT from being activated. B. Upon hypoxia, HIFα can no longer be hydroxylated, which prohibits VHL-regulated degradation, and allows stabilized HIFα to translocate to the nucleus and then upregulates its downstream targets such as VEGF. VEGF in turn activates PI3k-AKT pathway and upregulates miR-132/212 expression as well. Upregulated miR-132/212 inhibits PTEN expression which in turn prolongs AKT activity. C. VHL loss-of-function phenocopies hypoxic conditions even in the presence of oxygen (pseudo-hypoxia).

References

1.   Baldewijns, M.M., et al., VHL and HIF signalling in renal cell carcinogenesis. J Pathol, 2010. **221**(2): p. 125-38.
2.   Cancer Genome Atlas Network, Comprehensive molecular characterization of human colon and rectal cancer. Nature, 2012. **487**(7407): p. 330-337.
3.   Frantzen, C., et al., Pregnancy-related hemangioblastoma progression and complications in von Hippel-Lindau disease. Neurology, 2012. **79**(8): p. 793-6.
4.   Shen, J. and M.C. Hung, Signaling-Mediated Regulation of MicroRNA Processing. Cancer Res, 2015.
5.   Anand, S., et al., MicroRNA-132-mediated loss of p120RasGAP activates the endothelium to facilitate pathological angiogenesis. Nat Med, 2010. **16**(8): p. 909-14.
6.   van Rooijen, E., et al., Zebrafish mutants in the von Hippel-Lindau tumor suppressor display a hypoxic response and recapitulate key aspects of Chuvash polycythemia. Blood, 2009. **113**(25): p. 6449-60.
7.   van Rooijen, E., et al., von Hippel-Lindau tumor suppressor mutants faithfully model pathological hypoxia-driven angiogenesis and vascular retinopathies in zebrafish. Dis Model Mech, 2010. **3**(5-6): p. 343-53.
8.   van Rooijen, E., et al., A zebrafish model for VHL and hypoxia signaling. Methods Cell Biol, 2011. **105**: p. 163-90.
9.   Choorapoikayil, S., et al., Loss of Pten promotes angiogenesis and enhanced vegfaa expression in zebrafish. Dis Model Mech, 2013. **6**(5): p. 1159-66.
10.   Jiang, B.H. and L.Z. Liu, PI3K/PTEN signaling in angiogenesis and tumorigenesis. Adv Cancer Res, 2009. **102**: p. 19-65.
11.   Jin, W., et al., Small RNA sequencing reveals microRNAs that modulate angiotensin II effects in vascular smooth muscle cells. J Biol Chem, 2012. **287**(19): p. 15672-83.
12.   Remenyi, J., et al., Regulation of the miR-212/132 locus by MSK1 and CREB in response to neurotrophins. Biochem J, 2010. **428**(2): p. 281-91.
13.   Lei, Z., et al., MicroRNA-132/212 family enhances arteriogenesis after hindlimb ischaemia through modulation of the Ras-MAPK pathway. J Cell Mol Med, 2015.
14.   Gomes, R.S., et al., Efficient pro-survival/angiogenic miRNA delivery by an MRI-detectable nanomaterial. ACS Nano, 2013. **7**(4): p. 3362-72.
15.   Kumar, A., et al., AKT kinase pathway: a leading target in cancer research. ScientificWorldJournal, 2013. **2013**: p. 756134.
16.   Hubbard, P.A., C.L. Moody, and R. Murali, Allosteric modulation of Ras and the PI3K/AKT/mTOR pathway: emerging therapeutic opportunities. Front Physiol, 2014. **5**: p. 478.
17.   Samatar, A.A. and P.I. Poulikakos, Targeting RAS-ERK signalling in cancer: promises and challenges. Nat Rev Drug Discov, 2014. **13**(12): p. 928-42.
18.   Ge, Y.Z., et al., A tumor-specific microRNA signature predicts survival in clear cell renal cell carcinoma. J Cancer Res Clin Oncol, 2015.
19.   Acunzo, M., et al., MicroRNA and cancer - A brief overview. Adv Biol Regul, 2015. **57**: p. 1-9.
20.   Braicu, C., et al., Clinical and pathological implications of miRNA in bladder cancer. Int J Nanomedicine, 2015. **10**: p. 791-800.
21.   Qin, X., et al., The Tumor Cytosol miRNAs, Fluid miRNAs, and Exosome miRNAs in Lung Cancer. Front Oncol, 2014. **4**: p. 357.
22.   Shuch, B., et al., Defining early-onset kidney cancer: implications for germline and somatic mutation testing and clinical management. Journal of Clinical Oncology, 2014. **32**(5): p. 431-437.
23.   Ma, W., et al., Hepatic vascular tumors, angiectasis in multiple organs, and impaired spermatogenesis in mice with conditional inactivation of the VHL gene. Cancer Research, 2003. **63**(17): p. 5320-5328.
24.   Frew, I.J., et al., Combined VHLH and PTEN mutation causes genital tract cystadenoma and squamous metaplasia. Mol Cell Biol, 2008. **28**(14): p. 4536-48.

25.   Wang, S.S., et al., Bap1 is essential for kidney function and cooperates with Vhl in renal tumorigenesis. Proc Natl Acad Sci U S A, 2014. **111**(46): p. 16538-43.

26.   Alimov, A., et al., Somatic mutation and homozygous deletion of PTEN/MMAC1 gene of 10q23 in renal cell carcinoma. Anticancer Res, 1999. **19**(5B): p. 3841-6.

27.   Kondo, K., et al., PTEN/MMAC1/TEP1 mutations in human primary renal-cell carcinomas and renal carcinoma cell lines. Int J Cancer, 2001. **91**(2): p. 219-24.

28.   Velickovic, M., et al., Intragenic PTEN/MMAC1 loss of heterozygosity in conventional (clear-cell) renal cell carcinoma is associated with poor patient prognosis. Modern pathology, 2002. **15**(5): p. 479-485.

29.   Lin, Y.C., et al., SCP phosphatases suppress renal cell carcinoma by stabilizing PML and inhibiting mTOR/HIF signaling. Cancer Res, 2014. **74**(23): p. 6935-46.

Supplementary figure materials
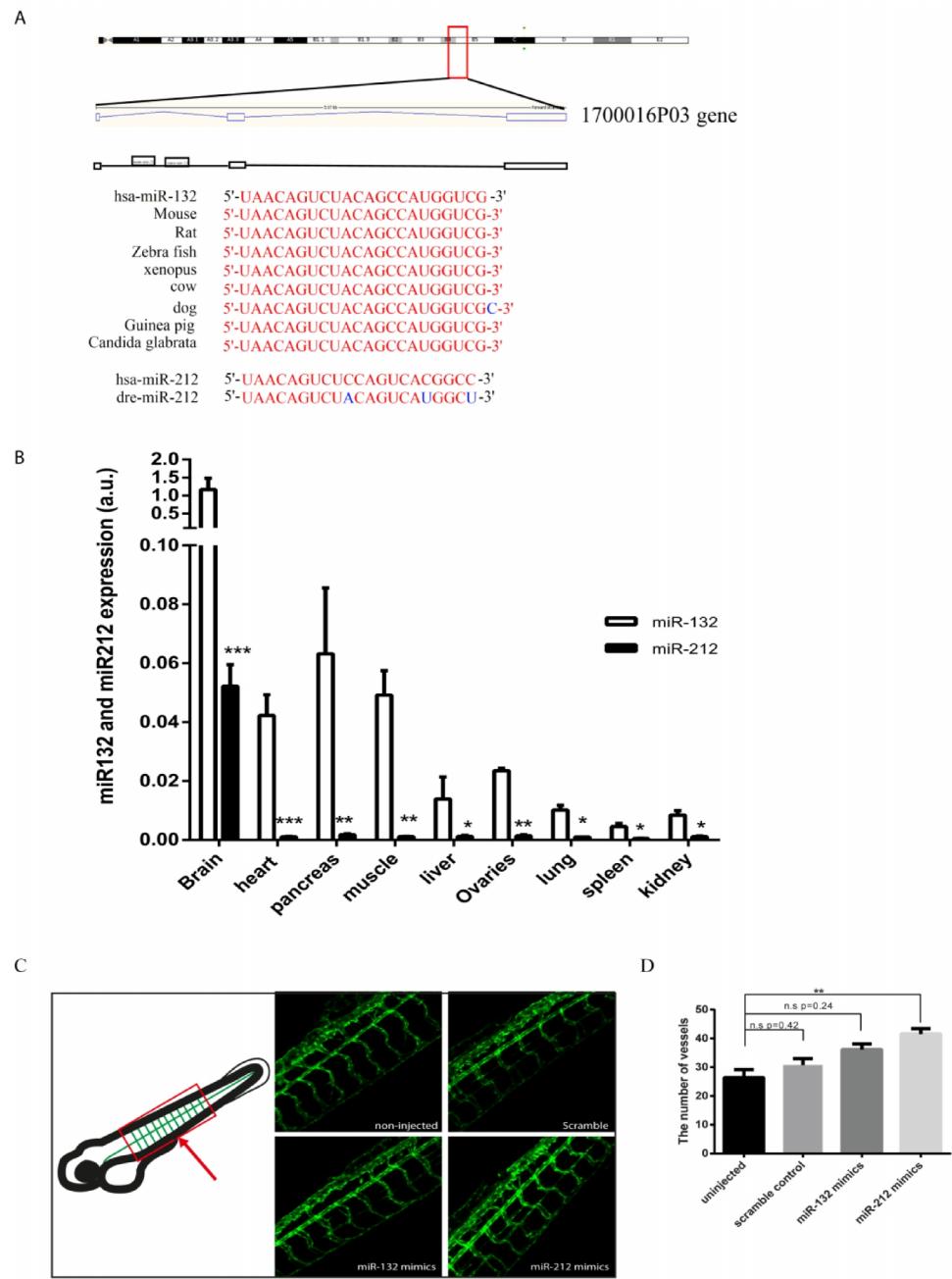
Supplementary figure. A. miR-132/212 location in human genome and conservation of miR-132/212 between different species. B. The relative expression of miR-132 and -212 in different tissues in mouse. Note miR-132 expression is considerably higher than miR-212. n=3. C. Representative images of tail vascular structures in WT *zebrafish* after being injected with scrambled, miR-132, or miR-212 mimics on DPF5. D. Quantification of vascular branching after injected with scrambled, miR-132, or miR-212 mimics.

Chapter 6

MiR-132/212 Impairs Cardiomyocytes Contractility in the Failing Heart by suppressing SERCA2a and PTEN Expression

Zhiyong Lei[1, 5], Christine Wahlquist[2] , Hamid el Azzouzi[1], Janine C. Deddens[1], Diederik Kuster[3], Alain van Mil[1], Agustin Rojas-Munoz[2], Manon M. Huibers[4], Mark Mercola[2], Roel de Weger[4], Jolanda Van de Velden[3,5], Taro Fukao[6], Junjie Xiao[7], Pieter A. Doevendans[1,5] and Joost. P.G. Sluijter[1,5*]

1. Department of Cardiology, Division Heart and Lungs, University Medical Center Utrecht, Utrecht, the Netherlands

2.   Department of Bioengineering, University of California, San Diego, and the Muscle Development and Regeneration Program, Sanford-Burnham Medical Research Institute, 10901 North Torrey pinesroad, La Jolla, California 92037, USA

3. Department of Physiology, Institute for Cardiovascular Research, VU University Medical Center, Amsterdam, the Netherlands

4. Department of Pathology, University Medical Center Utrecht, the Netherlands
5. ICIN, Netherlands Heart Institute, Moreelsepark 1, 3511 EP, Utrecht, the Netherlands

6. Planck Institute of Immunobiology and Epigenetics, Freiburg, Germany

7. Regeneration and Ageing Lab, School of Life Science, Shanghai University, Shanghai, China

Abstract

Background: One of the hallmarks in heart failure is the compromised cardiac function, mostly appearing as decreased contractile capacity due to dysregulated calcium handling. The pathomechanisms causing impaired calcium handling are still not fully understood.

Methods and Results: We have previously identified the miR-132/212 family as a regulator of the sarcoplasmic reticulum Ca2+-ATPase pump SERCA2a and calcium decay in a mouse cardiomyocyte cell line. In this study, we further investigated the role of miR-132/212 in modulating cardiomyocyte contractility in the context of pathological progression of heart failure. We found that the miR-132/212 family is consistently upregulated in all examined hypertrophic heart failure mice models. The overexpression of miR-132/212 prolongs calcium decay in neonatal isolated rat cardiomyocytes, whereas cardiomyocytes isolated from miR-132/212 KO mice display enhanced contractility in comparison to wild type controls. Upon pressure-overload, miR-132/212 KO mice show a blunted worsening (deterioration) of cardiac function. Using a combination of biochemical approaches and in vitro assays, we confirmed that miR-132/212 regulates SERCA2a by targeting the 3' end untranslated region of SERCA2a. Additionally, we also identified PTEN as a direct target of miR-132/212 which may participate in the modulation of cardiac contractility. We observed that miR-132/212 is upregulated in end-stage heart failure patients, which was associated with reduced SERCA2a expression and unaltered PTEN.

Conclusions: The upregulation of miR-132/212 in heart failure impairs cardiac contractile function by targeting SERCA2a and PTEN, suggesting that pharmaceutical inhibition of miR-132/212 maybe a promising therapeutic approach to promote cardiac function in heart failure patients.

Keywords: miR-132/212 family, cardiac contractility, heart failure

Introduction

Intracellular calcium and cardiomyocyte contractility act in a well concerted manner, known as excitation and contraction coupling [1]. In a normal heart contraction-relaxation cycle, the cardiac action potential triggers calcium entry into the cell via L-type calcium channels. This small increase of cytosolic calcium then stimulates a bulk release of calcium from the sarcoplasmic reticulum (SR) into the cytosol via the Ryanodine receptor (Ryr2) [1]. The elevated cytosolic calcium concentration stimulates the contractile machinery of the myofilaments. For relaxation and diastolic filling to occur, cytosolic calcium has to be removed in order to turn off the contractile machinery. In mammalian cells, cytosolic calcium undergoes reuptake by the SR mainly via the sarcoplasmic-endoplasmic reticulum Ca^{2+} ATPase 2 (SERCA2) [2].

In the failing heart, cardiomyocytes cannot maintain a proper excitation and contraction coupling which is still not fully understood, but often associated with a decreased expression or reduced SERCA2a expression, which results in an impaired re-uptake of Ca^{2+} into the SR [3, 4]. Significant efforts have been made to rescue cardiac contractile function through restoration of the expression of SERCA2 directly [5-7] or through indirect enhancement of its activity [8], but the recent results from Phase 2b CUPID2 trial which failed to show ang significant treatment effect as reported by Celladon in April, 2015. In order to develop an effective pharmaceutical treatment to restore SERCA2 expression level, understanding the underlying mechanism of the down-regulation of SERCA2 in failing hearts is still warranted.

MicroRNAs (miRNAs) are small non-coding RNAs that play an important role in regulating cardiac development and maintenance of cardiac function. Dysregulation of miRNAs have been associated with the progressive pathological development of several cardiac diseases [9] and pharmaceutical targeting of miRNAs has been shown to be beneficial in slowing down disease progression [10]. MiRNAs can modulate protein expression through either the degradation or translational inhibition of their target messenger RNA (mRNA) molecules. As certain miRNAs exert an inhibitory effect on gene expression and up-regulation of miRNAs have been reported in the failing heart [11], it is possible that up-regulated miRNAs suppress SERCA2 expression. Removing or blocking those

miRNAs might be a way to maintain SERCA2 expression level. In order to identify those miRNAs, we previously screened for miRNAs which can suppress SERCA2 expression and regulate cardiomyocyte calcium decay kinetics [12]. In this screen, the miR-132/212 cluster was identified as one of the top hits [12]. This miR-132/212 family is highly conserved among many species (Fig 1A) and has been reported as being up-regulated in both heart failure patients and mouse heart failure models [11, 13, 14]. However, their role in cardiac contractile regulation and development of heart failure remains to be defined.

In this study, we reveal that the miR-132/212 family is involved in the regulation of calcium handling and that the up-regulation of these miRNAs may impair cardiac contractility in failing hearts. We show that neonatal cardiomyocytes overexpressing miR-132/212 have a prolonged calcium decay *in vitro* and cardiomyocytes isolated from miR-132/212 KO mice exhibit enhanced contractility *ex vivo*. Moreover, the miR-132/212 KO mice are protected against pressure overload-induced cardiac dysfunction. This suggests that pharmaceutical inhibition of miR-132/212 maybe a promising therapeutic approach to promote cardiac function in heart failure patients.

Results

Expression of miR-132/212 in the heart of hypertrophic mouse models

Since we have previously identified the miR-132/212 family which can suppress GFP expression of the GFP/SERCA2-3'UTR reporter and prolong cardiomyocyte calcium decay kinetics [12], we decided to check the expression of miR-132/212 in normal hearts and in different rodent models for heart failure. miR132/212 mRNA expression was compared between healthy, transverse aortic constriction (TAC)-operated [15], Angiotensin-II infused [16], Calcinurin overexpressing [17], and muscle LIM protein (MLP) KO mice [18]. We observed that levels of both miR-132 and miR-212 were indeed up-regulated in all hypertrophic heart failure mouse models, indicating a common mechanism in these heart failure models (Figure 1B and C).

To further determine which cell types are expressing miR-132/212, we performed miRNA *in situ* hybridization. We observed that miR-132/212 localized mainly in cardiomyocytes (Figure 1D), with some detection also in large vessels (Figure 1D. d'). In accordance with the qPCR assay results (Figure 1B and C), miR-132 was found to be significantly up-regulated in cardiomyocytes from TAC animals (Figure 1D, d').

Overexpression of miR-132/212 suppresses cardiomyocyte contractility

Since miR-132/212 can regulate GFP/SERCA2a-3'-UTR expression and delays calcium decay kinetics in HL-1 cells [12], we decided to confirm the effect of miR-132/212 overexpression on cardiomyocyte contractility in isolated neonatal rat cardiomyocytes (RNCM). Using automated calcium kinetic imaging [12, 19], we found that miR-132 and miR-212 overexpression indeed significantly prolonged the decay of calcium transients (Figure 2A, B, C, and D). This effect was reversed by using antimiR-132 or antimiR-212, respectively (Figure 2A, B, C, and D). Interestingly, we also observed a slower Ca^{2+} influx in cardiomyocytes overexpressing miR-132 but not in the miR-212 overexpressing cells (Figure 2. A and C). These results indicate that both miR-132 and miR-212 may regulate calcium re-uptake, thereby explaining the prolongation of calcium kinetics. Additionally, miR-132 may play a role in calcium release.

To further investigate the physiological role of miR-132/212 in the regulation of cardiomyocyte contractility, taking advantage of our miR-132/212 knockout (KO) mice [20], we isolated individual cardiomyocytes from these KO mice and their littermate wildtype (WT) controls. Using an IonOptix calcium and sarcomere shortening imaging system (figure 2F), we are able to simultaneously record the calcium kinetics and sarcomere shortening of these individual cardiomyocytes. We found that in accordance with the prolonged calcium decay by overexpressing miR-132/212 in RNCM, the loss of miR-132/212 significantly enhanced cardiomyocyte contractility. This is indicated by the enhanced Ca^{2+}- release and Ca^{2+}-decay velocities of the calcium tracing in cells from the KO animals (Figure 2E), and by the diastolic sarcomere length, the enhanced shortening velocity, the shortening amplitude, the fractional shortening and the relengthening velocity of isolated cells from the KO animals (Figure 2G). We also noticed that the KO animals have lower diastolic calcium, longer diastolic sarcomere length which indicated less residual Ca^{2+}, thus a faster calcium reuptake after contraction (Figure 2E).

SERCA2a and PTEN as potential targets of miR-132/212

To explore the mechanism of miR-132/212 in regulating cardiomyocyte Ca^{2+} handling, we selected several potential miR-132/212 targets as predicted by Targetscan, namely SERCA2a, Ryr2, PTEN, and VDAC2 (Supplementary Figure 1 A). We hypothesize that knockdown of the targets of miR-132/212 should at least partially mimic the phenotype of overexpression of miR-132/212 in prolongation of calcium decay. Therefore, we knocked down these potential targets by siRNA and compared with miR-132/212 overexpression. We observed that knockdown of SERCA2a and PTEN could significantly prolong the calcium decay phase, which mimic the calcium kinetics trace of overexpression of miR-132/212 in RNCM (Figure 3. A and B). Meanwhile, knockdown of Ryr2 and VDAC2 did not display such mimicry (Figure 3. A and B). These results suggest that SERCA2a and/or PTEN maybe the targets of miR-132/212 involved in calcium handling in RNCM.

Since PTEN is an established target of miR-132 by 3'-UTR luciferase reporter assays [21], we evaluated SERCA2a similarly. We observed that miR-132 and miR-212 significantly suppress the

luciferase activity of the full length SERCA2a 3'-UTR reporter but not of a mutated SERCA2 3'-UTR reporter (Figure 3C and supplementary Figure 1. B). Likewise, SERCA2a and PTEN protein expression was inhibited by transfection of miR-132 and miR-212 mimics in RNCMs (Figure 3D and E). Additionally, also in our miR-132/212 KO animals the expression of SERCA2 and PTEN are significantly increased (Figure 3F and G). Interestingly, although the calcium kinetics did not show significant effect after Ryr2 knockdown in RNCMs, we did observe an increased Ryr2 expression in KO animals (Figure 3F and G). Taking together, these results show that SERCA2 and PTEN can be regulated by miR-132/212.

Loss of miR-132/212 blunts the pressure overload-induced worsening of cardiac contractile function

To assess the role of miR-132/212 on calcium handling and subsequent cardiac contractility during pathological heart failure progression, we performed TAC on miR-132/212 KO mice and wildtype control litter mates. Seven weeks after TAC induction, we did not observe a difference in heart/body weight ratio between KO and WT mice (Figure 4A and B). Interestingly, by echocardiography analysis we observed a better preserved cardiac function in KO mice (Table 3), as indicated by better preserved Left VentricularFractional Shortening (LVFS) and preserved LV Ejection Fraction (LVEF) at 7 weeks after TAC (Figure 4 C and D). In addition, KO hearts showed lower expression of cardiac damage markers Bnp and a lower βMHC/αMHC ratio, which is indicative for a less diseased phenotype (Figure 4. E). A non-significant trend towards lower Anp and fibrotic remodeling in KO hearts was observed (Figure 4. E). In line with their better contractile function, KO mice showed a higher expression of SERCA2 and PTEN but not Ryr2 (Figure 4F). These results suggest that animals without miR-132/212 are more resistant to pressure overload induced heart failure probably due to the absence of miR-132/212-mediated suppression of SERCA2 and PTEN.

Expression of miR-132/212 and their targets in the failing human heart

We further investigated whether miR-132/212 and their associated targets are similarly dysregulated in failing human hearts as in the mouse. First, we detected increased RNA expression levels of the mir-

132 in failing hearts from dilated cardiomyopathy (DCM), hypertrophic cardiomyopathy (HCM) and ischemic cardiomyopathy (IHD) patients, as compared to the left ventricular free wall of healthy controls (Figure 5. A). A similar pattern was also observed for miR-212, though differences did not reach significance due to larger variations (Figure 5. A). By using miRNA *in situ* hybridization on LV sections of healthy hearts and HCM patients, we observed a larger cross-sectional diameter of the cardiomyocytes with a significantly increased presence of miR-132 in the HCM patients (Figure 5. B).

As expected, DCM, HCM and IHD patients display higher expression of the cardiac damage markers ANP and BNP when compared with healthy controls (Figure 5. C). Only HCM patients failed to reach significance in ANP expression (Figure 5. C). We subsequently examined the expression of miR-132/212 targets in end stage heart failure patients. We observed SERCA2 is down-regulated in DCM, HCM, and IHD patients at both the mRNA and protein levels (Figure 5. D and E), which have been frequently observed in the failing heart [3, 4]. The downregulation of SERCA2a in human heart failure patients was further confirmed by immunofluoresence staining (Figure 5. I). These results suggest that SERCA2a could be a target of miR-132/miR-212 in the failing heart. Western blotting did not confirm the downregulation of total PTEN in heart failure patients (Figure 5.D and E); however, immunofluorescent staining showed reduced PTEN expression levels in cardiomyocytes, while PTEN appeared to be upregulated in other non-cardiomyocyte regions (Figure 5. H).

Discussion

Here we show that the upregulation of miR-132/212 in heart failure impairs cardiac contractile function by targeting SERCA2 and PTEN, suggesting pharmaceutical inhibition of miR-132/212 may be a promising therapeutic approach to restore SERCA2 and PTEN expression, thereby promoting cardiac function in heart failure patients.

The upregulation of miR-132/212 in the stressed or failing hearts has been repeatedly observed, including mouse and human heart failure following pressure overload [11, 13, 14]. We confirmed the upregulation of miR-132/212 in different categories of end stage heart failure patients and cardiac hypertrophic mouse models. But how this upregulation is regulated is still unclear. Recently, four CREB (cAMP-response element binding) sites have been identified within the miR-132/212 genomic loci [22]. It is possible that stress, hormones or growth factors such as Ca^{2+}, cAMP, or TGFβ induces CREB activation and thereby activates many downstream transcripts including miR-132/212 [23, 24]. Consistent with this hypothesis, it is has been shown *in vitro* that miR-132/212 can be upregulated by stimulating the βAR (adrenergic receptor) pathway via βAR agonists (e.g. PE, Angiotensin II) [13]. Since activation of the βAR pathway is a common mechanism by which cardiac contractility is enhanced, it is plausible that an over-stimulated βAR pathway could drive expression of miR-132/212 as a feedback control system, thereby suppressing contractility as a consequence of chronic βAR stimulation (Figure 6).

The upregulation of miR-132 in the failing heart is mainly localized in cardiomyocytes. Using miRNA *in situ* hybridization, we were able to provide additional details regarding the location of the expression of miR-132. We did detect the expression of miR-132 in other cell types, though expression level was relatively low, suggesting a secondary role in other cell types [25-27].

The upregulation of miR-132/212 found in failing heart cardiomyocytes might be detrimental to contractile function *in vivo*. Our results expand upon our previous finding that overexpression of miR-132/212 prolonged calcium decay kinetics in the mouse cardiomyocyte cell line HL-1 [12]. Here, we show that miR-132/212 can prolong calcium decay in RNCM and that this prolongation can be

121

blocked with specific miR-132 or miR-212 inhibitors. This similarity between mouse and rat models suggests that miR-132/212 induced prolongation in calcium decay is well conserved in mammals. On the other hand, cardiomyocytes isolated from miR-132/212 KO mice displayed enhanced contractile capability and these KO mice display better preservation of cardiac function under chronic pressure overload stress. These loss-of-function studies suggest that blocking the upregulation of miR-132/212 could be beneficial in both maintaining cardiac contractile function and slowing the progression towards heart failure.

MiR-132/212 modulates cardiomyocyte contractility at least in part through their regulation of SERCA2a. This is in line with our previous findings that miR-132/212 can suppress GFP expression in the SERCA2a 3'-UTR reporter [12]. This suppression can be eliminated by three nucleic acid mutations within the miR-132/212 seed sequence binding site. Furthermore, endogenous SERCA2a levels declined after transfection of miR-132/212 in neonatal rat cardiomyocytes and miR-132/212 KO mice showed higher levels of SERCA2a protein than wildtype controls, both in normal and stressed hearts. These results suggest that it is possible to increase SERCA2a expression through removal of its inhibitors [12].

Additionally, we identified PTEN as a direct target of miR-132/212 and thereby affect cardiomyocyte contractility. Since maintenance of the calcium gradient – namely, high calcium in the systolic phase and extremely low calcium in the diastolic phase – is key in the regulation of cardiomyocytes contractility, this is well balanced and controlled at different levels (Figure 6). Upon either agonist or hormonal stimulation, the βAR is activated, upon which adenylyl cyclase gets activated and converts AMP into cAMP. cAMP, the secondary messenger, activates protein kinase A (PKA) which eventually activates several downstream targets – including phospholambam (PLN). PLN inhibits the activity of SERCA2 until PLN is phosphorylated by cAMP-activated PKA. Therefore, cAMP concentration is crucial for regulation of cardiomyocyte contractility. *In vivo*, cAMP is degraded by PDE4, which is regulated by PI3Kγ and PTEN: PI3Kγ promotes cAMP degradation activity while PTEN prevents its degradation. Loss of PTEN in cardiomyocytes results in dramatic decrease in contractility [28, 29], but the underlying mechanism still has to be fully characterized. We therefore

postulate that elevated PTEN may raise cAMP levels and thereby activate PKA activity, in turn phosphorylating PLN and increasing the cardiac contractility of the KO mice.

Our results are in accordance with most of the phenotypes observed in antimiR-132 treated TAC animals [13]. For instance, we observe more cardiac function preservation after TAC in miR-132/212 KO mice, including less fibrosis, better ejection fraction and fraction shortening. We did not detect a significant difference in the heart/body weight ratio, although we did observe better functional autophagic response in the KO mice and overexpression of miR-132/212 in RNCM induced hypertrophy (data is not shown). The lack of hypertrophic differences might be caused by a follow-up of 7 weeks after TAC in our mice while the previous study terminated their mice at 3 weeks after TAC. Here, we report that in addition to a better autophagic response, calcium dynamics are directly regulated by this miR-132/212 as well as in cardiomyocytes.

To summarize, our results suggest that the upregulation of miR-132/212 in the failing heart may impair cardiac contractile function and accelerate the progression of heart failure. The pharmaceutical inhibition of miR-132/212 may therefore be a promising therapeutic approach to preserve cardiac function and slow the progression of heart failure in patients.

Materials and Methods

Generation and genotyping of miR-132/212 KO mice

The generation of miR-132/212 KO mice has been described previously[20]. For genotyping, genomic DNA was extracted from ear clippings using genomic DNA isolation kit (Sigma, Cat. XNATS). PCR was done with the GC-Rich PCR kit (TAKARA, Cat. RR002C) with miR-132/212 primers as shown in supplementary. PCR products were separated on 1% agarose gel: WT gave a band at 1076 bp and the KO at 392 bp.

Human cardiac tissue

The used of human cardiac tissue was approved by the Medical Ethics Committee of the University Medical Center Utrecht, The Netherlands.The left ventricular wall of patients with end stage heart

failure (HCM, DCM, IHD) was used while the left ventricular tissue from refused donor hearts was used as healthy controls.

TAC mouse model and Echocardiography

This study was approved by the Animal Ethical Experimentation Committee (Utrecht University) and was carried out in accordance with the Guide for the Care and Use of Laboratory Animals. Transverse aorta constriction was performed as previously described [15]. In brief, 12 weeks old miR-132/212 KO mice or their WT control litters were subjected to TAC or sham surgery. Surgical procedures were performed under sterile conditions with breathing pump and mice were anesthetized with fentanyl (0.05mg/kg), midazolam (5mg/kg), and medetomidine (0.5mg/kg) by intraperitoneal injection. After exposure of the transverse aorta, a 27 gauge constriction was made between the first and second branch of the aortic as previously described. After closure, mice recovered upon atipamezole (2.5mg/kg) and flumazenil (0.5mg/kg). After surgery, Temgesic (0.1mg/kg) was given as painkiller every 8 hours for 2 days. Echocardiography and cardiac function testing were performed both before and 7 weeks following TAC with the Vevo® 2100 System (Visualsonics) and analyzed with Vevo2100-1.6.0 (Visualsonics) software as previously described. During the measurement, mice were under anesthesia with isoflurane and their body temperature was maintained at 37C.

Ex vivo *cardiomyocyte calcium imaging and sarcomere shortening measurement*

Freshly explanted mice hearts were canulated and perfused with perfusion-buffer (11.3mM NaCl, 0.47mM KCl, 60mM KH2PO4, 60mM Na2HPO4, 120mM $MgSO_4$, 1.2mM NaHCO3, 1mM KHCO3, 1mM HEPES and 3mM Taurine) for 10 min at 37C, then switched to an enzyme solution (1x perfusion buffer, 5.5mM glucose and 5.0mM 2, 3-Butanedione monoxide with Roche's Liberase) for about 17 minutes. The hearts were then removed from the perfusion device and placed on petri-dish with stop buffer. The left ventricle was removed and cut into 10 pieces before being gently triturated with a plastic Pasteur pipet to release single cardiomyocytes. After centrifuging, myocytes were resuspended in 1mM $CaCl_2$ with the final concentration gradually adjusted to 2mM. Cells were loaded with Fura-4 at 1μM in Hepes buffer for 30 minutes. After washing, cells were placed under the

IonOptix imaging system, paced at 1HZ, 20mV at 1ml/min continuous flow at 37C. Cells with normal cardiomyocyte morphology (rod shaped, clear striations) and sarcomeres (without bubs or sign of spontaneous contraction) are recorded. Data was analyzed by Ionwizard 6.0.

miRNA in situ hybridization

The procedure for miRNA *in situ* hybridization has been described previously and was applied with minor modifications [30]. Briefly, 10mm sections were fixed with 4% PFA for 10 min before proteinase K treatment (5 mg/ml) for 10 minutes. Subsequently, sections were re-fixed with 0.16M EDC (PI-22980 Thermo Fisher) in 0.13M 1-methylimidazole for one hour at 37℃, then acetylated for 10 mins at room temperature. After incubation for 1 hour with urea based hybridization buffer, DIG labeled miRCURY LNA miRNA detection probes (Exiqon) for miR-132 (38031-15), negative control mir-159 (99003-15), and positive control U6 (99002-15) were applied to the sections overnight. After washing, sections were subsequently blocked for one hour before overnight incubation with anti-DIG alkaline phosphatase antibody (1:1,500, Roche). To block endogenous alkaline phosphatase activity, sections were incubated with levamisole solution (X302130, DAKO). NBT/BCIP (K059811, DAKO) substrate was then added for visualization. Blood vessels in mouse tissue were stained with lectin BS-1 (1:200, Sigma). Nuclei were stained with Hoechst 33342 (Life Technologies). Cardiomyocytes were stained with Troponin (ab47003, Abcam). Images were taken by Zeiss LSM710 and analyzed using Zen 2012 (Zeiss).

RNA isolation and RT-PCR

For miRNA quantification, RNA was extracted with Tripure (Roche) following manufacture instruction, generation of cDNA and qPCR was conducted with the Taqman® miRNA Reverse Transcription Kit and Taqman® miRNA Assay Kit. For gene expression quantification, RNA was prepared with a RNA isolation kit (Macherey-Nagel, Nucleospin RNA kit), transcribed to cDNA using the iScript cDNA Synthesis Kit (Bio-Rad) according to manufacturer instructions, and quantitative

real-time qPCR was performed on a RT-PCR system (Bio-Rad) as described previously [31]. All the primers used for qPCR analysis are listed in the supplementary Table 1.

Immunofluorescent staining

Sections were fixed with cold methanol and subsequently blocked with 10% normal goat serum plus 2% BSA in TBST, containing 0.1% Tween-20. Sections were then incubated with primary antibodies diluted in 0.5% BSA in TBST overnight at 4°C. Images were taken by Zeiss LSM700 and analyzed using ZEN 2012 software (Zeiss). Antibodies and concentrations used in this study are listed in supplementary table 2.

Western blotting

Cells or cardiac tissue were lysed with lysis buffer (50mm Tris-HCL pH 7.4, 100mm NaCl, 1% NP40, 0.1% SDS, 0.5% sodium deoxycholate) supplemented with 1x protease/phosphatase inhibitor cocktail (Cell Signaling, #5872). Protein concentrations were measured with BCA protein assay kit (Thermo Scientific, 23227), 5g cell lysate or 20g tissue lysate was loaded on Nupage bis-tris Precast gels (Life Technologies), and transferred to PVDF membrane with iblot2 Western blotting system (Life Technologies), according to manufacturer instructions. Membranes were first blocked with 5% blotting grade blocker (Bio-Rad #170-6404). After washing, primary antibodies were diluted in 5% TBST and applied to the membrane overnight at 4C. After washing, appropriate horseradish peroxidase HRP-conjugated secondary antibodies were used for enhanced chemiluminescent (ECL) detection (Sigma). All the antibodies used in this studies and their dilution are listed in supplementary table 2.

Cell culture and transfection

HL-1 cells were cultured in Claycomb media (Sigma, 51800C) according to manufacturer instructions. HL-1 cells were transfected with either 20 nmol/L mirVana miRNA mimic negative control (4464085), hsa-miR-132-3p mimics (MC10166), hsa-miR-212-3p mimics (MC10340), mirVana miRNA inhibitor negative control1 (4464077), hsa-miR-132-3p inhibitor (AM10166), hsa-miR-212-

3p inhibitor (AM10340) using RNAiMAX (Life Technologies). After 6 hours, media was replaced with fresh Claycomb media and cells maintained for 72 hours before harvest.

### 3'-untranslated region (3'-UTR) reporter generation and luciferase assay

A 0.8 kb fragment of SERCA2a 3'-untranslated region (3'-UTR) was cloned into the pMIR-REPORT Luciferase vector (Ambion), as described previously [30]. Mutations in the seed-region were generated by Q5 Site-Directed Mutagenesis kit (New England Biolabs) as indicated in figure 3A. All the primers used for cloning and mutagenesis are listed in supplementary table 1. To test suppression efficiency of miR-132 and 212 on luciferase activity, HEK293 cells were co-transfected with 200 ng of pmir-REPORT-3'-UTR Luciferase vectors, or one of the mutated vectors, and a pMIR-REPORT β-gal control plasmid to normalize for transfection efficiency together with 25 nmol/L miRNA mimic controls, miR-132 mimics, or miR-212 mimics with Lipofectamine 2000 (Life Technologies). Luciferase and β-galactosidase activity was measured after 48h with the Luciferase Assay System and β-galactosidase Enzyme Assay System (both from Promega), respectively, as previously described [31].

Statistical analysis

Data was analyzed using Graphpad Prism 6 and comparisons were performed with t-test or paired t-test between two groups, and ANOVA with Bonferroni correction for multiple comparisons. Data are presented as mean ± SEM. *$p < 0.05$ is considered as significant different.
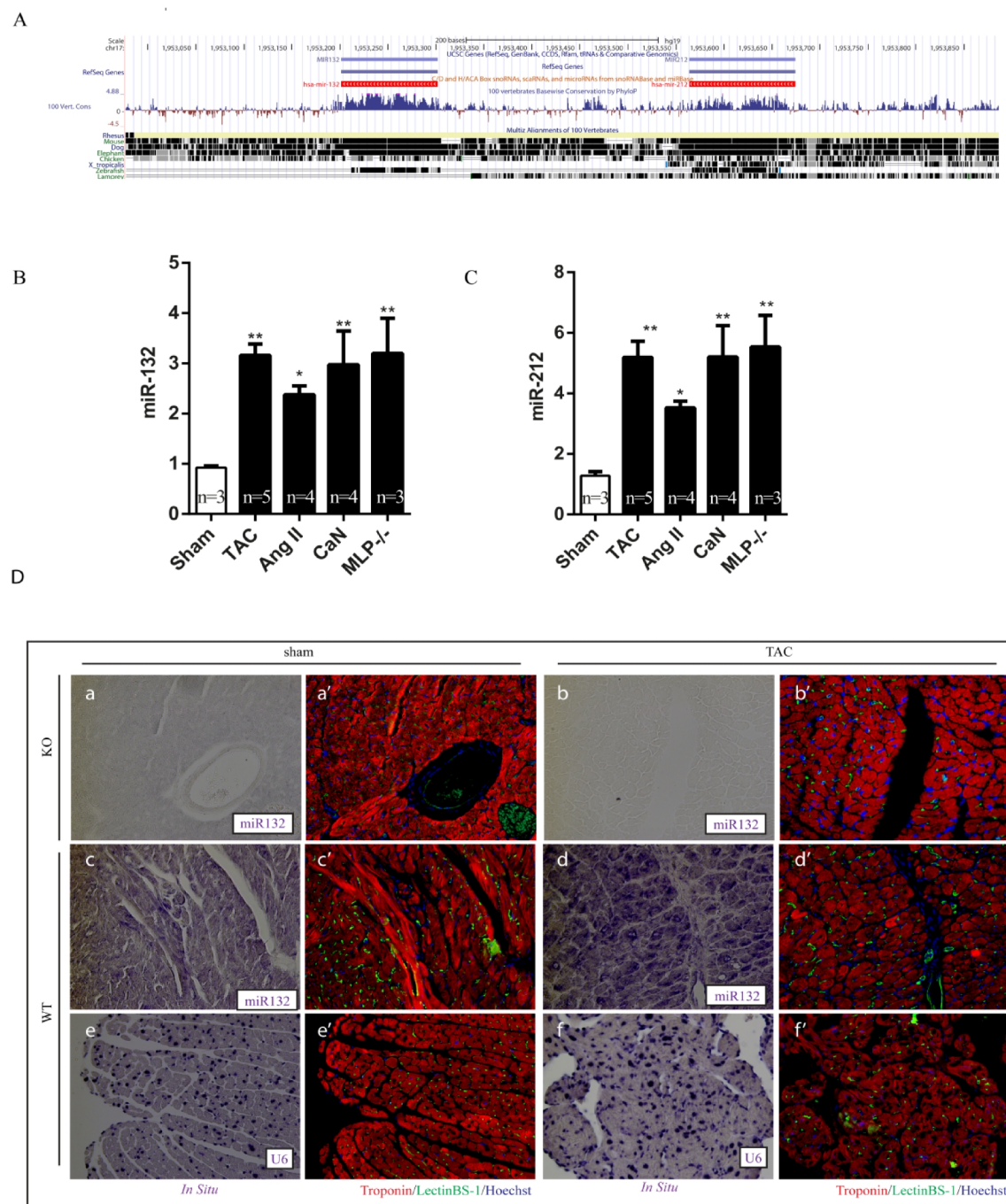
Figure 1 Dysregulation of miR-132/212 expression in left ventricle from hypertrophic mouse models and heart failure patients. A. The location of miR-132/212 loci in human genome (chr17:1,953,129-1,953,734) and conservation of miR-132 and miR-212 between different species [32]. B. The relative expression of miR-132 in left ventricle from Sham, TAC, Ang II, can, MLP^{-/-} induced hypertrophic mouse hearts. RNU6 is used as internal control. C. The relative expression of miR-212 in left ventricle from Sham, TAC, Ang II, can, MLP^{-/-} induced hypertrophic mouse hearts. RNU6 is used as internal control. D. In situ detection of miR-132 in Sham operated miR-132/212 KO mice (a and a'), TAC (b and b') in sham operated wildtype mice (c and c'), TAC (d and d'), in situ detection of U6 served as a control in sham operated wildtype mice (e and e'), TAC (f and f'). Immunofluorescent staining for Lectin BS-1 for endothelial cells in green, Troponin I for viable cardiomyocytes in red, nuclei in blue
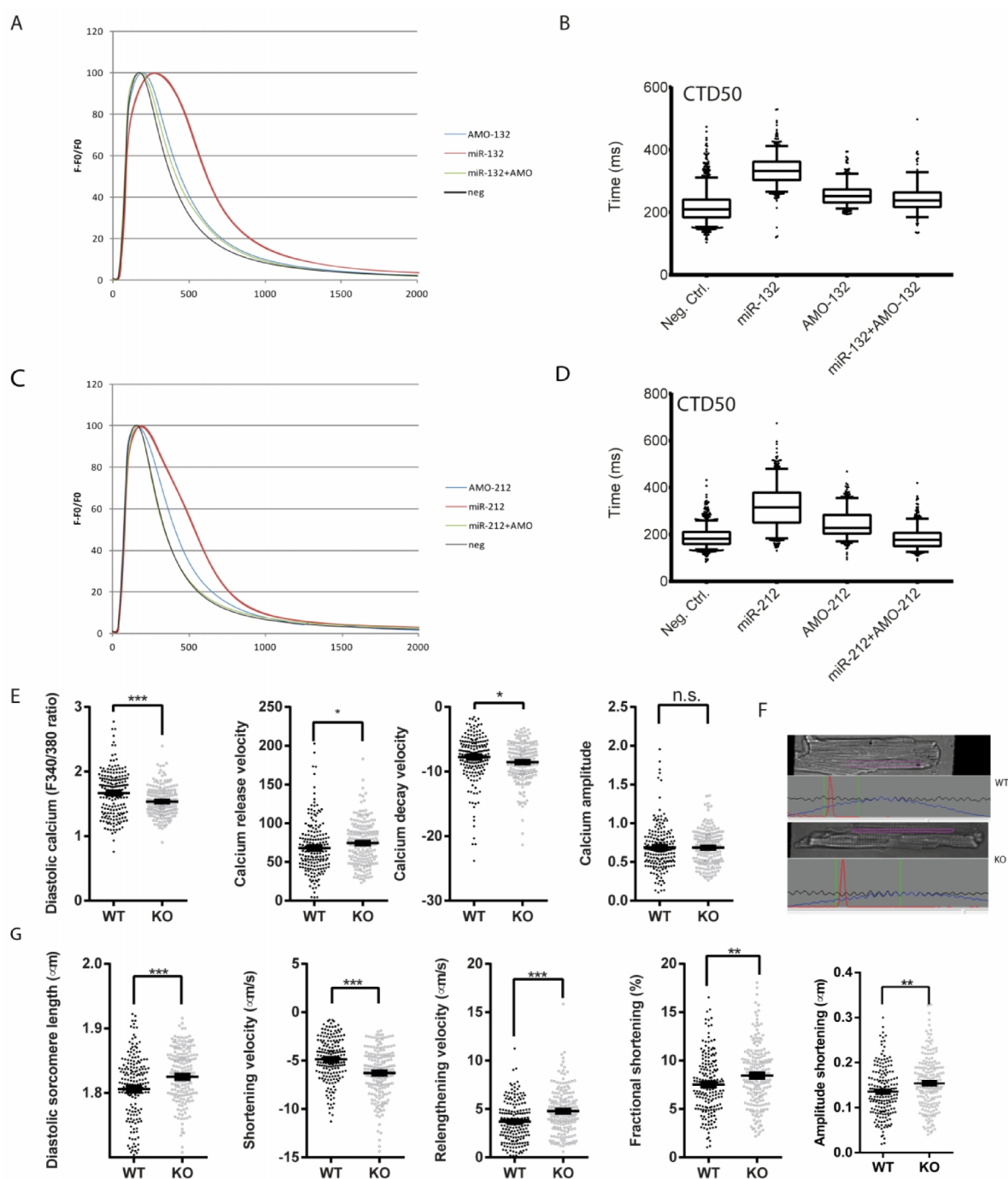
Figure 2 effect of loss or gain of function of miR-132/212 on cardiomyocytes contractility. A. calcium kinetics after overexpression and inhibition of miR-132 on as measured by Fluo-4 intensity. B. The decay time CTD_{50} after overexpression and inhibition of miR-132. C. calcium kinetics after overexpression and inhibition of miR-212 on as measured by Fluo-4 intensity. D. The decay time CTD_{50} after overexpression and inhibition of miR-212. E. Diastolic calcium (F340/380), calcium release velocity, calcium decay velocity and the calcium amplitude of the Fura-2 trace in cardiomyocytes isolated from WT and KO mice. F. Representative image sarcomere shortening analysis of cardiomyocytes isolated from WT and KO mice. G. The diastolic sarcomere length, shortening velocity, relengthening velocity, fractional shortening and the amplitude shortening of cardiomyocytes isolated from WT and KO mice.
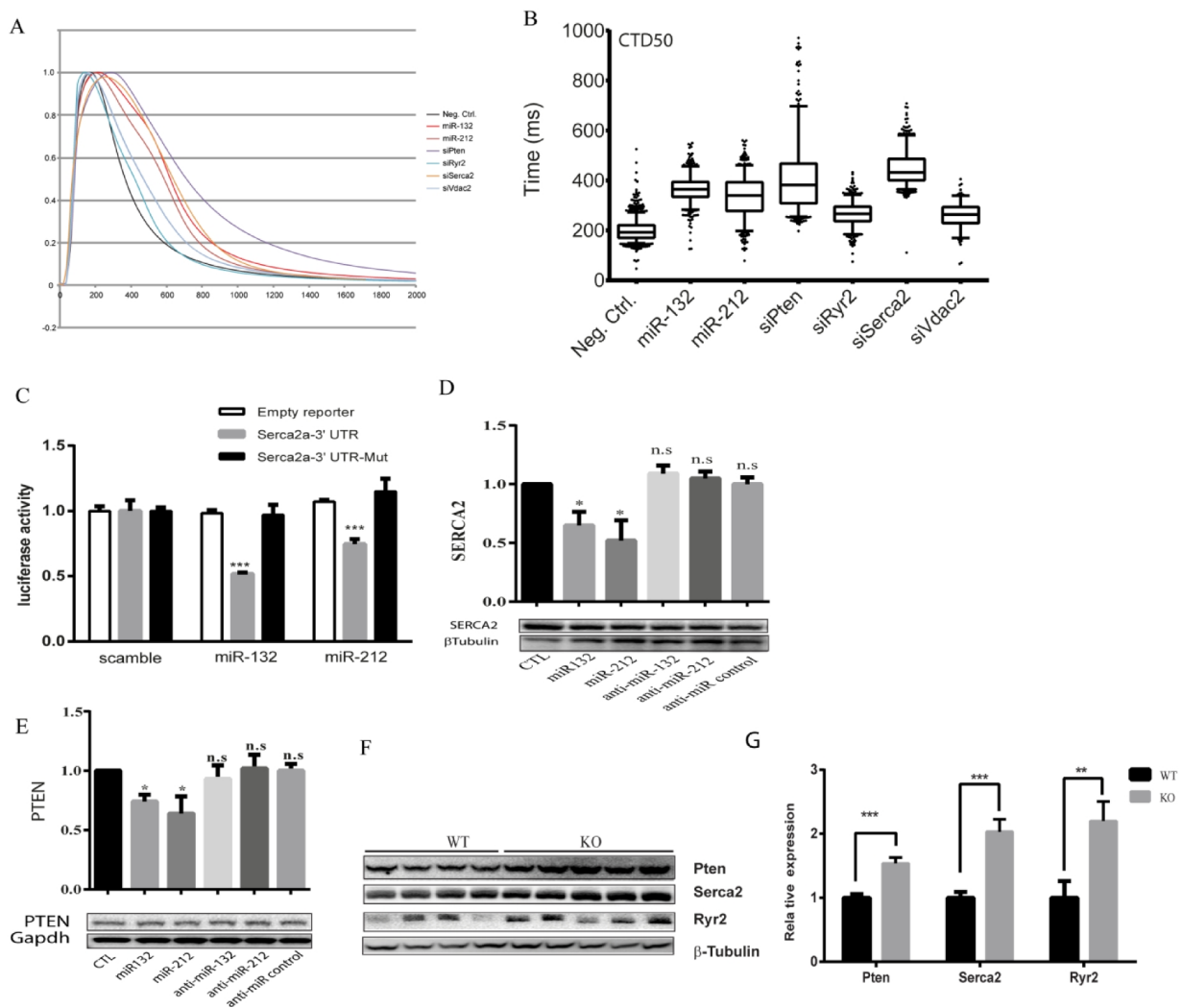
Figure 3. Serca2a and PTEN as potential targets of miR-132/212. A. The effect of knockdown predicted targets of miR-132/212 PTEN, Ryr2, VDAC2 and SERCA2 on calcium kinetics in RNCM as measured by Fluo-4 intensity. B. The decay time CTD_{50} of Fluo-4 signal after PTEN, Ryr2, VDAC2 and SERCA2 knockdown and miR-132/212 overexpression. C. Luciferase activity assay of luciferase reporter with intact SERC2a-3'UTR or 3 nucleic acids mutated 3'-UTR after transfection of synthetic miRNA mimics for scramble, miR-132 or miR-212 corrected by b-gal activity. D. Total endogenous Serca2 expression after transfection of scramble mimics, miR-132, miR-212, antimiR-132, antimiR-212 and antimiRs control by Western blot. Quantification of Serca2 expression corrected by -Tubulin is plotted above. E. Total endogenous PTEN protein after transfection of scramble mimics, miR-132, miR-212, antimiR-132, antimiR-212 and antimiR mimics by Western blot. Quantification of PTEN expression corrected by GAPDH is plotted above. F. PTEN, SERCA2 and Ryr2 protein level between WT and miR-132/212 mice by Western blot. G. Quantification of PTEN, SERCA2 and Ryr2 protein in figure G corrected by -Tubulin

130
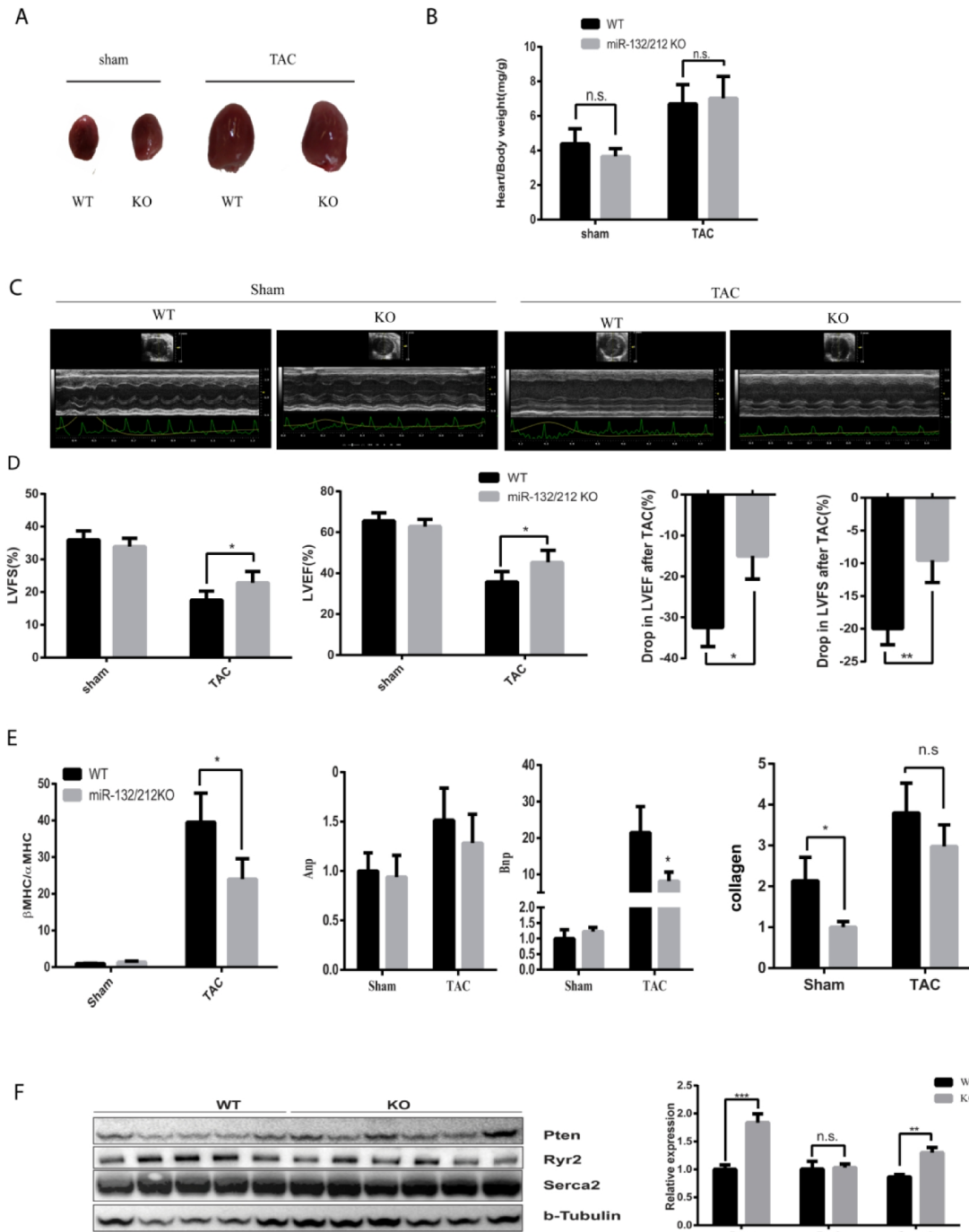
Figure 4 miR-132/212 KO mice are more resistant to pressure overload induced loss of contractility. A. Representative images of explanted WT and KO mice hearts 7 weeks after surgery. B. Gravimetric analysis of heart weight of WT and KO mice 7 weeks after sham or TAC surgery. C. Representative images of cardiac function assessment of WT and KO mice 7 weeks after sham or TAC surgery by echocardiography. D. cardiac function assessment of WT and KO mice 7 weeks after sham or TAC surgery by doppler echocardiography and the drop of cardiac function WT and KO mice before and after 7 weeks TAC. E. Expression of cardiac stress marker Anp, Bnp and βMHC/αMHC ratio and quantified fibrotic area by Picrosirius *Red staining. G. The expression of PTEN, Ryr2 and Serca2 in* WT and KO mice 7 weeks after TAC detected by Western Blot and the quantification.
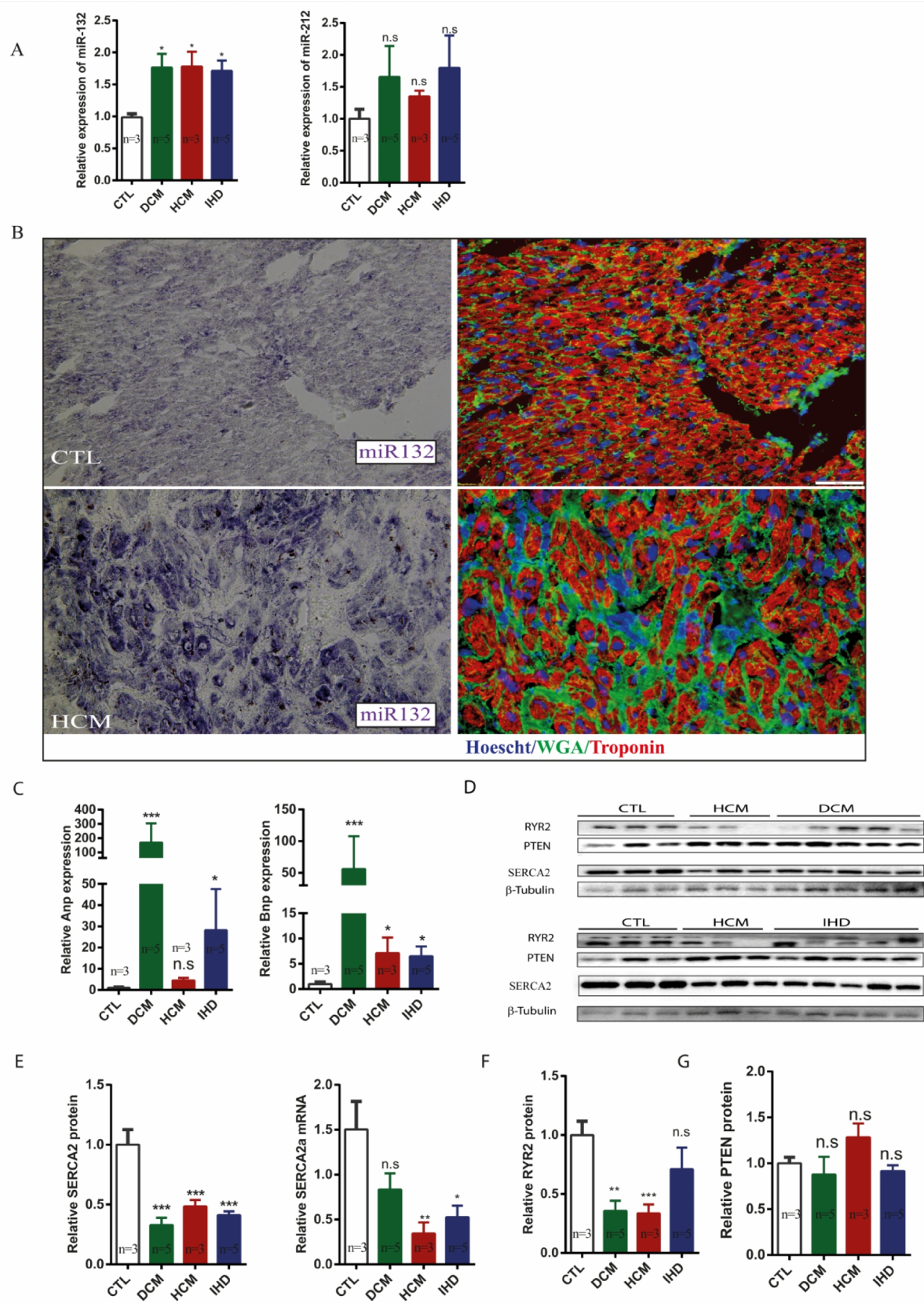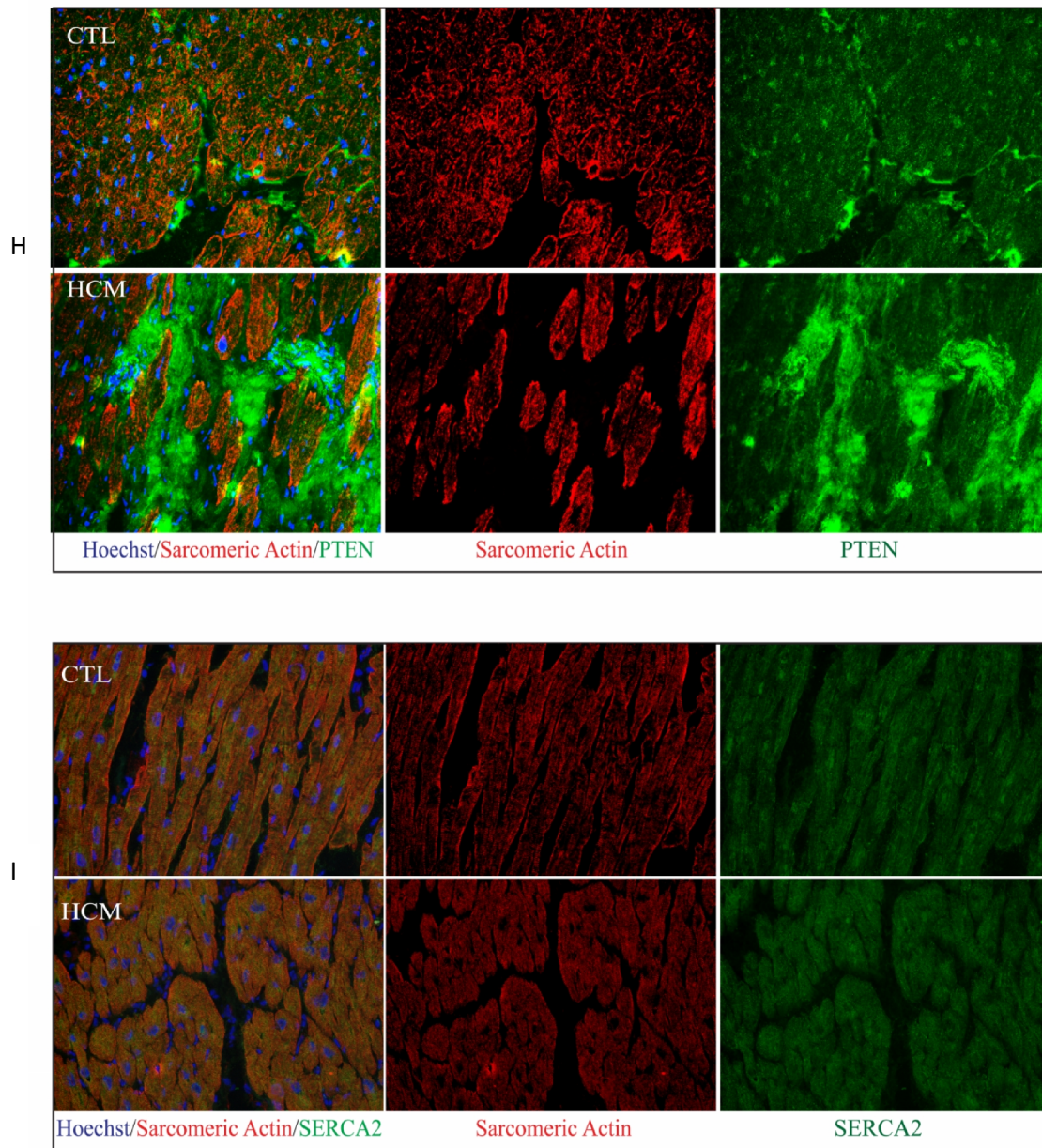
Figure 5. Expression of miR-132/212 and their targets in heart failure patients. A. The relative expression of miR-132 and miR-212 in left ventricle from healthy control, DCM, HCM and IHD heart failure patients. RNU6 is used as internal control. B. *in situ* detection of miR-132 (in purple blue) in healthy controls and HCM patients; immunofluorescent staining for WGA for extracellular matrix in green, Troponin I for viable cardiomyocytes in red, nuclei in blue. C. The relative expression of ANP and BNP mRNA in left ventricle from healthy control, DCM, HCM and IHD heart failure patients. GAPDH is used as internal control. D. The relative expression of RYR2, PTEN and SERCA2 protein in left ventricle from healthy control, DCM, HCM and IHD heart failure patients as detected by Western Blot. β-Tubulin is used as internal control. E. The relative expression of SERCA2a protein quantified from D and mRNA measured by qPCR in left ventricle from healthy control, DCM, HCM and IHD heart failure patients. GAPDH is used as internal control. F. and G Quantification of total endogenous RYR2 and PTEN in D corrected by β-Tubulin. H. and I. Representative image of immunofluorescent detection of PTEN and SERCA2 protein in health control and HCM heart failure patient left ventricle. Sarcomere Actinin is shown in red, PTEN in green and nuclei in blue.
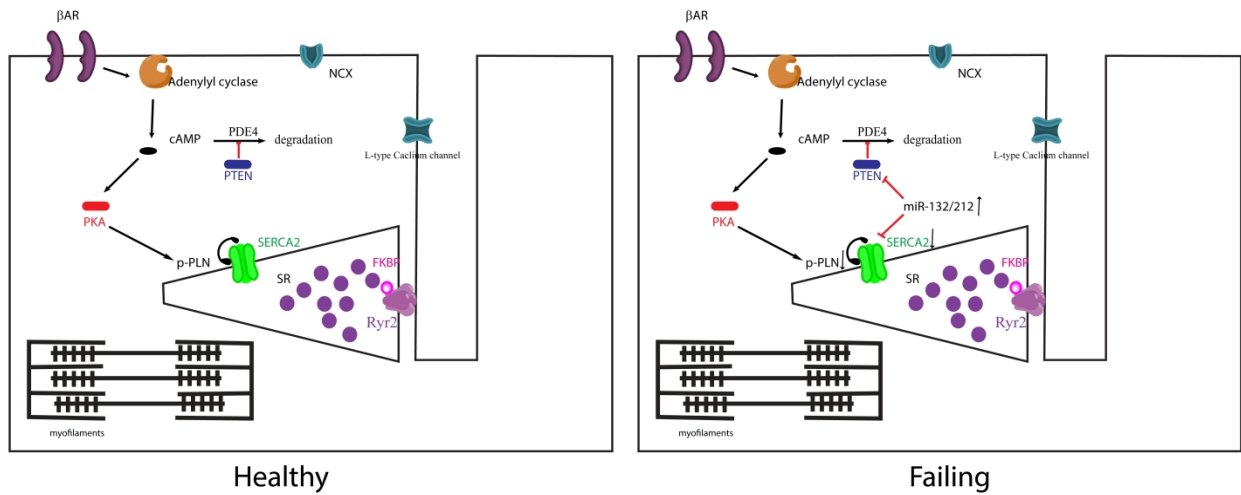
Figure 6 Schematic views for miR-132/212 regulation of cardiac contractility in the healthy and failing heart.

References

1. Bers, D.M., Cardiac excitation–contraction coupling. Nature, 2002. **415**(6868): p. 198-205.
2. Frank, K.F., et al., Sarcoplasmic reticulum Ca2+-ATPase modulates cardiac contraction and relaxation. Cardiovascular research, 2003. **57**(1): p. 20-27.
3. Borlak, J. and T. Thum, Hallmarks of ion channel gene expression in end-stage heart failure. FASEB J, 2003. **17**(12): p. 1592-608.
4. Meyer, M., et al., Alterations of sarcoplasmic reticulum proteins in failing human dilated cardiomyopathy. Circulation, 1995. **92**(4): p. 778-84.
5. Niwano, K., et al., Lentiviral vector-mediated SERCA2 gene transfer protects against heart failure and left ventricular remodeling after myocardial infarction in rats. Mol Ther, 2008. **16**(6): p. 1026-32.
6. Jessup, M., et al., Calcium Upregulation by Percutaneous Administration of Gene Therapy in Cardiac Disease (CUPID): a phase 2 trial of intracoronary gene therapy of sarcoplasmic reticulum Ca2+-ATPase in patients with advanced heart failure. Circulation, 2011. **124**(3): p. 304-13.
7. Greenberg, B., et al., Design of a phase 2b trial of intracoronary administration of AAV1/SERCA2a in patients with advanced heart failure: the CUPID 2 trial (calcium up-regulation by percutaneous administration of gene therapy in cardiac disease phase 2b). JACC Heart Fail, 2014. **2**(1): p. 84-92.
8. Ziolo, M.T., et al., Adenoviral gene transfer of mutant phospholamban rescues contractile dysfunction in failing rabbit myocytes with relatively preserved SERCA function. Circ Res, 2005. **96**(8): p. 815-7.
9. van Rooij, E., et al., Control of stress-dependent cardiac growth and gene expression by a microRNA. Science, 2007. **316**(5824): p. 575-9.
10. Kwekkeboom, R.F., et al., Targeted delivery of miRNA therapeutics for cardiovascular diseases: opportunities and challenges. Clin Sci (Lond), 2014. **127**(6): p. 351-65.
11. Thum, T., et al., MicroRNAs in the human heart: a clue to fetal gene reprogramming in heart failure. Circulation, 2007. **116**(3): p. 258-67.
12. Wahlquist, C., et al., Inhibition of miR-25 improves cardiac contractility in the failing heart. Nature, 2014. **508**(7497): p. 531-5.
13. Ucar, A., et al., The miRNA-212/132 family regulates both cardiac hypertrophy and cardiomyocyte autophagy. Nat Commun, 2012. **3**: p. 1078.
14. van Rooij, E., et al., Dysregulation of microRNAs after myocardial infarction reveals a role of miR-29 in cardiac fibrosis. Proc Natl Acad Sci U S A, 2008. **105**(35): p. 13027-32.
15. el Azzouzi, H., et al., The hypoxia-inducible microRNA cluster miR-199a approximately 214 targets myocardial PPARdelta and impairs mitochondrial fatty acid oxidation. Cell Metab, 2013. **18**(3): p. 341-54.
16. Crowley, S.D., et al., Angiotensin II causes hypertension and cardiac hypertrophy through its receptors in the kidney. Proc Natl Acad Sci U S A, 2006. **103**(47): p. 17985-90.
17. Chu, G., et al., Enhanced myocyte contractility and Ca2+ handling in a calcineurin transgenic model of heart failure. Cardiovasc Res, 2002. **54**(1): p. 105-16.
18. Arber, S., et al., MLP-deficient mice exhibit a disruption of cardiac cytoarchitectural organization, dilated cardiomyopathy, and heart failure. Cell, 1997. **88**(3): p. 393-403.
19. Whittaker, R., et al., Simultaneous recording of action potentials and calcium transients from stem cell-derived cardiomyocytes: Applications for cardiotoxicity testing. Journal of Pharmacological and Toxicological Methods, 2013. **68**(1): p. e47.
20. Kayo, H., et al., miR-212 and miR-132 are dispensable for mouse mammary gland development. Nat Genet, 2014. **46**(8): p. 802-4.
21. Jin, W., et al., Small RNA sequencing reveals microRNAs that modulate angiotensin II effects in vascular smooth muscle cells. J Biol Chem, 2012. **287**(19): p. 15672-83.
22. Remenyi, J., et al., Regulation of the miR-212/132 locus by MSK1 and CREB in response to neurotrophins. Biochem. J, 2010. **428**: p. 281-291.

23. Shaywitz, A.J. and M.E. Greenberg, CREB: a stimulus-induced transcription factor activated by a diverse array of extracellular signals. Annual review of biochemistry, 1999. **68**(1): p. 821-861.

24. Mayr, B. and M. Montminy, Transcriptional regulation by the phosphorylation-dependent factor CREB. Nature Reviews Molecular Cell Biology, 2001. **2**(8): p. 599-609.

25. Lei, Z., et al., MicroRNA 132/212 family enhances arteriogenesis after hindlimb ischaemia through modulation of the Ras MAPK pathway. Journal of cellular and molecular medicine, 2015.

26. Eskildsen, T.V., et al., Angiotensin II regulates microRNA-132/-212 in hypertensive rats and humans. International journal of molecular sciences, 2013. **14**(6): p. 11190-11207.

27. Kumarswamy, R., et al., Vascular importance of the miR-212/132 cluster. European heart journal, 2014: p. ehu344.

28. Crackower, M.A., et al., Regulation of myocardial contractility and cell size by distinct PI3K-PTEN signaling pathways. Cell, 2002. **110**(6): p. 737-49.

29. Ruan, H., et al., Inducible and cardiac specific PTEN inactivation protects ischemia/reperfusion injury. J Mol Cell Cardiol, 2009. **46**(2): p. 193-200.

30. Sluijter, J.P., et al., MicroRNA-1 and -499 regulate differentiation and proliferation in human-derived cardiomyocyte progenitor cells. Arterioscler Thromb Vasc Biol, 2010. **30**(4): p. 859-68.

31. van Mil, A., et al., MicroRNA-214 inhibits angiogenesis by targeting Quaking and reducing angiogenic growth factor release. Cardiovasc Res, 2012. **93**(4): p. 655-65.

32. Karolchik, D., et al., The UCSC genome browser database. Nucleic acids research, 2003. **31**(1): p. 51-54.

A

```
5' -CAGUC-UCAGAGGACCUGACUGUUC-3'          RYR2 225-232
       |   | | |      | | | | | |
   3'-CCGGCACUGACCU------CUGACAAU-5'       Hsa-miR-212
   3'-GCUGGUACCGACAU------CUGACAAU-5'      Hsa-miR-132
   5'-AUUUAAAUGUAUUUAACUGUUA-3'            VDAC2 221-228
                     | | | | | | |
   3'-GCUGGUACCGACAUCUGACAAU -5'           Hsa-miR-132
     3'-CCGGCACUGACCUCUGACAAU-5'           Hsa-miR-212
   5'-CUUUAGAAAACAUUGACUGUUA-3'            VDAC2  318-326
                    | | | | | | |
   3'-GCUGGUACCGACAUCUGACAAU -5'           Hsa-miR-132
     3'-CCGGCACUGACCUCUGACAAU-5'           Hsa-miR-212
   5'-UUUUAAAUGUCAUUAACUGUUAG-3'           PTEN 1246-1252
                      | | | | | |
   3'-GCUGGUACCGACAUCUGACAAU -5'           Hsa-miR-132
     3'-CCGGCACUGACCUCUGACAAU-5'           Hsa-miR-212
  5'-UUAUAAUGGGCUUUUGCACUGUUA-3'           PTEN 2257-2263
       | |  | | |   | | | | | | |
   3'-GCUGGUACC------GACAUCUGACAAU-5'      Hsa-miR-132
     3'-CCGGCACUGACCUCUGACAAU-5'           Hsa-miR-212
   5'-CGUUUACCUUUAAAUACUGUUAA-3'           PTEN 2919-2925
                    | | | | | | |
   3'-GCUGGUACCGACAUCUGACAAU -5'           Hsa-miR-132
     3'-CCGGCACUGACCUCUGACAAU-5'           Hsa-miR-212
   5'- CAUGUUUGACUUUAGACUGUAA-3'           SERCA2a 4236-4257
       :   | |  | |   | | | | | | |
   3'-GCUGGUACCGACAUCUGACAAU -5'           Hsa-miR-132
     3'-CCGGCACUGACCUCUGACAAU-5'           Hsa-miR-212
```

B


```
              3kb                    0.8kb
        [     SERCA2a      ][      3'-UTR      ]

   5'- CAUGUCUGACUGUAGUCUGUAA-3'     rat Serca2 4176-4197
   5'- CAUGUUUGACUUUAGACUGUAA-3'     mouse Serca2a 4236-4257
   5'- CAUGUUUGACUUUAGACUGUAA-3'     human SERCA2a 4236-4257
       :   | |  | |   | | | | | | |
   3'-GCUGGUACCGACAUCUGACAAU -5'     Hsa-miR-132
     3'-CCGGCACUGACCUCUGACAAU-5'     Hsa-miR-212
```
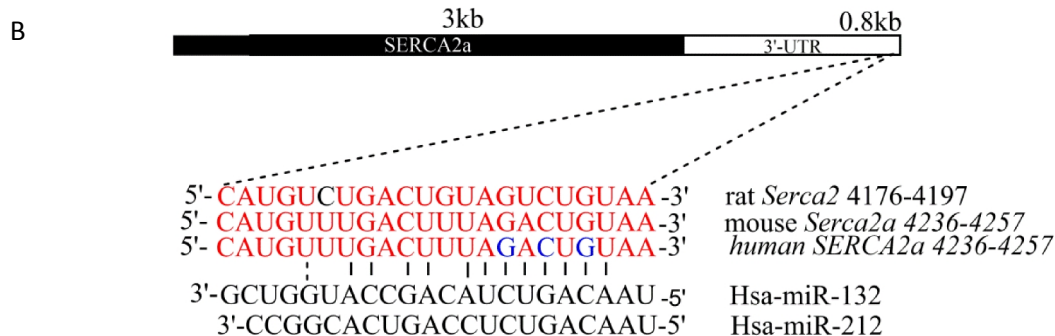
Supplementary material

Supplementary Figure 1. A. Predicted miR-132/212 targeting site on 3'-UTR of Pten, Ryr2 and VDAC2. B. Predicted miR-132/212 targeting site on 3'-UTR of SERCA2a, and site mutation on the 3'-UTR.

Table 1 Primers and oligo used in this study

Primer name	Sequence(5'-3')	Species	Application
Mir132-KO-GT-P1	ATCCTTTCAAGAAAGTGGGGAGA	mouse	genotyping
Mir132-KO-GT-P2	TCTGAGGAGGATGTTCAGACAC	mouse	genotyping
Gapdh_F	GGCATGGACTGTGGTCATGA	mouse	qPCR
Gapdh_R	TTCACCACCATGGAGAAGGC	mouse	qPCR
Serca2a_3'utr_SpeI	ATCGACTAGTCAATACTGGAGTAACCGCTTCCT	mouse	luciferase assay
Serca2a_3'utr_HindIII	ACTGAAGCTTCATAGAATAGATTTATTTACCTGAA	mouse	luciferase assay
Anp_F1	CCTGTGTACAGTGCGGTGTC	mouse	qPCR
Anp_R1	CCTAGAAGCACTGCCGTCTC	mouse	qPCR
Bnp_F1	GTTCTTTTGTGAGGCCTTGG	mouse	qPCR
Bnp_R1	CTGAAGGTGCTGTCCCAGAT	mouse	qPCR
αMHC_F1	GGTCCACATTCTTCAGGATTCTC	mouse	qPCR
αMHC_R1	GCGTTCCTTCTCTGACTTTCG	mouse	qPCR
βMHC_F1	CAGGCCTGTAGAAGAGCTGTACTC	mouse	qPCR
βMHC_R1	TCTCCTGCTGTTTCCTTACTTGCT	mouse	qPCR
PTEN_F1	TGGATTCGACTTAGACTTGACCT	mouse	qPCR
PTEN_R1	GCGGTGTCATAATGTCTCTCAG	mouse	qPCR
Q5_SERCA2a_3UTR_Mut_F	GTCTAAATAGAGATCAGTTTGTTTCTTTC	mouse	luciferase assay
Q5_SERCA2a_3UTR_Mut_R	TGTAAAGTCAAACATGCGCAGTG	mouse	luciferase assay
Serca2a(b)_F1	TGGAACCTTTGCCGCTCATT	mouse	qPCR
Serca2a_R1	CGGTTACTCCAGTATTGCGG	mouse	qPCR
Serca2b_R1	CTGCACACACTCTTTACCGG	mouse	qPCR

Table 2 reagents used in this study

Product name	Company	Catology No.	Dilution	Application
anti-PTEN (138G6) antibody	Cell signaling	9559S	1/1000	WB
anti-RyR2 antibody	Thermo Scientific	MA3-925	1/1000	WB
anti-GAPDH antibody	Cell signaling	#2118S	1/1000	WB
anti-Vimentin	Abcam	ab45939	1/1600	WB
anti-Dig-AP Fab fragment	Roche	11093274910	1/1500	ISH
β-Tubulin (9F3)	Cell signaling	#6181	1/1000	WB
BCIP/NBT	DAKO	K0598	1/1000	ISH
anti-Vimentin antibody V9	Sigma	V6630	1/1000	WB
β-actin antibody AC-15	Sigma	A5441	1/1000	WB
anti-SERCA2 [2A7-A1]	Abcam	ab2861	1/1000	IF
anti-SERCA2 (N-19)	Santa Crutz	sc-8095	1/1000	WB
Lectin BS-I	Sigma	L2895	1/200	IF
WGA	Sigma	L4895	1/500	IF

WB: Western blot; ISH: in situ hybridization; IF: immunfluorescence staining

Table 3 Echocardiography assessment of cardiac function

	7 weeks Sham		7 weeks TAC	
	WT(n=6)	KO(n=9)	WT(n=12)	KO(n=8)
Heart_Rate(BMP)	548.9±11.5	442.8±12.9**	467.3±14.2	463.5±13.9
Diameter_systolic(mm)	2.6±0.2	2.4±0.2	3.4±0.2	3.0±0.3
Diameter_diastolic(mm)	4.0±0.1	3.7±0.2	4.0±0.2	3.9±0.2
Volume_systolic(a.u)	25.3±4.5	24.0±4.7	49.4±6.4	38.8±7.4
Volume_diastolic(a.u)	70.8±5.8	61.6±7.8	73.3±6.5	66.4±7.8
Stroke_volume(a.u)	45.5±2.7	37.6±4.6	23.9±2.6	27.6±2.1
Ejection_Fraction(%)	65.6±3.9	62.5±3.5	35.7±5.0	45.4±5.8*
Fraction_shortening(%)	35.9±2.8	33.6±2.5	17.5±2.8	22.8±3.4*
Cardiac_Output (a.u.)	25.0±1.6	16.6±2.0*	10.9±1.0	12.8±1.0
IVS_d(mm)	0.99±0.05	1.14±0.05	1.03±0.04	0.99±0.03
IVS_S(mm)	1.42±0.08	1.56±0.05	1.36±0.06	1.25±0.07
LVID_d(mm)	3.82±0.21	3.45±0.10	3.71±0.13	4.03±0.21
LVID_s(mm)	2.61±0.22	2.42±0.09	3.05±0.16	3.38±0.24
LVPW_d(mm)	1.17±0.11	1.12±0.07	1.22±0.08	0.98±0.04
LVPW_s(mm)	1.48±0.13	1.45±0.08	1.34±0.07	1.19±0.06
LV_mass(mg)	166.56±11.96	152.52±6.53	170.96±11.96	159.61±11.37
LV_mass_corrected(mg)	133.25±9.58	122.02±5.22	136.77±9.57	127.69±9.09

Chapter 7

Loss of miR-132/212 has no long-term beneficial effect on cardiac function after permanent coronary occlusion in mice

Zhiyong Lei[1], Janine C. Deddens[1], Corina H.G. Metz[1], Esther C.M. van Eeuwijk[1], Alain van Mil[1], Dries Feyen[1], Hamid el Azzouzi[1], Taro Fukao[3], Pieter A. Doevendans[1,2] and Joost. P.G. Sluijter[1,2]*

[1]Department of Cardiology, Division Heart and Lungs, University Medical Center Utrecht, Utrecht, the Netherlands Taro Fukao[3]

[2]ICIN, Netherlands Heart Institute, Moreelsepark 1, 3511 EP, Utrecht, the Netherlands

[3]Max Planck Institute of Immunobiology and Epigenetics, Freiburg, Germany

In preparation

Background:

Myocardial infarction (MI) is caused by occlusion of the coronary artery and induces ischemia in the myocardium and eventually a massive loss in cardiomyocytes. Studies have shown many factors or treatments that can affect the healing and remodeling of the heart upon infarction, leading to better cardiac performance and clinical outcome. Previously, miR-132/212 has been shown to play an important role in arteriogenesis in a mouse model of hindlimb ischemia and in the regulation of cardiac contractility in hypertrophic cardiomyopathy in mice. In this study, we explored the role of miR-132/212 during ischemia in a murine MI model.

Methods and Results:

miR-132/212 knockout mice show enhanced cardiac contractile function at baseline compared to wild-type controls, as assessed by echocardiography. One day after induction of MI by permanent occlusion, miR-132/212 knockout mice display similar levels of cardiac damage as wild-type controls, as demonstrated by infarction size quantification and LDH release, although a trend towards more cardiomyocyte cell death was observed in the knockout mice as shown by TUNEL staining. Four weeks after MI, miR-132/212 knockout mice show no differences in terms of cardiac function, expression of cardiac stress markers, and fibrotic remodeling, although vascularization was reduced. In line with these *in vivo* observation, overexpression of miR-132 or miR-212 in neonatal rat cardiomyocyte suppress hypoxia induced cardiomyocyte cell death.

Conclusions:

Although we previously observed a role in collateral formation and myocardial contractility, the absence of miR-132/212 did not affect the overall myocardial performance upon a permanent occlusion of the coronary artery. This suggests an interplay of different roles of this miR-132/212 before and during MI, including an inhibitory effect on cell death and angiogenesis, and a positive effect on cardiac contractility and autophagic response. Thus, spatial or tissue specific manipulation of this microRNA family may be essential to fully understand the roles and to develop interventions to reduce infarct size. .

Keywords: miR-132/212, cardiac function, adverse cardiac remodeling

Introduction

Although the mortality rate of MI in patients is going down due to recently developed post-infarction treatments and secondary prevention, MI is still one of the leading causes of mortality [1]. 12.5% of patients that suffered a MI with ST-segment elevation will die within 6 months [2], suggesting that novel effective treatments are still required.

microRNAs are small non-coding RNAs that play important roles in cardiac development and progression of pathological progression of cardiac diseases. Therapeutic interventions have been shown to be beneficial to slow down the myocardial pathological progression [3-8] and therefore microRNAs have been considered as promising therapeutic targets for cardiovascular diseases [9, 10]. In search of novel microRNA targets for cardiovascular disease treatment, we and others have found a beneficial role for miR-132/212 during hind-limb ischemia to promote arterial growth (chapter 4) and a detrimental role in regulation of cardiomyocyte contractility and the cardiac autophagic response under stress (chapter 6). However, the regulation and biological function of this family in the response to a MI has never been investigated. We therefore used the miR-132/212 genetic knockout (KO) mice and induced MI by permanent occlusion of the coronary artery to explore the functional effects on cardiac function compared to wild-type controls.

Materials and Methods

Generation and genotyping of miR-132/212 KO mice

The miR-132/212 KO mice have been generated as described previously [11]. For genotyping, DNA samples were obtained by ear clipping and used in a GC-Rich PCR kit (Roche, cat. 12140306001) with miR-132/212 primers as shown in supplementary table 1. PCR products were revealed on a 1% agarose gel: WT genotype display a predicted band at 1076 bp and the KO genotype at 392 bp.

LAD ligation and Echocardiography

This study was approved by the Animal Ethical Experimentation Committee (Utrecht University) and was carried out in accordance with the Guide for the care and use of Laboratory Animals.
MI was induced by ligation of the Left anterior descending artery (LAD) and applied on 10-12 weeks old WT (C57B6) and miR-132/212 KO mice, as described previously[12]. In brief, mice were anesthetized with fentanyl (0.05mg/kg), midazolam(5mg/kg) and medetomidine (0.5mg/kg) by intraperitoneal injection and surgical procedures were performed under sterile conditions. LAD was ligated just below the left atrial appendage with an 8-0 Ethilon monifil suture. The chest was then closed and animals received atipamezole (2.5mg/kg) and flumazenil (0.5mg/kg) to recover quickly. Temgesic (0.1mg/kg) was given every 8 hours after surgery for 6 times to reduce discomfort. Cardiac function was assessed with echocardiography (Vevo® 2100 System , Visualsonics) and analyzed with

Vevo2100-1.6.0 (Visualsonics) before and after the surgical procedure (days 0, 7, 14 and 28, supplementary figure 1A). During the procedure, the animals were kept under 2% isoflurane anesthesia and the body temperature was strictly maintained between 36.5°C- 37.5°C.

Neonatal Rat Cardiomyocytes isolation and hypoxia treatment

Neonatal rat cardiomyocytes isolation was performed with Pierce Primary Cardiomyocyte Isolation Kit (Life Technologies, Cat. 88281) following manufacture's instruction. In brief, neonatal rat hearts were collected within 3 days after birth. After washing with ice cold HBSS, hearts are cut into small pieces before enzymatic digestion for 35 min. After digestion, pieces are washed with cold HBSS once again and disassociated with cardiomyocyte culture medium with 10% FBS and single cells generated by filtrating over a 40 m filter to remove undigested tissue. After centrifuge, cells were resuspended in culture medium with 10% FBS and seeded at 2.5×10^5 cells/cm^2. The next day, cells were transfected with microRNA mimics with RNAi Maxi at 50nM following manufacture's instruction. Six hours after transfection, medium was replaced with fresh DMEM medium with 10% FBS containing 1x Cardiomyocyte Growth Supplement. Forty-eight hours after transfection, cells were transferred to a hypoxia chamber with 5% CO_2 and 1% O_2 for 24 hours. Then cells were fixed with 4% PFA for 15 min before TUNEL staining.

TUNEL staining

Twenty-four hours after MI surgery (n=4/group), mice were terminated. Hearts were explanted, rinsed and fixed with 0.2 PFA in 15% sucrose at 4°C overnight before cryopreservation with Tissue Tek for sectioning. Ten m cryosections were prepared. For TUNEL staining, sections were first dried for 10min at room temperature, then digested with 5 g/ml proteinase K (cat. Roche)for 20 min at 37°C. Sections were subsequently used for TUNEL staining (In situ Death Detection Kit, Cat. 1684795, Roche) following manufacturer's instructions. After TUNEL, sections were counterstained with Hoechst for nuclei and Troponin for cardiomyocytes. Images were taken and analyzed by a blinded investigator with Cellsens imaging system at 20x magnification. TUNEL staining for hypoxia treated Rat neonatal cardiomyocytes (RNCM) was performed in a similar approach, but without Proteinase K treatment.

Infarct Size Quantification

Twenty-four hours after MI surgery (n=6/group), infarct size (IS) was determined as a percentage of the area at risk (AAR). Four % Evans Blue solution was injected via the thoracic aorta and hearts were explanted, rinsed and filled with paper before placement in -20°C freezer for 1 hour. Hearts were subsequently sliced into 1mm cross sections and incubated with 1% triphenyltetrazolium chloride (TTC, Sigma) for 1 hour at 37 °C, then fixed with formaldehyde 4% for 15 min. Images from both

sides of the cardiac sections were taken sequentially. IS, AAR and left ventricular area were measured with Photoshop and reconstructed as previously described in ImageJ [13].

Lactate Dehydrogenase and Troponin measurement

After termination at 24 hours post-MI, blood samples (n=4/group) were collected by cardiac puncture. Samples were centrifuged at 12000xg for 10min and cleared plasma then transferred to another tube. For total lactate dehydrogenase assay (LDH), 10 ml of plasma was used to determine total LDH concentration using the Toxicology Assay kit (Cat. TOX7-1KT, Sigma) according to manufacturer's instructions with an arrayscan at 492nM (Thermo Fisher). cTnI levels were measured by ELISA (Synchron Lxi 725 integrated clinical chemistry, Beckman Coulter) in the Laboratorium Klinische Chemie en Haematologie (LKCH) of UMC Utrecht as previously described [14].

Histological analysis and immunohistochemical staining

28 days after MI (long-term group, n=6/group), mice were terminated. Hearts were explanted, rinsed and fixed with 0.2 PFA in 15% sucrose at 4 °C overnight before cryopreservation with Tissue Tek for sectioning. HE staining and Picrosirius red staining were performed for morphological and fibrotic remodeling assessment, respectively, as described before[15]. To evaluate large vessels, sections were first blocked with 2% BSA for 30min, FITC-labeled anti- SMA antibody was applied for 1 hour at room temperature. After incubating the slides with 1 mg/ml Hoechst to visualize the nuclei, sections were mounted in fluoromount G (Southern Biotech). The complete sections were then scanned for both SMA and Hoechst channel. Images were analyzed with ImageJ. All the SMA positive signal larger than 500 arbitrary unit (a.u.) (proximately 2 nuclei) were considered as a vessel. The vessel coverage was calculated by total vessel area divided by total number of cells and vessel density was calculated by the total number of vessels divided by the total number of the cells.

RNA isolation and RT-PCR analysis

DNA-free RNA was extracted with Tripure (Roche applied science). To perform qPCR for gene expression, RNA is transcribed to cDNA using the iScript cDNA Synthesis Kit (Bio-Rad) according to manufacturer's instructions, and quantitative real-time PCR was performed on a MyIQ single-color qRT-PCR system (Bio-Rad), as described previously [16]. All primers used for qPCR analysis are listed in the supplementary table 1. Mature miR-132 and miR-212 expression levels were measured by TaqMan® MicroRNA Assay following manufactory's instruction, using U6 as control.

Statistical analysis

Data was analyzed using Graphpad Prism 6 and comparisons were performed with t-test between two groups. Data are presented as mean ± SEM. p<0.05 is considered as significant.

Results

miR-132/212 knockout mice show more damage after MI

Consistent with our previous observations, miR-132/212 knockout mice display enhanced cardiac contractile function as shown by higher left ventricular fraction shortening (LVFS), left ventricular ejection fraction (LVEF) and myocardial performance index (MPI) at baseline, as shown in Supplementary Figure 1C.

To assess the role of miR-132/212 in the setting of an acute MI, LAD ligations were performed in miR-132/212 knockout and WT control mice (Supplementary Figure 1A). 24 hours post-MI, cardiac damage was assessed by TTC staining on cardiac slices from operated WT and KO mice (Figure 1 A). No significant differences were observed in infarct size (IS), as measured both in percentage of LV (IS/LV) and in percentage of area at risk (IS/AAR). Although KO mice display a trend towards higher IS/AAR (Figure 1B), circulating Lactate Dehydrogenase (LDH) levels and Troponin levels, markers for cardiac damage, did not differ between WT and KO mice (Figure 1B).

 TUNEL staining was performed on cross sections of infarcted hearts 24 hours post-MI to determine differences in cell death. A trend to an increased percentage of TUNEL positive cells in the KO mice is observed in both border zone and infarcted area compared to WT control hearts (Figure 1C) which indicated that KO mice may have a higher potential for infarct expansion over time.

To further explore the effect of miR-132/212 in cell death, we overexpressed miR-132 and miR-212 in hypoxic RNCM for 24 hours. Cardiomyocytes with overexression of miR-132 or miR-212 are more resistant to ischemia induced cell death as shown by TUNEL staining (Figure 1. D) indicating that miR-132 and 212 are indeed protective for ischemia in cardiomyocytes.

Loss of miR-132/212 shows no benefit in cardiac function preservation or adverse cardiac remodeling

To see the long term consequence of miR-132/212 loss post-MI, we exposed another set of mice to MI and followed their cardiac function by echocardiography for 4 weeks (Supplementary Figure 1A). Consistent with the previously observed difference in cell death, we observed that KO mice demonstrated a stronger reduction in cardiac function than WT mice within the first 2 weeks (Figure 2A and B). However, eventually both WT and KO animals display similar cardiac function at 4 weeks, exemplified by a similar reduction in ejection fraction and fractional shortening (Figure 2 A and B).

After termination of these mice at 4 weeks post-MI, we further characterized their hearts at the morphological and molecular level. Both WT and KO displayed extensive cardiac remodeling and expansion of the IS (Figure 2C). No differences in fibrotic remodeling, both in the infarct and remote

areas could be observed between WT and KO mice (Figure 2D and E). To assess the stress status of the hearts, we checked the expression of several cardiac stress markers, but no significant difference was detected in Anp, Bnp nor in the βMHC/αMHC ratios (Figure 2F).

Neovascularization has been shown to play a role in cardiac healing and remodeling after MI [17, 18] and we have previously observed that miR132/212 did affect the arteriogenic response after hind-limb ischemia (see chapter 4). To see if the loss of miR-132/212 could also affect the neovascularization after MI, we stained for αSMA to visualize larger vessels. We observed that KO mice display lower number of vessels upon MI. There was a trend towards a lower vessel density and vessel coverage rate in the KO mice, but these were not significant (Figure 2 G and H).

Discussion

In this study, we tested the role of miR-132/212 during MI using genetic knockout mouse both on the short and long term post-MI. Although KO mice display similar infarct sizes (IS/AAR) as the WT mice, KO mice did show slightly increased cardiomyocytes in apoptosis. This was in line to the faster drop in cardiac function in the first week post-MI. However, 4 weeks after MI loss of miR-132/212 did not show any differences in the cardiac function or adverse cardiac remodeling. These results indicated that general inhibition of miR-132/212 in the setting of MI has no beneficial effect in the preservation of cardiac function.

Loss of miR-132/212 did not show any beneficial effects on cardiac function at 4 weeks, both on cardiac function as well as histological levels. This 4 weeks post-MI result may be caused by several distinct mechanisms. First, we and others found that miR-132/212 modulate Ras-MAPK pathway by synergistically suppressing multiple intrinsic inhibitors of the Ras-MAPK (Rasa1[19], Spred1 and Spry1) and PI3K-AKT pathway (PTEN) in Human Umbilical Vein Endothelial Cells (HUVECs) (chapter 4 and 5). It also has been shown that miR-132/212 has an anti-apoptotic role by activating the PI3K-AKT pathway in a mouse cardiomyocyte line[20]. Thus, miR-132/212 may have a positive effect on cardiomyocyte cell death by directly regulating survival signaling during ischemia. Secondly, miR-132/ 212 regulates the contractility of the heart (chapter 6). Reducing wall stress after MI, either by mechanically unloading the heart [21] or pharmaceutically by using ACE inhibitors or beta blockers [22], has been shown to be beneficial to cardiac healing after MI. Therefore we believe that the loss of miR-132/212 enhances cardiac contractility and increases stress levels post-MI. In this sense, miR-132/212 inhibition may induce more damage following MI, a detrimental effect undesirable in the clinical setting.

Although miR-132/212 plays a protective role in the immediate early phase post-MI, associated with an early increase in expression 12h post-MI, its expression is decreased at 24h but increased again in a second wave in later phases (Supplementary figure 1B). The upregulation of this miR-132/212 in the

later phase is then impairing cardiac contractility and potentially the autophagic response[20]. It remains to be tested if inhibition of miR-132/212 at later stages after MI may still help to maintain cardiac contractile function while keeping or even increasing the expression of miR-132/212 in the early phase. For that purpose, conditional knockout mice, antagomiRs or better targeting of therapeutics should be used [23], and at least a substantial amount of viable myocardium has to be preserved before any effect of miR-132/212 inhibition can be observed. Nevertheless, our results demonstrate yet another example for multifunction properties of a single microRNA, emphasizing that a spatial and/or tissue specific intervention may be critical to achieve desired therapeutic effects [23].
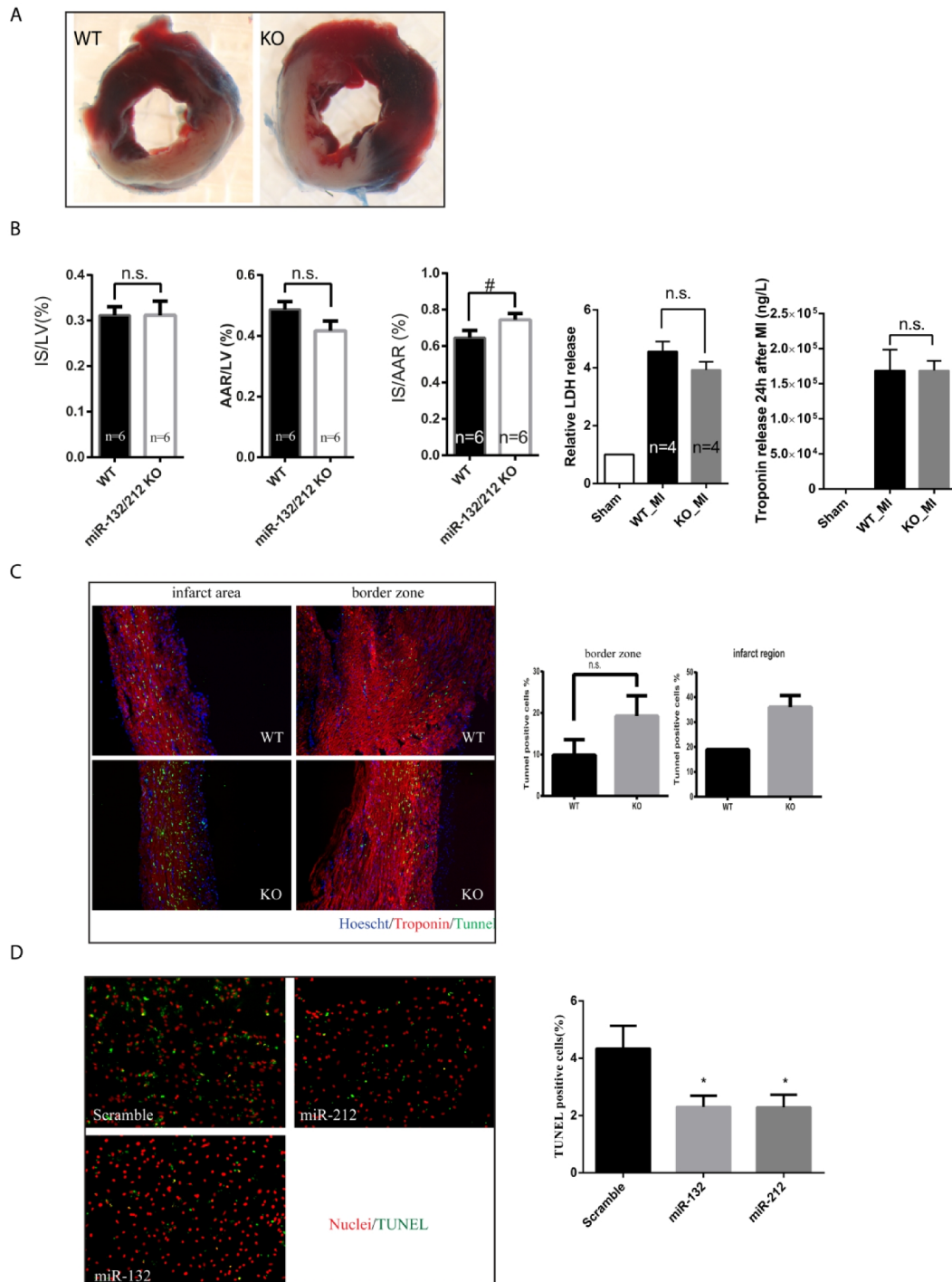
Figure1. Characterization of cardiac damage after MI by TTC and TUNEL staining. A. representative images of WT and KO hearts stained with TTC 24h after MI. B. Quantification of infarct size(IS), area at risk (AAR) of left ventricle (LV), LDH and Troponin release in the serum at 24 hours after MI as measured by ELISA. C. Representative images of TUNEL staining on the left ventricle 24 hours after MI and their quantifications. D. representative images of TUNEL staining on rat neonatal cardiomyocytes, transfected with indicated microRNA mimics or scramble controls and treated for 24h of ischemia and the quantification of TUNEL positive cells .
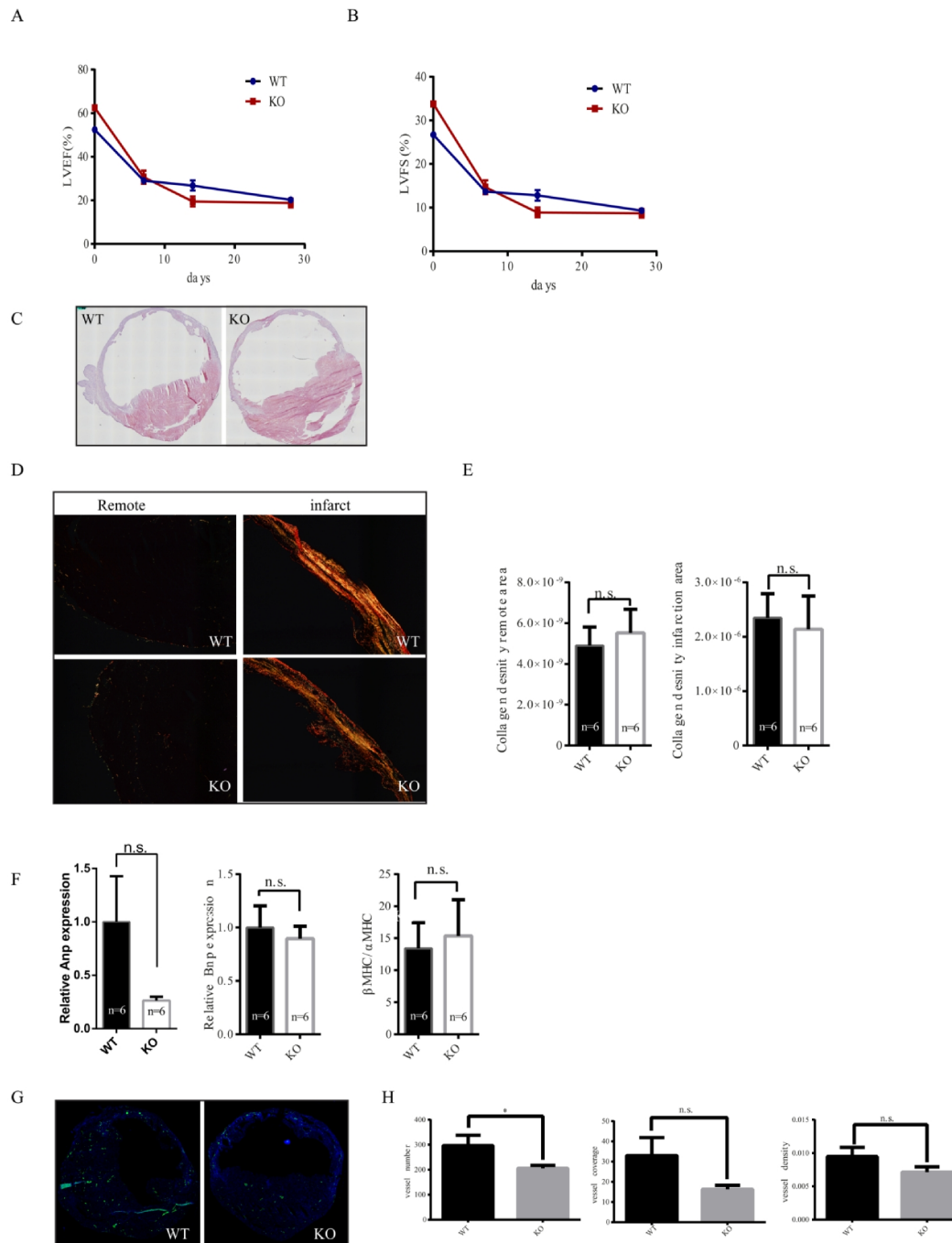
Figure 2. Characterization of cardiac function of miR-132/212 knockout mice by echocardiography 4 weeks after MI. A. LVEF as a percentage in WT and KO mice during 4 weeks post- MI. B. LVFS as a percentage in WT and KO mice during 4 weeks post- MI. C. representative images of HE staining of the WT and KO cardiac section 4 weeks post-MI. D. representative images of Picrosirius red staining for collagen content of the WT and KO cardiac section. E. Quantification of collagen density as shown in D. F. Molecular characterization of the hearts 4 weeks post-MI by qPCR for cardiac stress markers: Anp, Bnp and βMHC/ αMHC ratio. G. Representative images of αSMA staining in WT and KO cardiac section. H. Quantification of number of the SMA positive vessel, normalized vessel coverage and vessel density as shown in G.

Reference

1.	Mozaffarian, D., et al., *Heart disease and stroke statistics--2015 update: a report from the American Heart Association.* Circulation, 2015. **131**(4): p. e29-322.
2.	Steg, P.G., et al., *ESC Guidelines for the management of acute myocardial infarction in patients presenting with ST-segment elevation.* European heart journal, 2012. **33**(20): p. 2569-2619.
3.	Montgomery, R.L., et al., *Therapeutic inhibition of miR-208a improves cardiac function and survival during heart failure.* Circulation, 2011. **124**(14): p. 1537-47.
4.	Grueter, C.E., et al., *A cardiac microRNA governs systemic energy homeostasis by regulation of MED13.* Cell, 2012. **149**(3): p. 671-83.
5.	Wahlquist, C., et al., *Inhibition of miR-25 improves cardiac contractility in the failing heart.* Nature, 2014. **508**(7497): p. 531-5.
6.	Montgomery, R.L., et al., *Therapeutic inhibition of miR-208a improves cardiac function and survival during heart failure.* Circulation. **124**(14): p. 1537-47.
7.	Bonauer, A., et al., *MicroRNA-92a controls angiogenesis and functional recovery of ischemic tissues in mice.* Science, 2009. **324**(5935): p. 1710-3.
8.	Hullinger, T.G., et al., *Inhibition of miR-15 protects against cardiac ischemic injury.* Circulation research, 2012. **110**(1): p. 71-81.
9.	van Rooij, E., *MicroRNA therapeutics for cardiovascular disease.* HEART AND METABOLISM, 2014: p. 4.
10.	van Rooij, E. and S. Kauppinen, *Development of microRNA therapeutics is coming of age.* EMBO molecular medicine, 2014: p. e201100899.
11.	Kayo, H., et al., *miR-212 and miR-132 are dispensable for mouse mammary gland development.* Nat Genet, 2014. **46**(8): p. 802-4.
12.	Grundmann, S., et al., *MicroRNA-100 regulates neovascularization by suppression of mammalian target of rapamycin in endothelial and vascular smooth muscle cells.* Circulation, 2011. **123**(9): p. 999-1009.
13.	Koudstaal, S., et al., *Necrostatin-1 alleviates reperfusion injury following acute myocardial infarction in pigs.* European journal of clinical investigation, 2015.
14.	Oerlemans, M.I., et al., *Early assessment of acute coronary syndromes in the emergency department: the potential diagnostic value of circulating microRNAs.* EMBO molecular medicine, 2012. **4**(11): p. 1176-1185.
15.	Timmers, L., et al., *Toll-like receptor 4 mediates maladaptive left ventricular remodeling and impairs cardiac function after myocardial infarction.* Circulation research, 2008. **102**(2): p. 257-264.
16.	van Mil, A., et al., *MicroRNA-214 inhibits angiogenesis by targeting Quaking and reducing angiogenic growth factor release.* Cardiovasc Res, 2012. **93**(4): p. 655-65.
17.	Zarrinpashneh, E., et al., *Ablation of SGK1 impairs endothelial cell migration and tube formation leading to decreased neo-angiogenesis following myocardial infarction.* PLoS One, 2013. **8**(11): p. e80268.
18.	Takeda, Y., et al., *Treatment with recombinant placental growth factor (PlGF) enhances both angiogenesis and arteriogenesis and improves survival after myocardial infarction.* Circ J, 2009. **73**(9): p. 1674-82.
19.	Katare, R., et al., *Transplantation of human pericyte progenitor cells improves the repair of infarcted heart through activation of an angiogenic program involving micro-RNA-132.* Circ Res, 2011. **109**(8): p. 894-906.
20.	Ucar, A., et al., *The miRNA-212/132 family regulates both cardiac hypertrophy and cardiomyocyte autophagy.* Nat Commun, 2012. **3**: p. 1078.
21.	Kapur, N.K., et al., *Mechanically unloading the left ventricle before coronary reperfusion reduces left ventricular wall stress and myocardial infarct size.* Circulation, 2013. **128**(4): p. 328-336.
22.	Gajarsa, J.J. and R.A. Kloner, *Left ventricular remodeling in the post-infarction heart: a review of cellular, molecular mechanisms, and therapeutic modalities.* Heart failure reviews, 2011. **16**(1): p. 13-21.

23. Kwekkeboom, R.F., et al., *Targeted delivery of miRNA therapeutics for cardiovascular diseases: opportunities and challenges.* Clinical Science, 2014. **127**(6): p. 351-365.
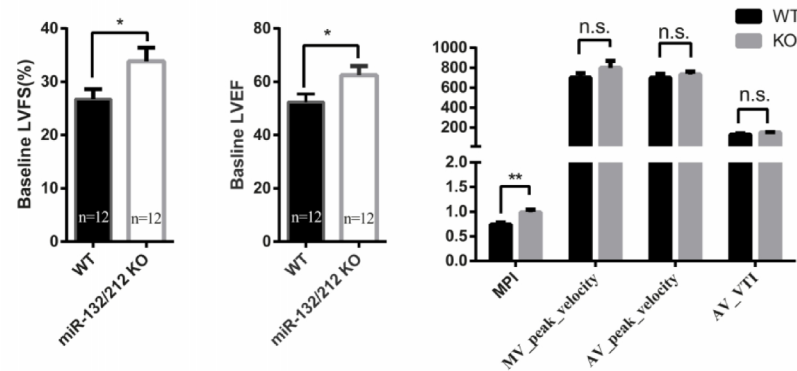
A
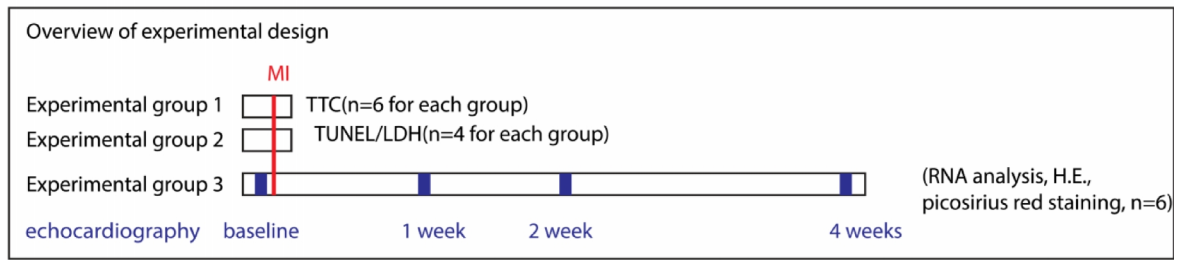
B
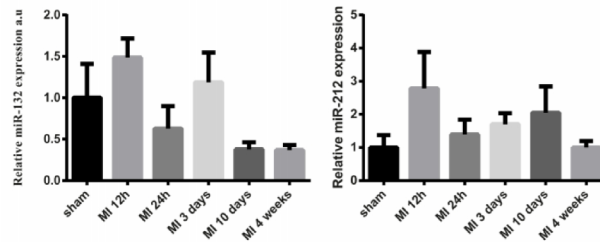
C

Supplementary figures and Table. A. Overview of experimental study design and the number of the animals used in this study. B. Expression of miR-132/212 after MI in mouse as observed in microarray and RT-PCR validation. The relative expression of miR-132and miR-212 at 12h, 24h, 3 days, 10 days, 28 days normalized by RNU6. C. Cardiac function analysis of miR-132/212 knockout and WT mice by echocardiography at baseline: LVFS; LVEF; myocardial performance index (MPI), peak velocity of MV and AV.

Table Echocardiography assessment of cardiac function

	Base line		1 week after MI		2 weeks after MI		4 weeks after MI	
	WT (n=12)	KO (n=12)	WT (n=6)	KO (n=5)	WT (n=6)	KO (n=5)	WT (n=5)	KO (n=5)
Heart_Rate	460.9±10.4	485.4±8.0	643.49±69.1	501.92±11.23	456.2±21.1	398.7±12.9	614.8±96.3	506.6±16.2
Diameter_systolic	2.8±0.1	2.4±0.1	4.18±0.28	3.86±0.25	4.4±0.4	5±0.4	5.1±0.2	5.1±0.5
Diameter_diastolic	3.8±0.1	3.7±0.1	4.83±0.24	4.51±0.14	5.1±0.3	5.5±0.4	5.7±0.2	5.6±0.5
Volume_systolic	30.2±2.6	22.6±3.1	80.59±12.49	66.18±9.48	94.5±15.5	123.9±21.9	126.9±8.7	131.2±24.3
Volume_diastolic	63.0±3.1	57.8±4.2	110.96±12.31	93.7±6.65	124.3±15.7	151.6±24.1	159.1±11.4	160.1±29.4
Stroke_volume	32.8±2.6	35.2±2.4	30.38±3.08	27.52±5.31	29.8±2.6	27.6±6.7	32.3±4.8	28.9±9.5
Ejection_Fraction	52.4±3.1	62.5±3.5*	29.06±3.67	30.61±6.72	26.8±5.6	19±5.1	20.2±2	18.8±4.6
Fraction_shortening	26.7±1.9	33.8±2.6*	13.69±1.81	14.68±3.54	12.8±3	8.9±2.5	9.3±1	8.7±2.2
Cardiac_Output	15.3±1.6	17.1±1.3	20.13±3.73	14.04±3.03	13.5±1.1	10.9±2.5	19.2±2.8	15±5.4

152

Chapter 8

Development of PEG-based amphiphilic nanopolymers for targeted delivery of microRNA therapeutics

Zhiyong Lei[*,1], Vera Verhage[*,1], Bhavna Gupta[*,2], Esther CM van Eeuwijk[1], Eric Aiazian[3], Rene JP Musters [4], Pieter AF Doevendans[1,5], Arthur C Watterson[2], Joost PG Sluijter[1,5]

[1] Department of Cardiology, Experimental Cardiology Laboratory, University Medical Centre Utrecht, the Netherlands
[2] Department of Chemistry, University of Massachusetts Lowell, Lowell, USA
[3] Axle International, Nieuwe Uitleg 28, 2514 BR, the Hague, the Netherlands
[4] Department of Physiology, VU University Medical Center, Van der Boechorststraat 7, 1081 BT, Amsterdam, the Netherlands
[5] Interuniversity Cardiology Institute of the Netherlands (ICIN), Moreelsepark 1, 3511 EP, Utrecht, the Netherlands

*Authors contributed equally

Abstract

MicroRNAs (miRNAs) play important roles in pathological development of many different diseases, therefore consider as promising therapeutic targets for the future. However, a safe and effective delivery technology for miRNA therapeutics is still lacking. In this study, using an enzyme-chemical approach, we synthesized a series of different amino group functionalized PEG-based nanopolymers aiming for miRNA therapeutics delivery. We characterized the effect of the different amino groups on the binding and complexation capacity to anti-miRNAs and pre-miRNAs *in vitro*. Based on their binding capacity, NB183-2 was selected for further functional testing thereby including cellular toxicity, cellular uptake and luciferase reporter assays. We observed that incorporation of a positive charged *N*-boc butyl amine group in the copolymer NB-183-2 improved the binding capacity of the nanopolymer. This polymer can form stable complexes with both pre- and anti- miRNAs, and can be taken-up efficiently by cells without showing any cellular toxicity. By using NB-183-2, however, miR-214 failed to suppress the luciferase activity of a validated miR-214 reporter (QKI-3'UTR reporter). By direct immune fluorescence labelling, we observed that NB-183-2 and antimiR complexes were trapped in the endolysosomal compartment, whereas traditional transfection reagents like Lipofectamine 2000 can deliver functional miRNA therapeutics.

Introduction

Most cardiovascular diseases are multi-factorial in nature [1] and clear therapeutic options are limited, continually awaiting for novel treatment modalities [1, 2]. Recently, small single stranded RNA molecules, termed microRNAs (miRNAs) [3], have been found to regulate a variety of physiological functions and have great impact on cardiovascular diseases, including cardiac hypertrophy [4-11], reperfusion injury, ischemic heart disease [12-16] and peripheral vascular disease [17-19]. The potential role of miRNA in the progression of several diseases stimulated the development of specific inhibitors to modulate its activity via a RNA anti-sense mechanism [20]. The impressive specific, strong and long- lasting effects make miRNA interventions a powerful new therapeutic modality [21]. Systemic injection of these inhibitors either directly into the circulation or via intraperitoneal administration, demonstrated a powerful inhibition of miRNA functionality lasting for at least three months. However, systematic delivery results in rather low organ specificity and side-effects in other cells and organs [22]. Therefore, this systematic delivery of miRNA inhibitors has major drawbacks including cost-ineffectiveness and lacking control of the site of action.

Poly (ethylene glycols) PEG copolymers-based amphiphilic polymeric micelles which has been used to encapsulate both hydrophobic and hydrophilic drug are very promising miRNA therapeutic delivery systems due to their chemical properties [23]. The PEG shell is known for its wide range in solubility, high biologically stability *in vivo*, and well tolerated by living organisms, thereby widely used in polymer-based drug delivery systems [23, 24]. The PEG copolymers-based amphiphilic polymeric micelles, which take the advantage of both PEG and the flexibility of the amphiphilic block copolymer, which can be tailored with different functionalized groups for different types of drugs or with different cell specific targeting peptides [23, 24]. These features make them suitable for targeted drug delivery, and therefore holds a promise for targeted delivery of miRNA therapeutics.

In this manuscript, we tried to design and synthesize a PEG-based polymer with flexible hydrophilic copolymers that have RNA -binding capacity and appropriate targeting properties. We synthesized different self-assembling amphiphilic copolymers with a similar PEG exterior shell but different internal hydrophobic side chains [24] and tested their capability in regard to their miRNA binding capacity.

Methods

Synthesis of backbone polymer

Dimethyl -5-hydroxyisophthalate (1, 1.0 mmol) and PEG 1000 (2, 1.0 mmol) were placed in a three neck round-bottom flask and stirred until homogeneous, Novozyme 435 (10% by weight with respect to monomers) and 4Å molecular sieves (10% by weight with respect to PEG) were added. The resultant reaction mixture was stirred using a magnetic bead at 90 °C under vacuum for 48 h and for additional 12 h with overhead stirrer at 90 °C under vacuum and then quenched by adding chloroform. The enzyme and molecular sieves were removed by filtration and the filtrate was concentrated to get the crude product, which was redissolved in deionized water for dialysis using membrane (MWCO 6000). After the completion of dialysis, the pure product polymer 3 was obtained as a waxy off-white solid by freeze-drying.

Synthesis of NB-183-2

Poly[(polyoxy ethylene-1000)-oxy-5-hydroxyisophthaloyl] (3) was reacted with 4-bromo-*N*-boc butyl amine using potassium carbonate as a base in acetonitrile solvent at room temperature to obtain *N*-boc butyl amine substituted polymer derivative(10) .This derivative was treated with 5% hydrochloric acid solution at 45^0C to obtain crude product and was further purified by dialysis to afford NB-183-2. The synthesis route for NB-183-2 is illustrated in details in Supplementary figure 1. A.

Synthesis of NMS-08

Poly[(polyoxy ethylene-1000)-oxy-5-hydroxyisophthaloyl] (3) was reacted with 1-azido 6-bromohexane 4 under mild basic conditions using potassium carbonate in acetonitrile solvent at room temperature to obtain alkyl azide bearing phenoxy derivative 5. Compound 5 has been confirmed by the spectroscopic data *viz* NMR, IR and UV. Click reaction was performed using the azide derivative 5 and *N*-propynyl, *N,N,N*-trimethyl ammonium iodide 2, with copper acetate (15 mol %) and sodium ascorbate (15 mol %) in THF: H2O (1:1) at room temperature for 15 hours. Compound 2 was prepared from *N*-propynyl, *N,N*-dimethyl amine 1, by stirring with methyl iodide in chloroform at room temperature for 1 hour. The course of the click reaction was examined by recording ^{1}H NMR of crude reaction mixture. After 3 hours, ^{1}H NMR of an aliquot of the reaction showed the presence of starting polymer. But after 15 hours the disappearance of azide methylene protons (triplet at δ 3.29 ppm) confirms the complete transformation to afford compound 6. Despite complete consumption of starting polymer 5, the unreacted *N*-propynyl, *N,N,N*-trimethyl ammonium iodide 2, was observed. The unreacted starting compound 2 was eliminated by dialysis using dialysis membrane with molecular weight cutoff: 500 in methanol medium for 24 hours to yield pure cationic triazole polymer

derivative 6 (NMS-08). The synthesis route for NMS-08 is illustrated in details in Supplementary figure 1. B.

Synthesis of NMS-16

Another triazole cationic derivative was prepared under similar click reaction conditions. Azide bearing polymer 5 was reacted with *N*-boc propynyl amine 7 in presence of copper acetate (15 mol %) and sodium ascorbate (15 mol %) in THF: H_2O (1:1) at room temperature for 15 hours. After completion of the reaction as indicated by crude mixture NMR, the reaction was stopped and the polymer derivative 8 was purified by precipitation with anhydrous ethyl ether. *N*-boc protected triazole polymer 8 was confirmed by all spectroscopic data. This compound was further subjected to acid treatment with 5% aq. HCl at 45° C overnight to affect the cleavage of boc protecting group to afford free amine hydrochloride salt of triazole polymer 9 (NMS-16). The synthesis route for NMS-16 is illustrated in details in Supplementary figure 1. C.

Synthesis of NMS-44

Commercially available, glucose diacetonide (GDA) was coupled with dibromo hexane to form ether linkage, which affords compound GDA-hexyl bromide 28. This compound has been confirmed by spectroscopic analysis of NMR and IR. In the next step, GDA-hexyl bromide 28, was reacted with the phenol moiety of backbone polymer 3 under mild basic conditions in acetonitrile at room temperature afforded the compound 29, in good yields. Compound 29 has been characterized by the spectroscopic analysis of NMR, IR and UV spectral data. Finally, the masked hydroxyls of acetonide protections were freed by acid hydrolysis with 5% aqueous HCl at 45 °C for 3 hour to produce the polymer NMS-44. This polymer has been purified by dialysis in methanol. The synthesis route for NMS-44 is illustrated in details in Supplementary figure 1. C.

Nanopolymer-miRNA binding and agarose gel shift assay

Nanopolymer and miR/antmiRs polyplex formation is based on their nitrogen/phosphate (N/P) ratios. We therefore mixed the polymer and miRNA therapeutics at different N/P ratios (ranging from 0.5-160) in DEPC-H2O and incubated for 1 hour at 37°C to form polyplexes. Polyplexes gel shift assay was subsequently analyzed using 4% agarose gel. As for precursor miRNAs, we have used 6-carboxyfluorescein (FAM) Labeled Pre-miR Negative control #1 (Ambion, Cat#AM17121), and a plant-specific miRNA, ath-miR-159a (UUUGGAUUGAAGGGAGCUCUA, Cat. # 4464066) and miR-214 mimics (MC12124, Cat. #4464066). For miRNA inhibitors, previously designed anti-miR-214 [25] was used in this study with the following modifications: 5`-a*c*ugccugucugugccugc*u*g*u*-3', modified via 5`Cy5-modification, 2`O-methyl-RNA of the whole oligo, 4xPTO-linkage 3`-side; 2x PTO-linkage 5`-side (* in provided sequence) (VBC Biotech Services GmbH), As positive controls, we used polyethylenimine (PEI) (Cat. 23966-2, Polyscience),

Lipofectamine® RNAiMAX (Cat. 13778030, Life technologies) and Lipofectamine 2000 (Cat. 11668027, Life technologies) according the manufactures instructions.

MiRNA functionality upon polyplex formation

The NB-183-2 and anti-miRs polyplex formation was performed as described above. Interaction of polymer NB-183-2 and miRNA therapeutics was studied by Dynamic Light Scattering (DLS) to measure changes in particle size and ζ potential of the polyplexes formed, at different concentrations of polymer and miRNA. The stability and particle size distributions of the formed polyplexes were analyzed by Nanoparticle Tracking Analysis (NTA) on a NanoSight NS500 (Malvern), according to the supplier's instruction. The polyplexes were kept for 3 days at 4 degree and resuspended before measurement again.

In vitro transfection and visualization:

Human microvascular endothelial cells (HMECs) were grown on fibronectin in MCDB 131 supplemented with EGF, hydrocortisone, L-glutamine, and 10% FBS. Cultured HMECs were reverse-transfected with formed polyplexes, as described above. For microscope analysis of fluorescently labeled miRNAs or antimiRs treated cells, cells were fixed with 4% paraformaldehyde in PBS for 15 min at room temperature (RT). Nuclei were stained with 0.2 µg/ml Hoechst 33342 (Invitrogen) and mounted in Fluoromount-G (SouthernBiotech, Birmingham, AL). To study the location of anti-miR and nanopolymer polyplexes, the following antibodies were used: anti-CD63 (Cat. CBL553, Millipore), anti-Caveolin-1 (Cat. 610059, BD transduction labs) overnight at 4℃ followed by appropriate secondary antibodies for visualization.

Quantitative real time-PCR:

Total RNA was isolated with TriPure Isolation Reagent (Roche Applied Science, Penzberg, Germany) and treated with RNase-free DNase I (Qiagen, Venlo, The Netherlands). MiR-159 expression was subsequently validated by TaqMan MicroRNA Assay (Cat. # 4427975, Applied Biosystems) using TaqMan® Universal Master Mix II, no UNG (Applied Biosystems) and normalized to RNU19 (assay ID: 001003, Applied Biosystems), as previously described [26].

Luciferase activity assay:

To determine if NB-183-2 mediated miRNA transfection was biologically functional, we performed luciferase activity assay using a pMIR-REPORT Luciferase vector (Ambion) carrying sequences of the QKI 3'-untranslated region (UTR) which have been shown to be targeted by miR-214, as described before [25]. HEK293 cells were co-transfected with 200 ng pMIR-QKI-3'UTR reporter and pMIR-REPORT β-gal Control Plasmid as an internal control for transfection efficiency first. The next

day cell medium was replaced with miR-214 or scramble controls complexed with NB-183-2 and incubated overnight. We also tried to perform polyplex incubation of the cells first, then performed the pMIR-QKI-3'UTR and pMIR-REPORT β-gal transfections. For controls, pMIR-QKI-3'UTR, pMIR-REPORT β-gal and miR-214 or scramble miRNAs were mixed together and transfected at the same time as described before [25]. Finally, to promote endolysosome escape, 25μm chloroquine was supplemented for polymer transfected HEK293 cells throughout the experiment. The activity of Luciferase and β-galactosidase was assessed by Arrayscan after 48 hours with the Luciferase Assay System at 405nM and β-galactosidase Enzyme Assay System at 570nm (Promega), respectively. Luciferase activity was calculated by luciferin signal normalized by β-galactosidase activity according manufacturer's instructions.

Results

Our first objective was focused on the design and synthesis of polymeric nanoparticles that demonstrate RNA binding. As a basis, we used our previously described flexible chemo-enzymatic approach that allows design and synthesis of a complex polymer structure[24], which self-assembles into spherical nanoparticles. The PEG-based copolymer has a pendent functional group and this hydroxyl functional group can be further tailored (Figure 1). Several novel groups were attached to the basic copolymer (Figure 2 and supplementary figure 1) and basic characterizations were performed to assure proper synthesis and assembly by 1H NMR (data not shown), as described before [27].

As a basis for selection, we selected only those polymers that demonstrated a clear shift of the anti-miRNA on an agarose gel (Figure 2 and 3). Among all polymers generated only NB183-2 and NMS-016 demonstrated a clear dose-dependent shift upward, an indication for miRNA therapeutics binding and thereby neutralizing the negatively charged RNA molecules (Figure 2 and 3). Polymer NB183-2, which showed a stronger binding capacity than NMS-16, was thereby selected and repeatedly synthesized to see reproducibility in its method of synthesis and behavior of polymer-miRNA binding. At a concentration of 1 mg/ml, the average size of the particle of the NB183-2 is about 80.30 nm and the ζ potential is about 3.9 mV. Upon binding to the miRNAs, the average size shift to 114.7 nm, and the ζ potential changes to10.8 mV, which is indicative for binding of miRNA antimiRs. These observations could be further confirmed by Nanoparticles Tracking Analysis (NTA) (Figure 4), which demonstrated a relative small size distribution of the polymer by itself (Figure 4A) and shifted to a larger complex upon miRNA therapeutic binding (Figure 4B). This complexation is relative stable as can be seen in figure 4C and D. Upon vigorous mixing, the binding is still present on agarose separation and NTA. And analysis of the polyplexes 48 hours after preparation still demonstrated

larger complexes in solution. Upon 48 hours, some larger sized complexes become visible as well, probably caused by the interaction and fusion of different polyplexes in time (Figure 4D).

Since we anticipated developing a generic miRNA therapeutic delivery platform, the generated novel polymer should not only be able to bind anti-miRNA therapeutics but also precursor miRNA molecules. By mixing either the inhibitors or the precursor with the NB183-2 polymer, we could clearly observe a dose dependent shift on agarose gel in both of them (Figure 5).

Subsequently, we tested whether the formed polyplexes were able to have functional interaction with cultured endothelial cells (ECs) as observed for the basic polymer before [24]. We exposed the cells for 24-28 hours with the formed complexes and used PEI and RNAiMax as positive controls for transfection efficiency. Both fluorescently labelled anti-miRNA and pre-miRNA molecules could be observed in the cultured ECs which indicated that the formed complexes could interact with the cells and are internalized (Figure 6A). By using the plant-specific miRNA-159 precursor, we were able to quantitatively determine the transfection efficiency of these approaches. We found that the transfection efficiency of NB-183-2 is higher than PEI even though it is lower than that of RNAiMax (see Figure 6B).

Finally, binding and internalization of the miRNA therapeutics are very promising but a functional effect in the targeted cells is essential to proceed with the development of the polymer. For this, we performed a luciferase-assay using a validated target sequence for miRNA-214 [25]. With this we are able to determine if there is a direct effect upon binding of the miR-214 precursor upon complexation with the polymer after encapsulation by the target cell. Although our positive control (Lipofectamine 2000) did show more than 50% reduction in target expression, treating our cells with the miRNA-polymer complex in combination with the target sequence at the same day (see Figure 7A), two consecutive days (see Figure 7B), or even in the presence of a lysosome inhibitor Chloroquine (see Figure 7C) did not show a reduction in target expression. These results indicate that our miRNA therapeutic is bound by the polymer, is internalized in the target cells, but probably cannot be released intracellularly for proper functioning. Indeed, 48 hours after transfection, in nanopolymer transfected cells, Cy5-labeled antimiRs are still trapped in the endolysosomal compartment while Lipofectamine 2000 transfected show a more diffused pattern (Figure 8).

Conclusion and discussion

In this study, using an enzyme-chemical approach, we have synthesized and characterized a series of different amino group-functionalized PEG-based nanopolymers. Based on the binding capacity to pre- and anti-miRs, we selected NB-183-2 for further functional testing, including cellular toxicity, cellular uptake and miRNA luciferase activity assay. We observed that incorporation of the *N*-boc butyl amine group in the copolymer demonstrated a miRNA binding potential. We also observed that this polymer can form stable complexes with both pre- and anti-miRs, which can be efficiently taken-up by cells without showing any cellular toxicity. Unfortunately, NB-183-2 with pre- or antimiR complexes was trapped in the endolysosomal compartments after cellular uptake and can therefore not become functional.

Obviously, the first property for nanopolymers as a carrier for miRNA therapeutics is their direct RNA binding capacity, which is in our compounds based on a positive charge. Incorporation of a positive charged group significantly improved the binding capacity of the nanopolymers such as NB-183-2. However, attaching more and stronger positively charged groups such as NMS-16, NMS-08, and NMS-45 did not improve the binding capacity of the nanopolymers further. Although, we did not explore the structural mechanism of these consequences, it seems that a combination of both the positive charges and structural organization could influence the binding.

Another challenge for a nanopolymer carrier is a proper intracellular release of the therapeutics and the demonstration of functional effects. Although NB-183-2 can form complexes with pre- and anti- miRs and is present in the cells, no suppression of luciferase reporter activity could be detected when cells were treated. Moreover, we could not see an effect on endothelial cell migratory capacity either (data not shown) by the miR-214 treatment as we have seen before [25]. The lack of functional suppression may be caused by the binding affinity between NB-183-2 and the miRNAs, which is too strong to be released. In this regards, NMS-16, which shows weaker small RNA binding capacity, maybe a better candidate for follow-up. Further investigation on this polymer is therefore warranted. Given the different reducing potential within the cytosol, introducing some disulfide bonds in the backbone of the polymer that can be cleaved after entering the cytosol might be helpful for miRNA therapeutics to be released from the polymer [28]. Another possible reason for the entrapment might be that the complexes cannot escape from the lysosomal compartments into the cytosol. Forty-eight hours after transfection, we can still detect fluorescent-labeled anti-miRs trapped in the endolysosomal compartments, as indicated by the CD63 staining [29]. This is commonly seen in polymer-based nucleic acid delivery studies; however, the underlying mechanism of the endolysosomal escape is not fully understood [30]. Interestingly it was found that viruses can escape from endolysosomal compartment by expression of some fusogenic proteins and modifying polymers with these fusogenic

peptide can promote endolysosomal escape [30]. Therefore, it is worth to try to incorporate those fusogenic peptides in the polymer to facilitate the endolysosomal escape.
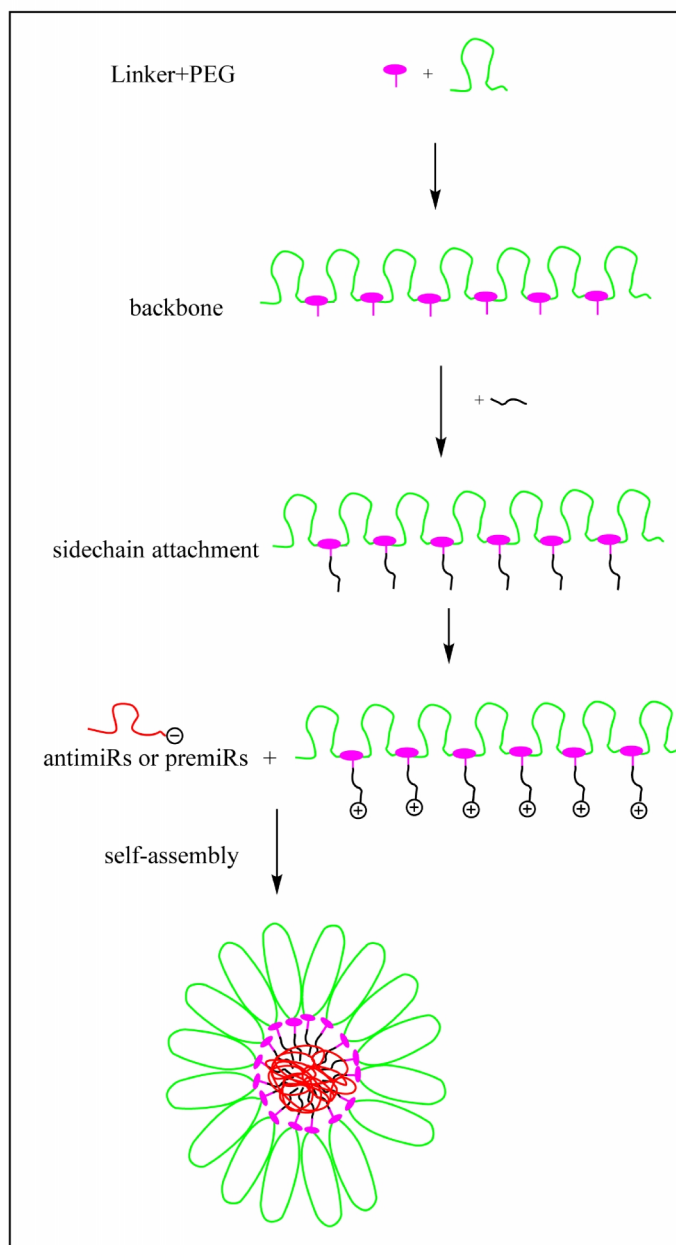
In summary, we have synthesized polymer NB-183-2 that can bind both pre- and anti-miRNAs, which were delivered intracellularly into endothelial cells. Although promising as miRNA carrier, functional effects were lacking and further developments are needed to promote e.g. lysosomal release.
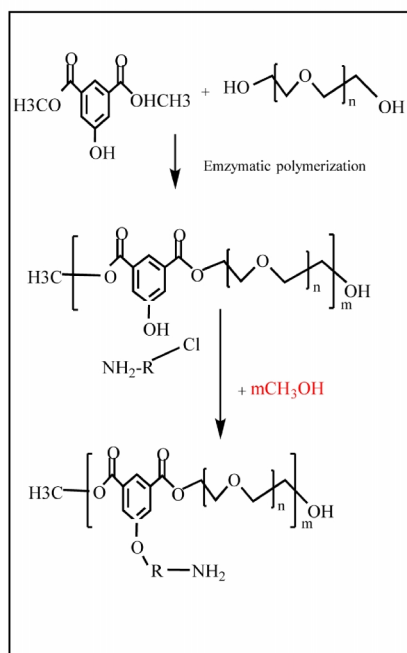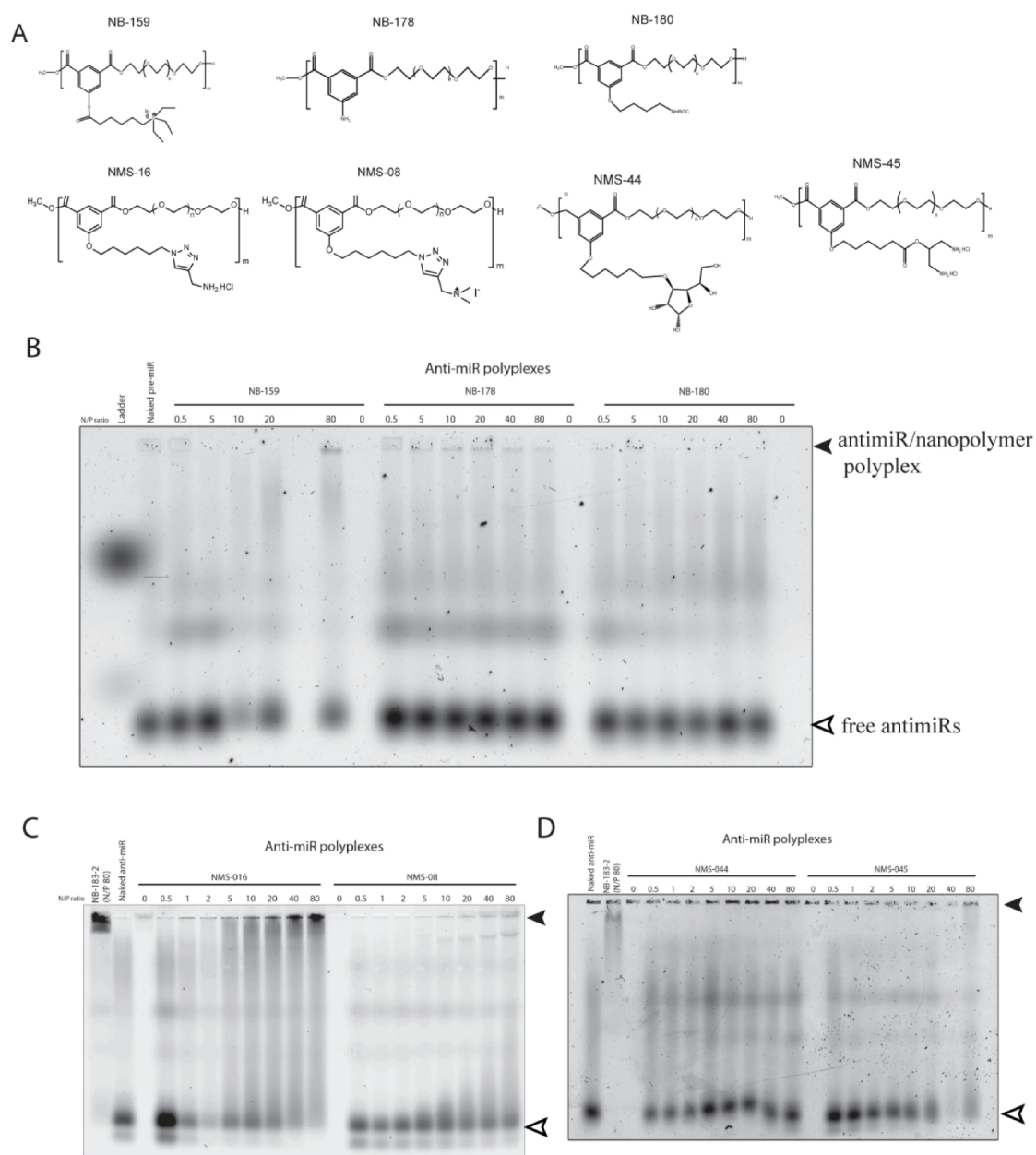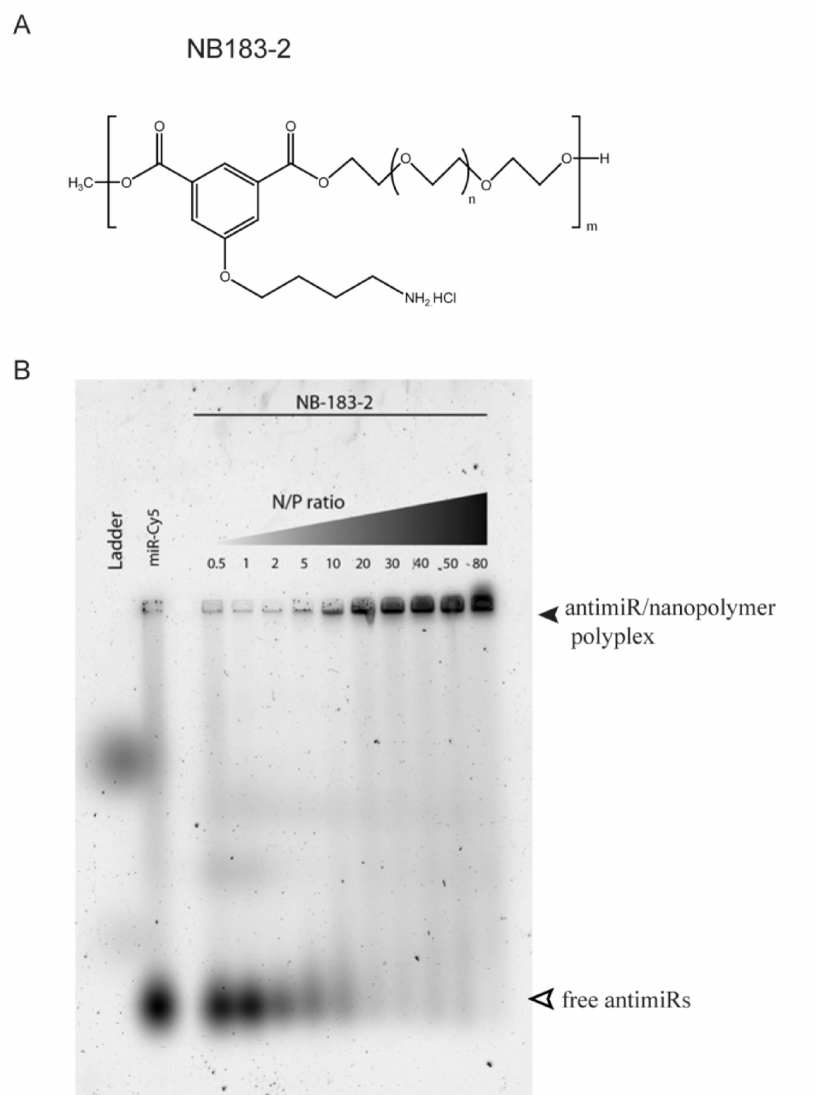
Figure 1. Overview of the polymer synthesis (A) and a schematic cartoon for polymer synthesis and polyplex formation with antimiRs or pre-miRs in solution (B).

Figure 2. The structure of NB-159, NB-178, NB-180, NMS-16, NMS-08, NMS-44 and NMS-45 (A) and gel shift assays for polyplex formed by incubation with NB-159, NB-178 and NB-180 (B), NMS-16 and NMS-08 (C), NMS-44 and NMS-45 (D).

Figure 3. **The structure of Nb-183-2 (A) and gel shift assay for different N/P ratios of NB-183-2 and Cy5-labeled antimiRs complexes (B).**
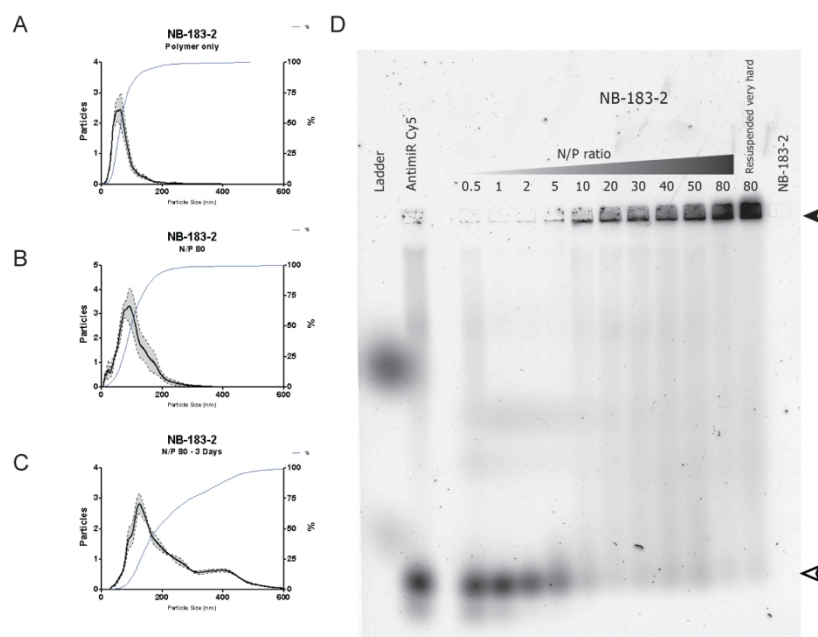
Figure 4. The size and stability of NB-183-2 and antimiRs polyplexes. (A). Size distribution of empty NB-183-2 as measured by nanosight (B). The size distribution of NB-183-2 and antimiRs polyplexes as measured by nanosight. Note that the size become larger compared to the empty NB-183-2. (C). The size distribution of NB-183-2 and antimiRs polyplexes 3 days after formation of polyplexes as measured by nanosight. (D). The stability of NB-183-2 and antimiRs polyplex at different N/P ratios. Note that the polyplex stay intact even after vigorous resuspending.
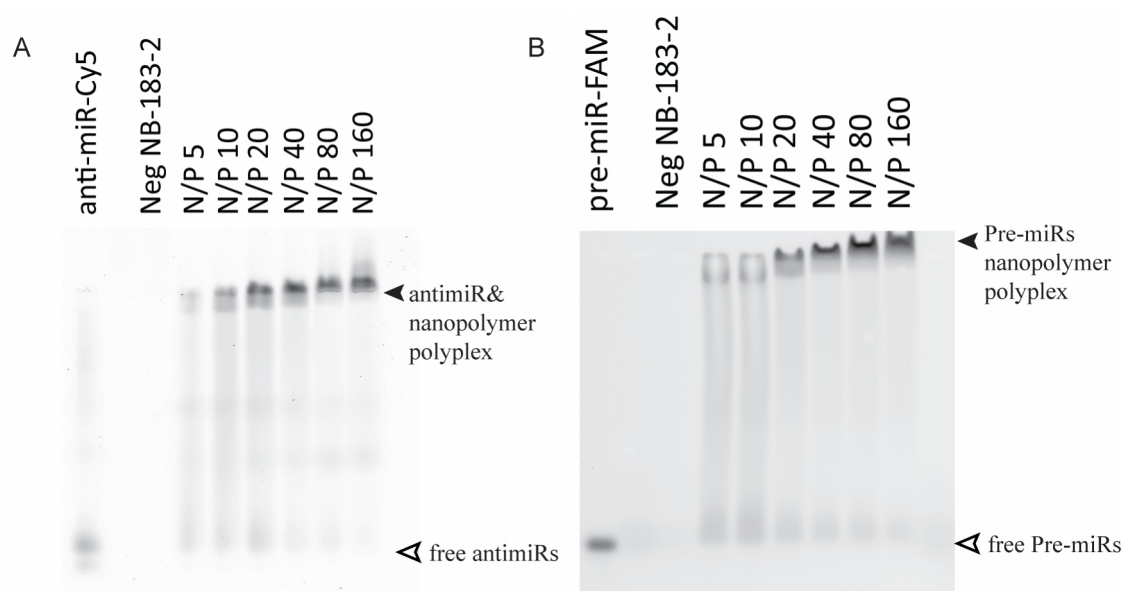
Figure 5. Gel shift assay for different N/P ratios of NB-183-2 and Cy5-labeled antimiRs complexes (A) and with FAM labeled pre-miRNA (B).
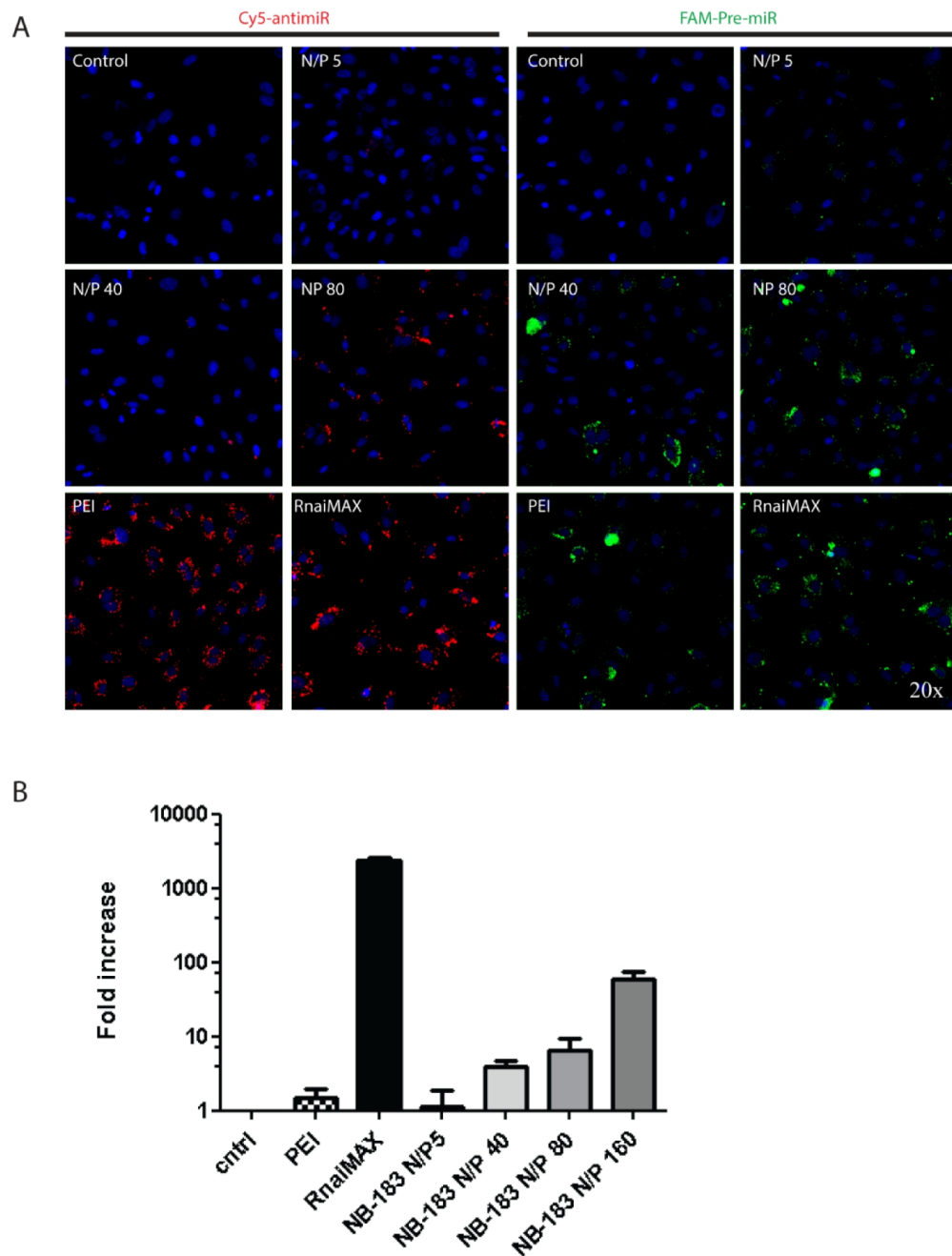
Figure 6. NB-183-2 mediated cellular uptake of antimiR and pre-miR. (A). Representative pictures of Cy5-labeled antimiRs and FAM labeled pre-miRs complexed with NB-183-2 in HMECs at different N/P ratios. PEI and RnaiMAX were used as positive controls. (B). Quantification of transfection efficiency of pre-miR-159a by NB-183-2 in HMECs using RNU19 as endogenous control. Results are normalized to control treatment.
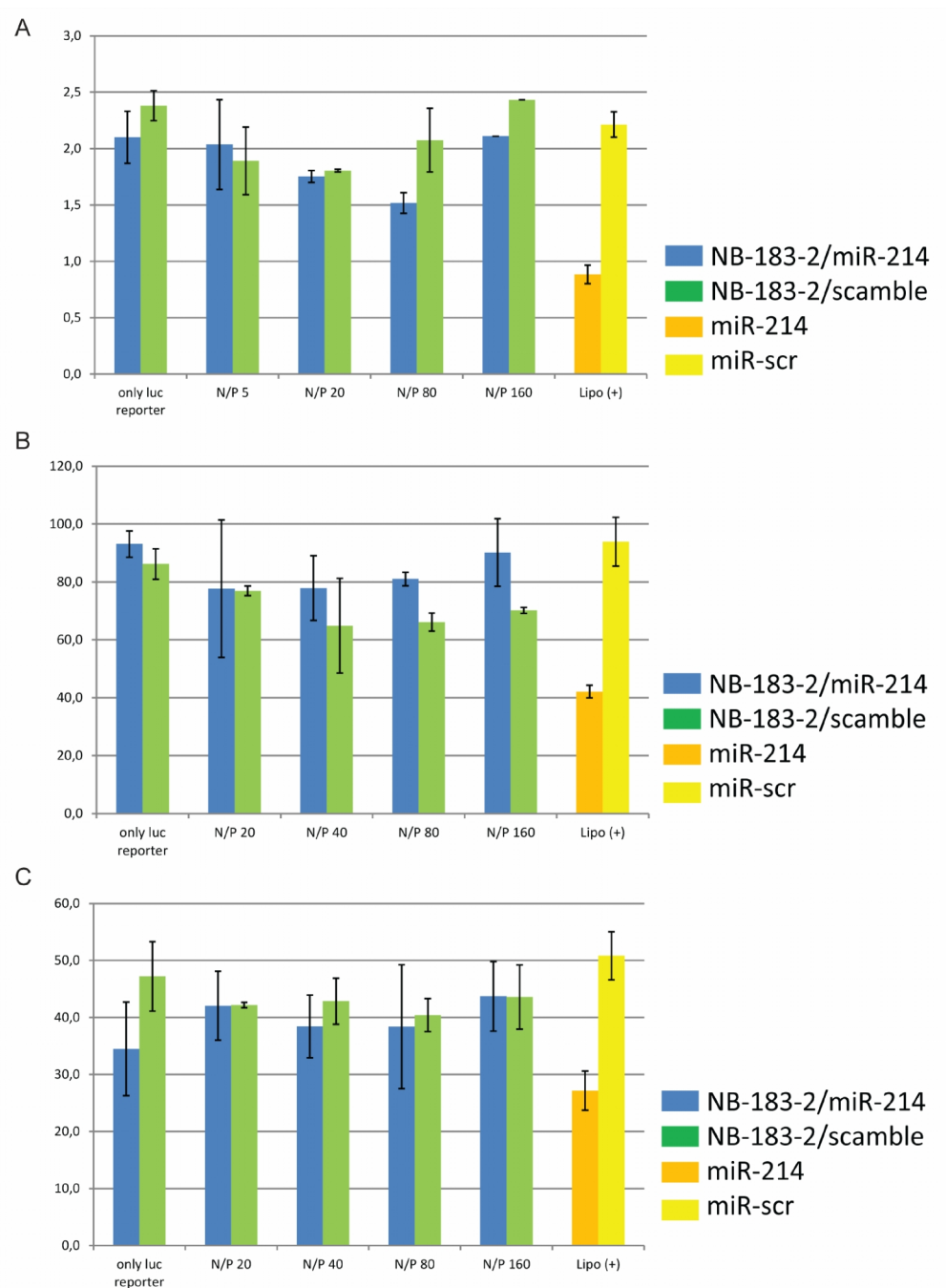
Figure 7. Functional test for NB-183-2 in miR-214 and QKI-3'UTR luciferase activity assay. (A). Luciferase activity of QKI-3'UTR reporter. Cells were transfected with miR-214 with NB-183-2, and reporter plasmids were transfected by Lipofectamine 2000 on the same day. (B). Luciferase activity of QKI-3'UTR reporter. Cells were first transfected by Lipofectamine 2000, and then reporter plasmids were transfected with miR-214 with NB-183-2 on the next day. (C). Luciferase activity of QKI-3'UTR reporter in presence of endolysosome inhibitor: 25μM Chloroquine.
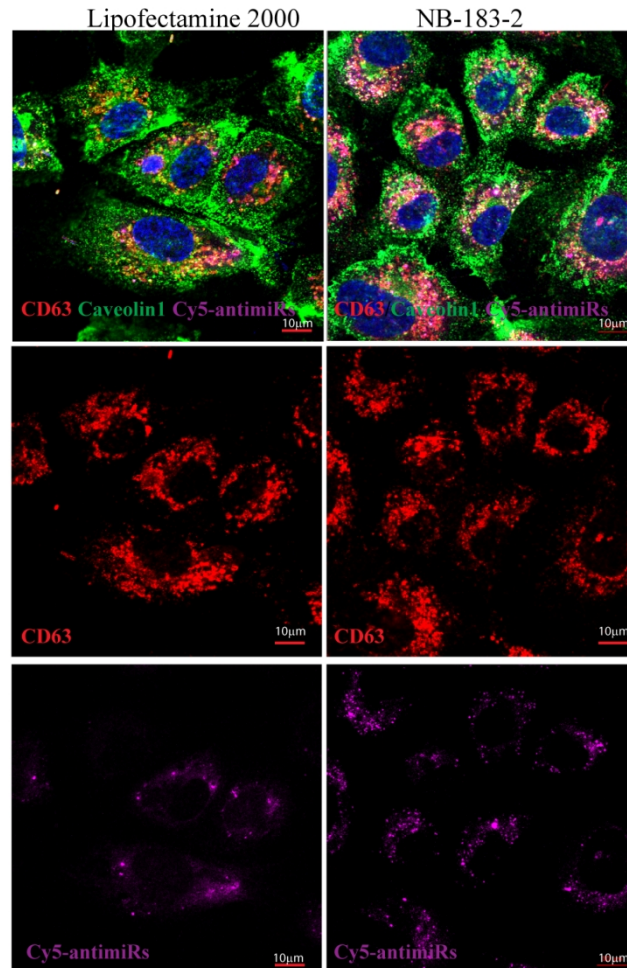
Figure 8. Localization of Cy5-labeled antimiRs 24 hours after treatment with Lipofectamine 2000 and NB-183-2, characterized by microscopic analysis. Endolysosome marker CD63 is shown in red, endocytosis marker Caveolin1 is shown in green, Cy5-labeled antimiRs are shown in Magenta. Note that in both Lipofectamine 2000 and NB-183-2 transfected cells, Cy5 signal mainly localized in CD63 positive endolysosome domain but not in Caveolin1 positive regions.

References

1. Go, A.S., et al., Heart disease and stroke statistics--2014 update: a report from the American Heart Association. Circulation, 2014. **129**(3): p. e28.
2. Steg, P.G., et al., ESC Guidelines for the management of acute myocardial infarction in patients presenting with ST-segment elevation. European heart journal, 2012. **33**(20): p. 2569-2619.
3. Krol, J., I. Loedige, and W. Filipowicz, The widespread regulation of microRNA biogenesis, function and decay. Nat Rev Genet, 2010. **11**(9): p. 597-610.
4. Ganesan, J., et al., MiR-378 controls cardiac hypertrophy by combined repression of mitogen-activated protein kinase pathway factors. Circulation, 2013. **127**(21): p. 2097-106.
5. Ucar, A., et al., The miRNA-212/132 family regulates both cardiac hypertrophy and cardiomyocyte autophagy. Nat Commun, 2012. **3**: p. 1078.
6. Yang, T., et al., MicroRNA-214 provokes cardiac hypertrophy via repression of EZH2. Biochem Biophys Res Commun, 2013. **436**(4): p. 578-84.
7. Huang, Z.P., et al., MicroRNA-22 regulates cardiac hypertrophy and remodeling in response to stress. Circ Res, 2013. **112**(9): p. 1234-43.
8. Heymans, S., et al., Macrophage microRNA-155 promotes cardiac hypertrophy and failure. Circulation, 2013. **128**(13): p. 1420-32.
9. Seok, H.Y., et al., Loss of MicroRNA-155 protects the heart from pathological cardiac hypertrophy. Circ Res, 2014. **114**(10): p. 1585-95.
10. Callis, T.E., et al., MicroRNA-208a is a regulator of cardiac hypertrophy and conduction in mice. J Clin Invest, 2009. **119**(9): p. 2772-86.
11. Care, A., et al., MicroRNA-133 controls cardiac hypertrophy. Nature medicine, 2007. **13**(5): p. 613-8.
12. Bonauer, A., et al., MicroRNA-92a controls angiogenesis and functional recovery of ischemic tissues in mice. Science, 2009. **324**(5935): p. 1710-3.
13. Hu, S., et al., MicroRNA-210 as a novel therapy for treatment of ischemic heart disease. Circulation. **122**(11 Suppl): p. S124-31.
14. Hu, S., et al., MicroRNA-210 as a novel therapy for treatment of ischemic heart disease. Circulation, 2010. **122**(11 Suppl): p. S124-31.
15. Aurora, A.B., et al., MicroRNA-214 protects the mouse heart from ischemic injury by controlling Ca(2)(+) overload and cell death. J Clin Invest, 2012. **122**(4): p. 1222-32.
16. Hullinger, T.G., et al., Inhibition of miR-15 protects against cardiac ischemic injury. Circulation research, 2012. **110**(1): p. 71-81.
17. Sluijter, J.P., MicroRNAs in Cardiovascular Regenerative Medicine: Directing Tissue Repair and Cellular Differentiation. ISRN Vascular Medicine, 2013. **2013**.
18. van Rooij, E. and S. Kauppinen, Development of microRNA therapeutics is coming of age. EMBO molecular medicine, 2014: p. e201100899.
19. Urbich, C., A. Kuehbacher, and S. Dimmeler, Role of microRNAs in vascular diseases, inflammation, and angiogenesis. Cardiovasc Res, 2008. **79**(4): p. 581-8.
20. Krutzfeldt, J., et al., Silencing of microRNAs in vivo with 'antagomirs'. Nature, 2005. **438**(7068): p. 685-9.
21. Mil, A.v., P.A. Doevendans, and J.P. Sluijter, The potential of modulating small RNA activity in vivo. Mini reviews in medicinal chemistry, 2009. **9**(2): p. 235-248.
22. Kwekkeboom, R.F., et al., Targeted delivery of miRNA therapeutics for cardiovascular diseases: opportunities and challenges. Clinical Science, 2014. **127**(6): p. 351-365.
23. Koli, P., et al., Synthesis and Characterization of Novel Encapsulating Materials Based on Functionalized Amphiphilic Block Copolymers. Journal of Macromolecular Science, Part A, 2014. **51**(9): p. 729-736.
24. Kumar, R., et al., Supramolecular assemblies based on copolymers of PEG600 and functionalized aromatic diesters for drug delivery applications. J Am Chem Soc, 2004. **126**(34): p. 10640-4.
25. van Mil, A., et al., MicroRNA-214 inhibits angiogenesis by targeting Quaking and reducing angiogenic growth factor release. Cardiovasc Res, 2012. **93**(4): p. 655-65.

26.   Sluijter, J.P., et al., MicroRNA-1 and -499 regulate differentiation and proliferation in human-derived cardiomyocyte progenitor cells. Arterioscler Thromb Vasc Biol, 2010. **30**(4): p. 859-68.

27.   Kumar, R., et al., Chemo-enzymatic synthesis and characterization of novel functionalized amphiphilic polymers. Journal of Macromolecular Science, Part A, 2002. **39**(10): p. 1137-1149.

28.   Lin, C., et al., Novel bioreducible poly (amido amine) s for highly efficient gene delivery. Bioconjugate chemistry, 2007. **18**(1): p. 138-145.

29.   Lau, A.W. and M.M. Chou, The adaptor complex AP-2 regulates post-endocytic trafficking through the non-clathrin Arf6-dependent endocytic pathway. Journal of cell science, 2008. **121**(24): p. 4008-4017.

30.   Pack, D.W., et al., Design and development of polymers for gene delivery. Nature Reviews Drug Discovery, 2005. **4**(7): p. 581-593.
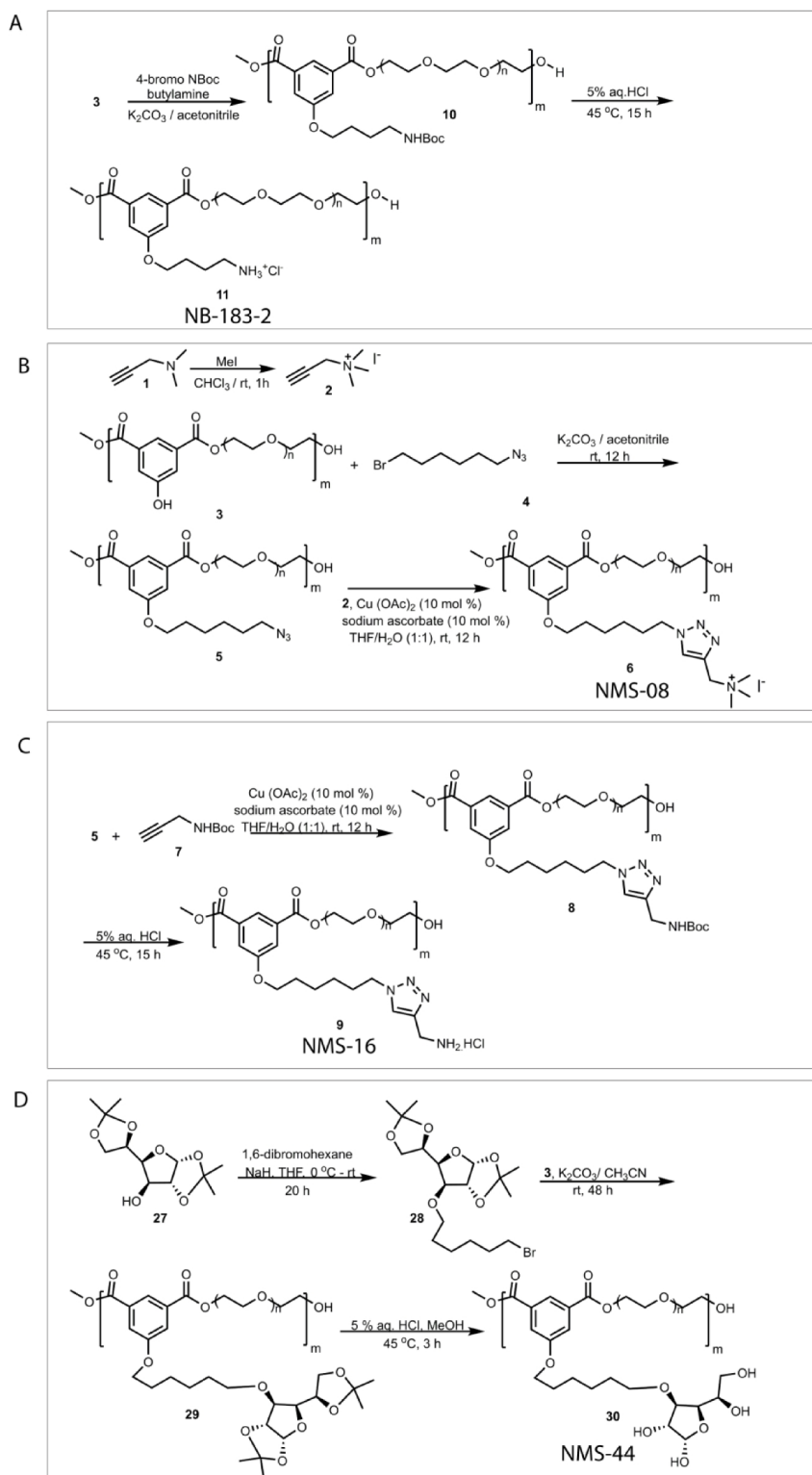
Supplementary figure: The synthesis of nanopolymers NB-183-2 (A), NMS-08 (B), NMS-16 (C), NMS-44 (D) in details.

Chapter 9

Ultrasound and Cationic Microbubble Induced Local Delivery of microRNA-based Therapeutics both *in vitro* and *in vivo*.

Rick F J Kwekkeboom[*], Zhiyong Lei[†], Sylvia J P Bogaards[*], Eric Aiazian[‡, §], Otto Kamp[§], Walter J Paulus[*], Joost P G Sluijter[†], René J P Musters[*].

[*]Department of Physiology, VU University Medical Center

[†]Department of Experimental Cardiology, University Medical Center Utrecht

[‡]Axle International, Nieuwe Uitleg 28, 2514 BR, the Hague, the Netherlands

[§]Department of Cardiology, VU University Medical Center

Abstract

MicroRNAs are involved in many pathological processes and are a promising class of molecules to therapeutically target. However, successful localized, minimally invasive delivery of miRNA-based therapeutics is lacking. In the present study, cationic ultrasound-responsive microbubbles (MB) were studied for their ability to deliver microRNA blockers and mimics *in vitro* and *in vivo*. Cationic MB successfully delivered microRNA blockers into the intracellular compartments of primary isolated human endothelial cells *in vitro* with a transfection percentage of 22% and a 50% reduction in microRNA-expression. This *in vitro* US protocol however was not successful in local delivery of miR mimics *in vivo* whereas a US-protocol which is routinely used for contrast-imaging increased local delivery 2.8-fold. Additionally, antimir and antagomir molecules were bound to cationic MB and locally delivered using US-protocols causing inertial cavitation at 7 MHz and 2 MHz. Antimir delivery was only slightly increased to the extracellular compartments of the muscle whereas antagomir delivery was both significantly increased to the capillaries, myocytes and extracellular space both at 7 and 2 MHz. Antagomir are a more suitable miRNA blocker to use in combination with MB and US for local delivery then antimir.

Keywords: ultrasound, microbubbles, microRNA, antimir, antagomir, drug delivery, endothelial cells.

Introduction

Since the recognition of microRNA (miR) as a class of regulatory RNAs in 1993 [1-3] and the discovery of the first miR in humans [4], miR have been quickly recognized as a potential target for pharmaceutical therapy [5] in for instance cancer [6], heart disease [7, 8] and acute ischemia [9]. Overall, two strategies have been developed using either gain of function (e.g. with miR mimics) or inhibition (e.g. with antimirs or antagomirs) of miR. Antimirs are single stranded RNA molecules with an exact complementary base-sequence to a specific miR and are nuclease resistant [10]. Antimirs are hydrophilic and therefore have problems crossing the endothelial barrier after intravascular injection resulting in limited pharmaceutical effect. Antimir can be modified to create an antagomir by adding a cholesterol group to the 3` end of the antimir, resulting in its cellular uptake upon systemic injection [11]. However, miR inhibition should ideally be confined to a specific organ or tissue to avoid side effects, which limits the potential systemic use of antagomirs in a clinical setting, especially if the targeted miR is not tissue-specific.

An alternative approach in miR-therapeutics is to boost miR-activity through the application of miR mimics. Developments in miR mimic chemistry, however, have fallen behind to antimir development, leading to substantial difficulties in *in vivo* miR mimic delivery [12]. Ideally, both antimir and miR mimics would be injected in the blood and taken up by specific tissues or cells. Development of drug delivery vehicles for antimir and miR mimics is still in its infancy [13-15], and localized delivery of antimir, antagomir and miR mimics remains a challenge.

A previously described type of drug delivery vehicle for localized delivery is the microbubble [16]. Microbubbles (MBs) are gas-filled spheres with a micrometer diameter (typically 1-10 μm) and are used as a contrast agent in ultrasonography. Additionally, these gas-filled spheres can be loaded with several types of molecules with therapeutic potential like pDNA [17-19], oligodeoxynucleotides [20], siRNA [21] and growth factors [22]. After intravenous injection of these 'loaded' MBs, ultrasound (US) can be applied locally, causing the MBs in the ultrasonic field to cavitate. Cavitation of MBs causes them to lose their payload and permeabilize the vasculature, leading to an increased localized release and uptake of therapeutics at the site of US treatment [17, 18, 20-22]. *In vitro* studies have shown that MB induced drug delivery to cells can be achieved at low mechanical index (MI) US causing stable oscillation of MB [23]. On the other hand, most *in vivo* studies report the use of high MI US, leading to destruction of MBs (inertial cavitation). These high MI *in vivo* approaches have been successful in local delivery of drugs without causing major damage [17, 18, 20-22]. This raises the question, however, whether US-parameters which are successful *in vitro,* which do not cause

inertial cavitiation, can also be successfully used for *in vivo* delivery of therapeutics [24] as this has not been demonstrated even though extensively studied and successfully employed *in vitro*.

The first goal of this study is to test whether antimir and antagomir molecules can be loaded upon cationic MB and subsequently be delivered intracellularly to cultured human umbilical cord endothelial cells (HUVECs) as has previously been done with siRNA [25]. Second goal of the study is to test whether US-settings that successfully deliver antimir and antagomir *in vitro* can be used for *in vivo* delivery of miR mimics (as a model small RNA) and how this compares to delivery when using US-settings that are used for US contrast imaging and do cause inertial cavitation of MB. Thirdly, a comparison between antimir and antagomir is made regarding tissue distribution after MB and US induced local delivery at 14 MHz and 2 MHz. Ultimately, this study aims to discuss the relevance of *in vitro* data concerning drug delivery using MB and US and aims to clarify what kind of miR blocking agent is most suitable for local delivery using MB and US.

Materials and Methods

Antimir, antagomir and miR mimics

For *in vitro* transfection experiments and *in vivo* delivery experiments, antimir and antagomir molecules targeting miR-214 were designed and synthesized as well as mismatch control antimir and antagomir (Supplementary figure A). For *in vivo* miR mimic delivery, a commercially available double-stranded Ambion^{TM} miR-159a mimic (Life Technologies, Bleiswijk, The Netherlands) was used. Since miR-159a is not endogenously expressed by mice, background levels or this miR are practically non-existent and signal to noise ratio of locally delivered miR-159a thus very good.

Cationic MB production and antimir complex formation

Cationic MB (cMB) design was based on earlier work by Christiansen et al. [18] and slightly altered to improve MB-antimir/antagomir binding. Di-stearoyl-phosphatidylcholine (DSPC, Avanti polar lipids, Alabama, USA), di-stearoyl-tri-ammoniumpropane (DSTAP, Avanti polar lipids) and PEG40-stearate (Life Technologies) were dissolved in glycerol (Invitrogen, Life Technologies) at 10 mg/ml at 70 °C. Subsequently, phospholipids and PEG40-stearate were transferred to a 2 ml reaction tube in a DSPC:DSTAP:PEG40-stearate weight ratio of 8:4:1. MB creation medium consisted of a H_2O:glycerol:propyleneglycol mixture with a 24:14:3 volume ratio. Perfluorobutane gas (C_4F_{10}, F2 Chemicals Ltd., Lancashire, UK) was added to the capspace of the reaction tube after which the

phospholipid mixture was placed in a Decon FS200 ultrasonic bath (Decon Ultrasonics Ltd., East Sussex, UK) for 10 min. Next, MB were created by high speed shaking (4500 rpm) using a Vialmix^{TM} device (Lantheus Medical Imaging inc., MA, USA) for 45 seconds. MBs were washed three times by means of centrifugal flotation. Subsequently, MB size-distribution and concentration were determined using a Multisizer 3^{TM} (Beckman Coulter Nederland B.V., Woerden, the Netherlands). Next, MBs were tested for their capability to load FITC-labeled antimir, antagomiR and Ambion miR mimic (Life Technologies) molecules. MB were diluted to $500*10^6$ MB/ml and antimir, antagomiR or miR mimic was added to a concentration of 1.4 nmol/ml, 2.9 nmol/ml and 3.3 nmol/ml respectively. Five minutes after adding antimir, antagomiR or miR-mimic to MB, complexes were visualized using DIC and FITC fluorescence imaging on a ZEISS Axiovert Marianas^{TM} 200M inverted fluorescence microscope [26] (Intelligent Imaging Innovations (I.I.I.), Denver CO, USA) in combination with Slidebook^{TM} 5.0 software (I.I.I.). Additionally, cMB payload was determined for antimir molecules. 2 nmol of FITC-labeled antimiR was added to $200*10^6$ cationic MB in a volume of 300 µl and allowed to form complexes for 10 min. Degassed H2O was subsequently added up to a volume of 3 ml and unbound antimir was separated from the cationic MB by means of centrifugal flotation at 300 g for 10 min. Unbound antimir was collected and its concentration was determined using a FLUOstar Galaxy microplate reader (MTX Lab systems, Virginia, USA) The percentage of antimir bound to the cMB was determined by subtracting the unbound amount of antimir from the added amount of antimir.

Microbubble induced transfection of HUVECs with antimir in *in vitro* system 1

A custom designed *in vitro* US treatment chamber (UTC) was manufactured for treatment of HUVEC monolayers on 12 mm Millicell culture plate inserts (Merck, Darmstadt, Germany) (Supplementary figure B, *In vitro system 1*). The UTC was used in combination with a V303-SU unfocused single element ultrasound transducer (Panametrics, Waltham, MA, USA), driven by an arbitrary waveform generator (AWG-5000 series, Tektronix, Oregon, USA) and custom build amplifier. Therefore, the scattering effect of the cylindrical metal casing of the UTC on the US wave was determined with a needle-hydrophone (Precision Acoustics, Dorchester, UK) (Supplementary Figure C).

HUVECs were isolated and cultured as described previously [26]. Passage 2 HUVECs were seeded on 12 mm diameter Millipore standing culture inserts (Merck). Three days after seeding, culture inserts with HUVEC monolayers were placed in the UTC. Cy3-labeled antimir was added to MBs to form MB-antimir complexes which were subsequently added to the culture medium (containing 20% serum) to form treatment medium, resulting in concentrations of $27*10^6$ microbubbles/ml and 112 pmol antimir/ml. Treatment medium was added to the UTC containing the HUVECs. Treatment

consisted of applying three different US protocols: short pulse, long pulse, or low pressure, or no US. Exact parameters of the ultrasound protocols are listed in table 1. After treatment, HUVECs were allowed to recover at 37 ^{o}C and 5% CO_2 in a humidified atmosphere for 60 minutes in treatment medium. After 60 minutes, HUVEC monolayers were fixed with 4% paraformaldehyde in phosphate buffered saline (PBS), stained for f-actin with Alex Fluor 488 Phalloidin (Life Technologies) and enclosed on a glass microscopy slide with mounting medium containing DAPI nuclear staining. Subsequently, fluorescence pictures of these monolayers were taken using filter sets for DAPI, FITC and Cy3 with 10x and 40x objectives (Carl-Zeiss, Sliedrecht, the Netherlands) on a ZEISS Axiovert Marianas[TM] 200M inverted microscope [26] (I.I.I.). Fluorescence microscopy images were analyzed with Slidebook[TM] 5.0 software (I.I.I.) both qualitatively and quantitatively. Pairs of groups were tested for differences in percentage of transfection using a Mann-Whitney U test. A HUVEC was considered transfected when the nucleus contained a Cy3-fluorescent staining.

Microbubble induced transfection of HUVECs with antimir in *in vitro* system 2

Transfection efficiency of MB and US was also tested in an alternative *in vitro* system, *in vitro system 2 (*Supplementary figure B: *in vitro* system 2). This system applies US at a 45 ^{o} angle, thus not pushing the MB directly to the cells and has been used successfully for the *in vitro* transfection of siRNA into aortic endothelial cells [25]. HUVECs were seeded on Opticell culture membranes and treated with MB+US (US protocol is listed in table 1; *in vitro* 2) in combination with either cy3-labeled antimir or antagomir after 3 days. Control cells received MB with bound antimir or antagomir, but no US. After treatment, medium was immediately replaced with serum-containing culture medium. Cells were fixed 1 h, 3 h, 18 h or 24 h after treatment, subsequently stained for F-actin and the nucleus and analyzed using the fluorescence microscope as previously described for *in vitro* system 1. Localization of transfected antimir and antagomir was analyzed for all timepoints. Additionally, transfection% and the number of membrane adherent cells for control cells and US-treated cells 1 h or 3 h after treatment was determined per 10x magnification window. To test for statistical significant differences, a student's t-test was performed.

Additionally, cells were treated with US+MB in combination with either antimir or antagomir targeting miRNA-214 or mismatch control-antimir/antagomir. 48 h after treatment, RNA was extracted from these cells and purified using the TriPure RNA isolation reagent (Roche Applied Science, Penzberg, Germany). miR-214 levels were determined with a TaqMan MicroRNA Assay (Applied Biosystems, Foster City, CA, USA) as published before [27]. In brief, 2 ng total RNA was used for miR-214-specific reverse transcription (Taqman® MicroRNA Reverse Transcription Kit,

Applied Biosystems). Amplification and detection of specific mature miRs was performed by specific TaqMan hybridization probes and Sybr Green (Applied Biosystems) in a MyIQ single-color quantitative real time polymerase chain reaction (qRT-PCR) system (Bio-Rad, Veenendaal, the Netherlands) at 95 °C for 10 min, followed by 40 cycles of 95 °C for 15 s and 60°C for 60 s. The cycle threshold (Ct) of each target gene was automatically defined, located in the linear amplification phase of the PCR, and normalized to the expression of the small nuclear RNA RNU6 (ΔCt value). miR-214 levels in US-treated cells were normalized to the levels of non-treated control cells. miR-214 levels of different groups were tested for statistical difference using a student's t-test.

In vivo miR mimic delivery

As a pilot study to determine what types of US-protocol were most feasible for *in vivo* miRNA/antimir/antagomir delivery, an animal study for miR-159 delivery was performed. All animal studies were approved by the institutional animal care and use committee at the VU University Medical Center. Male C57BL/6 mice (n=13, 20-24 g; Harlan, Horst, the Netherlands) were anesthetized with a mixture of azepromazine, fentanyl and midazolam through i.p. injection and placed on a homeothermic blanket (Panlab, s.l.u., Barcelona, Spain). For US+MB induced local delivery of miR mimics, mice received an i.v. injection of miR mimics alone (1 nmol ~ 70 μg/kg) or miR mimics (1 nmol ~ 70 μg/kg) complexed with cationic MB (200 * 10^6 MB) through the tail vein in a volume of 100 μl. Subsequently, the upper portion of the right hind limbs of mice were treated with ultrasound using different US treatment protocols; 'High intensity 7 MHz US only', 'Low intensity US' and 'High intensity 7 MHz'. Exact parameters of US-treatment protocols are listed in table 2. Directly after US-treatment, mice were whole-body-perfused with 40 ml of PBS over 15 min. After perfusion, muscles from the treated and non-treated hind-limb were isolated and frozen at -80 °C. Total RNA was isolated with TriPure Isolation Reagent. miR159a mimic levels were determined with a TaqMan MicroRNA Assay (Applied Biosystems, Foster City, CA, USA) as described earlier in this manuscript. The relative difference in miR mimic levels between the treated and non-treated hind limb was calculated (ΔΔCt) and presented as fold increase. The mean fold-increases of treatment groups were tested for statistical significant differences with a Mann-Whitney U non-parametric test.

In vivo antimir and antagomir delivery

After having established what kind of US-protocol is most feasible for local delivery of miRNA mimics, the same US-protocol was used in an animal study for antimir and antagomir delivery. Male C57BL/6 mice (n=36, 20-24 g; Harlan, Horst, the Netherlands) were anesthetized with a mixture of azepromazine, fentanyl and midazolam through i.p. injection and placed on a homeothermic blanket (Panlab, s.l.u., Barcelona, Spain). Subsequently mice received an i.v. injection through the tail vein of

either MB+antimir, MB+antagomir, antimir only or antagomir only. MB-dose was $200*10^6$ for all mice and antimir/antagomir dose was 2 nmol (~77 ug/kg of body weight). After i.v. injection mice received US-treatment of either 7 MHz with an MI of 1.8 (High intensity 7 MHz) or 2 MHz with an MI of 1.4 (High intensity 2 MHz) at the right hind limb. For a complete overview of treatment for the different groups we refer to supplementary table A. After US-treatment, mice were whole body perfused with 40 ml of PBS over 15 minutes after which the semimembranosus muscles of both the left and right hind limb were extracted and frozen in liquid nitrogen. Cryosections were cut and directly analyzed using our previously described fluorescence microscope. For both treated and control muscles, the peak intensity of fluorescence was measured in the capillaries and a line was drawn through 3 myocytes of which the mean intensity was determined, this mean intensity included both myocytes and extracellular space in one mean value. The fluorescence signal in the treated muscle was normalized for the non-treated muscle and means of fold-increase due to local US-application for each group were displayed in a graph. Differences between non-treated hindlimbs and treated hindlimbs were tested for statistical significance using a Wilcoxon signed-rank test. Additionally, cryosections were immunofluorescently stained for CD31 and for the nucleus for qualitative analysis.

In vivo effect of ultrasound protocols on MB integrity

In this study three different US-protocol were used for *in vivo* drug delivery. MB in the hind limb were visualized at the spot of treatment on the Siemens Sequoia in cadence mode at 14 MHz for treatment protocol 'Low intensity', 'High intensity 7 MHz' and 'High intensity 2 MHz'. Clips were recorded and stills from these clips just before US-application and directly after US-application were compared to visualize the effect of US-protocols on MB integrity.

Results

Microbubble size distribution and antimir, antagomir or miR-mimic loading

Polydisperse cMBs were created and washed, resulting in cMB with diameters between 1 and 6 μm (Fig 1A). MB yields ranged from $2.5*10^9$ - $3.5*10^9$ MBs per tube. These cMB were capable of homogeneously complexing with antimir, antagomir and fluorescently labeled miR mimic as observed by fluorescence microscopy (Fig 1B), based on fluorescence microscopy data antagomir showed a higher binding capacity to cationic MB compared to antimir and miR mimics. Additionally, the binding efficiency of antimir on cationic MB was determined to be at 46% (Fig 1C), corresponding to 0.92 nmol/$200*10^6$ MB (1,3 μg/$200*10^6$).

Microbubble induced transfection of HUVECs with antimir in *in vitro* system 1

HUVECs were grown to confluent monolayers in three days. The experimental procedure, including the addition of MBs + antimir to cells (without US), did not affect the cell monolayer integrity (Fig 2 A). Treatment of HUVEC monolayers with MBs, antimirs and US (1 MHz, 200 kPa peak-negative pressure (PnP), 60 sec, pulse length 2000, pulse repetition frequency (prf) 10 Hz) lead to a disturbance of the monolayer as seen by fluorescence microscopy (Fig 2 B). This disturbance was seen in combination with nuclear presence of antimir.

Areas with and without transfected cells were analyzed at a higher magnification (40x). In areas without the transfected cells, monolayer integrity was not compromised (Fig 2 C, D, E). Within transfected areas two distinct HUVEC phenotypes were observed (Fig 2 F, G, H). Firstly, HUVECs with a clearly disrupted F-actin cytoskeleton and single-stranded antimir in their nucleus were seen. The second phenotype consisted of cells that did not have antimir in their nucleus and also did not show the clearly disrupted F-actin cytoskeleton.

Transfection percentage as a result of MB+antimir+US treatment was determined by means of fluorescence microscopy (see Fig 2 I). The short pulse US protocol resulted in an average transfection of 6.3% of total HUVECs. The long pulse US protocol resulted in transfection percentages ranging from 13-30% with an average of 22%. Treating HUVECs with US protocols low pressure or without US resulted in percentages below 1%. The long pulse US protocol resulted in statistically significant higher transfection percentages when compared to the low pressure and no US protocols ($p<0.05$), and a trend towards higher transfection percentage when compared to the short pulse US protocol ($p=0.06$).

Microbubble induced transfection of HUVECs with antimir in *in vitro* system 2

Transfection of antimir molecules to HUVECs was also tested in an alternative setup which applies US at a 45° angle and allows for the treatment of a higher number of cells which makes it possible to isolate a sufficient amount of miRNA for a qPCR. As in setup 1, MB+US treatment resulted in cellular uptake of antimir molecules and these antimir could be found most pronounced in the nucleus of the cells 1 h after treatment (Figure 3 A). The f-actin skeleton of transfected HUVECs was disturbed but to a lesser extent when compared to *in vitro* system 1. Antimir could still be found in the nucleus 3 h, 18 h and 24 h after treatment. Additionally, MB+US was used to transfect antagomir molecules to HUVECs. 1 h after treatment, antagomir could be found intracellularly in HUVECs both in the

cytoplasm and in the nucleus (Figure 3 A). Antagomir could still be found in the HUVECs 3 h, 18 h and 24 h after treatment (Figure 3 A). In addition to qualitative analysis, microscopic images were analyzed quantitatively with regards to the amount of membrane adherent cells per 10x magnification window and transfection% both for antimir and antagomir transfection for non-treated control cells and the 1 h and 3 h timepoints after treatment (Figure 3 B+C). MB+US treatment in combination with antimir resulted in a small, non-significant, decrease in membrane adherent cells from 337 cell/image window without US treatment to 300 cells/image window 1 h after treatment. 3 h after treatment a further decrease in membrane adherent was observed to 183 cell/image window which was statistically significant (p<0.0001) compared to no US treatment. Transfection% was 23% at 1 h and thus comparable to the transfection% of system 1. After 3 h, transfection% was 25%. Both percentages were statistically significantly different from non-treated control cells (p<0.05). Additionally, the correlation between transfection% and amount of membrane-adherent cells was studied both at 1 h and 3 h after treatment. Transfection% was clearly correlated to a lower amount of membrane-adherent cells, both at 1 h and 3 h after treatment and both for antimir transfection and antagomir transfection (Supplementary figure C).

Subsequently, the biological effect of transfected antimir and antagomir was tested by extracting RNA 48 h after treatment and determining the amount of miRNA-214 (Figure 3 D). Treatment of HUVECs with MB+US and a mismatch control-antimir did not result in a difference in miRNA-214 expression. However, MB+US treatment with an antimir-214 resulted in a statistically significant decrease in miRNA-214 expression compared to both non-treated control cells and mismatch control treated cells (p<0.05) of 50%. Treatment of HUVECs with MB+US and antagomir (both mismatch control and antagomir-214) resulted in a decrease in miRNA-214 expression compared to non-treated control cells . However, no difference could be found between mismatch control antagomir and antagomir-214. Overnight treatment of HUVECs with antagomir-214 however resulted in a drastic decrease of miRNA-214 expression of around 90%.

In vivo MB+US induced delivery of miR-mimics.

Mice were treated with three different US-protocols (Table 2). After treatment, no MB could be detected in treated hind limbs whereas MBs were still present in non-treated hind limbs. High intensity only treatment resulted in a 1.2 fold-increase (ranging from 0.5 to 2) of miR mimic delivery in treated tissue. Treatment of hind limbs with low intensity US resulted in a 0.88 fold-increase (ranging from 0.3 to 1.3). High intensity US treatment resulted in a 2.8 fold-increase (ranging from 2.6-3.7). The 2.8-

fold-increase of the high intensity US treatment group was statistically higher than the fold-increase of the low intensity US and miR only treatment groups (p<0.05).

In vivo MB+US induced delivery of antimir and antagomir.

Antimir and antagomir were locally delivered using the 'High intensity 7 MHz' or 'High intensity 7 MHz only' protocols as were used for miR mimic delivery. Antagomir could mostly be found in the smaller capillaries (diameter <10 μm) and to a lesser extent in arterioles (Figure 5 A) both in mice which received antagomir+MB and antagomir only (data for antagomir only not shown). Local treatment of US, only in the presence of MB, resulted in an increase of delivered antagomir to the capillaries and additionally caused an increase in extracellular space (probably due to edema), also containing antagomir. Additionally, antagomir could be found more pronounced at myocyte cell-cell contacts.

Antimir could mostly be found in the vessel wall of arterioles and a lesser extent the bigger capillaries (Figure 5 B) both in mice which received antimir+MB and antimir only (data for antimir only not shown). Local application of US to increase local delivery did not result in a difference in tissue distribution of antimir in the absence or presence of MB. Subsequently, antimir and antagomir were locally delivered using the 'High intensity 2 MHz' and 'High intensity 2 MHz only' protocols. Tissue distribution of antagomir was comparable to the 'High intensity 7 MHz' treated group, however, the US-transducer used for this treatment regimen has a bigger focus area resulting in a larger treatment area (Supplementary Figure E). Additionally, more microbleedings could be seen at 2 MHz compared to 7 MHz and a bigger increase in extracellular space was observed in the treated muscle at 2 MHz, in which antagomir was present. As with the 7 MHz protocols, the 2 MHz protocol did not have an effect on antimir distribution in the capillaries in the presence or absence of MB. However, an increase in extracellular space, in which antimir could be seen, was found after treatment with US at 2 MHz in the presence of MB.

Microscopy pictures were furthermore analyzed quantitatively by measuring the fluorescence intensity of antimir/antagomir signal in the capillaries and myocytes/extracellular space and determine the fold-increase over the non-treated control hind limb. Treatment with US at 7 MHz did not result in increased capillary delivery of antimir in the presence or absence of MB (Figure 6). In the presence of MB however, 7 MHz US treatment resulted in a slight, non-significant, increase in antimir levels in the myocyte/extracellular space compartment. For antagomir however, 7 MHz US treatment in the

presence of MB resulted in 2.5-fold increase in antagomir in the capillaries (p<0.05) and a significant increase in the myocyte/extracellular space compartment (p<0.05). In the absence of MB, no effect on antagomir levels in either capillary or myocyte/extracellular space was observed. The same pattern was observed when mice were treated with 2 MHz US (Figure 7). Localized US treatment at 2 MHz did not result in increased delivery of antimir to the capillaries (Figure 7) and a small, non-significant, increase in antimir levels in the myocyte/extracellular space compartment. For the antagomir however, in the presence of MB, 2 MHz US treatment resulted in a 2.3-fold increase of antagomir in the capillaries (p<0.05) and a statistically significant increase in the myocyte/extracellular space (p<0.05). In the absence of MB, no effect was observed.

Effect of US-protocols on MB integrity

The low intensity US protocol did not have an effect on MB integrity (Figure 8) whereas both the 7 MHz and 2 MHz high intensity US protocols caused MB destruction as can clearly be seen when looking at cadence images directly before and after application of these specific US-protocols.

Discussion

In the present study, antimir, antagomir and miR mimicking molecules were attached to cMB for *in vitro* and *in vivo* local delivery experiments. These MBs were capable of delivering antimir and antagomir to HUVECs upon ultrasound exposure, resulting in knockdown of the antimir target, but not of the antagomir target. Additionally, local delivery of miR mimics to the hind limb was increased 2.8-fold after US-treatment with 7 MHz at an MI of 1.8, but not with 1 MHz at an MI of 0.2. Furthermore, local 7 MHz US treatment in combination with MB increased delivery of antagomir, but not antimir, to capillaries, myocytes and extracellular space. The same effect was observed for US treatment at 2 MHz.

Nucleic acid-MB binding has been studied before [18, 21] using different protocols. Christiansen et al. attached pDNA to cationic MB by adding the pDNA to the MB after production. This resulted in a homogenous distribution of pDNA along the MB shell. More recently, Carson et al. [21] attached siRNA to cationic MBs by adding the siRNA to the phospholipid mixture before making the MBs. In the present study, antimir, antagomir and miR mimicking molecules were added after MB production and directly used for *in vitro* or *in vivo* testing. This strategy was chosen because of lower loss of antimir, antagomir and miR due to the absence of washing steps, the resulting homogeneous distribution of these small RNA molecules on the MB surface and comparable payloads (in the μg per

100 * 10^6 MB range) as in the Carson et al. study [21]. One drawback of this method is that 50% of the RNA that is injected is not bound to the cMB.

Furthermore, MB-antimir/antagomir complexes were tested in two *in vitro* setups to transfect primary isolated HUVECs. In both setups, antimir was successfully transfected to 22-23% of the HUVECs and transfection correlated with significant cell-loss. US-parameters that were most successful with regards to transfection% in the two different *in vitro* setups differed. In set-up 2, where US was applied at a 45° angle, US-treatment was shorter and employed a higher pressure, showing that even *in vitro*, US-parameters that are optimal for one setup do not necessarily translate to another setup. Setup 2 was chosen as the system to test for time-dependent trafficking and biological activity of delivered antimir and antagomir to determine which of the two molecules was most suitable for *in vitro* miR-knockdown in combination with US+MB. Transfected antimir could mainly be found in the nucleus of HUVECs 1h, 3h, 18h and 24h after treatment, and the intensity of the antimir signal declined over time indicating either a dilution of antimir due to cell division, trafficking out of the nucleus to the cytosol or loss of fluorescent intensity of the cy3-group coupled to the antimir. Transfected antagomir could be found both in the nucleus and the cytosol at all timepoints, and also for antagomir the intensity of the signal declined over time. Since the miR are localized in the cytoplasm, the antagomir seemed the more suitable of the two. However, transfection% for antimir was higher compared to antagomir at 1 and 3 h after treatment with the same US-treatment protocols. To answer the question which of these molecules is more suitable for *in vitro* miR-knockdown in combination with US+MB, we measured miR-214 levels 48 h after treatment with antimir-214 and antagomir-214. Interestingly, antimir-214 caused a 50% reduction in miR-levels compared to a mismatch control antimir whereas antagomir-214 had no effect on miR-levels compared to a mismatch control antagomir. Thus, for *in vitro* purposes, antimir are the more suitable molecule for specific miR-knockdown in combination with US+MB.

This is the first time that MB and US have been investigated for their capability to transfect antimir and antagomir *in vitro*. However, a structural homologue, the siRNA, has been studied extensively in *in vitro* MB+US mediated transfection. Our results regarding transfection% are somewhat lower compared to other studies [23, 28-30], which can be explained by our choice of primary isolated HUVECs which are known to be difficult to transfect [31]. Additionally, siRNA could be found more pronounced in the cytosol [25] compared to antimir in our study. A possible explanation is that siRNA is double-stranded whereas our antimir is single-stranded, making it easier for the antimir to travel through the nuclear membrane. The mechanism, in which transfection of antimir to the nucleus of cells in 23% of treated HUVECs leads to a 50% reduction of miR-expression, has yet to be elucidated.

In the present study, *in vivo* local delivery of miR mimics, antimir and antagomir by means of MB+US treatment was also studied. First we aimed to test whether the US-parameters which were successful in antimir and antagomir delivery *in vitro* and successful for siRNA delivery in a previous study [25] could locally increase miR mimic levels after i.v. injection of MB carrying this miR mimic and local US application. We choose miR-159 mimics as a model RNA since these are detectable by qPCR, meaning that even a very small increase in delivery could be picked up. We found that this low intensity 1 MHz US protocol, which did not cause MB destruction, did not increase local delivery of miR-159 to the treated muscle. Since previous studies on local delivery with US+MB use US protocols that cause MB destruction [21], we also tested the capability of our standard contrast imaging protocol, which does cause MB destruction at MI=1.8, to achieve local delivery of miR mimics. We found that treatment with this 7 MHz high intensity protocol resulted in a 2.8-fold increase of local miR mimic delivery. In contrast to *in vitro* findings, for *in vivo* delivery of small RNAs it seems necessary to destroy MB.

Subsequently we tested whether this 7 MHz high US protocol could also locally deliver antimir molecules and where in the treated muscle these could be found. We found that antimir could be found mostly in the vessel wall of arterioles and a to lower extent in bigger capillaries after i.v. injection of MB+antimir. The local application of US did not have an effect on antimir levels or distribution in these vessels. The application of US however did have a small, non-significant, effect on the extracellular space. Without application of US, myocytes were closely aligned and no extracellular space could be seen in between. However, US-treatment in the presence of MB caused edema, creating extracellular space in which antimir could be seen. Probably the miR mimics that were delivered earlier were situated in the extracellular space as well. The same pattern of antimir distribution was observed with the 2 MHz high intensity US protocol.

Previous studies regarding local delivery of siRNA using MB+US have claimed that siRNA only enters the vessel wall at the spot where US is applied, and not in remote areas [32]. However, in that particular study, blood flow was disrupted and the MB and siRNA were incubated in the lumen of the treated blood vessel without flow and blood pressure. Studies reporting on siRNA delivery after systemic injection, thus retaining flow and blood pressure, also report on successful effects of delivered siRNA. However, not all these studies include all the proper controls, for instance the non-US treated control with MB carrying specific siRNA directed the target mRNA is lacking in one study [33]. Another study that does include that control reports that ~50% of the therapeutic effect of MB+US+siRNA treatment might be attributed to MB+siRNA alone [21], and that local US-treatment doubles that effect. Whether that is due to a local increase of siRNA levels or increased cellular

permeability is not mentioned; the mechanistics in which MB increases the effectivity of siRNA *in vivo* is unclear. Increasing pressure is a well-established method for siRNA transfection *in vivo* [34]. Our results suggest that blood pressure in arterioles (~80-100 mmHg) [35] might be high enough to push the single-stranded antimir in the vessel wall and that the blood pressure in small capillaries is insufficient to do so. US does not have an additional effect on this process. However, local US-treatment does cause the MB to collapse, increasing vascular permeability and causing extravasation of fluid in which antimir leaves the blood and enters the extracellular compartment of the muscle. Antimir might subsequently slowly enter myocytes and endothelial cells even though antimir uptake over cellular membranes is generally considered low. In this sense, the effect of MB+US is mostly an increased delivery effect and less a sonoporation/increased cellular permeability effect.

We also tested the capability of MB+US to locally deliver antagomir molecules. Antagomir molecules are comparable to antimir regarding nucleotide length but contain a cholesterol-group at the 3'-prime end which increases their lipophilicity and subsequently their cellular membrane passage [11]. After i.v. injection of antagomir, both with or without cMB, these molecules could mostly be found in the smaller capillaries of the muscle. The local application of US, both at 2 MHz and 7 MHz with a high MI causing MB destruction, significantly increased local delivery of antagomir to the capillaries when antagomir was bound to cMB prior to i.v. injection. US-treatment in the presence of cMB and antagomir also caused extravasation of fluid into the muscle containing antagomir, further increasing the local delivery of antagomir. Since antagomir can cross cell membranes if given the time, as is also shown in our *in vitro* overnight antagomir-214 incubation, we expect the antagomir from the extracellular space to diffuse into the mycoytes and endothelial cells to knockdown its miR-target. When the antagomir delivery is compared to the antimir delivery, the local increase in capillary delivery is clearly in favor of the antagomir as is the delivery to the extracellular compartment. In addition to that, antagomir are more readily taken up by cells, making the antagomir a more feasible molecule for local delivery using cMB and local US-treatment. Our *in vitro* results however show that antagomir-214 delivery using cMB+US did not specifically knock-down miR-214 as the mismatch control antagomir showed a similar knockdown. However, antagomir that is deposited *in vivo* will remain there for a longer period of time and since our *in vitro* results clearly show that overnight incubation with antagomir-214 results in significant knock-down of miR-214 we expect similar results *in vivo*.

In summary, the present study showed that US+cMB treatment *in vitro* could both transfect endothelial cells with antimir and antagomir molecules. The antimir molecule however was successful in specifically knocking down its target where the antagomir was unable to. Additionally, *in vivo* experiments showed that MB+US treatment increased the local presence of delivered miR mimics 2.8-

fold only when a US-protocol was used that destroyed cMB. Furthermore, US+cMB treatment increased the local delivery of antagomir, but not of antimir, to the blood vessels both at 2 MHz and 7 MHz. Additionally, the treatment caused extravasation of fluid into the muscle containing antimir and antagomir, and this effect was more pronounced for antagomir. The combination of higher delivery of antagomir to both the capillaries and extracellular space and their increased capability to further enter cells through diffusion make the antagomir are more suitable molecule for local delivery with cMB and US compared to the antimir.

Ultimately we have shown that US-protocols that work best *in vitro* do not necessarily work for localized delivery *in vivo*. Additionally we've shown that successful molecules for miR-knockdown *in vitro* may not be the most suitable for *in vivo* use. The sonoporation mechanism which is used and studied *in vitro* is most probably not the driving mechanism behind the promising results which have been obtained *in vivo* local siRNA delivery over the past years.

Tables and figures

Table 1 Ultrasound treatment protocols for *in vitro* transfection of HUVEC monolayers.

Protocol:	*Frequency:*	*PnP:*	*Pulse duration:*	*PRF:*	*Treatment duration:*
Short pulse	1 MHz	100 kPa	20 cycles	1000 Hz	60 seconds
Long pulse	1 MHz	100 kPa	2000 cycles	10 Hz	60 seconds
Low pressure	1 MHz	50 kPa	2000 cycles	10 Hz	60 seconds
In vitro 2	1 MHz	200 kPa	2000 cycles	20 Hz	30 seconds

Exact parameters for the different ultrasound treatment protocols for the *in vitro* treatment of HUVEC monolayers. PnP: peak-negative-pressure, PRF: pulse repetition frequency.

**Table 2 Ultrasound treatment protocols for *in vivo* delivery of miR mimics, antimir and antagomir**.

Protocol:	I.v. injection:	US-machine:	Freq:	MI:	Pulsing:	Treatment duration:
High intensity 7 MHz only	miR mimic or antimir or antagomir only	Siemens Sequoia C512	14 MHz	0.22-1.8	Imaging in cadence mode at MI=0.22 with 1 second MB destruction (MI=1.8) every 10 seconds.	15 minutes
Low intensity US	miR mimic + MB	AWG+V303-SU	1 MHz	0.2	Intermittently 10 seconds US on/off. PRF: 10 Hz, pulse duration: 2000 cycles.	15 minutes
High intensity 7 MHz	miR mimic or antimir or antagomir + MB	Siemens Sequoia C512	7 MHz	0.22-1.8	Imaging in cadence mode at MI=0.22 with 1 second MB destruction (MI=1.8) every 10 seconds.	15 minutes
High intensity 2 MHz only	antimir or antagomir only	Siemens Sequoia C512	2 MHz	0.2-1.4	Imaging in cadence mode at MI=0.20 with 1 second MB destruction (MI=1.4) every 10 seconds.	15 minutes
High intensity 2 MHz	antimir or antagomir + MB	Siemens Sequoia C512	2 MHz	0.2-1.4	Imaging in cadence mode at MI=0.20 with 1 second MB destruction (MI=1.4) every 10 seconds.	15 minutes

Treatment parameters for *in vivo* MB+US treatment of mice for local delivery of miR mimics, antimir and antagomir. AWG: arbitrary waveform generator, V303-SU: V303-SU unfocused single element ultrasound transducer, MI: mechanical index, PRF: pulse repetition frequency, Freq: frequency of US wave.

Table 3 Comparison of *in vitro* transfection protocols and *in vivo* delivery protocols

	In vitro 1	*In vitro 2*	*In vivo qPCR*	*In vivo fluorescence*
Type of MB	Cationic MB	Cationic MB	Cationic MB	Cationic MB
Type of molecule	antimir-cy3 (single-stranded)	Antimir-cy3 and antagomir-cy3	miR mimic (double-stranded)	Antimir-cy3 and antagomir-cy3
US parameters	Frequency: 1 MHz MI: 0.1 Pulse length: 20 or 2000 cycles PRF: 10 Hz	Frequency: 1 MHz MI: 0.2 Pulse length: 2000 cycles PRF: 20 Hz	Frequency: 1 or 7 MHz MI: 0.2 (1 MHz) or 1.8 (7 MHz)	Frequency: 2 or 7 MHz MI: 1.4 (2 MHz) or 1.8 (7 MHz)
MB concentration	$27*10^6$ MB/ml	$15*10^6$ MB/ml	$\sim100*10^6$ MB/ml	$\sim100*10^6$ MB/ml
(anti)miR concentration	213 pmol antimir/ml	190 pmol/ml	~500 pmol/ /ml	~1 nmol/ /ml
(anti)miR/$100*10^6$ MB	830 pmol	1270 pmol	500 pmol	1000 pmol
Medium	Culture medium (20% serum)	Culture medium w/o serum	Blood	Blood

In vitro and *in vivo* treatment protocols were different with regards to type of delivered miR-therapeutic, US protocol and concentrations.
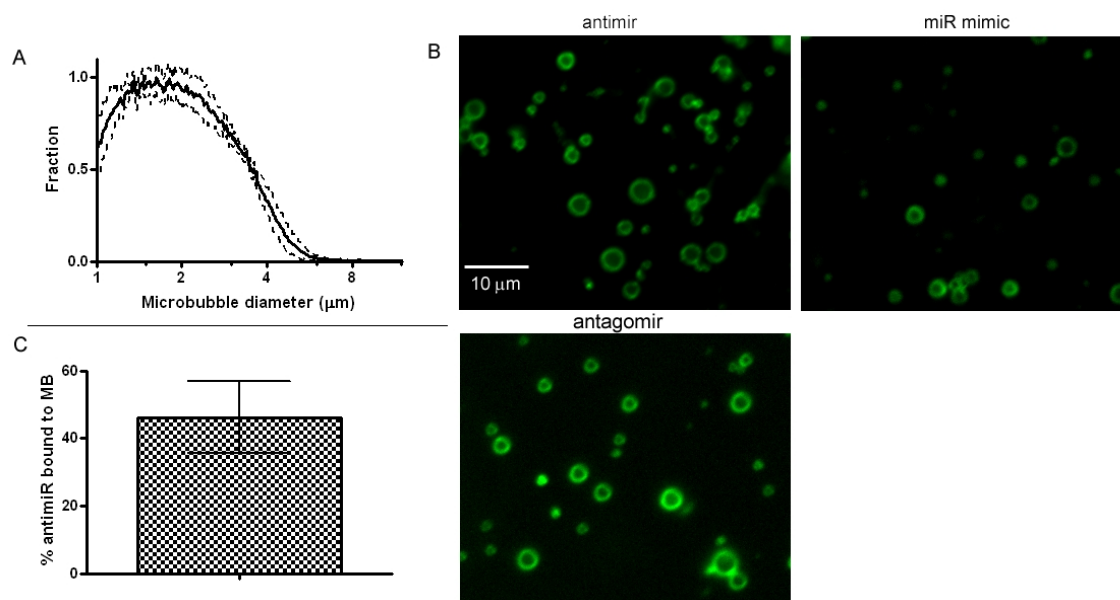
Figure 1 Cationic microbubbles. A) Size distribution of cationic microbubble populations after washing on as measured by a Multisizer 3^{TM} on a 2-log x-axis. Y-axis displays the abundance of fractions of MB normalized for the most abundant fraction. Dotted line represents +/- SD for 4 independent measurements. B) FITC-labeled antimir, miR mimic and antagomir binding to cMB. C) Quantification of the percentage of antimir which is attachment to cMB.
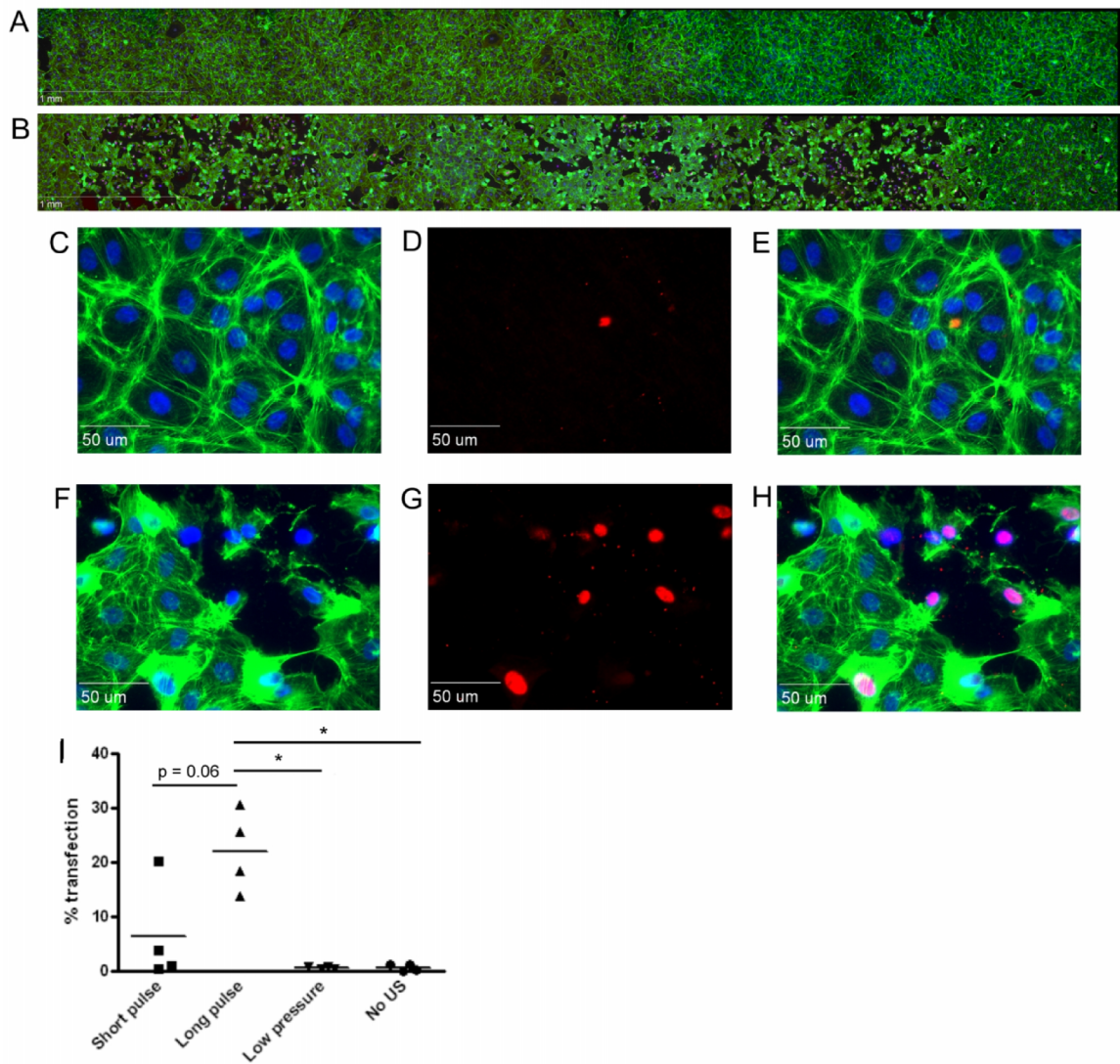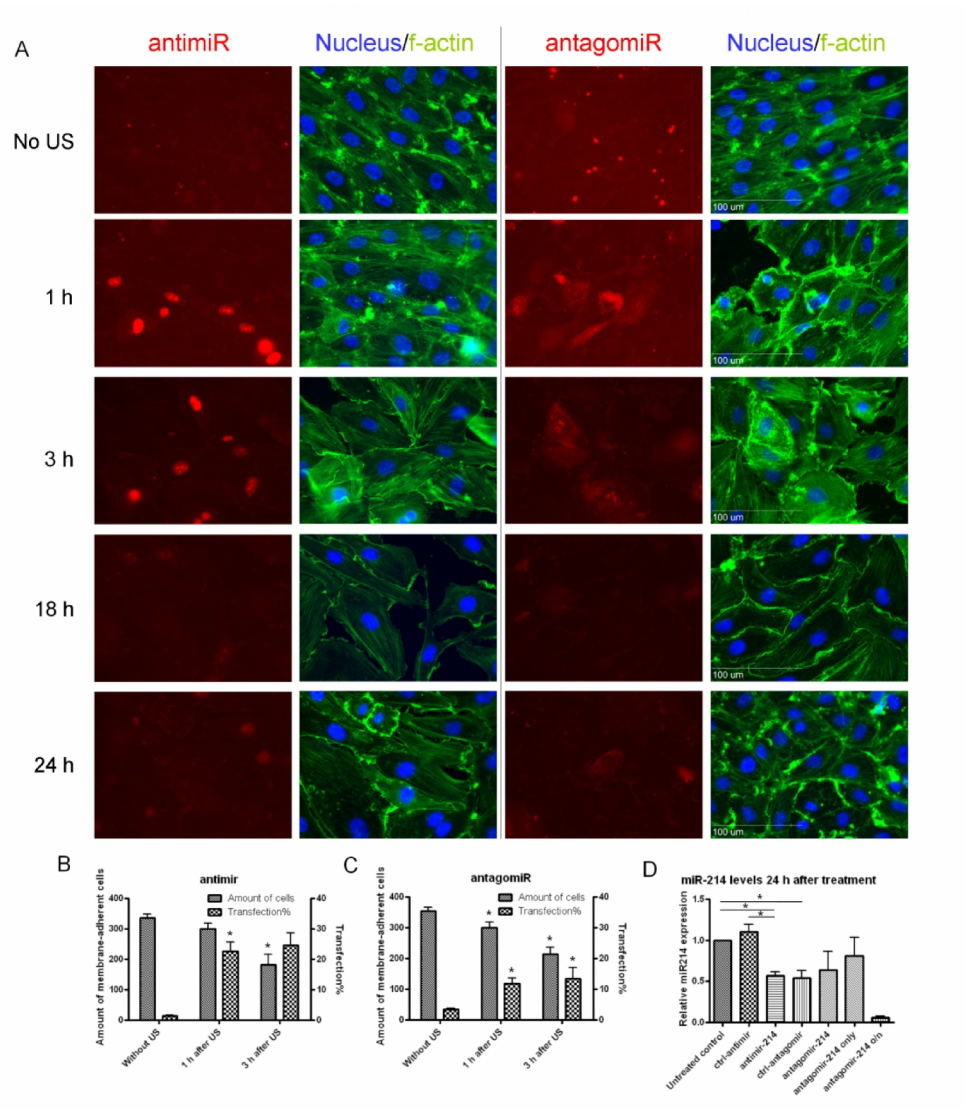
Figure 2 **Transfection of HUVEC *in vitro* system 1.** A) Montage image of MB+antimir (no US) treated HUVEC monolayer, B) Montage image of US+MB+antimir treated HUVEC monolayer. C, D, E) Detail images of a non-transfected US+MB+antimir treated HUVEC area with DAPI and FITC channels (C), Cy3 channel (D) or all three channels (E). F, G, H) Detail images of a transfected US+MB+antimir treated HUVEC area with DAPI and FITC channels (F), Cy3 channel (G) or all three channels (H). I) Quantification of transfection% as a result of different US-protocols. (* $p<0.05$) n=4

Figure 3 **Transfection of HUVEC *in vitro* system 2.** A) Fluorescence microscopy images of antimir and antagomir transfection in HUVECs without US-treatment and 1h, 3h, 18h and 24h after US-treatment. B) Quantification of fluorescence images regarding number of membrane-adherent cells and antimir transfection% per 10x magnification window. (* $p<0.05$ compared to Without US groups) C) Quantification of fluorescence images regarding number of membrane-adherent cells and antagomir transfection% per 10x magnification window. (* $p<0.05$ compared to Without US groups) D) Quantifcation of miR-214 expression in HUVECs 48 h after treatment with US, cMB and antimir/antagomir. Relative expression of miR-214 was normalized for untreated control cells. N=3 for fluorescence microscopy experiments and n=4 for miR-214 expression experiments. (* $p<0.05$)
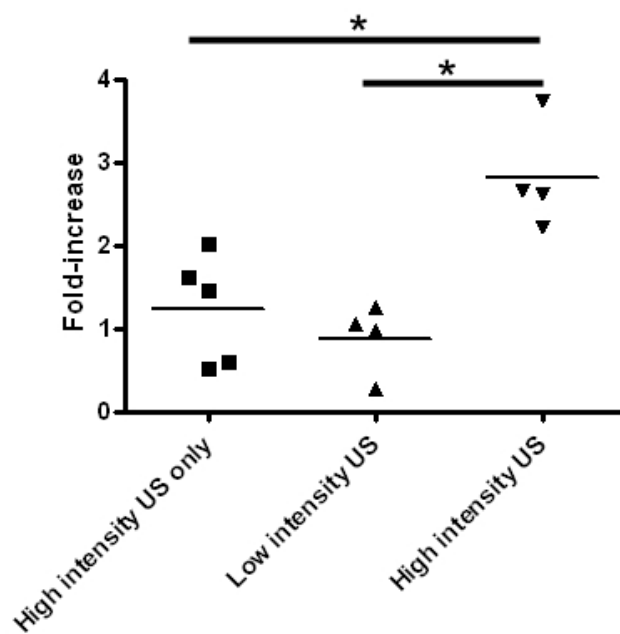
Figure 4 *In vivo* **US+MB induced local delivery of miR mimics.** For each mouse individually, the fold-increase of miR mimic content in the treated hind limb compared to the non-treated hind limb was determined and plotted. Each data point represents the fold-increase for one mouse. (*p<0.05)
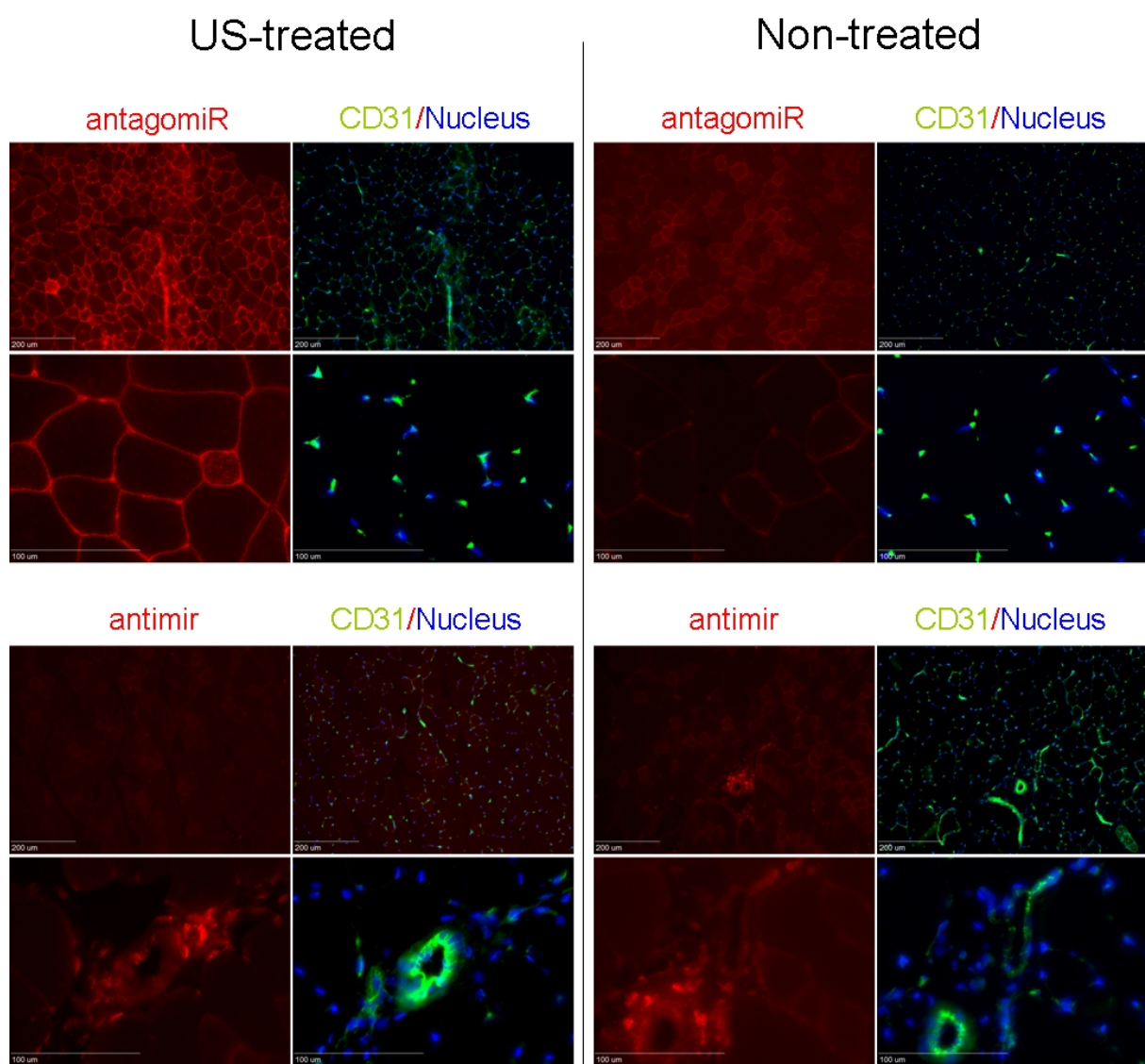
Figure 5 *In vivo* **US+MB induced local delivery of antimir and antagomir at 7 MHz.** Fluorescence microscopy images of cryosections of treated muscles of mice. Images are representative images for several experimental mice per group (antimir n=3, antagomir n=6).
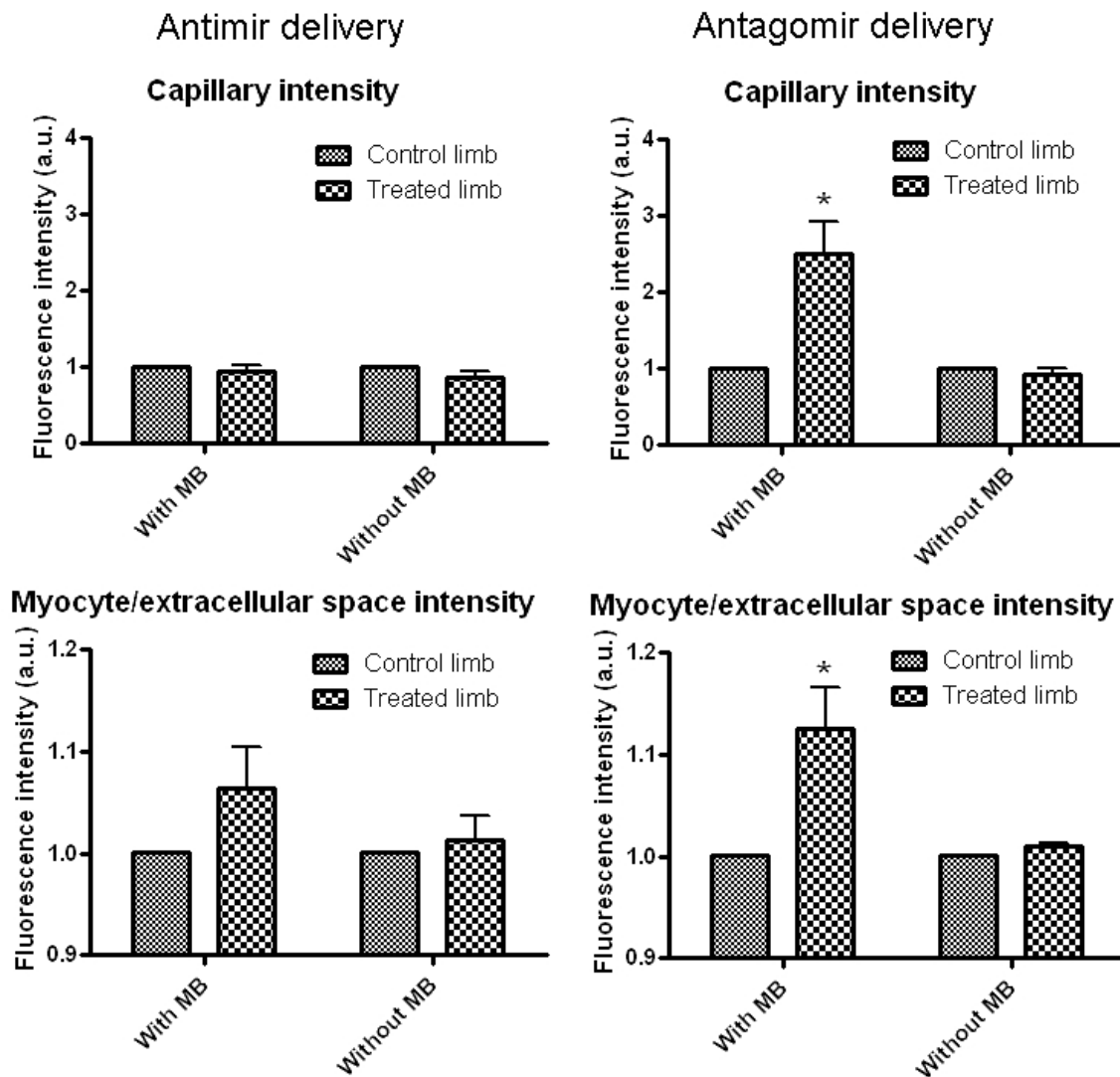
Figure 6 14 MHz antimir-antagomir delivery

Figure 6 **Quantification of antimir delivery to capillaries and myocytes/extracellular space in muscles treated with US at 7 MHz.** Quantification of antimir and antagomir signal intensity from fluorescence images. Capillary intensities and myocyte/extracellular space intensities were measured for each individual mouse and normalized for the intensity of the non-treated control hind-limb. (*p<0.05 compared to the non-treated control hind-limb.)
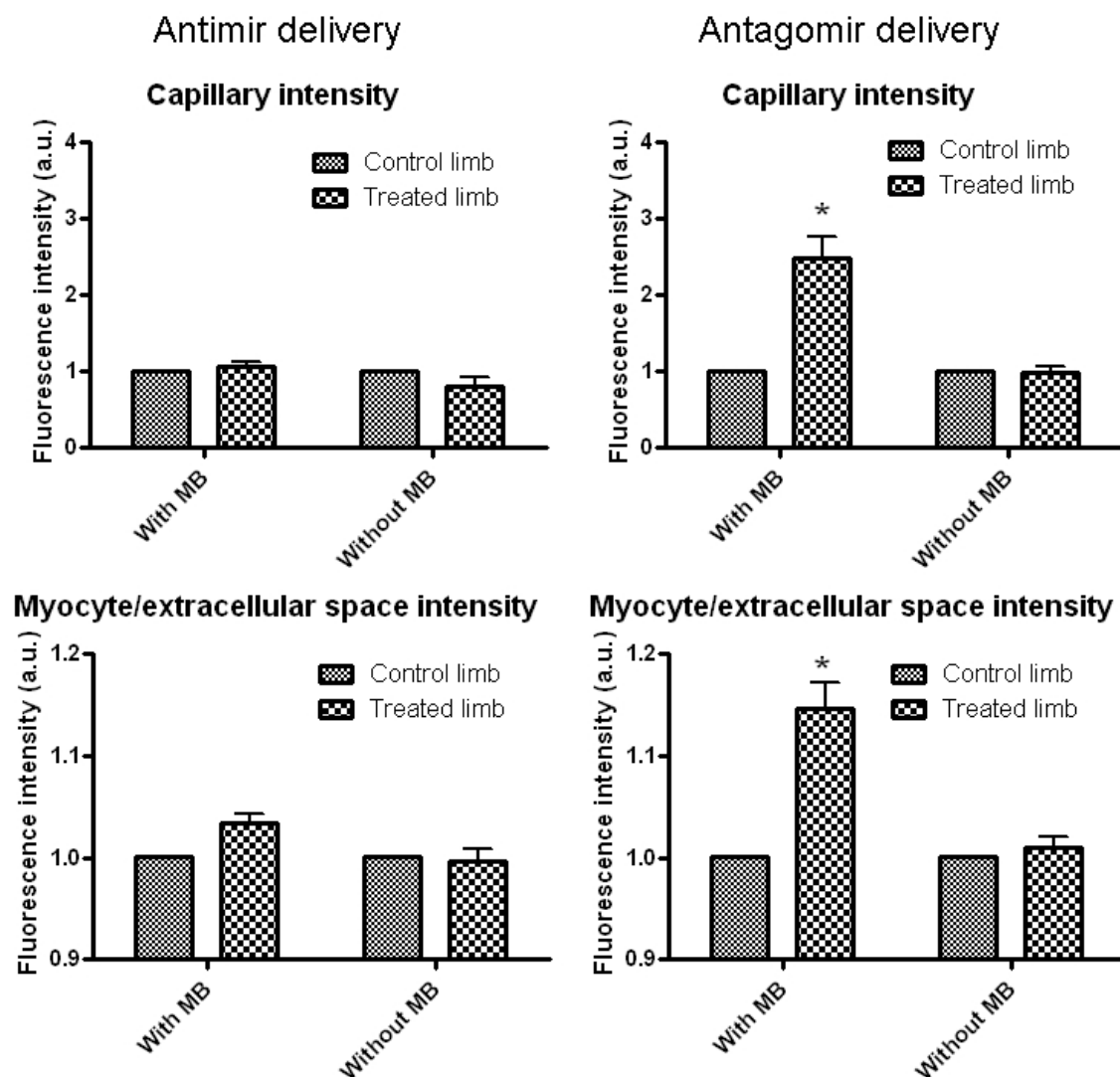
Figure 7 2 MHz antimir-antagomir delivery

Figure 7 **Quantification of antimir delivery to capillaries and myocytes/extracellular space in muscles treated with US at 2 MHz.** Quantification of antimir and antagomir signal intensity from fluorescence images. Capillary intensities and myocyte/extracellular space intensities were measured for each individual mouse and normalized for the intensity of the non-treated control hind-limb. (*$p < 0.05$ compared to the non-treated control hind-limb.)
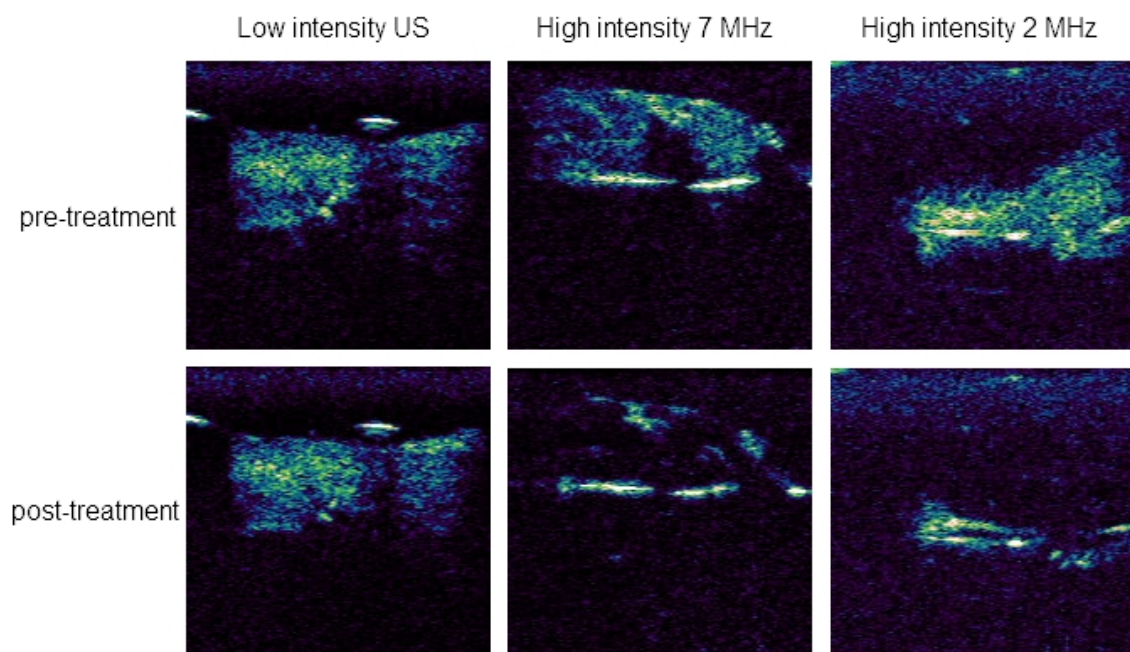
Figure 8 **Effect of *in vivo* US treatment protocols on MB integrity.** Cadence images of MB in the hind-limbs of mice pre- and after US-treatment with different US-protocols used throughout this study.

References

1. Lagos-Quintana, M., et al., *Identification of novel genes coding for small expressed RNAs.* Science, 2001. **294**(5543): p. 853-8.
2. Lau, N.C., et al., *An abundant class of tiny RNAs with probable regulatory roles in Caenorhabditis elegans.* Science, 2001. **294**(5543): p. 858-62.
3. Lee, R.C., R.L. Feinbaum, and V. Ambros, *The C. elegans heterochronic gene lin-4 encodes small RNAs with antisense complementarity to lin-14.* Cell, 1993. **75**(5): p. 843-54.
4. Pasquinelli, A.E., et al., *Conservation of the sequence and temporal expression of let-7 heterochronic regulatory RNA.* Nature, 2000. **408**(6808): p. 86-9.
5. van Mil, A., P.A. Doevendans, and J.P. Sluijter, *The potential of modulating small RNA activity in vivo.* Mini Rev Med Chem, 2009. **9**(2): p. 235-48.
6. Esquela-Kerscher, A. and F.J. Slack, *Oncomirs - microRNAs with a role in cancer.* Nat Rev Cancer, 2006. **6**(4): p. 259-69.
7. Sluijter, J.P., *microRNAs in cardiovascular regenerative medicine; directing tissue repair and cellular differentiation.* ISRN Vascular Medicine, 2013. **2013**: p. Article ID 593517.
8. van Rooij, E., W.S. Marshall, and E.N. Olson, *Toward microRNA-based therapeutics for heart disease: the sense in antisense.* Circ Res, 2008. **103**(9): p. 919-28.
9. Fasanaro, P., et al., *microRNA: emerging therapeutic targets in acute ischemic diseases.* Pharmacol Ther, 2010. **125**(1): p. 92-104.
10. Calin, G.A., et al., *Frequent deletions and down-regulation of micro- RNA genes miR15 and miR16 at 13q14 in chronic lymphocytic leukemia.* Proc Natl Acad Sci U S A, 2002. **99**(24): p. 15524-9.
11. Krutzfeldt, J., et al., *Silencing of microRNAs in vivo with 'antagomirs'.* Nature, 2005. **438**(7068): p. 685-9.
12. van Rooij, E. and E.N. Olson, *MicroRNA therapeutics for cardiovascular disease: opportunities and obstacles.* Nat Rev Drug Discov, 2012. **11**(11): p. 860-72.
13. Kota, J., et al., *Therapeutic microRNA delivery suppresses tumorigenesis in a murine liver cancer model.* Cell, 2009. **137**(6): p. 1005-17.
14. Akinc, A., et al., *A combinatorial library of lipid-like materials for delivery of RNAi therapeutics.* Nat Biotechnol, 2008. **26**(5): p. 561-9.
15. Thum, T., *MicroRNA therapeutics in cardiovascular medicine.* EMBO Mol Med, 2012. **4**(1): p. 3-14.
16. Hernot, S. and A.L. Klibanov, *Microbubbles in ultrasound-triggered drug and gene delivery.* Adv Drug Deliv Rev, 2008. **60**(10): p. 1153-66.
17. Leong-Poi, H., et al., *Therapeutic arteriogenesis by ultrasound-mediated VEGF165 plasmid gene delivery to chronically ischemic skeletal muscle.* Circulation research, 2007. **101**(3): p. 295-303.
18. Christiansen, J.P., et al., *Targeted tissue transfection with ultrasound destruction of plasmid-bearing cationic microbubbles.* Ultrasound Med Biol, 2003. **29**(12): p. 1759-67.
19. Yang, D., et al., *Inhibition of hepatic fibrosis with artificial microRNA using ultrasound and cationic liposome-bearing microbubbles.* Gene Ther, 2013. **20**(12): p. 1140-8.
20. Haag, P., et al., *Microbubble-enhanced ultrasound to deliver an antisense oligodeoxynucleotide targeting the human androgen receptor into prostate tumours.* J Steroid Biochem Mol Biol, 2006. **102**(1-5): p. 103-13.
21. Carson, A.R., et al., *Ultrasound-targeted microbubble destruction to deliver siRNA cancer therapy.* Cancer Res, 2012. **72**(23): p. 6191-9.
22. Chappell, J.C., et al., *Targeted delivery of nanoparticles bearing fibroblast growth factor-2 by ultrasonic microbubble destruction for therapeutic arteriogenesis.* Small, 2008. **4**(10): p. 1769-77.
23. Karshafian, R., et al., *Sonoporation by ultrasound-activated microbubble contrast agents: effect of acoustic exposure parameters on cell membrane permeability and cell viability.* Ultrasound Med Biol, 2009. **35**(5): p. 847-60.
24. Meijering, B.D., et al., *Ultrasound and microbubble-targeted delivery of macromolecules is regulated by induction of endocytosis and pore formation.* Circ Res, 2009. **104**(5): p. 679-87.

25. Juffermans, L.J., et al., *Ultrasound and microbubble-targeted delivery of small interfering RNA into primary endothelial cells is more effective than delivery of plasmid DNA.* Ultrasound Med Biol, 2014. **40**(3): p. 532-40.

26. Juffermans, L.J., et al., *Ultrasound and microbubble-induced intra- and intercellular bioeffects in primary endothelial cells.* Ultrasound Med Biol, 2009. **35**(11): p. 1917-27.

27. van Mil, A., et al., *MicroRNA-214 inhibits angiogenesis by targeting Quaking and reducing angiogenic growth factor release.* Cardiovasc Res, 2012. **93**(4): p. 655-65.

28. Otani, K., et al., *Nonviral delivery of siRNA into mesenchymal stem cells by a combination of ultrasound and microbubbles.* J Control Release, 2009. **133**(2): p. 146-53.

29. Tlaxca, J.L., et al., *Analysis of in vitro transfection by sonoporation using cationic and neutral microbubbles.* Ultrasound Med Biol, 2010. **36**(11): p. 1907-18.

30. Zhao, Y.Z., et al., *Comparing transfection efficiency and safety for antisense oligodeoxyribonucleotide between phospholipids-based microbubbles and liposomes.* J Drug Target, 2006. **14**(10): p. 687-93.

31. Hunt, M.A., et al., *Optimizing transfection of primary human umbilical vein endothelial cells using commercially available chemical transfection reagents.* J Biomol Tech, 2010. **21**(2): p. 66-72.

32. Suzuki, J., et al., *Ultrasound-microbubble-mediated intercellular adhesion molecule-1 small interfering ribonucleic acid transfection attenuates neointimal formation after arterial injury in mice.* J Am Coll Cardiol, 2010. **55**(9): p. 904-13.

33. Tsunoda, S., et al., *Sonoporation using microbubble BR14 promotes pDNA/siRNA transduction to murine heart.* Biochem Biophys Res Commun, 2005. **336**(1): p. 118-27.

34. Mukai, H., et al., *Pressure-mediated transfection of murine spleen and liver.* Hum Gene Ther, 2009. **20**(10): p. 1157-67.

35. Fronek, K. and B.W. Zweifach, *Microvascular pressure distribution in skeletal muscle and the effect of vasodilation.* Am J Physiol, 1975. **228**(3): p. 791-6.

Supplementary figure A:

hsa/mmu-miR-214:   acagcaggcacagacaggcagu

antimir-214:   FITC/cy3-5'-a*c*ugccugucugugccugc*u*g*u*-3'

mismatch control-antimir: FITC/cy3-5'-a*c*u**ccc**ug**ccu****uu**c**ccu****ua***u*g*u*-3'

antagomir-214:   FITC/cy3-5'-a*c*ugccugucugugccugc*u*g*u*-3'-CHOLESTEROL

mismatch control-antagomiR: FITC/cy3-5'-a*c*u**ccc**ug**ccu****uu**u**ccu****ua***u*g*u*-3'-CHOLESTEROL

Antimir-214 and antagomir-214 consists of the inverse complementary mature miR-214 sequence. The mismatch control antimir and antagomir contains 6 mismatches (underlined). Antagomirs are 3'cholesterolmodificated,

2'O-methylated, and contain PTO-linkages (*) at the first two and last four

nucleotides.

Supplementary table A

	7 MHz	2 MHz
Antimir only	N=3	N=3
Antimir + cMB	N=3	N=3
Antagomir only	N=6	N=6
Antagomir + cMB	N=6	N=6

Antimir and antagomir treatment groups for localized delivery using cMB and US. For antimir and antagomir delivery 8 different treatment groups were created. The table represents these groups and the amount of mice treated for each individual group.

Supplementary figure B
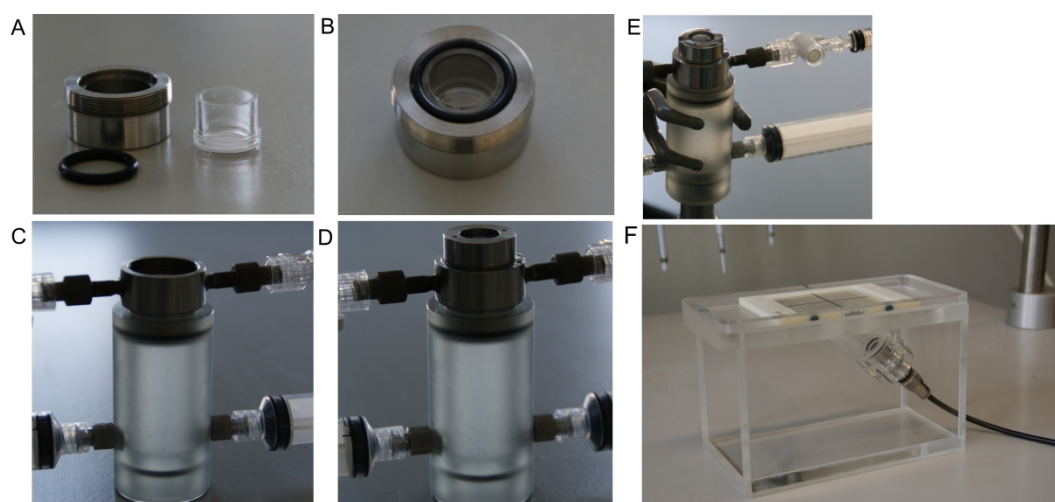
***In vitro* systems 1 and 2 for US+MB induced HUVEC transfection.** A custom designed metal ring was created for fitting 12 mm culture plate inserts (A). The culture plate insert was placed in the metal insert holder and sealed with a rubber ring (B). A plastic spacer with inlets for degassed H_2O to conduct ultrasound was attached to the bottom part of the UTC metal casing with in- and outlets to insert treatment medium. The metal ring and plastic spacer were separated by a membrane cut out of an Opticell[®] (Thermo Scientific, MA, USA) (C). The two metal rings were connected placing the membrane of the insert on top of the system (D). For ultrasound treatment the V303-SU ultrasound transducer was inserted in the plastic spacer at the bottom after which the plastic spacer was filled with degassed H_2O. Phosphate buffered saline (PBS) was added on top of the culture plate insert and a syringe was attached to the metal casing inlet to inject treatment medium (E). *In vitro* system 2 applied ultrasound at a 45°. Cells were cultured in an Opticell culture system which contains two membranes on one of which HUVECs were grown. The Opticell was placed in the system with the HUVEC attached side up (F).

Supplementary figure C
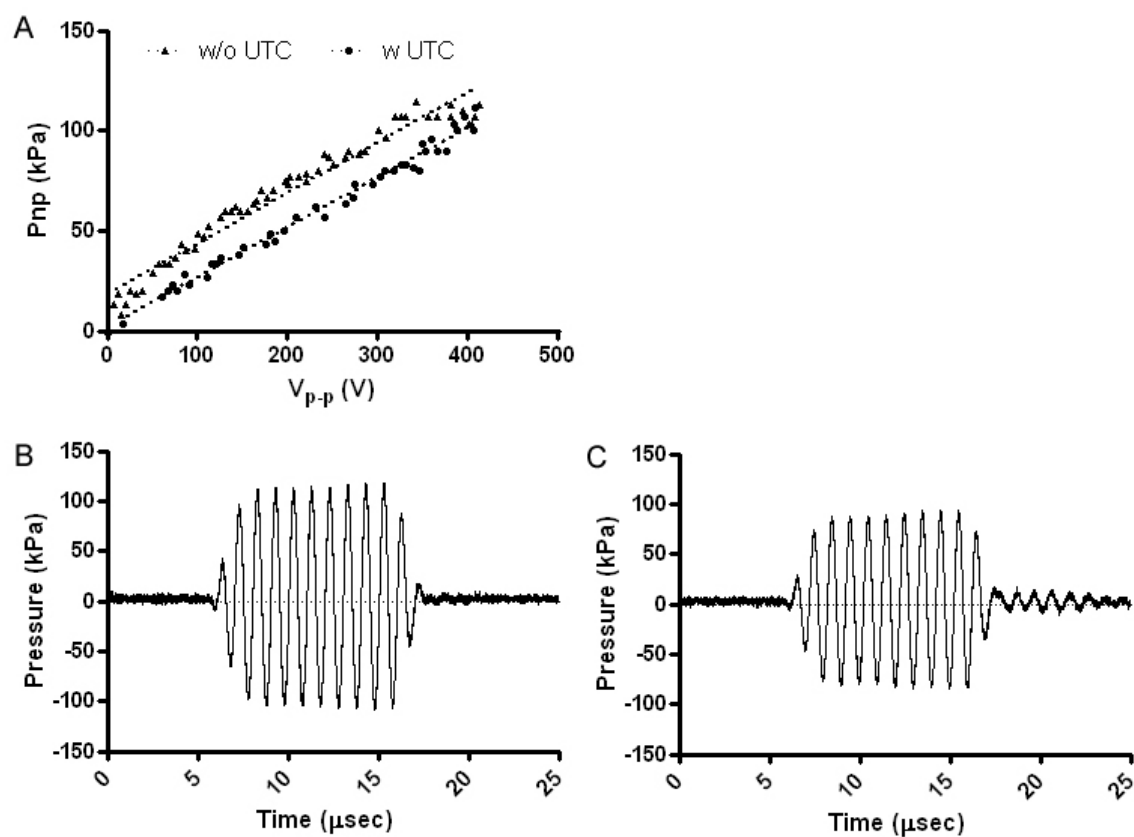
The effect of the UTC on the ultrasound wave from a V303-SU. A) Calibration curves of the V303-SU transducer both without (w/o) and with (w) UTC. B) Shape of a 10 cycle ultrasound pulse from the V303-SU. C) Shape of a 10 cycle ultrasound pulse after placing the UTC in between transducer and hydrophone.

Supplementary figure D
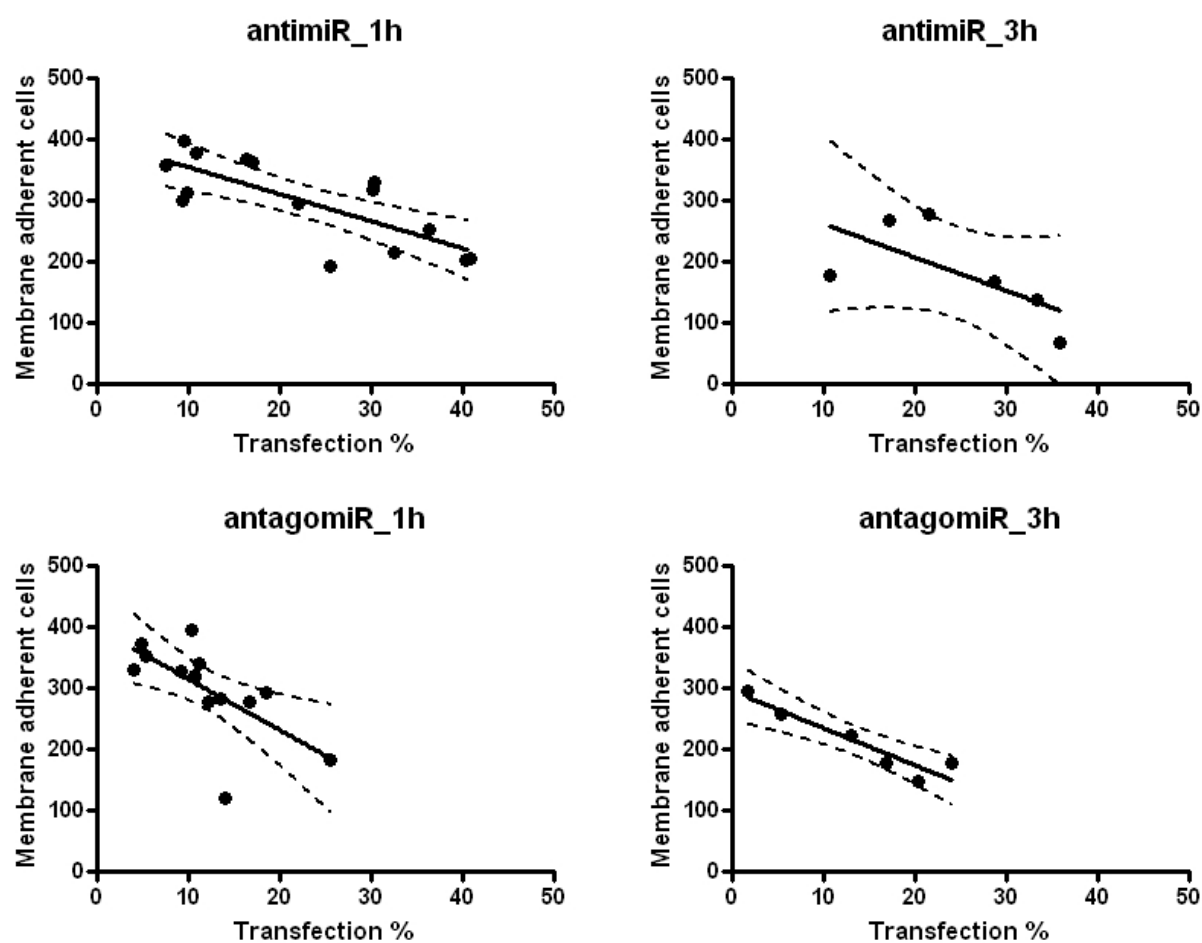
Correlation of antimir/antagomir transfection and membrane adherent cell numbers in *in vitro* system 2. Analysis of 10x magnification windows regarding transfection% and amount of membrane adherent cells were plotted with transfection% on the x-axis and membrane adherent cells on the y-axis to visualize the relation between the two.

Supplementary figure E
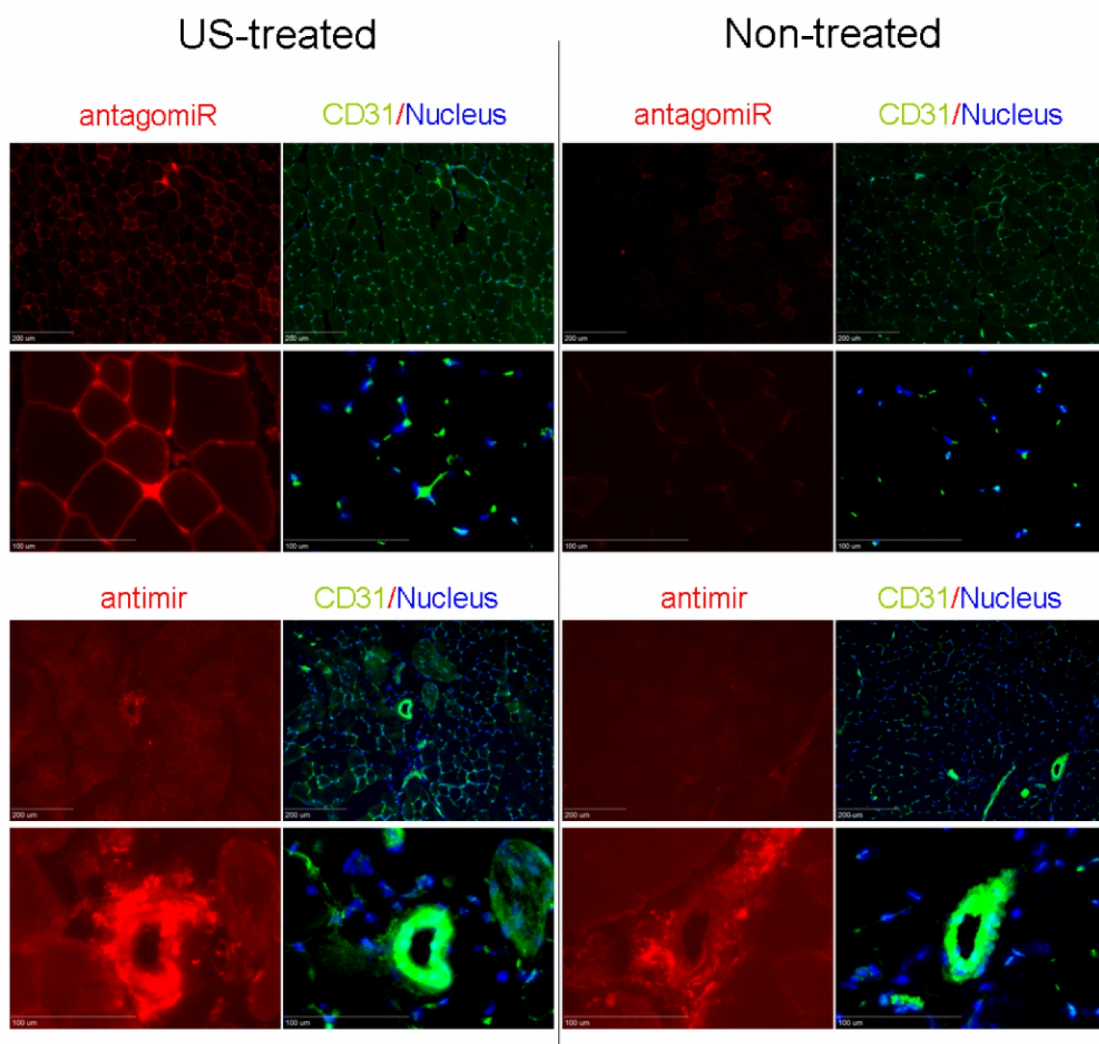
In vivo **US+MB induced local delivery of antimir and antagomir at 2 MHz.** Fluorescence microscopy images of cryosections of treated muscles of mice. Images are representative images for several experimental mice per group (antimir n=3, antagomir n=6).

Chapter 10 General discussion and future perspectives

MicroRNAs (miRNAs) are small, non-coding RNA species, and play an inhibitory role either by inhibiting the translation of or degrading its targeted mRNAs. In normal conditions, miRNAs may function as a filter to reduce the fluctuation of gene expression noise and thereby "fine tune" cellular responses in response to environmental stimuli. Under pathological or stress conditions, however, their regulatory roles become more pronounced [1]. Using various *in vivo* models, a lot of studies have provided insights on the actions of miRNAs in different processes in cardiovascular diseases. These studies have revealed important roles for miR-195, 208a, 133, 132, 25, 23a, 199b, and 499 in cardiac hypertrophy [2-8], for miR-29, 133a, and 30 in cardiac fibrosis[9-11], for miR-499, 24, and 15b in cardiomyocyte survival [12-14], for miR-126, 92a, 210, and 24 in cardiac angiogenesis [15-18], for miR-143 and 145 in vessel remodeling [19, 20], and for miR-208a in cardiac metabolic control [21]. The essential roles of miRNA in cardiovascular diseases and the relative ease of either decreasing or increasing individual miRNA levels *in vivo* make miRNA-based therapeutics one of the most promising therapeutic strategies in the coming years.

The main goal of this thesis was to define new roles of miRNAs involved in diseases progression and to explore the feasibility of using miRNA therapeutics to treat cardiovascular diseases in the clinic. However, before miRNA-based therapeutics may enter the clinical arena safely, several issues are needed to be addressed to achieve optimal therapeutic effects and to minimize potential side effects. Firstly, a better understanding of the role of miRNAs in the complex cardiovascular system is required: where is the miRNA expressed, how is it regulated and what are its targets (part I and part II). Secondly, a safe and efficient miRNA therapeutic *in vivo* delivery strategy is investigated (part III).

Part 1. Developing new techniques to understand miRNA biology

In situ detection of miRNA by in situ hybridization

Due to the fact that expression of miRNAs is tightly regulated and that its effect is relying on their local presence at the cellular level, defining the exact localization of the miRNA expression is essential not only for understanding its biology but also for choosing different therapeutic intervention strategies later on. For instance, to study a cardiac specific miRNA such as miR-1, it is will be reasonable to investigate its function in the cardiomyocyte instead of in neural cells. For a widely expressed miRNA, a systematic strategy may be used to manipulate its expression. However, to effectively manipulate a brain specific expressed miRNA such as miR-124 [22-24], using a strategy which will be able to penetrate the blood brain barrier or even a direct application to the brain is crucial.

In general, in situ hybridization is the most used technique to detect the expression of microRNAs at the cellular and subcellular level, even though the abundance of one particular microRNA can be easily measured by qPCR or Northern Blot. The concept of miRNA *in situ* is similar to the traditional mRNA *in situ* hybridizations: a pre-labeled nucleic acid sequence, so called probe, which is complementary to the selected miRNA is used to visualize the localization of the specific miRNA. As a result, a multicolor image can be created by combining high sensitive *in situ* hybridization with immunofluorescent staining, with this protocol, we have performed *in situ* hybridization for miR-132 (chapter 2,4,5 and 6), miR-155 (chapter 2), and miR-222 (chapter 2) on various tissues including both human and mice. It provides us in-depth information about their expression locations. For example, we found that miR-132 is mildly expressed in cardiomyocytes in healthy heart, but is significantly upregulated mainly in cardiomyocytes of diseased hearts. This insight prompt us to focus on the function of this miRNA in cardiomyocytes (in chapter 6 and 7) instead of angiogensis [25, 26], fibrosis [27] or inflammation [28-30] which has been assigned to this miR-132/212 family in other organs or disease conditions.

miRNA targets identification

Although identifying the targets of the miRNA is vital to understand its function, however, it is very challenging. Bioinformatics-based target prediction and experimental validation of these targets is very laborious and time-consuming. To better define the biological targets of these miRNAs, we tried to develop a miRNA-free Simple-cell system for target identification and individual miRNA functional study in cardiovascular cells, as illustrated in Figure 1. The rational of the Simple-cell is that cells which lack the essential genes for miRNA biogenesis, such as Dgcr8 which is responsible for pri-microRNA processing into precursor miRNAs in the nuclei, will result in a general loss of mature miRNAs populations. If we reintroduce one miRNA of interest into this Simple-cell, we can study the function of that single miRNA specifically and identify the targets of this miRNA by isolating and sequencing mRNAs which are bound by the miRNA.

Our data suggests that the development of a Simple-cell for cardiac miRNA target identification is not successful due to the fact that Dgcr8 knockout ES cells are defective in differentiation into cardiovascular lineages [31].We show that Dgcr8 KO ESCs are lacking a large population of small RNAs, including but not limited to mature miRNAs. In addition to a defect in miRNA processing, Dgcr8 KO embryonic stem cells are unable to form proper heterochromatin, to inactivate genotoxic centromeric repetitive elements including major and minor satellite RNAs and Line1 [31]. Although this issue can be solved to use a conditional Dgcr8 knockout ES line, the upcoming new technologies make it less appealing. Some of these technologies are discussed below.

With the development of next generation sequencing technology, miRNA targets identification can be readily approached in an alternative way. For instance, recently several similar technologies such as

Hits-CLIP [32], iCLIP [33], PAR-CLIP [34, 35], and CLASH [36] were developed which generate tissue/cells specific miRNA targets landscapes at single nucleic acid resolution. The rationale behind these techniques is rather simple as shown in Figure 2 below: first cross link miRNA with their targets within the RISC complexes, isolate these RISC complex containing both miRNA and their targets, then recover both miRNA and their targeted mRNA by cloning and sequencing [32-35]. These techniques allow us to create genome wide miRNA targets landscape in an unbiased manner under the physiological condition. Applying these techniques in the cardiovascular field will promote mechanistic studies of cardiac miRNAs but also may allow us to determine how successful a miRNA mimics or anti-miR treatment is. Based on this information, eventfully it will be also possible to design next generation miRNA mimics through rational design to achieve optimal targets spectrum.

Part 2. miR-132/212 in cardiovascular diseases

miRNA-132/212, a stress inducible miRNA [28], is initiatively identified as one of the most abundant miRNAs in the brain, but its role goes beyond the brain. In the hippocampus neurons, miR-132 is highly expressed in the active neurons. Loss of miR-132 results in less spine density, shorter dendrite length [37-39], and impaired synapse activation which is supposed to be critical for learning and memory [40]. Interestingly, the expression of miR-132 goes up when animals are placed in a stressful environment such as in a Maze, exposure to a predator or acute foot shock. The upregulated miR-132 may facilitate learning and memory process and also suppress stress-induced cognate damage [41]. The mechanism behind the stress induced upregulation of miR-132 was not clear until recently: Four CREB(cAMP-response element binding) sites were identified within the miR-132/212 genomic loci [42] indicating that stress hormones or growth factors such as Ca^{2+}, cAMP, TGF , VEGF may induce CREB activation, which activates many downstream transcripts including miR-132/212 [43, 44]. In this thesis, we mainly focused on miR-132/212 under different stress condition within the cardiovascular system.

In our study, we found that miR-132/212, a pro-angiogenic miRNA, plays an important role in both physiological and pathological angiogenesis (see Figure 3 for illustration). In chapter 4, we confirmed that miR-132/212 is upregulated in the femoral artery-ligated legs. This transient upregulation of miR-132/212 inhibits Rasa1, Spred1 and Spry1 expression, which are intrinsic inhibitors of the Ras-MAPK signaling pathway. This results in prolonged Ras-MAPK activation, and eventually promoting arteriogenesis [45]. As a result, miR-132/212 KO mice show slower blood perfusion recovery after femoral artery ligation. Using a KDR-eGFP *zebra fish*, we found that overexpression of miR-132 or miR-212 promotes vascularization in the fish, suggesting that the pro-angiogenic role of miR-132/212 is conserved at least between mouse and fish. It is also suggested that miR-132/212 may be used as a therapeutics to enhance neovascularization in ischemic diseases[25].

Inhibition of miR-132/212 suppresses VHL loss-of-function induced pathological angiogenesis. Von Hippel-Lindau (*VHL*) [46, 47] is an E3 ubiquitin ligase involved in the degradation of hypoxia inducible- transcription factor (HIFα). Under normal oxygen tension, hydroxylated HIFα can be recognized by ubiquitin complex containing VHL and is rapidly degraded. Upon hypoxia or VHL loss-of-function, HIFα-subunits cannot be hydroxylated and degraded anymore. Stabilized HIFα activates the expression of a large suite of downstream target genes (*EPO*, *VEGF* etc) which are vital in angiogenesis. We found that miR-132/212 is also upregulated in this artificial-induced hypoxia, induced by a loss of function mutation in VHL. Blocking miRNA132/212 with antimiRs can significantly alleviate the excessive vascular branching phenotype in *vhl*$^{-/-}$ mutant *zebrafish*. Moreover, using endothelial cells and pericytes in a coculture system, *VHL* knockdown in HUVECs promotes endothelial cells neovascularization capacity, which can be inhibited by antimiR-132/212 treatment. These results demonstrate an important role for miRNA132/212 in VHL loss-of-function induced pathological angiogenesis and suggest an interesting opportunity for pharmaceutical intervention using an inhibitor of miR-132/212 to inhibit blood vessel outgrowth in malignant tumors.

Next to involvement in angiogenesis, we discovered that miR-132/212 has a role in regulating cardiac contraction. In a normal cardiomyocyte contraction-relaxation cycle, the cardiac action potential triggers the opening of L-type calcium channels. It results in a small increase of calcium via the L type Ca^{2+} channel which eventually stimulating a bulk release of calcium from the sarcoplasmic reticulum (SR) into the cytosol via the Ryr2 [48]. This elevated cytosolic calcium initiates the contractile machinery of the microfilaments. After contraction, cytosolic calcium has to be removed to prepare for the next contraction. In mammalian cells, cytosolic calcium reuptake by the SR is mainly regulated via the sarcoplasmic-endoplasmic reticulum Ca^{2+} ATPase 2 (SERCA2) [49]. In the failing heart, however, very often an impaired uptake of Ca^{2+} occurs which mainly result from a decreased expression or reduced SERCA2a activity [50, 51]. Significant efforts have been made to rescue cardiac contractile function through restoration of the expression of SERCA2 directly [52-54] or through indirect enhancement of its activity [55], however, the clinical results thus far were very disappointing.

Given the fact that miRNAs play an inhibitory role at gene expression and that upregulation of miRNAs have been reported in the failing heart, it is possible that these upregulated miRNAs influence Ca-metabolism via targeting of SERCA2. A genome-wide screen for miRNAs, showed that miR-132/212 inhibits a SERCA2-3'UTR reporter vector and also prolongs calcium decay in a mouse cardiomyocyte HL-1 cell line [56]. We and others have observed upregulation of miR-132/212 in both human heart failure patients and heart failure mouse models [57, 58]. With miRNA *in situ* hybridization, we further defined that miR-132 upregulation is mainly localized in cardiomyocytes. Through manipulation of miR-132/212 *in vitro* and *in vivo* we confirmed SERCA2a and PTEN as a direct target of miR-132/212, hereby modulating cardiac contractility (see Figure 3 for illustration).

Furthermore, similar results are also observed in human heart failure patients showing upregulation of miR-132/212 and the subsequent downregulation of their targets SERCA2 and PTEN in these hearts.

Psychosocial stress in some extreme cases, such as depression has been identified as one of the risk factors for heart failure by epidemiological studies [59]. Experimental studies show that animals under chronic stress display compromised cardiac functions [60, 61]. Given the fact that miR-132/212 play a role both in neural system and cardiovascular system, both of which can be linked by stress, it is interesting to look into the possible role of this miRNA in this association in the future.

Part 3. Developing novel targeted delivery technologies

Our study on miR-132/212 revealed some common features of miRNA biologymiR-132/212 regulates different biological process, (Figure 3), as transient stimulation of miR-132/212 in the vessels promoted angiogenesis while in the heart it impaired cardiac contractility. Therefore, appropriate delivery of these miRNAs as therapeutic agents is not only vital but quite demanding to avoid any potential side-effects. Next to avoiding side-effect, other reasons to focus on targeted delivery of miRNAs are related to reducing costs by minimizing the therapeutically effective dosage. For this, there is a persistent need for methods to increase miRNA therapeutic delivery, prevent off-target uptake, and increase tissue-specific uptake [62].

Recent developments in drug delivery vehicles for siRNA have resulted in proper protection of siRNA in the blood, successful exit from the circulation, and intracellular delivery of siRNA. Important lessons can be learned from these siRNA delivery methods. Several strategies to improve cardiac uptake and targeting of delivery vehicles are being developed and encouraging results are being obtained with antibodies, cardiac targeting peptides, and pH sensitive targeting peptides. These results, however, still need to be translated to delivery vehicles for miRNA therapeutics [62].

Nanoploymers

By an intensive and multi-disciplinary approach we designed, and tested, different nanopolymers for the delivery of miRNA mimics or anti-miRs. After extensive characterization of these nanopolymers, we show that different amino groups of these nanopolymers affect the binding and complex formation capacity with anti-miR or pre-miR binding *in vitro*. One of the nanopolymers, NB-182-2 can form stable complexes with both pre- and anti-miRs and is taken-up by cells efficiently without showing any cellular toxicity. However, NB-183-2 pre- or antimiR complexes cannot escape from endolysosomal compartments into the cytosol to become functional. Although we still need to test, we reasoned that the affinity between polymer and antimiRs are too strong for anti-miR release from the complexes or due to the stable structural properties that cannot break in the endolysosomal membrane.

Given the reducing potential within the endolysosomal compartment, introducing some disulfide bonds in the backbone of the polymer will facilitate miRNA therapeutic release from the polymer and eventually escape from the endolysosomal compartment [63].

Ultrasound guided microbubbles

Next to the chemical strategy, we developed a mechanical strategy that includes ultrasound-guided microbubbles [64]. Microbubbles are gas-filled spheres with a micrometer diameter (typically 1-10 μm) and are used as contrast agent in ultrasonography. These gas-filled spheres can be loaded with several types of molecules with therapeutic potential, like plasmid DNA [65-67], oligodeoxynucleotides [68], siRNA [69] and growth factors [70]. After intravenous injection of these 'loaded' microbubbles, ultrasound can be applied locally, causing the microbubbles in the ultrasonic field to cavitate. Cavitation of microbubbles causes them to lose their payload and permeabilizes the vasculature, leading to an increased localized release and uptake of therapeutics at the site of treatment.

By keeping negatively charged nucleic acid in mind, we generated cationic ultrasound-responsive microbubbles and studied them for their ability to deliver miRNA inhibitors and mimics *in vitro* and *in vivo*. Cationic microbubbles successfully delivered miRNA inhibitors, including antimiRs and antagomiRs, into the intracellular compartments of primary isolated human endothelial cells *in vitro*. AntagomiRs are comparable to antimiRs regarding nucleotide length but contain a cholesterol-group at the 3'-prime end which increases their lipophilicity and subsequently their cellular membrane passage. AntimiRs and antagomiRs molecules were bound to cationic microbubbles and locally delivered using ultrasound protocols causing inertial cavitation at 7 MHz and 2 MHz. AntimiR delivery was only slightly increased to the extracellular compartments of the muscle whereas antagomiRs delivery was both significantly increased to the capillaries, myocytes and extracellular space. These properties render antagomiRs more suitable to be used in combination with microbubbles and ultrasound for local delivery. An interesting concept would be to combine nanopolymers with ultrasound guided microbubbles for local targeted delivery of miRNA therapeutics to achieve maximal loading capacity and specificity at the same time.


Perspectives

Towards miRNA-based therapeutics for cardiovascular diseases

With more and more miRNAs being identified to be involved in different processes of cardiovascular diseases in preclinical discoveries influencing angiogenesis, fibrosis, cardiomyocyte hypertrophy, cell death and many others, we foresee that miRNA therapeutics will take a great leap towards clinic testing. Along with the already ongoing clinical trials [71], the next areas that includes cardiovascular diseases will follow as well. The first generation of miRNA mimics adopted double stranded structure

trying to mimic miRNA precursors so that they can be loaded into RISC complex properly and function like endogenous miRNA. This design made them less flexible, less tolerant to chemical modifications than its counterpart inhibitors, and therefore more problematic for *in vivo* application. In the future, the second generation miRNA mimics with single strand miRNA structural design such as agomiR will significantly push the application of miRNA mimics forward. Moreover, in order to target complicated diseases such as cardiovascular disease, the usage of cocktails to manipulate several miRNAs will be necessary. As an example, myocardial infarction involves numerous processes such as the stability of atherosclerosis plaque, cell death, inflammation, angiogenesis and fibrosis in which several miRNAs may play distinct roles in each of these processes. Thus, it will be very interesting to apply several different miRNA therapeutics for one disease either as a cocktail or in a sequential manner. Finally, the usage of miRNA therapeutics in combination with other established therapies, such as heart transplantation or stem cell therapy, will be available. For example, stem cell therapy has been widely tested in human clinical trial for various cardiovascular diseases showing limited beneficial result, whereas other studies show that miRNA play important roles in mobilization, differentiation and survival of transplanted stem cells. Thus, it is expected that combining the strength of miRNA therapeutics with other existing therapy or upcoming therapeutics such as stem cell therapy will be an interesting field to explore. In either of these applications, fundamental understanding of miRNA biology as well as its targeted delivery strategies will be key for the successful application of miRNA therapeutics in the clinic.
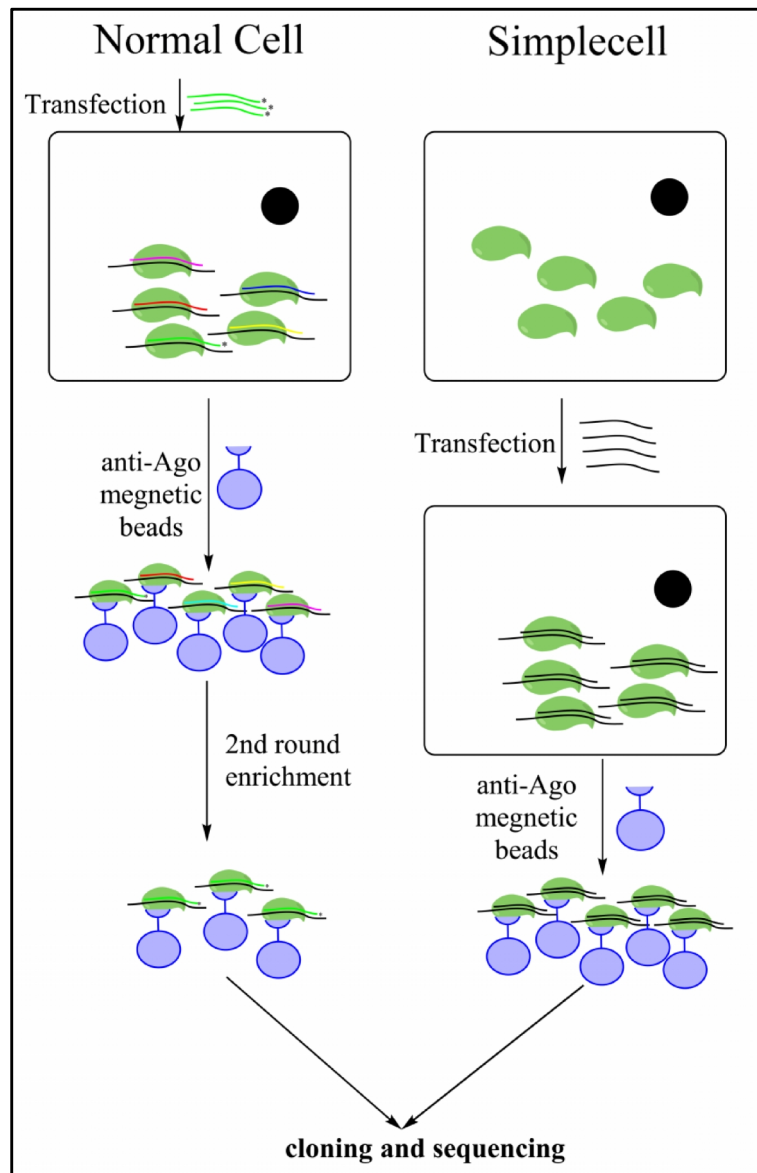
Figure 1. The concept of using Simple-cell for miRNA targets identification. In a normal cell, RISC complexes were isolated by immunoprecipitation which contains all the miRNAs and their targets. Then a second round selection based on the pre-labeled miRNA was used to enrich one particular miRNA. In the Dgcr8 KO Simplecell on the right, one miRNA of interested was introduced into the Simpecell. Then cells were lysized and RISC complex containing only the miRNA and its targets were cloned and sequenced.
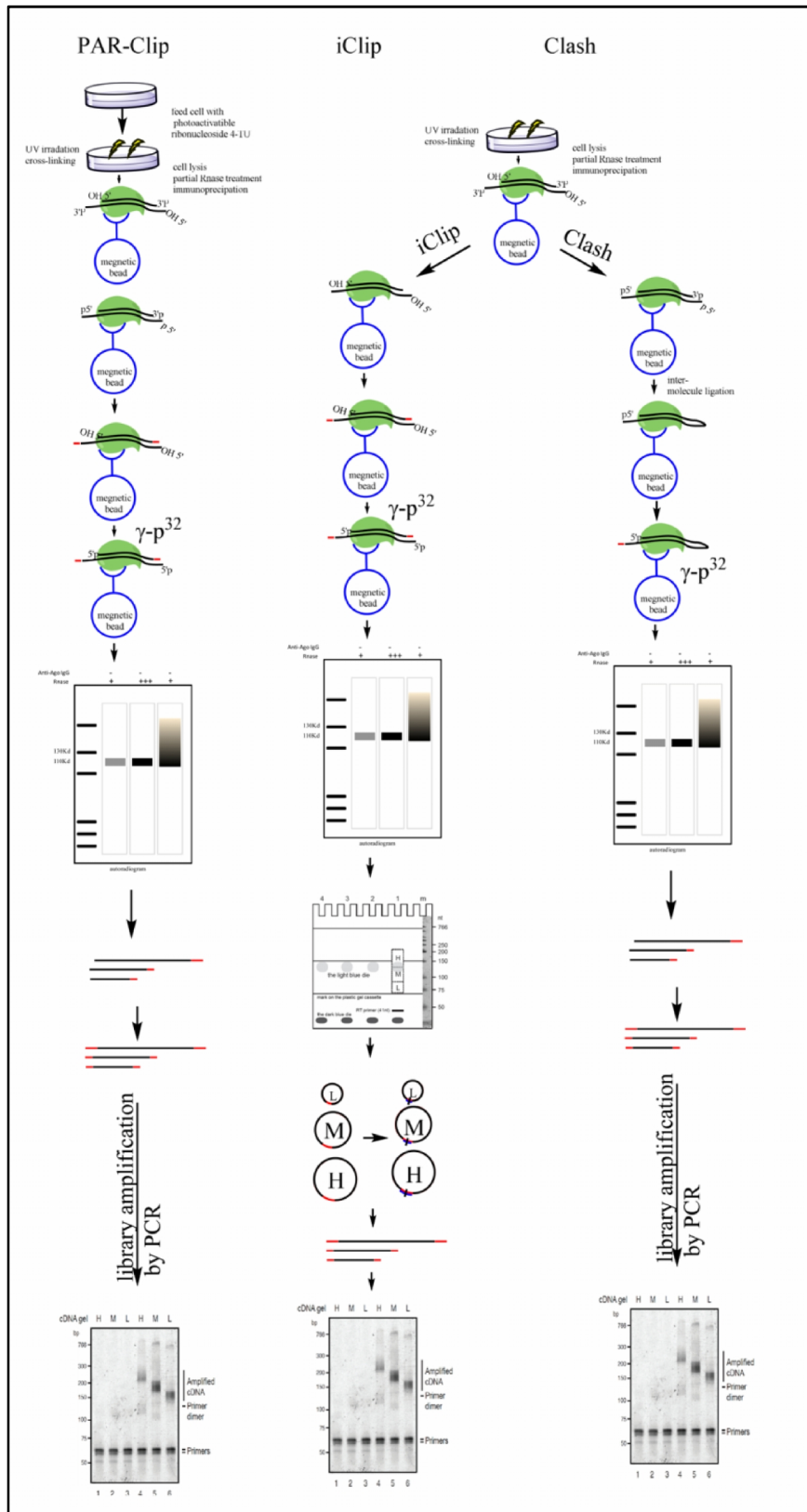
Figure 2. The workflow of different CLIP techniques for miRNA targets identification: first cross link miRNA with their targets within the RISC complexes, isolate these RISC complex containing both miRNA and their targets, then recover both miRNA and their targeted mRNA by cloning and sequencing.
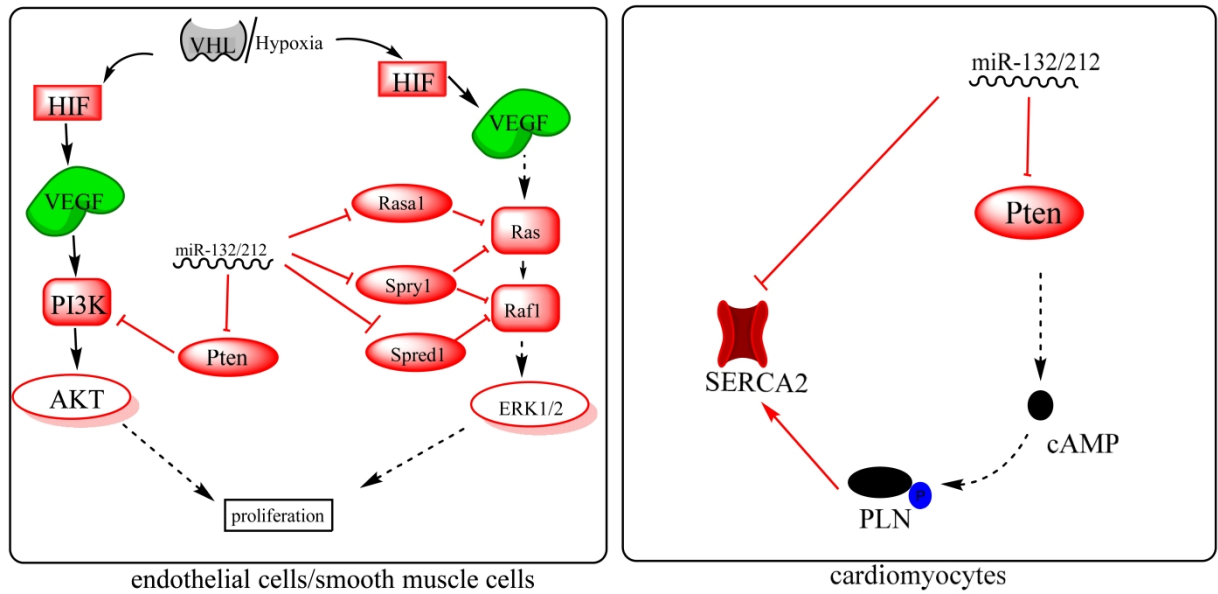
Figure 3. A summary of miR-132/212 in regulation of neovascularization in endothelial cells/smooth muscle cells and cardiac contractility in the cardiomyocytes.
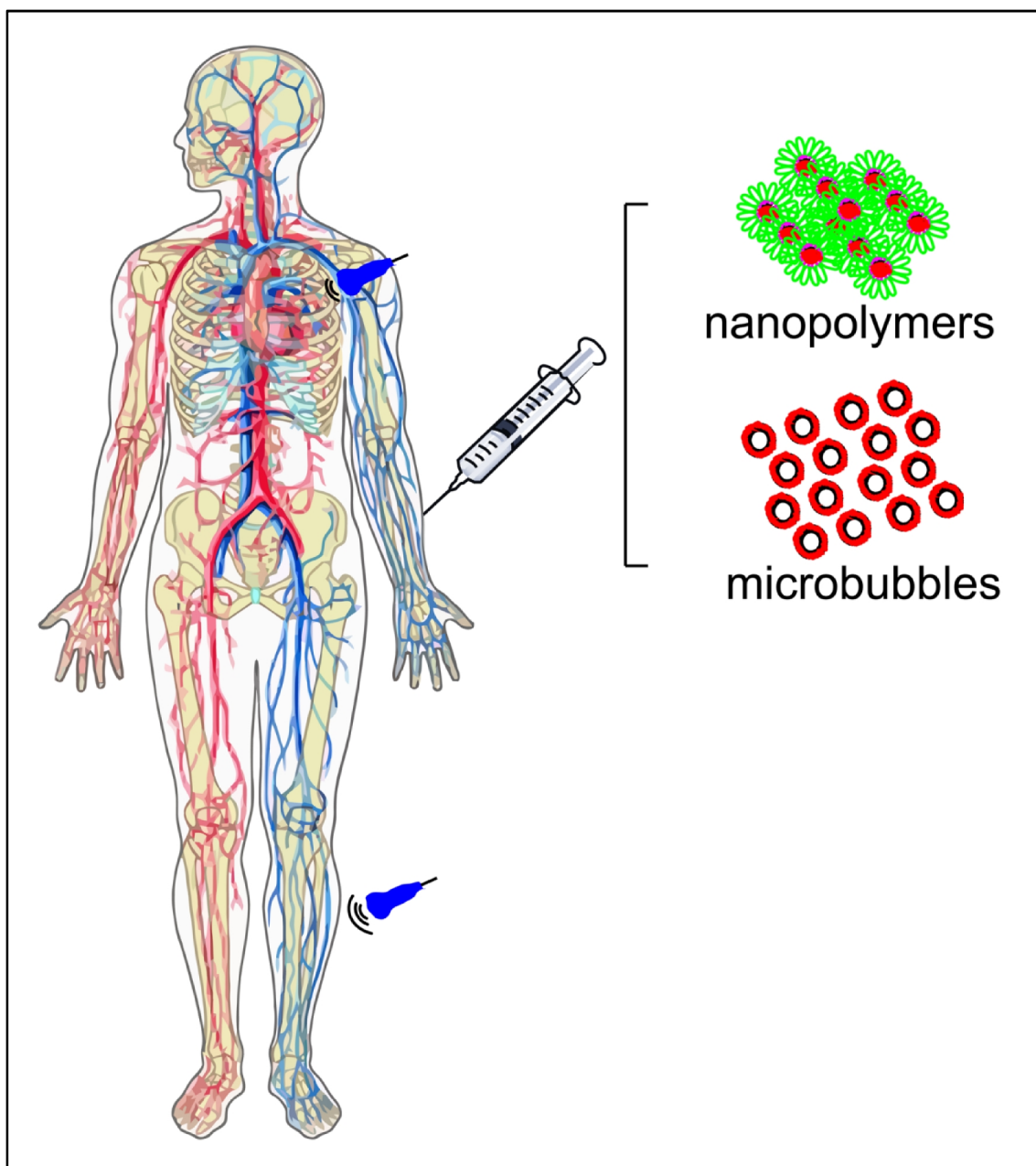
Figure 4 A cartoon about the nanoploymer and ultrasound guided microbubbles mediated targeted delivery of miRNA therapeutics in the cardiovascular system. miRNA therapeutics (miRNA mimics or antimiRs) can be loaded directly on the nanopolymers or microbubbles and then injected into circulation. Targeted delivery is achieved by targeting peptide on the nanopolymers or localized ultrasound treatment.

References

1. Small, E.M. and E.N. Olson, Pervasive roles of microRNAs in cardiovascular biology. Nature, 2011. **469**(7330): p. 336-42.
2. van Rooij, E., et al., Control of stress-dependent cardiac growth and gene expression by a microRNA. Science, 2007. **316**(5824): p. 575-9.
3. van Rooij, E., et al., A signature pattern of stress-responsive microRNAs that can evoke cardiac hypertrophy and heart failure. Proceedings of the National Academy of Sciences of the United States of America, 2006. **103**(48): p. 18255-60.
4. da Costa Martins, P.A., et al., MicroRNA-199b targets the nuclear kinase Dyrk1a in an auto-amplification loop promoting calcineurin/NFAT signalling. Nature cell biology, 2010. **12**(12): p. 1220-7.
5. Care, A., et al., MicroRNA-133 controls cardiac hypertrophy. Nature medicine, 2007. **13**(5): p. 613-8.
6. Callis, T.E., et al., MicroRNA-208a is a regulator of cardiac hypertrophy and conduction in mice. The Journal of clinical investigation, 2009. **119**(9): p. 2772-86.
7. Shieh, J.T., et al., Elevated miR-499 levels blunt the cardiac stress response. PloS one, 2011. **6**(5): p. e19481.
8. Lin, Z., et al., miR-23a functions downstream of NFATc3 to regulate cardiac hypertrophy. Proceedings of the National Academy of Sciences of the United States of America, 2009. **106**(29): p. 12103-8.
9. van Rooij, E., et al., Dysregulation of microRNAs after myocardial infarction reveals a role of miR-29 in cardiac fibrosis. Proceedings of the National Academy of Sciences of the United States of America, 2008. **105**(35): p. 13027-32.
10. Matkovich, S.J., et al., MicroRNA-133a protects against myocardial fibrosis and modulates electrical repolarization without affecting hypertrophy in pressure-overloaded adult hearts. Circulation research, 2010. **106**(1): p. 166-75.
11. Duisters, R.F., et al., miR-133 and miR-30 regulate connective tissue growth factor: implications for a role of microRNAs in myocardial matrix remodeling. Circulation research, 2009. **104**(2): p. 170-8, 6p following 178.
12. Wang, J.X., et al., miR-499 regulates mitochondrial dynamics by targeting calcineurin and dynamin-related protein-1. Nature medicine, 2011. **17**(1): p. 71-8.
13. Hullinger, T.G., et al., Inhibition of miR-15 protects against cardiac ischemic injury. Circulation research, 2012. **110**(1): p. 71-81.
14. Qian, L., et al., miR-24 inhibits apoptosis and represses Bim in mouse cardiomyocytes. The Journal of experimental medicine, 2011. **208**(3): p. 549-60.
15. Bonauer, A., et al., MicroRNA-92a controls angiogenesis and functional recovery of ischemic tissues in mice. Science, 2009. **324**(5935): p. 1710-3.
16. Wang, S., et al., The endothelial-specific microRNA miR-126 governs vascular integrity and angiogenesis. Developmental cell, 2008. **15**(2): p. 261-71.
17. Hu, S., et al., MicroRNA-210 as a novel therapy for treatment of ischemic heart disease. Circulation, 2010. **122**(11 Suppl): p. S124-31.
18. Fiedler, J., et al., MicroRNA-24 regulates vascularity after myocardial infarction. Circulation, 2011. **124**(6): p. 720-30.
19. Elia, L., et al., The knockout of miR-143 and -145 alters smooth muscle cell maintenance and vascular homeostasis in mice: correlates with human disease. Cell death and differentiation, 2009. **16**(12): p. 1590-8.
20. Xin, M., et al., MicroRNAs miR-143 and miR-145 modulate cytoskeletal dynamics and responsiveness of smooth muscle cells to injury. Genes & development, 2009. **23**(18): p. 2166-78.
21. Grueter, C.E., et al., A cardiac microRNA governs systemic energy homeostasis by regulation of MED13. Cell, 2012. **149**(3): p. 671-83.
22. Farh, K.K.-H., et al., The widespread impact of mammalian MicroRNAs on mRNA repression and evolution. Science, 2005. **310**(5755): p. 1817-1821.

23. Cheng, L.-C., et al., miR-124 regulates adult neurogenesis in the subventricular zone stem cell niche. Nature neuroscience, 2009. **12**(4): p. 399-408.

24. Makeyev, E.V., et al., The MicroRNA miR-124 promotes neuronal differentiation by triggering brain-specific alternative pre-mRNA splicing. Molecular cell, 2007. **27**(3): p. 435-448.

25. Lei, Z., et al., MicroRNA-132/212 family enhances arteriogenesis after hindlimb ischaemia through modulation of the Ras-MAPK pathway. J Cell Mol Med, 2015.

26. Anand, S., et al., MicroRNA-132-mediated loss of p120RasGAP activates the endothelium to facilitate pathological angiogenesis. Nat Med. **16**(8): p. 909-14.

27. Eskildsen, T.V., et al., The microRNA-132/212 family fine-tunes multiple targets in Angiotensin II signalling in cardiac fibroblasts. J Renin Angiotensin Aldosterone Syst, 2014.

28. Shaltiel, G., et al., Hippocampal microRNA-132 mediates stress-inducible cognitive deficits through its acetylcholinesterase target. Brain Struct Funct, 2013. **218**(1): p. 59-72.

29. Nahid, M.A., et al., Regulation of TLR2-mediated tolerance and cross-tolerance through IRAK4 modulation by miR-132 and miR-212. J Immunol, 2013. **190**(3): p. 1250-63.

30. Shaked, I., et al., MicroRNA-132 potentiates cholinergic anti-inflammatory signaling by targeting acetylcholinesterase. Immunity, 2009. **31**(6): p. 965-73.

31. Lei, Z., et al., Dgcr8 is Indispensable for Cardiac Lineage Specification in Embryonic Stem Cells. Journal of Stem Cell Research & Therapy, 2015.

32. Chi, S.W., et al., Argonaute HITS-CLIP decodes microRNA-mRNA interaction maps. Nature, 2009. **460**(7254): p. 479-86.

33. Broughton, J.P. and A.E. Pasquinelli, Identifying Argonaute binding sites in Caenorhabditis elegans using iCLIP. Methods, 2013. **63**(2): p. 119-25.

34. Hafner, M., et al., Transcriptome-wide identification of RNA-binding protein and microRNA target sites by PAR-CLIP. Cell, 2010. **141**(1): p. 129-41.

35. Hafner, M., et al., Genome-wide identification of miRNA targets by PAR-CLIP. Methods, 2012. **58**(2): p. 94-105.

36. Helwak, A., et al., Mapping the human miRNA interactome by CLASH reveals frequent noncanonical binding. Cell, 2013. **153**(3): p. 654-65.

37. Pathania, M., et al., miR-132 enhances dendritic morphogenesis, spine density, synaptic integration, and survival of newborn olfactory bulb neurons. PLoS One, 2012. **7**(5): p. e38174.

38. Remenyi, J., et al., miR-132/212 knockout mice reveal roles for these miRNAs in regulating cortical synaptic transmission and plasticity. PLoS One, 2013. **8**(4): p. e62509.

39. Magill, S.T., et al., microRNA-132 regulates dendritic growth and arborization of newborn neurons in the adult hippocampus. Proc Natl Acad Sci U S A, 2010. **107**(47): p. 20382-7.

40. Mellios, N., et al., miR-132, an experience-dependent microRNA, is essential for visual cortex plasticity. Nat Neurosci, 2011. **14**(10): p. 1240-2.

41. Wanet, A., et al., miR-212/132 expression and functions: within and beyond the neuronal compartment. Nucleic acids research, 2012: p. gks151.

42. Remenyi, J., et al., Regulation of the miR-212/132 locus by MSK1 and CREB in response to neurotrophins. Biochem. J, 2010. **428**: p. 281-291.

43. Shaywitz, A.J. and M.E. Greenberg, CREB: a stimulus-induced transcription factor activated by a diverse array of extracellular signals. Annual review of biochemistry, 1999. **68**(1): p. 821-861.

44. Mayr, B. and M. Montminy, Transcriptional regulation by the phosphorylation-dependent factor CREB. Nature Reviews Molecular Cell Biology, 2001. **2**(8): p. 599-609.

45. Lei, Z., et al., MicroRNA 132/212 family enhances arteriogenesis after hindlimb ischaemia through modulation of the Ras MAPK pathway. Journal of cellular and molecular medicine, 2015.

46. Baldewijns, M.M., et al., VHL and HIF signalling in renal cell carcinogenesis. J Pathol, 2010. **221**(2): p. 125-38.

47. Network, C.G.A., Comprehensive molecular characterization of human colon and rectal cancer. Nature, 2012. **487**(7407): p. 330-337.

48. Bers, D.M., Cardiac excitation–contraction coupling. Nature, 2002. **415**(6868): p. 198-205.

49.   Frank, K.F., et al., Sarcoplasmic reticulum Ca2+-ATPase modulates cardiac contraction and relaxation. Cardiovascular research, 2003. **57**(1): p. 20-27.

50.   Borlak, J. and T. Thum, Hallmarks of ion channel gene expression in end-stage heart failure. FASEB J, 2003. **17**(12): p. 1592-608.

51.   Meyer, M., et al., Alterations of sarcoplasmic reticulum proteins in failing human dilated cardiomyopathy. Circulation, 1995. **92**(4): p. 778-84.

52.   Niwano, K., et al., Lentiviral vector-mediated SERCA2 gene transfer protects against heart failure and left ventricular remodeling after myocardial infarction in rats. Mol Ther, 2008. **16**(6): p. 1026-32.

53.   Jessup, M., et al., Calcium Upregulation by Percutaneous Administration of Gene Therapy in Cardiac Disease (CUPID): a phase 2 trial of intracoronary gene therapy of sarcoplasmic reticulum Ca2+-ATPase in patients with advanced heart failure. Circulation, 2011. **124**(3): p. 304-13.

54.   Greenberg, B., et al., Design of a phase 2b trial of intracoronary administration of AAV1/SERCA2a in patients with advanced heart failure: the CUPID 2 trial (calcium up-regulation by percutaneous administration of gene therapy in cardiac disease phase 2b). JACC Heart Fail, 2014. **2**(1): p. 84-92.

55.   Ziolo, M.T., et al., Adenoviral gene transfer of mutant phospholamban rescues contractile dysfunction in failing rabbit myocytes with relatively preserved SERCA function. Circ Res, 2005. **96**(8): p. 815-7.

56.   Wahlquist, C., et al., Inhibition of miR-25 improves cardiac contractility in the failing heart. Nature, 2014. **508**(7497): p. 531-5.

57.   Ucar, A., et al., The miRNA-212/132 family regulates both cardiac hypertrophy and cardiomyocyte autophagy. Nat Commun, 2012. **3**: p. 1078.

58.   Thum, T., et al., MicroRNAs in the human heart a clue to fetal gene reprogramming in heart failure. Circulation, 2007. **116**(3): p. 258-267.

59.   Van der Kooy, K., et al., Depression and the risk for cardiovascular diseases: systematic review and meta analysis. International journal of geriatric psychiatry, 2007. **22**(7): p. 613-626.

60.   Sgoifo, A., L. Carnevali, and A.J. Grippo, The socially stressed heart. Insights from studies in rodents. Neuroscience & Biobehavioral Reviews, 2014. **39**: p. 51-60.

61.   Groban, L., et al., Effect of depression and sertraline treatment on cardiac function in female nonhuman primates. Psychosomatic medicine, 2014. **76**(2): p. 137-146.

62.   Kwekkeboom, R.F., et al., Targeted delivery of miRNA therapeutics for cardiovascular diseases: opportunities and challenges. Clinical Science, 2014. **127**(6): p. 351-365.

63.   Lin, C., et al., Novel bioreducible poly (amido amine) s for highly efficient gene delivery. Bioconjugate chemistry, 2007. **18**(1): p. 138-145.

64.   Kwekkeboom, R.F., et al., Ultrasound and microbubble-induced local delivery of MicroRNA-based therapeutics. Ultrasound Med Biol, 2015. **41**(1): p. 163-76.

65.   Leong-Poi, H., et al., Therapeutic arteriogenesis by ultrasound-mediated VEGF165 plasmid gene delivery to chronically ischemic skeletal muscle. Circ Res, 2007. **101**(3): p. 295-303.

66.   Christiansen, J.P., et al., Targeted tissue transfection with ultrasound destruction of plasmid-bearing cationic microbubbles. Ultrasound Med Biol, 2003. **29**(12): p. 1759-67.

67.   Yang, D., et al., Inhibition of hepatic fibrosis with artificial microRNA using ultrasound and cationic liposome-bearing microbubbles. Gene Ther, 2013. **20**(12): p. 1140-8.

68.   Haag, P., et al., Microbubble-enhanced ultrasound to deliver an antisense oligodeoxynucleotide targeting the human androgen receptor into prostate tumours. J Steroid Biochem Mol Biol, 2006. **102**(1-5): p. 103-13.

69.   Carson, A.R., et al., Ultrasound-targeted microbubble destruction to deliver siRNA cancer therapy. Cancer Res, 2012. **72**(23): p. 6191-9.

70.   Chappell, J.C., et al., Targeted delivery of nanoparticles bearing fibroblast growth factor-2 by ultrasonic microbubble destruction for therapeutic arteriogenesis. Small, 2008. **4**(10): p. 1769-77.

71.   van Rooij, E. and S. Kauppinen, Development of microRNA therapeutics is coming of age. EMBO molecular medicine, 2014: p. e201100899.